

Strathclyde Institute of Pharmacy and Biomedical

Sciences

University of Strathclyde

Glasgow G4 0RE

Submitted September 2024



Decipher, Disarm and Disengage:

Understanding the biosynthesis and self-resistance mechanisms of kirromycin-like elfamycin producing, *Streptomyces*.

Robyn Elizabeth Braes: 202085988

Principal Investigator: Professor Paul A Hoskisson

Secondary Supervisor: Professor Glenn Burley

Doctoral Thesis submitted in fulfilment of the requirement for the degree of Doctor of
Philosophy.

Declaration of Authenticity and Author's Rights:

This thesis is the result of the author's original research. It has been composed by the author and has not been previously submitted for examination which has led to the award of a degree.

The copyright of this thesis belongs to the author under the terms of the United Kingdom Copyright Acts as qualified by University of Strathclyde Regulation 3.50.

Due acknowledgement must always be made of the use of any material contained in, or derived from, this thesis.

Signed: 

Date: 29/09/24

Previously published material:

1. McHugh, R.E., Munnoch, J.T., Braes, R.E., McKean, I.J.W., Giard, J., Taladriz-Sender, A., Peschke, F., Burley, G.A., Roe, A.J., Hoskisson, P.A., 2022. Biosynthesis of Aurodox, a Type III Secretion System Inhibitor from *Streptomyces goldiniensis*. *Applied and Environmental Microbiology* 88. <https://doi.org/10.1128/aem.00692-22>

Contribution - Data Curation and draft preparation/review.

2. Preprint - McHugh, R. E., Giard, J., Braes, R.E., McKean, I., Roe, A.J., Hoskisson, P.A., 2023. Optimisation of aurodox production by *Streptomyces goldiniensis*. *Access Microbiology*. <https://doi.org/10.1099/acmi.0.000572.v1>

Contribution - Data Curation and original draft preparation.

3. Larcombe, D.E., Braes, R.E., Croxford, J.T., Wilson, J.W., Figurski, D.H., Hoskisson, P.A., 2024. Sequence and origin of the *Streptomyces* intergenetic-conjugation helper plasmid pUZ8002. *Access Microbiology* 6. <https://doi.org/10.1099/acmi.0.000808.v3>

Contribution - Formal analysis, Methodology and draft preparation/review.

Acknowledgements

These acknowledgements are in no way comprehensive, but I hope they show my appreciation for those that have made my PhD journey possible:

I'd like to thank the University of Strathclyde, not only for the Student Excellence Award which allowed me to pursue this PhD research, but also for being my home for the past 8 years.

Next, I'd like to thank my supervisor, Professor Paul Hoskisson, who has provided me with continuous support, for which I'm profoundly grateful. Your knowledge, ability to think creatively, and give me a kick up the bottom was valued, especially in times of perfection paralysis. In my undergraduate thesis I said thank you for 'educating, inspiring and most importantly showing me how fascinating the complex world of microbiology is.' Something that rings even more true to this day. I hugely appreciate your mentorship for the past 8 years.

To professor Andrew Roe at the University of Glasgow, thank you equally for your support and mentorship which is exemplary. Being an adopted member of your lab group was a privilege and one I am incredibly grateful for.

To my lab mother and aurodox pioneer, Dr Rebecca McHugh, I am struggling to find the words to show my appreciation. Continuing a project and following in the footsteps of those before you can be difficult in the world of science, but your faith, trust and support were unwavering. Thanks for letting me run with it, I hope I've done it justice.

Let's have some secco!

To past and present members of the Hoskie group, particularly JB, Dan and our adopted chemist Admir, thank you for all of your help over the past few years. I couldn't have asked to collaborate with a better bunch. Equally, to all members of the Strathclyde Micro Group, thank you. You truly have been the loveliest, funniest, most talented and driven group of researchers I have ever have the pleasure of working

with. The community we have is second to none and working with you has helped to forge some incredible friendships that I will never forget.

Speaking of... to Elmira, Eilidh, Ada and Molly (better known as the garlic girls). Thank you for the laughs, kitchen discos, megapints of French martini, and a glass of vino when I have really, really, needed it. As the last of us to become 'Dr', thanks for waiting... I'll see you in wine country.

I'd like to thank my family and friends for their continued support during my PhD. Though you had no clue what I was on about, you always asked. Mum and Dad I guess you could say the experiments finally worked (sort of).

Lastly, I would like to thank my partner James, who funnily enough, without this PhD I would never have met. It's a long way from Worcester to Glasgow, I'll always be thankful you made the move. I want to thank you for the love, passion, patience and acceptance. Thank you for reminding me that we suffer more in our imagination than we do in reality, even in the darkest of times. Your unwavering support and motivation has made all of this possible. I truly can't thank you enough, but I hope I can return the favour. After all, it's your turn now...

Contents

Abstract	10
Chapter 1: Introduction.....	12
1.1 Antimicrobial Resistance and the need for alternative therapies.....	13
1.1.1 Antimicrobial Resistance – A Global Health Emergency.....	13
1.1.2 Molecular Basis of Antimicrobial Resistance (AMR).....	13
1.1.3 The Global Impact of AMR.....	16
1.1.4 The Hunt for New Antibiotics	18
1.1.5 Repurposing Old Pipeline Antibiotics.....	22
1.1.6 Anti-Virulence Therapies.....	22
1.2 <i>Escherichia coli</i> as a Pathogen.....	25
1.2.1 Introduction to <i>Escherichia coli</i>	25
1.2.2 <i>Enteropathogenic E. coli</i> (EPEC).....	28
1.2.3 <i>Enterohaemorrhagic E. coli</i> (EHEC).....	29
1.2.4 The Role of the T3SS in EPEC and EHEC.....	32
1.2.5 Antivirulence Therapies.....	34
1.2.6 T3SS: A Potential Target for Antivirulence Therapies.....	34
1.3 The Actinomycetota and <i>Streptomyces</i>.....	35
1.3.1 The Phylum Actinomycetota and the genus <i>Streptomyces</i>	35
1.3.2 Taxonomy, Phylogeny and Current tools for Species Identification.....	36
1.3.3 <i>Streptomyces</i> Life Cycle and Related Morphology.....	37
1.4 Natural products and <i>Streptomyces</i> metabolism.....	41
1.4.1 Natural Products.....	41
1.4.2 Primary Metabolism in <i>Streptomyces</i>	41
1.4.3 Secondary Metabolism in <i>Streptomyces</i> and a Change in Terminology.....	41
1.4.4 Clinical Importance of natural products.....	43
1.5 Biosynthetic gene clusters.....	45
1.5.1 Biosynthetic Gene Clusters.....	45
1.5.2 Expression Under Laboratory Conditions.....	45
1.5.3 NRPS/PKS containing gene clusters.....	48
1.5.4 Evolution of Biosynthetic Gene clusters.....	51
1.5.5 Regulation of Biosynthetic Gene Clusters.....	54
1.5.6 BGC Associated Immunity Genes.....	58
1.6 The Elfamycins.....	59
1.6.1 Introduction to the Elfamycins.....	59
1.6.2 Mechanism of action.....	59
1.6.3 Elfamycin Classification.....	60
1.6.4 The kirromycins.....	63
1.7 Aurodox.....	67
1.7.1 Introduction to Aurodox.....	67
1.7.2 Chemical Structure and Properties.....	68

1.7.3 Inhibition of the <i>E. coli</i> T3SS by aurodox.....	71
1.7.4 Whole genome sequencing and mining of <i>S. goldiniensis</i>	74
1.7.5 Deciphering the aurodox biosynthetic gene cluster.....	74
1.8 Rationale and specific aims.....	76
1.8.1 Rationale.....	76
1.8.2 Specific Aims.....	76
Chapter 2: Materials and Methods.....	77
2.1 Chemicals and Reagents.....	78
2.2 Growth, Maintenance of Bacteria and Media.....	79
2.2.1 Bacterial growth and Maintenance.....	79
2.2.2 Strains and Plasmids.....	80
2.2.3 Media and Antibiotics.....	84
2.2.4 Gravimetric Dry-Weight Analysis of <i>Streptomyces</i> Growth.....	86
2.3 Molecular Biology.....	87
2.3.1 DNA Isolation.....	87
2.3.2 PCR Conditions.....	88
2.3.3 Oligonucleotide primer List.....	89
2.3.4 Gel electrophoresis.....	91
2.3.5 Restriction digests.....	91
2.4 Sequencing, Genome Assembly and Annotation.....	92
2.4.1 Whole genome sequencing using Illumina Technologies.....	92
2.4.2 Assembly of <i>S. ramocissimus</i> genome using Illumina short reads.....	92
2.4.3 Bioinformatic analysis of <i>S. ramocissimus</i> genome.....	92
2.4.4 16S rRNA Sequencing.....	93
2.4.5 Phylogenetic analysis	94
2.4.6 MinION Sequencing of Aurodox Phage artificial chromosome pESAC13-A_pAur.....	94
2.5 Assessing natural product production and bioactivity of <i>Streptomyces</i>.....	95
2.5.1 Solvent Extraction of aurodox from <i>Streptomyces</i> cultures.....	95
2.5.2 Liquid Chromatography Mass Spectrometry.....	95
2.5.3 Agar Plug and disc diffusion Bioassays Against ESKAPE Pathogens.....	96
2.6 Generation of aurodox derivatives in the heterologous host using the re-direct method.....	97
2.6.1 Redirect-PCR targeting system in <i>Streptomyces</i> for lambda-red mediated gene deletions on Phage Artificial Chromosomes.....	97
2.6.2 Preparation of electrocompetent <i>Escherichia coli</i>	97
2.6.3 Tri-Parental Mating.....	98
2.6.4 Intergenic conjugation of integrating vectors into <i>Streptomyces</i>	98
2.7 Cloning of key aurodox biosynthesis genes into pET-21a(+).	100
2.7.1 <i>In silico</i> cloning and plasmid construction.....	100

2.7.2 Plasmid construction using restriction cloning.....	100
2.8 Overexpression, identification and purification of Key aurodox biosynthesis genes in E. coli BL21 DE3.....	101
2.8.1 Hexa-His-tag protein expression using autoinduction media.....	101
2.8.2 Identification and purification of protein.....	101
2.8.3 Inclusion body solubilisation.....	101
2.8.4 SDS – PAGE and Coomassie brilliant blue staining.....	102
2.8.5 Protein Transfer, Wash and Antibody Treatment.....	102
2.8.6 Chemiluminescent detection of aurodox biosynthesis proteins.....	103
2.8.7 Protein preparation of aurodox biosynthesis proteins via French pressure cell	103
2.8.8 Protein purification via Immobilised Metal Affinity Chromatography.....	103
2.9 Overexpression and identification of EF-Tu2/EF-TuB in EHEC.....	105
2.9.1 Overexpression of <i>tuf2/tufB</i> in EHEC and gathering of Secreted proteins.....	105
2.9.2 Harvesting of cell lysate and secreted proteins.....	105
2.9.3 Western blotting for EF-Tu2.....	105
2.10 Experimental assays in this study.....	107
2.10.1 Analysis of the effect of Elfamycins and aurodox derivatives on <i>in vitro</i> growth and cell viability.....	107
2.10.2 <i>In vitro</i> GFP fusion reporter assays.....	107
2.10.3 Enzymatic methylation assay (AurM*).....	107

Chapter 3: Expanding the knowledge of kirromycin-like elfamycin biosynthesis and enzyme evolution within biosynthetic gene clusters.....	109
3.1 Introduction.....	110
3.2 Results.....	112
3.2.1 kirromycin-like elfamycin biosynthetic gene clusters share a conserved structure.....	112
3.2.2 Characterisation of key kirromycin-like Elfamycin producing strains.....	119
3.2.3 Sequencing of the <i>S. ramocissimus</i> genome.....	146
3.2.4 Assessing the biosynthetic potential of Elfamycin-producing strains.....	162
3.2.5 Deciphering the biosynthetic gene clusters of Elfamycins.....	173
3.2.5.1 PKS/NRPS (KirAI-KirAVI).....	173
3.2.5.2 Malonyl and ethylmalonyl transferase (KirCI and KirCII).....	174
3.2.5.3 Aspartate-1-decarboxylase and NRPS (KirD and KirB).....	174
3.2.5.4 Phosphopantetheinyl transferase (PPTase, KirP)...	178
3.2.5.5 Phytanoyl-CoA hydroxylase (PhyH, KirHVI).....	179
3.2.5.6 Crotonyl CoA (KirN).....	180
3.2.5.7 TetR family transcriptional regulator (KirR).....	180

3.2.5.8 Cytochrome p450 (KirO).....	181
3.2.5.9 Methyltransferase (KirM*/AurM*).....	188
3.2.6 Discovery of other potential kirromycin-like biosynthetic gene clusters.....	194
3.3 Summary.....	200
 Chapter 4: Elucidating gene function within the aurodox biosynthetic gene cluster.....	 203
4.1 Introduction.....	204
4.2 Results.....	207
4.2.1 Sequencing of pESAC-13A_AurI.....	207
4.2.2 Validation of <i>S. coelicolor</i> M1152 + pESAC-13A_AurI as a suitable heterologous expression system for aurodox biosynthesis.....	210
4.2.3 Generation of mutant PACs using the pESAC-13A_AurI aurodox BGC expression vector and the Streptomyces re-direct protocol.	215
4.2.4 Phenotypic and biochemical characterisation of the effect of key genes during aurodox biosynthesis using the <i>S. coelicolor</i> M1152 with pESAC-13A_AurI heterologous expression system.....	224
4.2.5 Analysis of the effect of aurodox derivatives from the <i>S. coelicolor</i> M1152 pESAC-13A_AurI_ΔX heterologous expression system on the T3SS of Enterohaemorrhagic <i>E. coli</i>	233
4.2.6 Creation of hexahistidine tagged aurodox biosynthesis genes.....	240
4.2.7 Optimising hexahistidine tagged protein overexpression and detection by Western Blot in <i>E.coli</i> BL21.....	248
4.2.8 optimising hexahistidine tagged AurM* protein purification by IMAC.....	255
4.2.9 Investigating the enzymatic role of AurM* in aurodox biosynthesis.....	259
4.3 Summary.....	265
 Chapter 5: Understanding the self-resistance mechanisms adopted by kirromycin-like elfamycin producers.....	 267
5.1 Introduction.....	268
5.2 Results.....	270
5.2.1 Analysis of EF-Tu copy number and phylogeny in kirromycin-like elfamycin producing strains.....	270
5.2.2 Predicting the structure of EF-Tu1-3 (<i>tuf1-3</i>) from <i>S. ramocissimus</i>	275
5.2.3 Predicting the structure of EF-Tu2 (<i>tuf2</i>) from <i>S. goldiniensis</i>	278
5.2.4 EF-Tu2 increases resistance to aurodox and increases aurodox production in the heterologous host <i>S. coelicolor</i> M1152 + pESAC-13A_AurI.....	281

5.3 Summary.....	287
Chapter 6: Investigating the role of EF-Tu in Type III Secretion by Enterohemorrhagic Escherichia coli.....	288
6.1 Introduction.....	289
6.2 Results.....	294
6.2.1 EF-Tu is not an effector of the T3SS of EHEC.....	294
6.2.2 Overexpression of EF-Tu2 in EHEC via the pVS45 expression vector.....	297
6.2.3 Overexpression of EF-Tu2 in EHEC via the pSEVA_238 expression vector reverses the T3SS knockdown effect of aurodox and kirromycin.....	303
6.2.4 Expression of the resistant Ef-TuB from <i>E. coli</i> in Enterohemorrhagic <i>Escherichia coli</i> via the pSEVA_238 expression vector reverses the T3SS knockdown effect of aurodox and kirromycin.....	310
6.3 Summary.....	316
Chapter 7: Discussion.....	319
7.1 Genome sequencing of <i>S. ramocissimus</i>	319
7.2 Annotation of the <i>S. ramocissimus</i> kirromycin BGC.....	320
7.3 Identification of a kirromycin-like BGC in a metagenome-assembled genome <i>S. ISL094</i>	321
7.4 Analysis of kirromycin-like elfamycin BGC evolution.....	322
7.5 Kirromycin, aurodox and its derivatives are capable of downregulation of the T3SS of EHEC.....	323
7.6 Cloning and overexpression of key aurodox biosynthesis genes.....	324
7.7 Purification of AurM* and enzymatic characterisation.....	325
7.8 EF-Tu copy number and elfamycin resistance profile varies among <i>Streptomyces</i>	326
7.9 EF-Tu reversed the T3S knockdown phenotype of Aurodox and Kirromycin and potentially plays a role in T3SSs in EHEC.....	327
Chapter 8: Conclusions and Future Work.....	329
Chapter 9: References.....	332

Abstract

Elfamycin antibiotics exhibit activity against Gram-positive bacteria by inhibiting translation via elongation factor EF-Tu. Elfamycins are characterised by mode of action rather than chemical structure, though minor structural modifications in these antibiotics can significantly alter their biological activity. Aurodox, a kirromycin-like elfamycin, was shown to inhibit the Type III Secretion System (T3SS) of Enteropathogenic (EPEC) and Enterohemorrhagic (EHEC) *Escherichia coli* along with effective anti-virulence treatment. This study aimed to investigate the diversity of kirromycin-like elfamycin biosynthetic gene clusters (BGCs), their evolution, resistance mechanisms, and how biosynthesis may be manipulated to create modified elfamycin variants which may be active against the T3SS of EHEC.

Genome sequencing of the kirromycin producer *Streptomyces ramocissimus* was performed, and the BGC responsible for kirromycin production through comparison to the BGC found in *Streptomyces collinus*. Comparative analyses between kirromycin-like BGCs revealed the potential for natural variation in producing identical compounds via different genetic pathways. Additionally, a kirromycin-like BGC was identified in *Streptomyces ISL094*, which contained an additional methyltransferase on the BGC, similar to the aurodox BGC of *S. goldiniensis*, suggesting it could be an aurodox producer.

Moreover, aurodox and kirromycin were found to downregulate the T3SS of EHEC, a trait previously thought to be unique to aurodox. Key genes within the aurodox BGC were manipulated and the BGC heterologously expressed to infer function of their roles in aurodox biosynthesis, where their derivatives showed similar effects on the T3SS. The protein, AurM*, thought to methylate the kirromycin molecule creating aurodox was assayed for methyltransferase activity *in vitro*, but activity was not demonstrated on kirromycin as a substrate. Finally, a potential "moonlighting" role for

EF-Tu proteins is suggested, indicating that they might have additional functions related to T3SS regulation, where the knockdown phenotype of aurodox on the T3SS of EHEC was reversed when EF-Tu was expressed in EHEC.

Chapter 1: Introduction

1.1 Antimicrobial Resistance and the need for alternative therapies

1.1.1 Antimicrobial Resistance – A Global Health Emergency

During its 'Golden Age', the discovery and utilisation of antibiotics increased exponentially. As such, global healthcare systems are now more dependent on the use of antibiotics than ever before (Hutchings et al., 2019). Unfortunately, this reliance on antibiotics has led to the misuse of these vital drugs by overprescribing from pharmacists and GPs, lack of patient compliance, overuse in agriculture, poor infection control and poor sanitation. These factors have led to the global emergence of antimicrobial resistance (McEwen and Collignon, 2017).

1.1.2 Molecular Basis of Antimicrobial Resistance (AMR)

Antimicrobial resistance arises when an infective microorganism survives exposure to an antimicrobial agent. This could be via mutation, known as mutational resistance, or horizontal gene transfer where the surviving microorganism can transfer its antimicrobial resistant genes to other microorganisms, conferring resistance from this antimicrobial to another bacterium (Munita et al., 2016).

Antibiotic resistance genes can be transferred via horizontal gene transfer (HGT) through a number of mechanisms. These commonly include transduction via bacteriophage, transformation with free DNA, conjugation involving plasmids and integrative conjugating elements (ICEs) and more recently, the role of membrane vesicles in HGT has been investigated (McInnes et al., 2020). Transduction is a process where bacteriophage drive bacterial evolution, and in turn AMR, through the transfer of genetic material from phage to bacteria (Leclerc et al., 2022). As the most abundant biological organisms on the planet, it is no wonder that phage are one of the main drivers of AMR through this transduction of resistant genes (Clokier et al., 2011). The process of transformation to acquire resistance genes does not require

cell to cell contact, and is best characterised in the Gram-positive bacteria, such as *Streptococcus pneumoniae* and *Bacillus subtilis* (Dubnau, 1999; Dubnau and Blokesch, 2019). Though no contact is required, the cells are required to be in a state of competency, to accept the DNA (Chen et al., 2005). Conjugation is a common mechanism for horizontal gene transfer which has been shown to be instrumental in the spread of antibiotic resistance among bacteria (Graf et al., 2019). In contrast to transformation, it is a contact-dependant process where the unidirectional transfer of DNA is fulfilled from a donor to a recipient cell via mating apparatus expressed by the donor (Sørensen et al., 2005). All genetic material that is required for conjugation is carried on the mobile genetic element (MGE) itself, these can include conjugative plasmids and ICEs (Johnson and Grossman, 2015). Studies have identified AMR genes as part of these MGEs, conferring antimicrobial resistance to the recipient cell after conjugation (Davies and Davies, 2010; Stokes and Gillings, 2011). Conjugation is widely considered to be the most important process of HGT in the dissemination of antimicrobial resistance genes, closely followed by transduction and transformation (von Wintersdorff et al., 2016). More recently, membrane vesicles (MVs) have been investigated in the context of AMR due to their ability to deliver cargo to target cells. In this process, the outer membrane bulges from cells and is released through constriction (Gill et al., 2019). These MVs then fuse with target cells releasing vesicle contents such as the β -lactamases of bacterioides, which protect target cells against β -lactam antibiotics (Stentz et al., 2015). However, the role of membrane vesicles in the transfer of antimicrobial resistance genes is not yet investigated.

The mechanistic basis of antimicrobial resistance can arise in a variety of ways (Baran et al., 2023; Blair et al., 2015; Munita et al., 2016). First, the antibiotic molecule itself can be modified, where bacteria produce enzymes that inactivate the antimicrobial or add chemical moieties to the compound resulting in destruction of the molecule

(Surette et al., 2021; Wilson, 2014), such as hydrolysis, through the action of β -lactamases (Abraham and Chain, 1988), or modification of the drug through addition of a moiety that results in a molecule which is unable to interact with its drug target (D'Costa et al., 2011). Another mechanism is through decreasing antibiotic penetration and/or increasing efflux. In this case, decreased permeability of the cell wall stops the antibiotic entering the bacterial cell and can prevent the antibiotic from eliciting its effects within the cell (Pagès et al., 2008) and the presence of efflux pumps can drive toxic compounds out of the bacterial cell allowing the cell to survive antibiotic treatment (Blair et al., 2014; Lorusso et al., 2022; McMurry et al., 1980), contributing to the antimicrobial resistance. Another antimicrobial resistance strategy for bacteria to develop is to prevent the antibiotic from interfering with its target site. Here, bacteria have evolved methods to protect the target site (Aldred et al., 2014; Connell et al., 2003) and mechanisms to modify the target site to prevent interaction of the antibiotic due to the decreased affinity of the antibiotic for the altered binding site (Campbell et al., 2001). This target alteration can be achieved through mutation, where the resulting bacteria is more resilient to antimicrobial treatment (Hooper, 2002; Leclercq, 2002; Weisblum, 1995). Finally, resistance to antimicrobials can arise as a result of global cell adaptations, where bacterial pathogens have devised strategies to evade disruption of essential cellular processes, which are so often the target of antimicrobials (Pogliano et al., 2012). Here, the bacteria evolve the resilience to antibiotic treatment by devising complex mechanisms to maintain cell wall synthesis and membrane homeostasis, protecting the bacteria from antimicrobial treatment (Dhar et al., 2018; Tan et al., 2022). With standard antimicrobial treatments for simple infections now ineffective due to the molecular basis and mechanisms used by bacteria, a clinical crisis has been declared; driving efforts to tackle this global crisis.

1.1.3 The Global Impact of AMR

Commissioned in 2014, Lord Jim O'Neill sought to analyse the global crisis of antimicrobial resistance and proposed actions to tackle this situation internationally. It was not until his findings were published in 2016, that the true nature and urgency of this global health crisis was observed. It was found that the antimicrobial resistance currently causes 700,000 deaths annually, which is predicted to soar to 10,000,000 by the year 2050 without intervention, surpassing those attributed to cancer (Fig. 1.1 O'Neill, 2016). The report made several tangible recommendations on how to address this issue, these included: the implementation of a massive global awareness campaign; improving hygiene to prevent the spread of infection; reducing the unnecessary use of antimicrobials in agriculture, preventing dissemination into the environment; improving global surveillance of antimicrobial usage; promoting rapid diagnostic and alternative therapies to reduce antimicrobial use; increasing industrial and research funding for antimicrobial resistance; and finally to build a global coalition to tackle this issue as one, much like the 'One Health Perspective' of McEwen and Collignon (McEwen and Collignon, 2017).

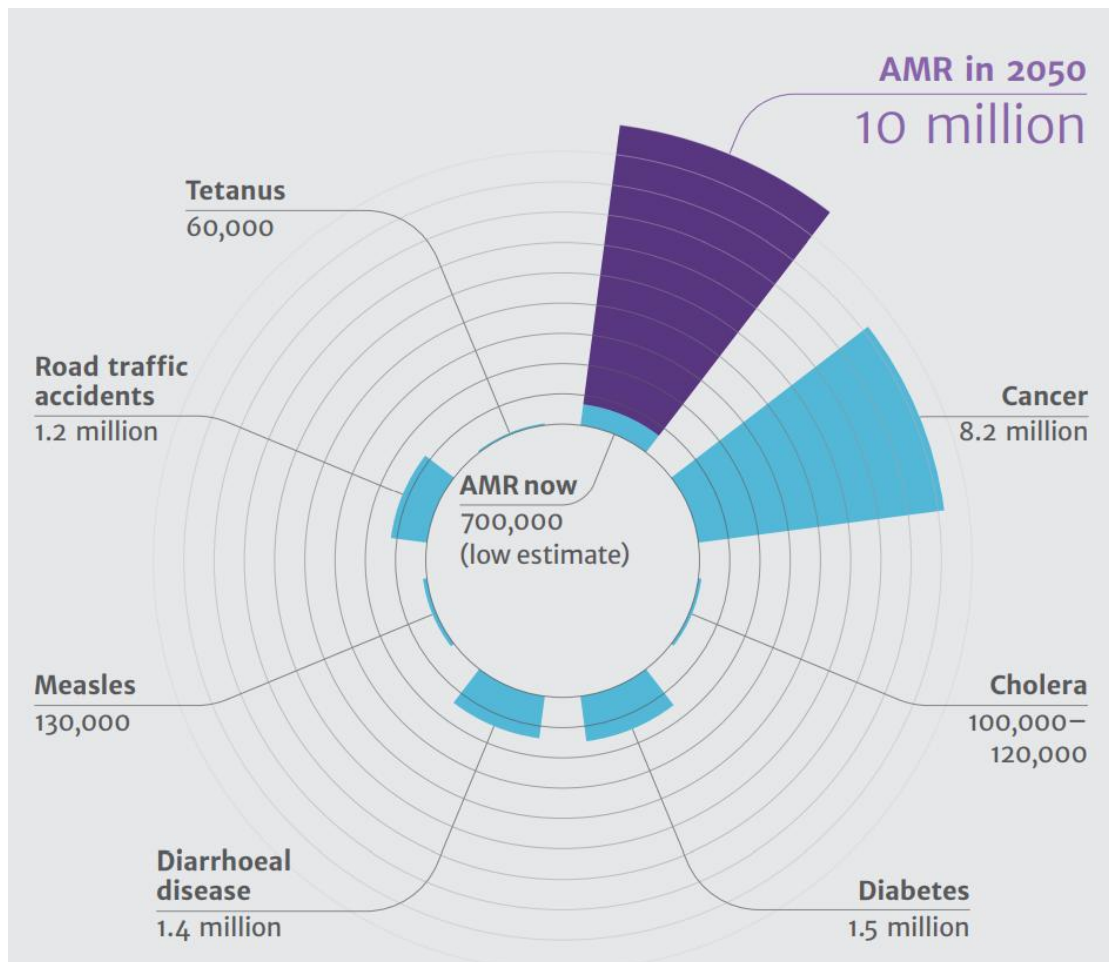


Figure 1.1: Death attributed to antimicrobial resistance is thought to reach 10 million people per year by 2050. Taken from O'Neill, 2016.

1.1.4 The Hunt for New Antibiotics

Two thirds of our clinically used antibiotics have been harnessed from Actinomycete species (van Bergeijk et al., 2020), the majority of which have been isolated from terrestrial environments (Bizuye et al., 2013) such as soil (Crits-Christoph et al., 2018). Due to the convenience of physical sampling, these terrestrial environments have been explored in depth since the beginning of the antibiotic era. As such, while looking to expand our antibiotic medicine cabinet, current research has now diverted into other environments as prospective sources for a new pipeline of antibiotics.

Some Actinomycete species have been found to exhibit extremophile characteristics as they can be isolated from environments such as the hyper arid conditions of The Atacama Desert (Bull et al., 2016; Crits-Christoph et al., 2013) and the harsh environments of Antarctica (Waschulin et al., 2022). These harsh environments have even been shown to be an ecological niche for some species which possess endemism, though the environments remain relatively unexplored (Kleinteich et al., 2017). Closer to home, they are found in more hospitable environments such as marine sediments (Gebreyohannes et al., 2013). The biodiversity of tropical marine environments has been studied considerably more than the temperate marine environments observed in the Atlantic and polar marine environments of the Arctic Oceans (Fuhrman et al., 2015). Studies have explored the marine biodiversity of temperate environments and specifically, the Actinomycete species present (Duncan et al., 2015). Other studies have shown *Streptomyces* species to be isolated from mangrove swamps (Zhang et al., 2023) and even the bodies of fungus cultivating ants, in a complex interaction where *Streptomyces* are horizontally acquired from the environment to form a protective microbiome for the ants against fungal pathogens (Batey et al., 2020). This symbiosis between natural product-producing bacteria and their symbiotic partners has been observed countlessly across a number of relationships (Seipke et al., 2012), including the aforementioned fungus farming ants

(Barke et al., 2010; Cafaro et al., 2010; Seipke et al., 2013, 2011; Sit et al., 2015), marine sponges (Selvin et al., 2009; Taylor et al., 2007), other insects such as solitary wasps (Kaltenpoth, 2009) and finally, the more well known symbiotic relationships with plants (Kruasuwan et al., 2023; Sousa and Olivares, 2016; Worsley et al., 2020). Though this new wave of antibiotic discovery has emerged, the terrestrial environment is not yet exhausted. Recent studies have identified potential bioactive compounds from the soil using metagenomic approaches (Brady et al., 2021) and from the microbiome of roots (Dror et al., 2020). This confirms the vast opportunities for novel antimicrobial compounds yet to be harnessed. With a world of possible isolation environments, each with the potential to harbour novel natural product producers, it is now more important than ever to consider the most fair and equitable sharing of benefits arising out of the sampling and genetic information from this research. Protocols such as the Nagoya protocol address this and have the ultimate objective to conserve and promote sustainable use of biodiversity (Leal et al., 2020; Overmann and Scholz, 2017).

Creating representative environmental conditions in a laboratory is extremely challenging, where culturing and maintaining isolated strains is problematic. Compared to their abundance in the natural environment, as little as 1% of microbes can be grown successfully under *in vitro* conditions (Torsvik et al., 1990). This 1% of the environmental microbiome has been a rich source of natural products, therefore, it is no surprise that traditional isolation techniques have progressed to utilising modern genomic applications such as Next Generation Sequencing (NGS) to identify the other 99% of organisms in a culture independent manner. This culture-independent isolation allows for larger discovery of microorganisms when compared to that of culture dependant methods. This theory was observed in the bacterial communities of the apple phyllosphere where culture-dependent and culture-independent methods were used for bacterial isolation. Yashiro, Spear and McManus

found culture-independent methods revealed greater numbers and greater richness of bacteria on apple leaves than found by culturing (Yashiro et al., 2011). The same was found for the diversity of mycorrhizal fungi in orchid species, where the culture-dependant approach identified half of the species detected by the culture-independent method (Mennicken et al., 2024). The same can be observed in the human microbiome, where integration of both culture-dependant and the addition of culture independent molecular methods of species identification allowed the greatest diversity ever described so far for anaerobic bacteria in the cystic fibrosis lung (Lamoureux et al., 2021).

For ecological analysis, using a metagenomic approach, Crits-Christoph et al., 2013 sampled various sites of the Atacama Desert looking at the microbial diversity of each site. They found that the phylum level composition of each sample was similar across all sample sites, and all sites were dominated by Actinobacteria at a composition of between 72% to 88%. In hyper arid zones, they also found the Actinomycetes were the most dominant Actinobacteria present, confirming their extremophile characteristic and proving the promise of culture-independent methods of identification.

Over the last decade, metagenomics has allowed an insight into the uncultured environment and has shown that a vast amount of the bacterial diversity on Earth is comprised of uncultured bacterial taxa. Despite the rise in metagenomic studies, only 2.1% of the global prokaryotic taxa are represented by sequenced genomes, with 97.9% of bacterial operational taxonomic units estimated as unsequenced (Zhang et al., 2020). This demonstrates that even with the combination of cultured and culture-independent methods, the microbial world still remains relatively uncharted.

One way to address this discrepancy has been through in situ culture methods such as the iCHIP (Nichols et al., 2010). The device has been utilised to study previously unculturable bacteria and has helped to identify new bacterial species and natural

products such as Teixobactin (Ling et al., 2015). Teixobactin is specialised metabolite of *Eleftheria terrae*, which targets cell wall precursors causing cell lysis making it a promising antimicrobial agent for antibiotic-resistant Gram-positive pathogens (Homma et al., 2016).

Another angle is to heterologously express the genes responsible for a specific antimicrobial's production in strains which are easily cultivated in the lab. This means that novel natural products identified during culture-independent methods can be expressed and the specialised metabolite produced under laboratory conditions. Work by Iqbal et al., 2016 saw them express, and produce, the novel natural product Metatricycloene from environmental eDNA in *Streptomyces albus*, a strain known for its acceptance of heterologous expression. Traditionally, heterologous expression is considered a time consuming process due to the construction and screening on large-insert genomic DNA libraries (Kang and Kim, 2021). Technological advancements in synthetic biology, genome engineering tools such as CRISPR (clustered regularly interspaced short palindromic repeats)/Cas9, DNA assembly and high efficiency *in vivo* or *in vitro* recombination have resulted in strategies which allow much faster cloning of BGCs directly from genomic DNA without the need for the construction of a cosmid or BAC library (Alberti and Corre, 2019). To further this, libraries of synthetic promoters and ribosome binding sites (RBSs) have allowed the re-designing and fine-tuning of the genes present in BGCs required for natural product biosynthesis (Ji et al., 2019, 2018) to improve natural product titre or activate silent BGCs. for *Streptomyces*, in particular, methods have been developed which use synthetic biology and novel genome modifications to aid in BGC discovery and expression (Moore et al., 2021; Sidda et al., 2016; Wang et al., 2016).

Other strategies for antibiotic discovery have harnessed bioinformatic tools for the mining of bacterial genomes for the discovery of novel antimicrobials and activating

the genetic machinery of bacteria to produce unexpressed metabolites, which will be discussed later.

1.1.5 Repurposing Old Pipeline Antibiotics

A secondary branch of natural product research has followed the opposite direction and looked back into the old pipeline of antibiotics for antimicrobials which did not make it to clinic. This could provide a promising source of untapped potential therapeutics. In 2019, the Global Antibiotic Research and Development Partnership (GARDP) performed an in-house review of the current clinical antibacterial and antituberculosis pipeline. Their findings highlighted that most of their current antimicrobials in the pipeline were of an old class of antibiotics which focus on an old target, with as little as one antimicrobial of a new class and of a new target (Theuretzbacher et al., 2019). Many old antibiotic classes and original targets are favourable for antimicrobials due to the wealth of knowledge and clinical awareness of their effects. There is also the benefit of the drug being previously approved for the clinic, therefore, drug licensing is less time consuming (Savoia, 2016). This presents the question as to if some of our old pipeline antibiotics could potentially have a new target or mode of action which could be exploited for therapeutic use to tackle the ongoing antimicrobial resistance crisis.

1.1.6 Anti-Virulence (AV) Therapies

With the current treatments for microbial infections resulting in a strong selection for a resistance phenotype, the use of anti-virulence compounds has been proposed. Where antibiotics are used to kill pathogens by inhibiting their key metabolic processes causing cell death, anti-virulence (AV) compounds differ from antibiotics through their mechanism of action (Allen et al., 2014). AV drugs are known to disarm the infecting bacteria of the virulence factors they utilise to colonise and promote

infection in the host. As a result of this, bacteria which have developed resistance profiles are less selected for in populations as the bacteria are not 'killed' but 'disarmed' (Cegelski et al., 2008). This helps to alleviate the ongoing burden of antimicrobial resistance as the fitness benefits associated with a bacterium being resistant, do not convey the same effects when it comes to treatment with an AV drug, and so are not selected for in the population (Clatworthy et al., 2007; Rasko and Sperandio, 2010). Work by Allen and co-workers explored this 'evolution-proof' prediction, where their work concluded that even though resistance to AV drugs has already been reported in certain cases, it is possible to reduce and/or reverse selection for resistance through appropriate combinations of target and treatment environment, affirming the potential AV drugs possess (Allen et al., 2014). Bacteria can elicit their virulence strategies in many ways, *Bacillus anthracis* and *Clostridia spp.* can produce toxins (Hedge et al., 2008; Schiavo and van der Goot, 2001), have adhesive mechanisms (Proft and Baker, 2009) and even have specialised secretion systems, such as the secretion systems of *Escherichia coli* and *Salmonella spp.* (Coburn et al., 2007; Kaper et al., 2004). Virulence factors are those that assist in bacterial colonization, immunoevasion, immunosuppression, obtaining nutrition and damaging host cells. Compounds to target these virulence factors act upon that which makes the strain virulent. In 2014, a study used gallium as an antivirulence drug to quench the siderophore secreted and shared among pathogenic *Pseudomonas aeruginosa* to scavenge iron. Their results found that extracellular quenching of bacterial public goods could offer an effective and evolutionarily robust control strategy for bacterial populations as gallium strongly inhibited bacterial growth *in vitro* without the development of bacterial resistance (Ross-Gillespie et al., 2014).

Targets for AV drugs can vary between intra or extracellular structures, however in all appropriate targets, there must be the incorporation of a factor which, if inactivated, will reduce the affinity of the pathogen to colonise and persist in the host. This

provides the cessation in infection needed for the innate immune response to clear the infection from the host (Mühlen and Dersch, 2015; Zambelloni et al., 2015). This AV treatment is then aided by the fact that most gut infections have a means of self-clearing, where the regular excretion of intestinal waste through defecation can facilitate the ridding of pathogenic bacteria from the gut naturally (Calvert et al., 2018; Totsika, 2016).

Some examples of recently discovered AV therapies include those that target adherence, such as Auranofin's reduction of Vancomycin resistant *Enterococci* in the murine internal organs after treatment (Abutaleb and Seleem, 2020). ToxR was found to be a efflux pump involved in the export of antimicrobials and so ToxR inhibitors such as PAβN could be used as adjuvants to traditional antibiotic treatment for cholera and potentially other Gram-negatives by targeting toxins and secretion systems (Weng et al., 2021). Studies have also suggested that bacteriophage could be an effective anti-virulence treatment, as phage's often target bacterial surface structures that may crucial to their virulence (Shen and Loessner, 2021).

Whether anti-virulent compounds are to be used alone, or in combinations with current antimicrobials, they show promise for potential therapies to replace or complement current antimicrobials (Hotinger et al., 2021). The implementation of which, should be explored and encouraged but also cautioned as recent studies have suggested that some compounds with anti-virulence properties can actually increase the pathogenicity of some microbial species (Juárez-Rodríguez et al., 2020).

1.2 *Escherichia coli* as a Pathogen

1.2.1 Introduction to *Escherichia coli*

Escherichia coli is often regarded as the best studied free-living organism on Earth. The model bacterium, *E. coli* is a Gram-negative rod-shaped organism belonging to the *Enterobacteriaceae*. First isolated from the human colon in 1885 by Theodor Escherich, the bacterium was termed *Bacterium coli*, however this was changed to reflect the discoverers name in 1954 (Friedmann, 2006). Characteristic of its isolation from the human gut, the organism is a facultative anaerobe which is found to grow exponentially at 37° C (Dunne et al., 2017). In line with the ongoing antimicrobial resistance crisis, *E. coli* has been identified as clinically relevant as in 2017, 58% of all *E. coli* species could be categorized as drug resistant across Europe.

Both the physiology and genetics of *E. coli* have been extensively characterised historically, and more-so now with the current global health crisis. *E. coli* K-12, a widely used clinically isolated lab strain, was one of the very first organisms to undergo whole genome sequencing (Blattner et al., 1997). Blattner et al., showed that the genome of *E. coli* K-12 is approximately 4.6 MB in size and predominantly contained one large chromosome. Work since then has assigned a function to almost all of the ~ 4300 genes in its genome (Baba et al., 2006). The in-depth of knowledge about the biochemistry and the non-pathogenic character of *E. coli* K-12 has made it widely considered to be the workhorse of molecular biology. No other organism is exploited more widely in research laboratories across the world for the manipulation of DNA, production of native and mutant proteins, and physiological comparisons for studies in a variety of experimental settings (Dunne et al., 2017; Mori et al., 2022).

In its natural environment, *E. coli* is a common member of the human gut microbiome where it provides beneficial characteristics such as the production of vitamin K, an essential vitamin used for the post-synthesis modification of proteins involved in blood

coagulation and for the control of binding of calcium in bones and other tissue (Bentley and Meganathan, 1982). However, in his original findings from its isolation, Theodor Escherich found the organism to be causative of diarrheal disease in children (Friedmann, 2006). It became apparent through further research that not only can *E. coli* cause sustained and profuse infection in the human gut, but it can also infect other niches in the human body. Uropathogenic *E. coli* (UPEC) is seen to cause approximately 90% of urinary tract infections (UTIs) and other strains of *E. coli* have also been found to infect the circulatory system causing sepsis and meningitis (Bonacorsi and Bingen, 2005; Rodrigues et al., 2022; Whelan et al., 2023; Wiles et al., 2008).

Acquisition of this bacteria is often due to animal reservoirs, where modern farming methods result in contamination of the food chain leading to sustained infection in humans (Ferens and Hovde, 2011; Kim et al., 2017). These infections are acquired through the faecal-oral route but the original source and causative pathogenicity of *E. coli* is often linked to serotype (Wasteson, 2001). *E. coli* which causes diarrhoea, often termed Enteric pathogenic *E. coli* (EPEC) or diarrhoeagenic, is classified based on its virulence characteristics (Table 1A, adapted from Allocati et al., 2013).

Table 1A: Summary of major pathogenic *E. coli* strains, symptoms and virulence factors. Adapted from Allocati et al., 2013. The two *E. coli* strains in red will be discussed further in this thesis.

Strain of <i>E. coli</i>	Abbrev.	Symptoms	Epidemiology	Reference
Enteric <i>E. coli</i>				
Enteropathogenic <i>E. coli</i>	EPEC	Watery diarrhoea, abdominal pain, vomiting.	Common in developing countries. Contaminated water often responsible. Faecal-oral route most likely. Person to person spread can occur	(Kaper et al., 2004; Pakbin et al., 2021)
Enterohemorrhagic <i>E. coli</i>	EHEC	Bloody diarrhoea, vomiting, severe abdominal cramps. Can result in haemolytic uremic syndrome.	Worldwide outbreaks, contaminated meat often responsible. Faecal-oral route most likely.	(Biliński et al., 2012; Kaper et al., 2004)
Enterotoxigenic <i>E. coli</i>	ETEC	Watery diarrhoea, abdominal pain.	Common in developing countries. Contaminated water often responsible. Faecal-oral route most likely mode of transmission.	(Al-Abri et al., 2005; Mirhoseini et al., 2018; Qadri et al., 2005)
Enteroadherent <i>E. coli</i>	EAgEC	Diarrhoea with mucus, vomiting, fever.	Common in travellers, ingestion of food. Person to person transmission unlikely.	(Servin, 2005)
Enteroinvasive <i>E. coli</i>	EIEC	Watery diarrhoea, abdominal pain, vomiting, dysentery.	Worldwide. Contaminated food main factor. Faecal-oral route most likely-person to person spread likely. Shigellosis like.	(Kaper et al., 2004; Nataro et al., 1998)
Verotoxigenic <i>E. coli</i>	VTEC	Bloody diarrhoea, vomiting, abdominal cramps.	Common in travellers, ingestion of food. Person to person transmission unlikely.	(Karmali, 1989)
Extraintestinal <i>E. coli</i>				
Uropathogenic <i>E. coli</i>	UPEC	Cystitis, pyelonephritis.	Sexual transmission, person to person spread without sexual transmission.	(Johnson and Stell, 2000; Kaper et al., 2004; Terlizzi et al., 2017)
Neonatal Meningitis <i>E. coli</i>	NMEC	Acute meningitis, sepsis.	Person to person contact, mother and child.	(Gaschignard et al., 2011; Pouillot et al., 2012)
Avian Pathogenic <i>E. coli</i>	APEC	Watery diarrhoea, abdominal pain, vomiting.	Zoonotic transmission, ingestion of food, person to person transmission unlikely.	(Johnson et al., 2007; Rodriguez-Siek et al., 2005)

1.2.2 Enteropathogenic *E. coli* (EPEC)

Enteropathogenic *E. coli* (EPEC) is a clinically relevant global pathogen causative of chronic diarrhoea and is accountable for approximately 800,000 deaths per year, severely effecting children under 5 in developing countries (Liu et al., 2012). EPEC infections are most commonly caused from the ingestion of water from a contaminated source (Gambushe et al., 2022; Ochoa and Contreras, 2011). Separated into two distinct groups based on their virulence characteristics, EPEC infections are often termed typical EPEC (tEPEC) or atypical EPEC (aEPEC). Historically, tEPEC strains are termed by their ability to attach and efface to gut microvilli, where the eventual formation of microcolonies is sustained. These tEPEC strains are typically isolated exclusively from human sources and include the universally used lab strain, *E. coli* E2348/69, with O126:H6 serotype (Hernandes et al., 2009; Iguchi et al., 2009). In contrast, aEPEC strains can be isolated from both animal and human reservoirs and are unable to form coherent effacing lesions and adhere in a more diffuse manner (Hernandes et al., 2009).

Treatment of EPEC infections pose a clinical challenge. Firstly, gut pathogens display an increase in probability of antimicrobial resistance due to expansive horizontal gene transfer between the gut microbiota (Modi et al., 2014). Secondly, the use of broad-spectrum antibiotics for the treatment of these infections can have negative consequence for the healthy gut microbiota resulting in depletion of helpful bacteria. A healthy gut microbiota is essential for the clearing of EPEC infections by the innate immune system, and so treatment with antibiotics can often be more deleterious than beneficial. In most EPEC infections, treatment is often limited to rehydration therapy to replace the water lost by diarrhoea (Sperandio et al., 2000).

1.2.3 Enterohaemorrhagic *E. coli* (EHEC)

Enterohaemorrhagic *E. coli* (EHEC) are pathogens of the small intestine commonly involved in foodborne outbreaks causing bloody diarrhoea. EHEC can continuously be isolated from the bovine rumen. The relationship between EHEC and cattle can be observed where EHEC infections can occur from the ingestion of cattle food products such as undercooked beef or unpasteurised milk (Ferens and Hovde, 2011). *E. coli* O157: H7 is the most studied serotype of EHEC and is responsible for many pathogenic outbreaks. In California, from 1992-1993, 732 people sustained infection with O157: H7 due to undercooked beef burgers. In recent years, food travels further distances to get to its final consumer and so there has been a greater spread in infectious serotypes observed globally due to this distribution of goods. This was observed in the outbreak of the chimeric O104:H4 EHEC strain associated with vegetables from Germany, where the outbreak resulted in over 2000 cases across 14 different countries (Böhnlein et al., 2016; Mellmann et al., 2011).

The symptoms associated with EHEC are much more severe than EPEC, largely due to the pathogens potential to secrete prophage-encoded shiga toxins (Nguyen and Sperandio, 2012). These shiga toxins can disseminate the EHEC infection from the gut to other sites in the body causing systemic infection. Namely, shiga toxins can be split into two groups, Stx1 and Stx2, where presence of these toxins in the kidney or brain can cause fatal effects. Stx is capable of inhibiting protein synthesis, by the cleaving of the 60S ribosomal unit, causing cytotoxic effects, in the kidney, this is termed Haemolytic Uremic Syndrome (HUS; (Karmali, 1989)). If a patient should contract HUS, they often require sustained treatment for the rest of their lives, including dialysis or kidney transplantation, and can lead to mortality (Tarr et al., 2005).

Scotland has a large problem with EHEC infections with the country developing three-times more infections per capita than rest of the UK (Herbert et al., 2014). This is

thought to be due to the rural lives many Scots lead, with higher direct contact to cattle, rural lifestyle, genetics, and most interestingly, a higher prevalence of EHEC in cattle which carry a prophage associated with a 'super shedding' phenotype (Chase-Topping et al., 2007).

Much like the treatment of EPEC with antibiotics, the use of traditional antibiotics on EHEC can associate the same problems, and therefore antibiotic treatment is neither advised or routine. In addition to the complications observed in EPEC, treating EHEC infections with antibiotics can result in the induction of the bacterial SOS response, induced by the denaturation of genomic double stranded DNA (DS-DNA), which can cause further disruption to the system. Here, single stranded DNA breaks (SS-DNA) are present in high volume after antibiotic treatment, the presence of SS-DNA can induce the upregulation of *recA*, a gene involved in the SOS response. The RecA protein is then able to cleave LexA repressors which regulate Stx expression and therefore increasing shiga toxin production and the induction of the SOS response (Fuchs et al., 1999; Fig. 1.2). Due to this activation of the SOS response and upregulation of Stx expression because of the DNA damage caused by treatments with antibiotics, an alternative therapy for treatment of EHEC infections, independent of the induction of *recA* is desirable (Huerta-Urbe et al., 2016).

Like EPEC and due to the complexities associated with the induction of the SOS response with antibiotic treatment, currently patients are limited to the treatment they can receive and often includes symptom-targeted care such as rehydration therapy and total blood volume expansion (Goldwater and Bettelheim, 2012). As a result, the discovery of alternative treatments for EHEC to that of traditional antibiotics could provide a much-needed solution for these infections.

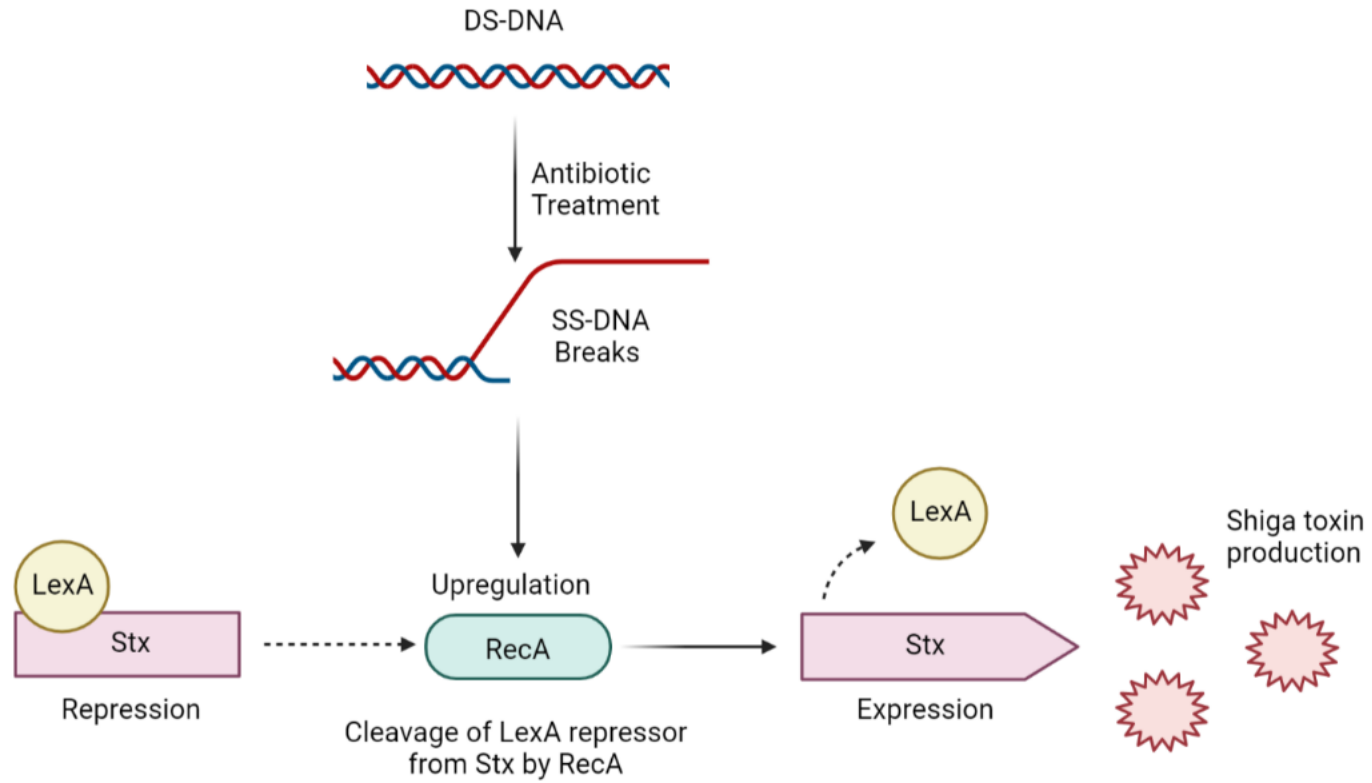


Figure 1.2: RecA mediates the induction of shiga toxin production in EHEC. Adapted from Fuchs et al., 1999. Figure made in BioRENDER.

1.2.4 The Role of the T3SS in EPEC and EHEC

Bacteria have evolved mechanisms to facilitate the transportation of small molecules and proteins to the extracellular space and/or to potential host cells (Costa et al., 2015). Transportation of these molecules is achieved via secretion systems, of which there are 10 types, which vary in size, shape and function (Type I – Type X Secretion Systems)(Gerlach and Hensel, 2007; Lauber et al., 2018; Palmer et al., 2021)

Type III Secretion Systems (T3SS) are often referred to as the ‘injectosome’ due to its needle-like machinery. It is present on the outer membrane of Gram-negative bacteria and is a proteinaceous structure which facilitates the translocation of effector proteins to the gut epithelium. In EPEC and EHEC infections, the utilisation of this T3SS is observed. This involves injection of these T3SS associated proteins, including the Translocated Intimin Receptor (Tir) and the Mitochondria Associated Protein (Map), that allow EPEC and EHEC to polymerise actin-filaments and form tight junctions with epithelial cells (Mills et al., 2008).

T3SS of EPEC and EHEC are encoded on a pathogenicity island in their genome termed the Locus of Enterocyte Effacement (LEE)(Deng et al., 2004). The LEE pathogenicity island is known to encode 42 genes, conserved on 5 operons, which are regulated by the H-NS-type master regulator Ler. Expression of *ler* can be regulated by specific regulators such as GrlA and GrlR and global regulators which control expression of the LEE pathogenicity island in response to environmental factors (Bingle et al., 2014). The structure and integration of the T3SS and the LEE pathogenicity island are shown (Fig. 1.3).

1.2.5 Antivirulence Therapies

The treatment of EPEC and EHEC currently deals with the symptoms associated with infection, with no treatments readily available for treating the underlying bacterial infection. This means novel approaches to treatment, independent of antibiotics, are required. The use of Anti-Virulence compounds has been proposed as a potential answer to this ongoing puzzle. For EPEC and EHEC infections in particular, many AV strategies have been investigated, most of which focus on the neutralisation of shiga toxin and the dissemination of biofilms (Huerta-Urbe et al., 2016; Kitov et al., 2000; Lee et al., 2014; Mühlen and Dersch, 2015).

1.2.6 T3SS: A Potential Target for Antivirulence Therapies

The T3SS is essential for colonisation in ruminants, it has, however, remained an ideal target for AV therapy (Beckham and Roe, 2014; Kimura et al., 2011; Pendergrass and May, 2019; Zambelloni et al., 2015). As T3SS facilitate the delivery effector proteins to the epithelium of the host resulting in attaching and effacing lesions, the T3SS could provide an ideal target for AV drugs. With no delivery of effector proteins, the bacteria would be unable to develop sustained infection in their host (Iyoda et al., 2006; Jarvis et al., 1995; Schmidt, 2010). An example of this the synthetic salicylidene acylhydrazide derivatives which effectively inhibit T3SS (Veenendaal et al., 2009). Unfortunately, these derivatives were found to have multiple targets and so therapy was paused due to the potential downstream effects. An Anti-Virulence compound identified for its inhibition of the bacterial Type III Secretion System is aurodox (Kimura et al., 2011). Produced as a natural product by *Streptomyces goldiniensis*, aurodox has shown promise as a potential AV drug targeting the T3SS (McHugh et al., 2019). The genus *Streptomyces* is well known for the prolific production of chemical compounds with therapeutic effects and may represent a valuable source for new metabolites to treat EPEC and EHEC infections.

1.3 The Actinomycetota and *Streptomyces*

1.3.1 The Phylum Actinomycetota and the genus *Streptomyces*

Actinomycetota are a phylum of Gram-positive bacteria which have high guanosine and cytosine (G+C) content in their genomes (Goodfellow, 2015; Oren and Garrity, 2021). They possess a well characterised filamentous morphology, resembling that of fungi (Bender et al., 2015). Often regarded as one of the most abundant bacterial phyla, the Actinomycetota possesses one of the largest bacterial families, the *Streptomycetaceae*. First described in 1943 after the isolation of *Streptomyces griseus*, the *Streptomycetaceae* are home to the genus *Streptomyces* which can be found extensively in terrestrial, aquatic, and extreme environments (Waksman and Henrici, 1943). *Streptomyces* maintain this filamentous morphology of the Actinobacteria and are found to be saprophytic, aerobic, and vastly morphologically diverse.

Streptomyces species, however, are most well-known for their prolific production of bioactive molecules. Through evolution, their capability to produce these natural products has expanded exponentially with some possessing antibacterial, antifungal, anti-virulent, anti-helminthic, anti-cancer, immunosuppressive and herbicidal properties (Gomez-Escribano et al., 2016). It is this production of natural products that make *Streptomyces* one of the most clinically relevant bacterial genera. The isolation of *Streptomyces griseus* in 1943 was closely followed by the discovery that the organism could produce Streptomycin in 1944, an antibiotic inhibiting protein synthesis in both Gram-positive and Gram-negative bacteria, securing this partnership between *Streptomyces* and the clinic (Schatz et al., 1944).

1.3.2 Taxonomy, Phylogeny and Current tools for Species Identification

Streptomyces are renowned for being phylogenetically diverse, where millennia of evolutionary events across all environments has led to great variation between species (Labeda et al., 2012). The clinical and industrial importance of *Streptomyces* has led to them being subject to extensive isolation and screening efforts. As a result, taxonomic classification of *Streptomyces* strains is challenging due to the genus having the greatest number of described species across all bacterial genera. In addition to the abundance of characterised species, *Streptomyces* are also difficult to taxonomically classify due to the evidence of extensive horizontal gene transfer events within the genus (Kiepas et al., 2023). Methods of classifying these diverse *Streptomyces* species have evolved through the years of working with the genus, from those based on morphological observations (Waksman, 1919; Waksman and Curtis, 1916) to subsequent classification based on numerical taxonomic analyses of standardised sets of phenotypic indicators (Williams et al., 1983) and most recently, to the use of molecular phylogenetic analysis of genomic sequences (Woese, Blanz and Hahn, 1984. Labeda et al., 2012).

The work of Woese, Blanz and Hahn (1984) proposed the use of the 16S ribosomal RNA gene (16S rRNA), a conserved housekeeping gene present across all bacterial species which contains species-specific polymorphisms. The 16S rRNA gene has allowed for characterisation of bacterial species based on these polymorphisms, where now, 16S rRNA gene sequencing is the most dominant method of primary phylogenetic identification of bacterial species (Tringe et al., 2008). In more recent work, there has been the suggestion that the 16S rRNA gene alone, is not sufficient evidence to identify or define *Streptomyces* species (Madhaiyan et al., 2022). This is due to many *Streptomyces* species having high sequence homology within their 16S genes causing low taxonomic resolution. To solve this, in addition to the 16S rRNA gene, multiple *Streptomyces* conserved genes such as *ssgA* and *ssgB* have been

sequenced to facilitate easier and more reliable identification and classification of *Streptomyces* species (Girard et al., 2013). However, it is widely regarded that for accurate phylogenetic analysis of *Streptomyces* species, robust whole genome analysis to elucidate the taxonomy and phylogeny of the Streptomycetes is recommended.

In more recent years, the addition of multi-locus sequence typing analysis to whole genome analysis, has proven beneficial in deciphering the complex *Streptomyces* genus. In work by Madhaiyan and co-workers, it can be seen that analysis of taxonomy further to that of 16S rRNA analysis provides deeper insight with higher resolution as to the diversity of the *Streptomycetaceae* family (Madhaiyan et al., 2022). Software such as AutoMLST software also uses an Automated Multi Locus Species Tree approach to determine phylogenetic and evolutionary relatedness among Actinobacterial species, helping to resolve species identity further than that of 16S rRNA sequencing alone (Alanjary et al., 2019). Though even AutoMLST is not without its limitations for resolving *Streptomyces* phylogeny.

1.3.3 *Streptomyces* Life Cycle and Related Morphology

Streptomyces' ability to ubiquitously populate their environments, and most importantly, sustain population in these environments is a result of their complex life cycle, involving formation and distribution of spores, which is under constant regulation by nucleotide secondary messengers, in response to environmental factors and stresses (Latoscha et al., 2019).

First, the initial germination of spores involves the swelling, growth polarisation and the emergence of one single germ tube that develops into vegetative hyphae capable of soil penetration. This process is activated in response to various signals in the surrounding environment suggesting that the environment is nutrient rich. These vegetative hyphae grow via tip extension which extend across and deeply penetrate

into the substrate giving rise to vegetative mycelia and exponential growth through branching (Nieminen et al., 2013). During the branching process, the polarisome, comprising of the proteins DivVA and Scy, is located at the pole of the cell and interacts with the cell wall biosynthesis machinery to form new points for branching. This process is governed by a gene responsible for a eukaryotic-type Serine/Threonine protein kinase called *asfK* which localises to hyphal tips and phosphorylates DivVA to modulate branching. This branching and formation of vegetative hyphae and mycelia to form bacterial colonies takes place in a nutrient rich environment (Claessen et al., 2003; Hempel et al., 2012). The next step in the *Streptomyces* life cycle is the formation of aerial hyphae which occurs during nutrient limitation or stress factors in the environment. Here, rodlin and chaplin proteins form a hydrophobic sheath over the polarisome and a third protein, SapB, a lantibiotic-like peptide, allows aerial hyphae to break surface tension and escape the aqueous substrate forming the hair-like structures of aerial hyphae (Elliot et al., 2003; Kodani et al., 2005, 2004; Willey and Gaskell, 2011). At this stage in development, each aerial hypha differentiates into a long chain of pre-spore compartments and active chromosome segregation machinery ensures that the multiple copies of that species of *Streptomyces*' genome is present in the hypha and are distributed so each pre-spore receives a single copy (Ohnishi et al., 2002). Pre-spores further differentiate and mature before release as dormant, thick-walled spores. When disturbed, these spores are released and dispersed into the environment where, if in favourable conditions, the process of spore germination and the *Streptomyces* life cycle can begin once again.

This sporulating nature of the *Streptomyces* possessing morphological differentiation as a multicellular unit is unique to the genus and is distinct among other bacteria (Yagüe et al., 2016). Though unique, this sporulation has allowed *Streptomyces* sustained survival in otherwise uninhabitable conditions but has also allowed the

distribution of *Streptomyces* species across ecological niches, such that the ecology and geography of the genus is an area of vociferous study.

Two classes of regulators are responsible for the tight control of the *Streptomyces* life cycle these are termed bald (*bld*) and white (*whi*) where the names of these proteins originate from their associated phenotype in deletion mutants (Chater and Chandra, 2006). Deletions in *bld* result in a bald phenotype as no aerial hyphae are produced, this means that *bld* regulators are involved the early stages of *Streptomyces* development, namely the production of aerial hyphae (Champness, 1988; Elliot et al., 1998, 2001; Salerno et al., 2013). Conversely, deletions in *whi* result in improperly formed mature spores suggesting that the *whi* regulators are involved in later stages of *Streptomyces* development by the conversion of spore chains to mature spores. These regulators are thought to be controlled by gene networks which are closely related to those that sense and respond to changes in the environment linking environmental change to change in *Streptomyces* development (Chater, 1972). Our understanding of this regulation was improved when it was revealed that *bld* and *whi* were mediated by cyclic-di-AMP as a second messenger which interacts with both regulators to moderate the *Streptomyces* life cycle (Bush et al., 2015) In addition to this, recent work by Latoscha et al., 2020 suggested that phosphodiesterase AtaC binds to and hydrolyses cyclic-di-AMP removing it from the cytoplasm of the cell allowing the life cycle to continue (Fig. 1.4).

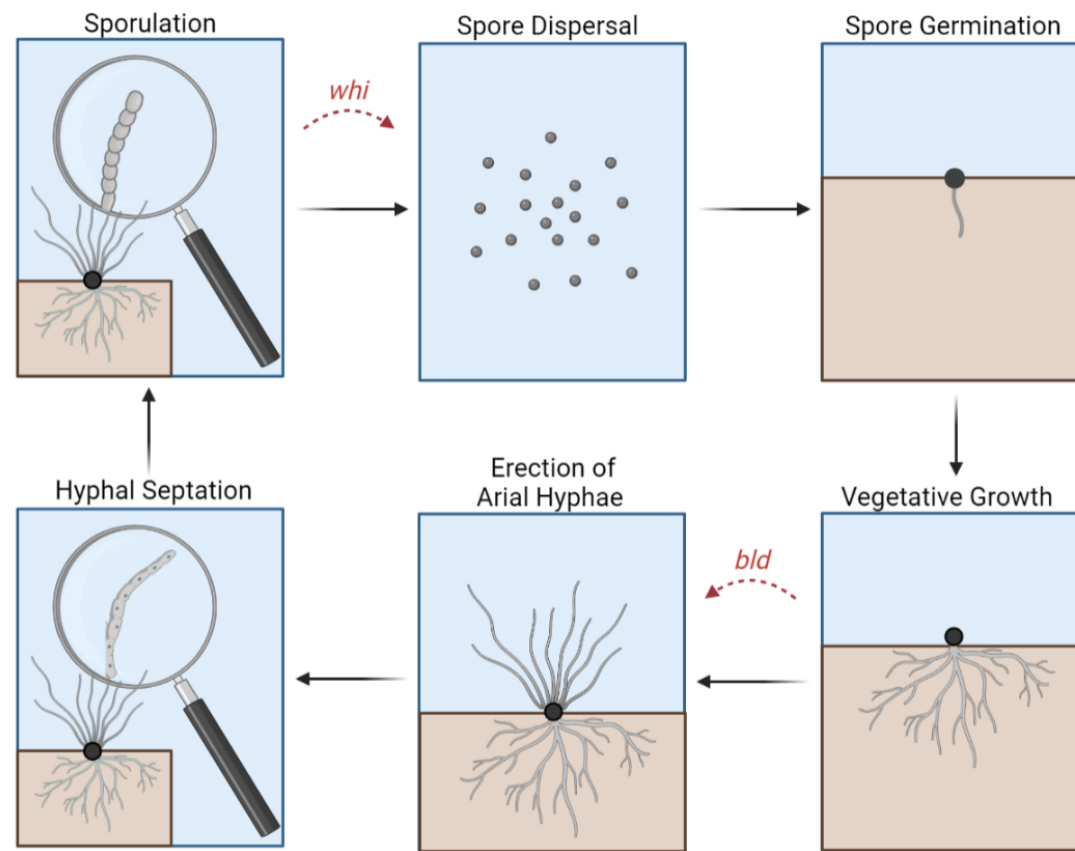


Figure 1.4: The *Streptomyces* life cycle is regulated by *bld* and *whi* genes. Regulatory stages mediated by *Bld* (erection of aerial hyphae) and *whi* genes (sporulation), shown in red.

1.4 Natural products and *Streptomyces* metabolism

1.4.1 Natural Products

Natural products are classified as chemical compounds which are produced by living organisms during their biochemical pathways of primary or secondary metabolism (Bérdy, 2005). The terms 'primary' and 'secondary' metabolism are often used to define both the catabolic and anabolic metabolic processes required for bacterial survival.

1.4.2 Primary Metabolism in *Streptomyces*

'Primary metabolism' is used to describe those cellular metabolic processes which are deemed essential to cellular survival. Primary metabolites are often involved in essential cellular processes such as normal growth, development, and reproduction. Production of the metabolites, therefore, is inherently linked with the exponential phase of growth allowing incorporation of essential chemical compounds required for cellular growth and reproduction (Chevrette et al., 2020b; Hodgson, 2000)

1.4.3 Secondary Metabolism in *Streptomyces* and a Change in Terminology

In contrast, 'secondary metabolites' have often been associated with the stationary phase of growth, with a previously well-regarded definition of being non-essential to cellular survival and reproduction (Van Wezel and McDowall, 2011). These compounds are historically diverse in their structure and were thought to provide help to the organism by aiding in protection from the environment, other organisms, competition with other organisms and assisting in species-species interactions (Katz and Baltz, 2016). Interestingly the production of secondary metabolites is unique to each organism, where each organism produces its own species-specific set of natural

products. This collection of unique small molecules is often termed the Parvome (Davies and Ryan, 2012) .

Work by (Schniete et al., 2018), shows that primary metabolism plays a role in in secondary metabolism in the Actinobacteria. The work demonstrates that the primary metabolic processes of expanding genetic repertoires, integrating functionality, and sensing and responding to metabolite concentrations affects and facilitates the production of secondary metabolites.

In *Streptomyces*, the simultaneous expression of genes essential for sporulation and those essential for the biosynthesis of secondary metabolites are inherently linked, where this process is called pleotropic switching. Genes which regulate sporulation are expressed during the stationary phase of growth alongside those which encode the production of secondary metabolites. The expression of these genes during the secondary growth phase are what helped to term the metabolites produced as secondary metabolites. However, as secondary metabolism was studied further, and the specific triggers to produce these secondary metabolites were analysed, it was found that the triggers of secondary metabolism showed great variability and could not be defined. As a result, the term 'secondary metabolism', with its association to non-essentiality to the organism cannot consistently be confirmed across bacterial species (Chevrette et al., 2020a). Following this observation, there has been much discussion within the natural product scientific community as to whether these 'secondary metabolites' should be re-termed to reflect their not-so-secondary nature. The switch to 'specialised metabolites' has been suggested (Davies, 2013), reflecting recent studies that suggest these compounds are essential for cellular survival in specific environmental conditions (Chevrette et al., 2020b). It has been postulated by Barona-Gómez and co-workers that the term specialised metabolism should be to describe a distinct area within secondary metabolism, where there is some knowledge of the role the natural product plays in the biology and ecology of the producer (Barona-Gómez

et al., 2023). Examples of specialised metabolism in secondary metabolites can be observed throughout the ecology of the producing organism. Siderophores are specialised metabolites used for iron uptake within bacteria, where iron acts as an enzyme co-factor to catalyse redox reactions involved in fundamental cellular processes (Kramer et al., 2020). Specialised metabolites produced by microorganisms such as gamma-Butyrolactones and the homoserine lactones are involved in quorum sensing to regulate group behaviours (Daer et al., 2018; Kudo et al., 2020). Germination inhibiting metabolites such as germicidin and those involved in spore coating have found to be produced from *Streptomyces* to aid in the developmental cycle (Aoki et al., 2011; Sigle et al., 2015). This observation of specialised metabolite having a role in essential cellular function can be observed, where the antibiotic-like peptide SapB, previously mentioned in the *Streptomyces* life cycle, encodes a polyketide spore pigment regulated by the white (*whi*) genes (Kodani et al., 2004). The same natural products with specialised function phenomenon can be observed for carotenoids (Li et al., 2020) and bioactive lipids (Murata et al., 2015), which are used as a source of antioxidants/UV protection and membrane structure respectively.

1.4.4 Clinical Importance of Natural Products.

Natural products produced by *Streptomyces* and other Actinomycetes are exploited for a wide range of therapeutic uses such as antibiotics, anti-fungals, antihelminthics, anti-cancer agents and immunosuppressives. In their natural environments, bacteria produce antibiotic compounds as a method of communication and defence. This activity has been exploited clinically for medicines to inhibit or kill pathogens without affecting the host, making them viable treatments for microbial infections in humans and animals. There are 15 main antimicrobial classes including the most used: β -lactams, tetracyclines, macrolides and glycopeptides (Aminov, 2017). Antibiotics have

been used clinically for over a century revolutionising the treatment of numerous infectious diseases. Prior to this 'Golden antibiotic' era, now easy to treat infections were the primary cause of human morbidity and mortality. In 1944, Schatz, Bugle, & Waksman discovered Streptomycin from *Streptomyces griseus*, an antibiotic capable of protein synthesis inhibition in both Gram-positive and Gram-negative bacteria (Schatz et al., 1944). Streptomycin was later used to effectively treat Tuberculosis; a lung infection caused by the bacteria *Mycobacterium tuberculosis*, and one of the most common causes of mortality prior to antibiotic use. The antibiotic Tetracycline was discovered in 1950 from *Streptomyces aureofaciens* and more recently, Platensimycin was discovered in 2006 from the bacterium *Streptomyces platensis* (de Lima Procópio et al., 2012). This relationship between *Streptomyces* species and antibiotic production from specialised metabolite can also be observed in *Streptomyces lucensis* which produces lucensomycin, a polyketide capable of inhibiting protein synthesis and is therefore classified as a macrolide antibiotic (Singh et al., 2009). With over 60% of clinically used antibiotics coming from *Streptomyces* species, the biosynthesis of these specialised metabolites by *Streptomyces* is of great importance (Bérdy, 2005; Genilloud, 2017).

1.5 Biosynthetic Gene Clusters

1.5.1 Biosynthetic Gene Clusters

The biosynthesis of these specialised metabolites is dependent on the expression of biosynthetic gene clusters (BGCs) present in the genome of microorganisms (Cimermancic et al., 2014; Slot, 2017). These BGCs are stretches of DNA containing the genes required for biosynthesis of these molecules. These gene clusters typically contain genes which encode core enzymes, used to convert substrates, and accessory enzymes, required for catalysis of the addition and conversion of accessory groups to the small molecules (Medema et al., 2014).

1.5.2 Expression Under Laboratory Conditions

Since the genomes of both *Streptomyces coelicolor* and *Streptomyces avermitilis* were sequenced and completed in 2002-2003, the 'genomics age' of antibiotic discovery began. Sequencing of the *Streptomyces coelicolor* genome revealed that the genome encoded a further 18 biosynthetic gene clusters than the 4 previously identified under laboratory conditions. This observation of *S. coelicolor* was also seen in other *Streptomyces* species such as *S. avermitilis* and *S. griseus* and was therefore regarded as a widespread phenomenon, rather than being unique to *S. coelicolor* (Ikeda et al., 2014; Ohnishi et al., 2002).

Since then, a rise in sequencing platform power and a lowering of genome sequencing cost has led to the mass sequencing of many bacterial species genomes. This newfound abundance of genomic data has driven the development of computational methods to mine bacterial genomes for BGCs such as AntiSMASH. AntiSMASH, was developed to aid in rapid identification, annotation, and analysis of specialised metabolite biosynthetic gene clusters (Medema et al., 2011). Since its implementation, its use around the world has allowed the identification of 52 different

types of BGC expanding on previous years with each update of the software (Blin et al., 2019). The data collected from AntiSMASH can be linked to natural product databases, such as MIBig, which is used to document the number of different gene clusters to date. By recording the minimum information about a biosynthetic gene cluster, and a comprehensive assessment of comparative analysis tools, the MIBig platform allows a unified place for analysis of bacterial, fungal and plant BGCs (Medema et al., 2015). To date, there are 2502 BGC entries into the database with just under half (1042) of these BGC's originating from the Actinobacteria. It is important to note, however, that these tools, and the databases they harness information from, are limited to discovery. Only the information known about BGC types and composition can be applied to the query and so there is a bias to identification and annotation. BGCs can also be analysed with networking-based tools such as BiG-SCAPE (Navarro-Muñoz et al., 2020) and BiG-SLiCE (Kautsar et al., 2021) which allow the visualisation of the relatedness of BGCs.

This new wave of natural product discovery has come with a wealth of literature showing that approximately 90% of the BGCs identified from genome sequencing are not expressed during standard lab conditions and do not result in the fabrication of specialised metabolites (Baltz, 2017; Ikeda et al., 2014). These unexpressed BGCs are often termed 'cryptic' or 'silent' where the two terms are used interchangeably throughout this wave of new literature. Recent work has seen a suggestion for uniformity of these terms where 'silent' and 'cryptic' are put into context for natural product discovery (Hokisson and Seipke, 2020; Fig. 1.5).

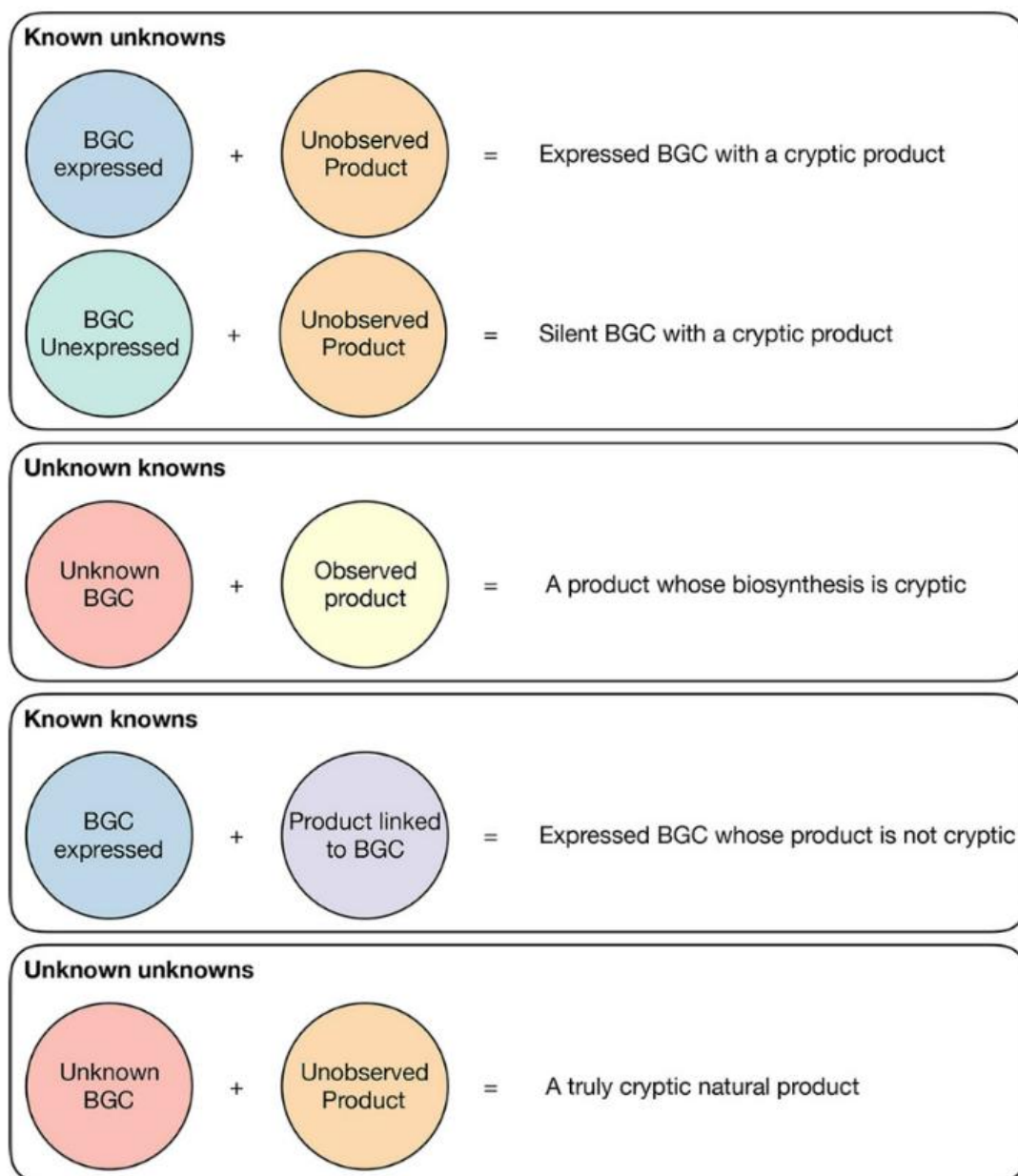


Figure 1.5: Description of various permutations of the cryptic or silent nature of secondary metabolism. Taken from Hoskisson & Seipke, 2020.

1.5.3 NRPS/PKS containing gene clusters

Since the emergence of tools like AntiSMASH for mining BGCs of Actinobacterial genomes, the wealth of information gathered about the architecture of biosynthetic gene clusters has vastly increased. Distribution of these BGCs across species has highlighted common trends among bacterial genus' providing essential information about the specialised metabolites commonly encoded for by each genus. This emergence of genome mining technology was used to analyse the distribution of biosynthetic and chemotherapeutic gene clusters across 1,107 *Streptomyces* genomes simultaneously using AntiSMASH (Belknap et al., 2020). Their work provides an in-depth analysis as to the general presentation of BGCs across *Streptomyces* genomes. It was shown that *Streptomyces* bacteria carry between 8–83 BGCs per genome where the number of these BGCs increases with genome size. Of their findings, the most common types of BGCs were non-ribosomal peptide synthetases (NRPSs) present in 1,062 genomes, and Type1 polyketide synthases (t1PKSs) present in 981 genomes, closely followed by terpenes, other ketide synthases and lantipeptides.

NRPSs are enzymes encoded for on BGCs, responsible for the production of non-ribosomal peptides (NRPs). NRPs are a family of specialised metabolite known for their clinical applications in human health and disease. Originally used by bacteria as bacteria-bacteria communication and signalling compounds, NRPs have been clinically exploited to produce a broad spectrum of treatments such as last resort antibiotics (daptomycin), antitumor drugs (bleomycin), antifungal drugs or as immunosuppressants (cyclosporin; Walsh, 2008). During NRP synthesis, catalytic domains of NRPSs select, activate or modify reaction components which have been covalently tethered together, in order to control the chain elongation of the peptide and eventual product release, independent of a ribosome (Strieker et al., 2010). The biosynthesis mechanism of these NRPs is now well understood due to extensive

biochemical and structural studies and shows an assembly line mechanism of mega-synthetases. They consist of a modular design and sequential biosynthesis mechanism; an adenylation (A) domain for amino acid selection and activation, thiolation (T) domain to carry the amino acid, condensation (C) domains for peptide bond formation and sometimes additional modifying domains such as an epimerisation domain (E) or methyltransferase (MT) are present. Unfortunately, the evolutionary diversity of these mega-synthetases which links the vast structural diversity of NRPs is poorly understood. Baunach et al., (2021) sought to elucidate this evolutionary diversity, regarding the vast structural diversity of the NRPs. Their work showed recombination that is the key driver in the evolution of NRPS across various phyla that gives NRPS the structural diversity. Their research also unveiled a network-like mosaic structure of NRPS genes that goes beyond the boundaries of the BGC and species giving crucial insight into bacterial ecology and evolution. From this, they generated a model of evolution in NRPS which strongly contradicts the common hypothesis that A and C domains co-evolve (Baltz, 2014). The multidomain structure of NRPS is outlined in Fig. 1.6, which has been adapted from (Guzmán-Chávez et al., 2018).

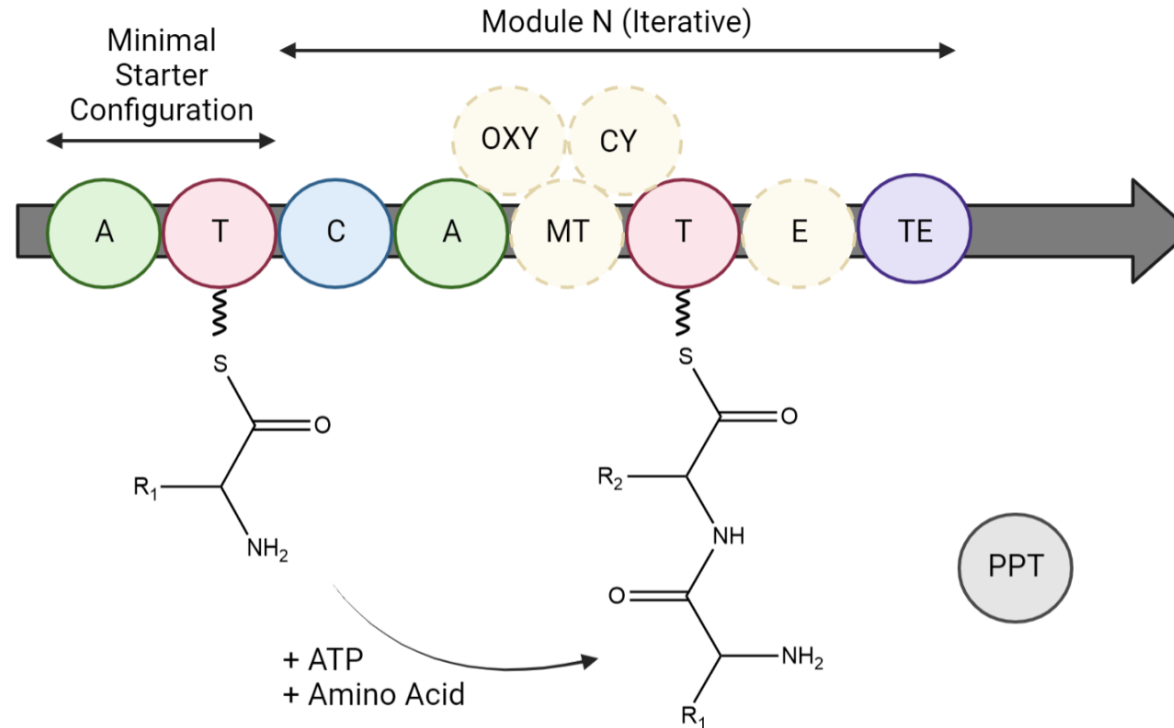


Figure 1.6: Non-ribosomal peptide synthetases (NRPSs) possess a multidomain structure. Where, adenylation (A) show in green, thiolation (T) shown in red, condensation (C) shown in blue, additional modifying domains such as an epimerisation domain (E), methyltransferase (MT) oxygenation (OXY), cyclisation (CY) are present and shown in yellow. Thioesterase (TE) shown in purple and 4'-phosphopantetheine transferase domain (PPT) shown in grey.

PKSs are enzymes encoded on BGCs which are responsible for the production of polyketides (PKs). Much like NRPs, PKs are a family of secondary metabolites which are of great clinical importance. PKS enzymes operate similarly to fatty acid synthases, where the range of PKs generated is extremely diverse. Here, the PKS enzymes begin the assembly of the PK by priming the starter molecule to the catalytic residue and then employs an extender unit for sequential chain elongation of the polyketide (Goukulan et al., 2014). Much like NRPS, PKS are often modular, where each module contains multiple domains that work sequentially to assemble polyketide chains through a series of condensation reactions. These domains include Acyl Transferase (AT) Domains, which select and transfer specific acyl groups from a CoA-thioester to the acyl carrier protein (ACP), a small, flexible protein domain that tethers the growing polyketide chain during biosynthesis. Other domains include Ketoreductase (KR) Domain, which catalyses the reduction of the β -keto group formed during the elongation process, converting it into a hydroxyl group, and Dehydratase (DH) Domains, which catalyse the dehydration of a β -hydroxy group from (KR) to form a double bond between two carbon atoms. Finally, thioesterase (TE) Domains are involved in chain termination. Other domains such as Methyltransferase (MT) Domains, Cyclase (CYC) Domains, and Epimerase (E) Domains can also be involved in the biosynthesis of these PKs. Based on structural architecture, PKSs have been classified into 3 types: type 1 PKS (t1PKSs), type 2 PKS (t2PKSs), and type 3 PKS (t3PKSs), where t1PKSs are the most abundant in *Streptomyces* bacteria (Belknap et al., 2020).

1.5.4 Evolution of Biosynthetic Gene clusters

The evolution of BGCs and, in turn, the development of interconnected metabolic networks signifies an important step forward in the diversification of not only natural product biosynthesis, but the diversification of life (Fondi et al., 2009). The knowledge

of the formation of these complex metabolic networks in genomes has expanded with the emergence of vast genomic data and has provided important insight into how metabolic and biosynthetic pathways have co-evolved via the convergence of different reactions and pathways. There are several mechanisms which have been proposed to facilitate genome evolution and the emergence of new metabolic pathways (Schmidt et al., 2003). These mechanisms are often considered in terms of adoption or recruitment, where genes are sourced and the genome expanded via; gene duplication, where genes are copied allowing the potential advantageous mutation of the non-coding gene (Näsvalld et al., 2012); expansion via HGT, where genes are acquired from another organism (Noda-García and Barona-Gómez, 2013); gene fusion, where genes that are used together repeatedly and persistently in a specific context are more likely to undergo fusion mutations in the course of evolution for mechanistic reasons (Bolotin et al., 2023; Fani et al., 2007); and finally, non-orthologous gene displacement, where original genes are replaced by a paralogue or non-homologue, of which comparative genomics has revealed many examples in which the same function is performed by unrelated or distantly related proteins from different cellular lineages (Forterre, 1999). The mechanisms of enzyme evolution are outlined (Fig. 1.7).

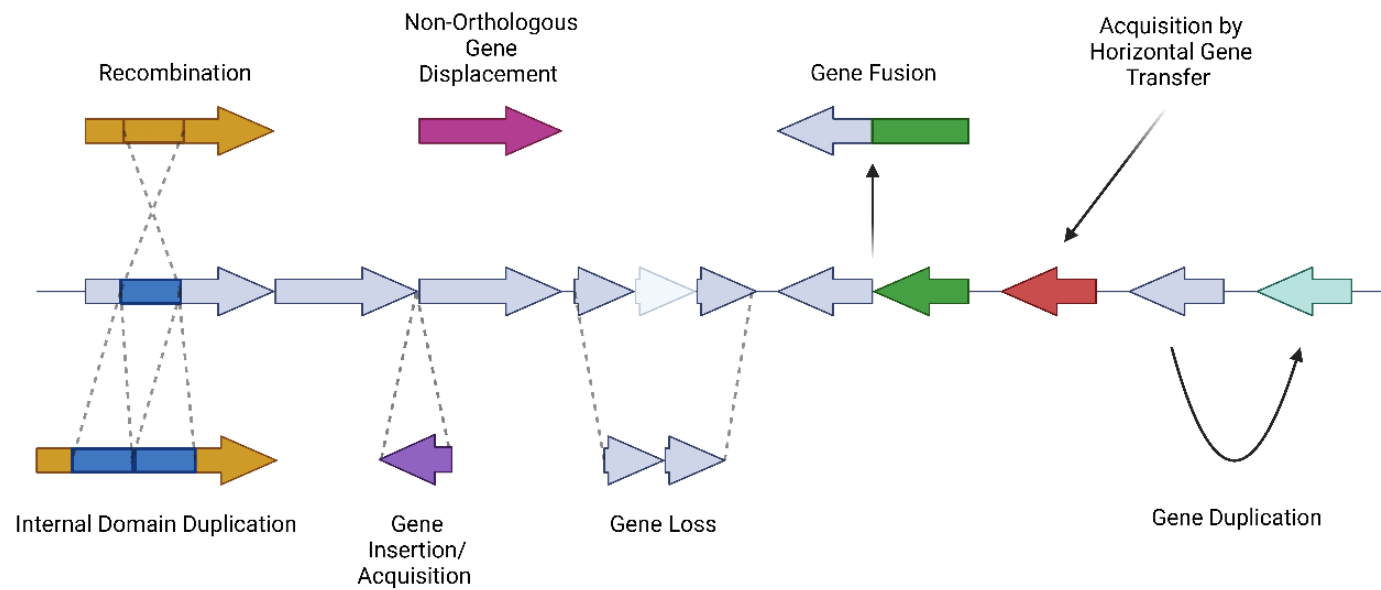


Figure 1.7: Many evolutionary mechanisms occur within biosynthetic gene clusters, driving BGC diversity and evolution. Adapted from Barona-Gómez et al., 2023.

1.5.5 Regulation of Biosynthetic Gene Clusters

Expression of biosynthetic gene clusters is dependent on complex regulatory mechanisms activated when the organism undergoes pleiotropic switching, the stage of life cycle where progression to the erection of aerial hyphae occurs (Van Wezel and McDowall, 2011). This regulation of gene clusters can be either specific to the cluster or global and be controlled by either one or two component systems.

The *Streptomyces* Antibiotic Regulatory Protein (SARP) is an example of a cluster situated regulator (CSR) which is controlled by a one component system. As the most common CSR in *Streptomyces*, the SARP can be found in various types of BGC encoding polyketide synthases (PKSs), ribosomal peptide synthetases (RPSs) and non-ribosomal peptide synthetases (NRPSs), and β -lactam antibiotics. The SARP activates biosynthetic gene cluster expression and, in turn, initiates production of these compounds by binding to repeat heptameric promoter sequences of the cluster they are tasked with regulating. Specifically, recent work suggests that overexpression of the SARP-type regulator gene *papR2* from *Streptomyces pristinaespiralis* could be used as an initiator of antibiotic biosynthesis in Actinomycetes due to its success in expression of the silent undecylprodigiosin gene cluster in *Streptomyces lividans* (Krause et al., 2020). There are also regulators which initiate biosynthesis in response to specific molecules. The Tet-R-type regulator of the kirromycin biosynthetic gene cluster is one example of this, where the regulators contain both a ligand-binding domain and a helix-turn-helix domain. Upon ligand binding of kirromycin, a conformational change is observed in the regulator causing a reduced affinity for DNA binding, enabling negative feedback expression (Robertsen et al., 2018). Expression of BGCs have also been seen to be globally regulated, where in *Streptomyces*, the life cycle associated regulator BldD activates gene cluster expression. This expression of BGC is initiated by BldD activating either a CSR, initiating expression or by directly targeting TTA codons (McLean et al., 2019a).

In addition to the previously mentioned one component systems, two component systems have also been found to regulate BGC expression. These systems respond to changes in their environment by utilisation of specialised sensor and DNA-binding proteins. These two component systems, much like one component systems can act on a specific BGC or at a global level (McLean et al., 2019b). This regulation by two component system is much less common than one-component regulation however should still be noted.

The γ -butyrolactones are small signalling molecules mainly produced by *Streptomyces* species in which they regulate antibiotic production and morphological differentiation (Sidda and Corre, 2012; Takano, 2006). The molecular mechanisms by which they elicit functions within *Streptomyces* has been investigated unveiling a complex system allowing the activation of morphological development and secondary metabolism (Kato et al., 2007; Zhou et al., 2021), of which we know is linked (Schniete et al., 2018). Though not specific to the *Streptomyces* species, γ -Butyrolactones and the receptors they act upon can also be found in other Actinobacterial species, suggesting that the γ -butyrolactones and their regulatory system for antibiotic production is well conserved (Xu and Yang, 2019). These regulatory systems have been elucidated in specific species such as *S. filipinensis* and *S. chattanoogensis* (Barreales et al., 2020; Du et al., 2011) and have gone on to be exploited for genetic manipulation due to their tight regulation and to control the regulation of previously silent secondary metabolite gene clusters (Waschulin et al., 2023).

In *Streptomyces*, the expression of specialised metabolites by BGC regulation is incredibly complex and often involves a network of integrated processes all working to streamline expression of the BGC. Understanding the regulation of these gene clusters and the environmental conditions which triggers their activation, allows us to understand the role of the secondary metabolites produced in their natural habitat, alongside supplying the information required for exploitation of these organisms as

sources of natural products for novel antibiotic sources (Hoskisson and Fernández-Martínez, 2018). The processes involved in regulation of the *Streptomyces* biosynthetic gene cluster are summarised (Fig. 1.8).

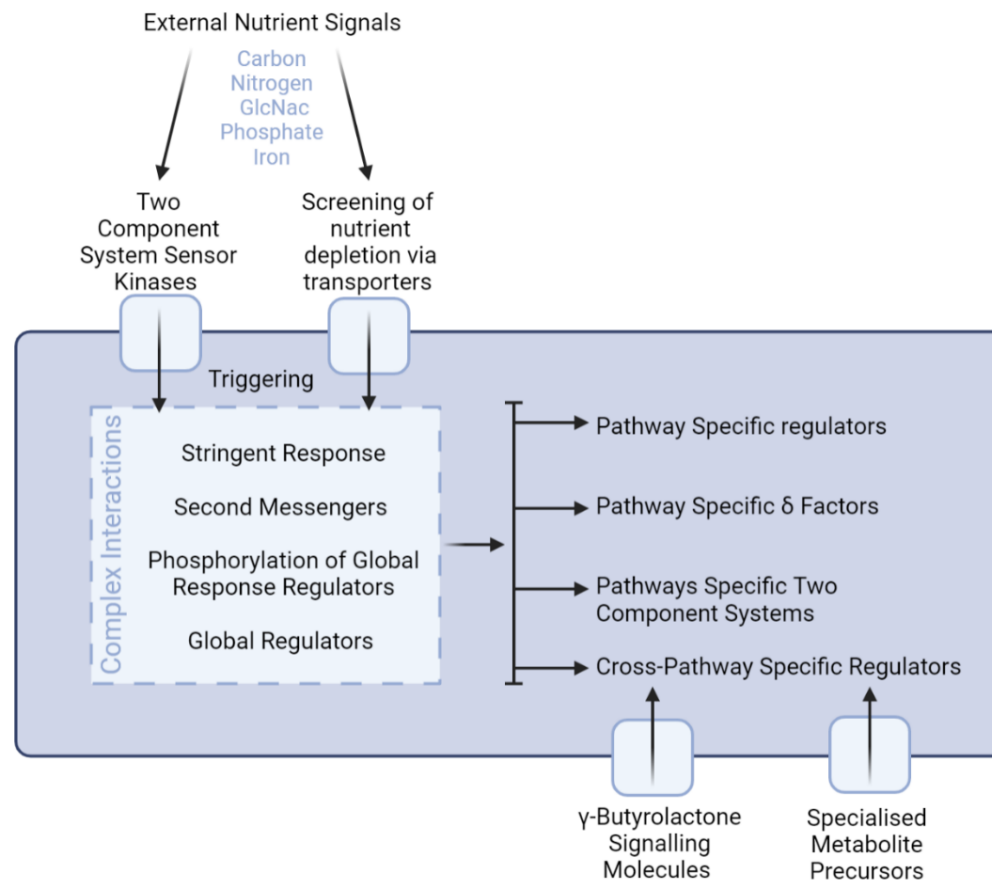


Figure 1.8: Actinobacterial specialised metabolite production is highly regulated. Adapted from Hoskisson & Fernández-Martínez, 2018.

1.5.6 BGC Associated Immunity Genes

Having the ability to produce specialised metabolites with antibiotic potential infers that the producing strain must have a degree of immunity or resistance to the natural products. Often this appears as a specialised export mechanism to rid the cell of specialised metabolite, especially if the producing organism also carries the conserved target present in the competitor. These resistance mechanisms are a feature of most specialised metabolite producing strains, which were originally thought to exist separate to the biosynthesis of the natural product. However, as further work has been taken on natural product biosynthesis and the associated resistance mechanisms, it has become clear that often, self-resistance is associated with the assembly machinery to aid in biosynthesis (Wu et al., 2022). An example of this is the β -Lactam Antibiotics of *Streptomyces*, where the resistance mechanism is encoded within the BGCs and have seen to co-evolve with the BGCs responsible for the metabolite production (Ogawara, 2016). Efflux pumps are the most common method of self-resistance for specialised metabolite producing strains (Blanco et al., 2016; Thaker et al., 2010). In *Streptomyces*, the Major-Facilitator-Superfamily-type (MFS) gene is the most common resistance gene, encoding a multi-drug efflux pump, which represents 40% of transport proteins within the genus (Zhou et al., 2016).

For most antibiotic specialised metabolites, it is the case that resistance mechanisms are located within the associated BGC (Alanjary et al., 2017). However, as an example, elfamycin compounds possess multiple genes conferring immunity which are encoded at distinct loci. This example of an alternative resistance mechanism will be illustrated later in this study.

1.6 The Efamycins

1.6.1 Introduction to the Efamycins

The Efamycins are a group of structurally diverse antibiotic compounds which target Elongation Factor Thermo unstable (EF-Tu), disrupting EF-Tu's role in translation during prokaryotic protein synthesis (Samantha M. Prezioso et al., 2017). The translation of messenger RNA (mRNA) transcripts into proteins within the cell is facilitated by the ribosome and is vital to cellular function. The ribosome is dependent on EF-Tu to deliver amino acyl-tRNAs (aa-tRNA) to the ribosome for protein elongation (Morse et al., 2020; Sprinzl, 1994), making EF-Tu essential in protein synthesis and an ideal target for Efamycins to disrupt cellular function as antibiotics (Hall et al., 1989).

1.6.2 Mechanism of Action

The crystal structure of EF-Tu was determined by Berchtold et al., in 1993, revealing binding domains corresponding to both tRNA and the ribosome. This discovery secured the role of EF-Tu in protein synthesis where its role is a catalyst for the synthesis of protein via tRNA and the ribosome (Berchtold et al., 1993). In this mechanism, EF-Tu forms a complex with GTP and delivers charged tRNA (aa-tRNA) to the A site of the ribosome for protein chain elongation. Upon binding to the A site of the ribosome, GTP is hydrolysed to GDP by EF-Tu causing EF-Tu to disassociate from the ribosome allowing continuation of the cycle (Fig. 1.9). This is possible as EF-Tu is a G protein, meaning that it possesses the intrinsic ability of hydrolysing GTP to GDP (Samantha M. Prezioso et al., 2017).

1.6.3 Efamycin Classification

Efamycins can be classified into four families of EF-Tu inhibitors, these are; pulvomycin, GE2270 A, enacylocin II, and kirromycin (Samantha M. Prezioso et al., 2017). The four families are not similar in structure, but their mechanism of action can be clearly grouped into two based on the stage at which the effect protein synthesis via EF-Tu. Pulvomycin and GE2270 A act on EF-Tu early in the protein synthesis cycle, where they are seen to inhibit EF-TU:GTP forming the ternary complex with aa-tRNA_b (Assmann and Wolf, 1979; Selva et al., 1991a). This prevents EF-Tu from associating with the ribosome and eliciting its enzymatic potential (Morse et al., 2020). In contrast, enacyloxin II and kirromycins prevent EF-Tu:GDP from disassociating with the ribosome by trapping EF-Tu on the ribosome and preventing the next round of chain elongation (Mahenthiralingam et al., 2011; Wolf et al., 1972). These four families of compounds are therefore determined by their target, rather than a conserved structure (Fig. 1.10).

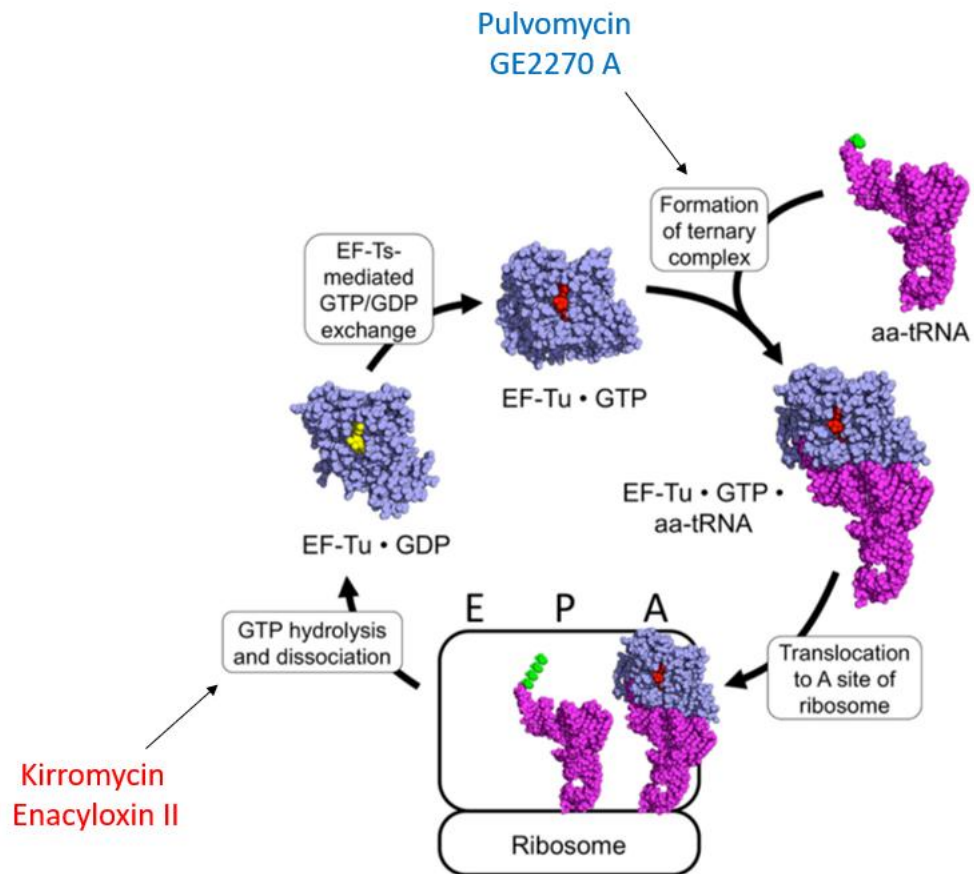


Figure 1.9: Elongation Factor Thermo-unstable is essential to prokaryotic protein synthesis and can therefore be targeted by elfamycin inhibitors such as the kirromycins. Taken from McHugh, 2020. Red molecules prevent GTP hydrolysis and dissociation from the ribosome and those in blue prevent the formation of ternary complex with aa-tRNA.

Pulvomycin was characterised in 1957 by Zief and co-workers and was found to be produced by *Streptoverticillium netropsis* (Zief et al., 1957). Multiple studies suggesting the discovery of similar antibiotics termed Antibiotic 1063-Z and labilomycin were later discovered to be identical to pulvomycin even though they were produced by *Streptoverticillium mobaraense*, *Streptomyces albosporeus* var. *labilomyceticus*, respectively. This indicates that multiple *Streptomyces* species are capable of the same elfamycin production (Assmann and Wolf, 1979; Schwartz et al., 1976). Pulvomycin was found to be active against select Gram-positive and Gram-negative bacteria, including the clinically relevant species such as *Bacillus brevis* and *E. coli* (Assmann and Wolf, 1979). Modern tools for harnessing antibiotic potential have also been used to develop pulvomycin as an antibiotic. Here, pulvomycin was expressed heterologously in the non-native producing strain, *Streptomyces flavopersicus*. Using alleles of a pleiotropic regulator of secondary metabolism from *S. coelicolor* to activate secondary BGCs. Heterologous expression of pulvomycin was achieved in *S. flavopersicus* and the pulvomycin produced was found to be active against *Burkholderia cepacia*, the opportunistic pathogen which display high levels of antibiotic resistance (McKenzie et al., 2010).

GE2270 A was found to be produced by the rare Actinomycete, *Planobispora rosea* in 1991. GE2270 is produced by *P. rosea* in 10 different forms which vary by their methylation state and their activity, both of which are inherently linked (Selva et al., 1991a, 1995). GE2270 A was found to be the most bioactive isoform of GE2270 with the highest antibacterial activity against a broad range of Gram-positive bacteria (Kettenring et al., 1991). Its mechanism of action on EF-Tu is similar to that of pulvomycin though the two vary on their binding sites and chemical structures (Parmeggiani et al., 2006).

Enacyloxin II is the only Elfamycin to be discovered in non-Actinomycetes. Produced by *Frateruria* sp. W-315, the linear polyenic antibiotic and its producer were identified

during an antifungal screen by Watanabe and co-workers in 1982 (Watanabe et al., 1982). During the screen the compound was found to be slightly active against fungi, the screen was extended to a range of Gram-positive and negative bacteria where enacyloxin IIa was found to be active against a range of both Gram serotypes (Watanabe et al., 1992). Enacyloxin IIa inhibits the function of EF-Tu by preventing its disassociation from the ribosome, where kirromycin acts with a similar function.

1.6.4 The Kirromycins

Kirromycin is a linear polyketide which is produced by *Streptomyces*. The first kirromycin producer was found in 1972 to be *Streptomyces collinus* Tü 365 (Wolf and Zähler, 1972) and later found to be produced by *Streptomyces ramocissimus* (Tieleman et al., 1997), though it was originally described as mocimycin and later found to be identical to kirromycin (Maehr et al., 1973). Kirromycin is the base molecule of a group of more than 20 compounds which are capable of inhibiting EF-Tu and are linear polyenes. The kirromycins can be further allocated into three subgroups based on their chemical structures, being kirromycin-like, L-681,217-like, and factumycin-like. It can be seen that the kirromycin-like subgroup is determined by the presence of an intramolecular ketal group called goldinonic acid, the L-681,217-like subgroup is characterised by the lack of the terminal pyridone ring and the factumycin-like subgroup contains a terminal pyridone ring but lacks the central furan ring (Fig. 1.10)

The first L-681,217-like antibiotic was found to be produced by *Streptomyces cattleya*, by Kempf and co-workers in 1986. Their work utilised the *S. cattleya* strain in industrial fermentation to produce analytical levels of the compound allowing them to characterise the structural and biological properties of L-681,217. The compound was found to be structurally similar to the kirromycin-like antibiotic aurodox, which has more recently been shown to be a methylated version of kirromycin, though it lacks

the pyridone ring associated with these compounds (Kempf et al., 1986). In recent years, *S. cattleya* has been shown to produce a methylated version of L-681,217, known as dimethyl- L-681,217, though the methylation of the compound has shown to have no effect on antibiotic activity (Sugai et al., 2016). In recent years, other L-681,217-like antibiotics have been identified through resistance-guided discovery, such as the phenelfamycins A and B, from *Streptomyces sulphureus*. During this study, Yarlagadda and co-workers identified Elfamycin-resistant copies of EF-Tu (EF-Tu^{KirR}) in the genomes of *Streptomyces Spp.* biosynthetic characterisation of gene clusters capable of Elfamycin biosynthesis were identified due to Elfamycin resistant copies of EF-Tu being encoded on the same BGC responsible for Elfamycin production. Genome mining identified *Streptomyces sulphureus* as a carrier of EF-Tu^{KirR} which was present on an Elfamycin BGC. Further elucidation of the structure of phenelfamycins A and B identified that the molecules lacked the terminal pyridone ring and therefore are classified as L-681,217-like Elfamycins (Yarlagadda et al., 2020).

Factumycin-like antibiotics were also found to be produced by *Streptomyces Spp.* First isolated from the culture broth of *Streptomyces lavendulae*, factumycin was identified to be a member of the kirromycin family, though lacking the central furan ring (Gullo et al., 1982). Thaker et al (2012) isolated the *Streptomyces Spp.* WAC5292, which produced a compound that had selective antibiotic activity against Gram-negative bacteria. Activity-guided purification of the compound against the ESKAPE pathogen, *Acinetobacter baumannii*, identified it as the well-known antibiotic factumycin, which the genome of the producer was later sequenced and the putative factumycin BGC identified. Interestingly, factumycin from *Spp.* WAC5292 was shown to be synergistic with tetracyclines, offering a new role for factumycin in Gram-negative targeted antibiotic combination therapy (Thaker et al., 2012).

The first kirromycin-like antibiotic was identified by Wolf and co-workers from *Streptomyces collinus* in 1972 as an inhibitor of the 30S rRNA subunit (Wolf et al., 1972). As one of the best characterised Elfamycins belonging to the kirromycin subclass, the molecule is the base for which the sub-classes are divided. The compound was later identified as an inhibitor of the biosynthesis of proteins acting on EF-Tu in by the same group in 1974 (Wolf et al., 1974). As research into kirromycin-like, kirromycin Elfamycins continued, it was found that more than one strain of *Streptomyces* was capable of the production of kirromycin-like compounds. The discovery of mocimycin, from *Streptomyces ramocissimus* was also in 1972 (Vijgenboom et al., 1994), alongside the discovery of Antibiotic X-5108, which would later be called aurodox (Maehr et al., 1973). Mocimycin was found to be identical to kirromycin and so the term mocimycin was rendered redundant. However, Antibiotic X-5108 was found to be the *N*-methylated form of kirromycin. To date, there are only three known producers of these kirromycin-like molecules, with *S. collinus* and *S. ramocissimus* producing kirromycin, and *S. goldiniensis* producing *N*-methyl kirromycin now known as aurodox (Berger et al., 1973).

Classification of Efamycin Antibiotics

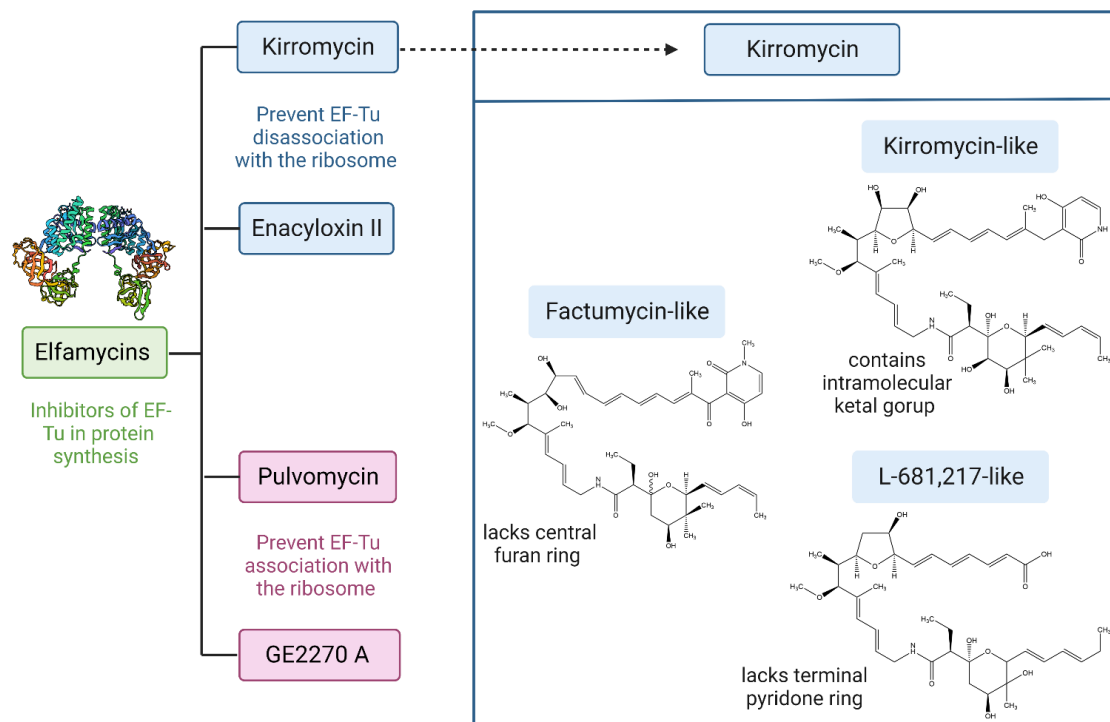


Figure 1.10: Efamycin antibiotics can be classified based on their target. Classification and sub-classification based on function and structure respectively. EF-Tu protein structure from *E. coli* (Abel et al., 1996). Kirromycin structure from *S. collinus*, factumycin from *Streptomyces* spp. WAC 5424, L-681,217 from *S. cattleya*. Chemical structures generated on ChemDraw (version 20.1). Figure generated on BioRender.

1.7 Aurodox

1.7.1 Introduction to Aurodox

One such kirromycin-like antibiotic is aurodox, often termed *N*-methyl kirromycin, produced by *Streptomyces goldiniensis*. In 1973, Berger and co-workers isolated the bacterium *S. goldiniensis* from soil from the Caribbean island of Bermuda (Berger et al., 1973). Using culture-dependant methods of assessing bioactive properties, it was found that *S. goldiniensis* could produce a compound which was active against a number of Gram-positive bacteria *in vitro*. This work also found the compound to be especially active *in vivo* against *Streptococcus pyogenes* infections in mice (Berger et al., 1973). They termed this molecule as a new antibiotic X-5108, most known in present day as aurodox. Subsequent work by Berger et al., characterised the antibiotic activity of aurodox where they found the compound to have strong activity against Gram-positive bacteria such as the aforementioned *Streptococcus pyogenes*, *Micrococcus luteus* and other species of *Streptomyces*. There was also weak activity against Gram-negative bacteria observed. Importantly, their work tested the resistance profile of aurodox showing that significant resistance to aurodox did not arise until after 64 generations of growth allowing this to be a potential antibiotic for use (Berger et al., 1973). These studies confirmed the bioactivity of aurodox and its potential as an antibiotic compound but in parallel they also designed and patented a fermentation method for production of aurodox, where the fermentation can be done in unrefined production media and the compound extracted from culture supernatant after approximately six days (Maehr et al., 1979).

1.7.2 Chemical Structure and Properties

Berger et al., (1973), elucidated the chemical formula of aurodox ($C_{44}H_{62}N_2O_{12}$.) and subsequent work by Maehr et al., (1979) elucidated the structure of the molecule using ¹³-Carbon Nuclear Magnetic Resonance. This study found the aurodox molecule is highly methylated and contains two unsaturated carbon chains connecting leucine and glycine derived groups. Interestingly, the structure of aurodox is highly similar to kirromycin, with the only variation of the structure being that aurodox has a methylation of the pyridone ring. The chemical structures of aurodox and kirromycin are shown (Fig. 1.11). In the same study, they found transmethylation to be responsible for the addition of these prolific methyl groups, while synthesis of synthetic analogues suggested that the pyridone moiety was responsible for the antibiotic activity of aurodox due to the decrease in bioactivity when this was altered.

Building on this, the work of Vogeley et al., (2001) established that aurodox was an Efmamycin antibiotic from the class of kirromycins meaning it can block translation by forming a complex with EF-Tu and GDP, blocking GTP Hydrolysis. This binding facilitates an irreversible conformational change in EF-Tu resulting in it become stuck in complex with the ribosome, unable to detach, preventing subsequent protein synthesis (Vogeley et al., 2001; Fig. 1.12). This blocking is seen both *in vitro* and *in vivo* where aurodox acts as a bactericidal causing cell death. The compound was commonly used for a growth promotor in animal livestock, however, even with its strong abilities to inhibit the growth of Gram-positive bacteria, aurodox was never licenced for use on humans due to its narrow spectrum of bactericidal activity.

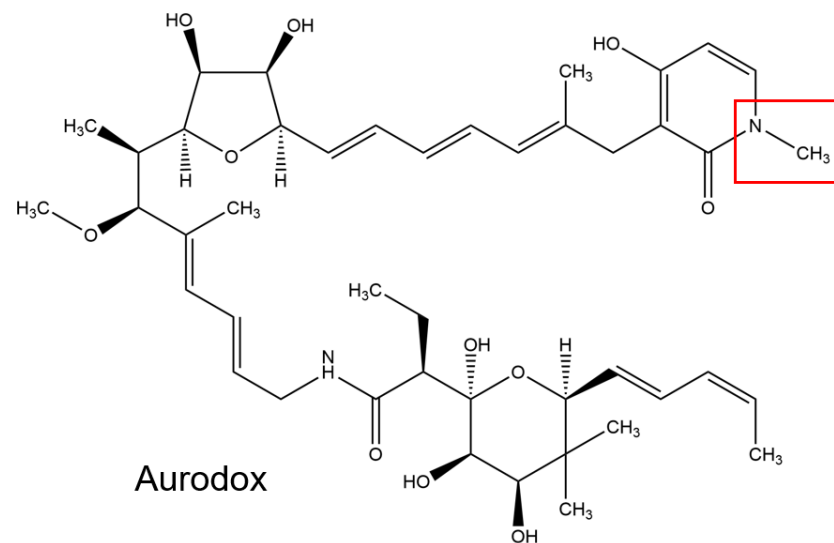
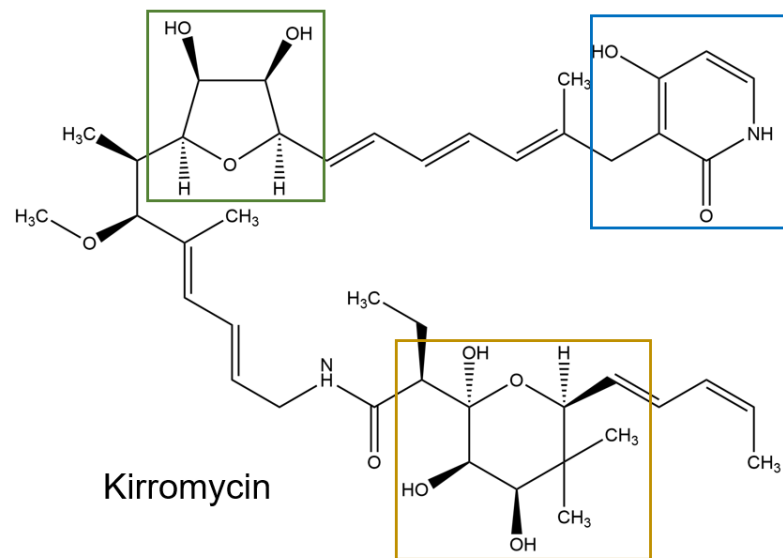


Figure 1.11: The chemical structures of kirromycin and aurodox are highly similar, with the exception of one methyl group. The blue box indicates the terminal pyridone ring, shown on kirromycin and the green and gold boxes indicate the central tetrahydrofuran ring and goldinonic acid, respectively. The red box indicates the methylated pyridone ring of aurodox.

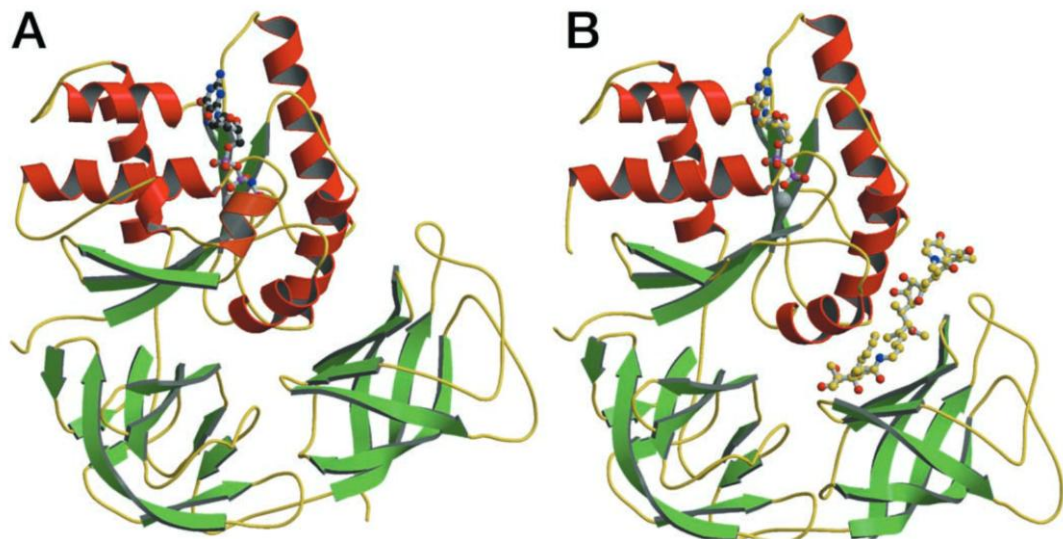


Figure 1.12: The crystal structure of aurodox binding to EF-Tu has been elucidated in *T. thermophilus* with GDP bound. Alpha helices are shown in red and beta helices in green, showing the tertiary structure of EF-Tu interacting with the ball and stick model depiction of aurodox and GDP/GTP. (A) showing the native conformation of EF-Tu with GTP bound and (B) showing the conformation of EF-Tu when aurodox is bound, blocking GTP Hydrolysis. Adapted from Vogeley et al., 2001.

1.7.3 Inhibition of the *E. coli* T3SS by aurodox

EPEC and EHEC infections are reliant on their T3SS to cause the initiation and persistence of infection in host cells, therefore, this has been identified as a potential target for novel therapies to combat these infections (Zambelloni et al., 2015). The need for AV compounds as a treatment for EPEC and EHEC infections is needed due to the problem treatment with traditional antibiotics causing the induction of the bacterial SOS response and the increased likelihood of antimicrobial resistance arising in the human gut (Imamovic and Muniesa, 2012). Recently it was demonstrated that aurodox from *Streptomyces goldiniensis* could inhibit the translocation of T3SS encoded effector proteins in EPEC infections. To complement these *in vitro* findings, the activity of the compound was tested *in vitro* using a *Citrobacter rodentium* murine infection model where mice treated with aurodox survived lethal infections with *C. rodentium* with limited negative effects on the intestinal tract (Kimura et al., 2011). This shows promise for aurodox as a potential AV drug and T3SS inhibitor due to the sufficient treatment of the EPEC infection and the lack of disruption to the intestinal tract as commonly observed when treating EPEC and EHEC with antibiotics.

Recently, work by (McHugh et al., 2019) sought to gain a better understanding of the mechanism of action of aurodox and inhibition of the T3SS's of EHEC and EPEC. They showed that aurodox down regulates the expression of the T3SS's of both EPEC and EHEC infections. They also demonstrated that this inhibition is modulated at the transcript level by the repression of the master regulator *ler*, where aurodox acts upstream of *ler* and not directly on the secretion system itself. Importantly, their work also revealed that treatment with aurodox does not induce the expression of RecA, which is essential for the production of Shiga toxin, confirming Aurodox's potential as an AV therapy for EPEC and EHEC infections (Fig. 1.13).

Until recently, the molecular target of aurodox has remained unclear. In 2024, chemistry and genetic biology-based approaches were used to show that aurodox binds to adenylosuccinate synthase (PurA), which suppresses the production of the secreted proteins from T3SS, resulting in the expression of bacterial virulence both in vitro and in vivo experiments (Watanabe et al., 2024.). As this data was not available until after the work was complete, we were unable to validate these findings.

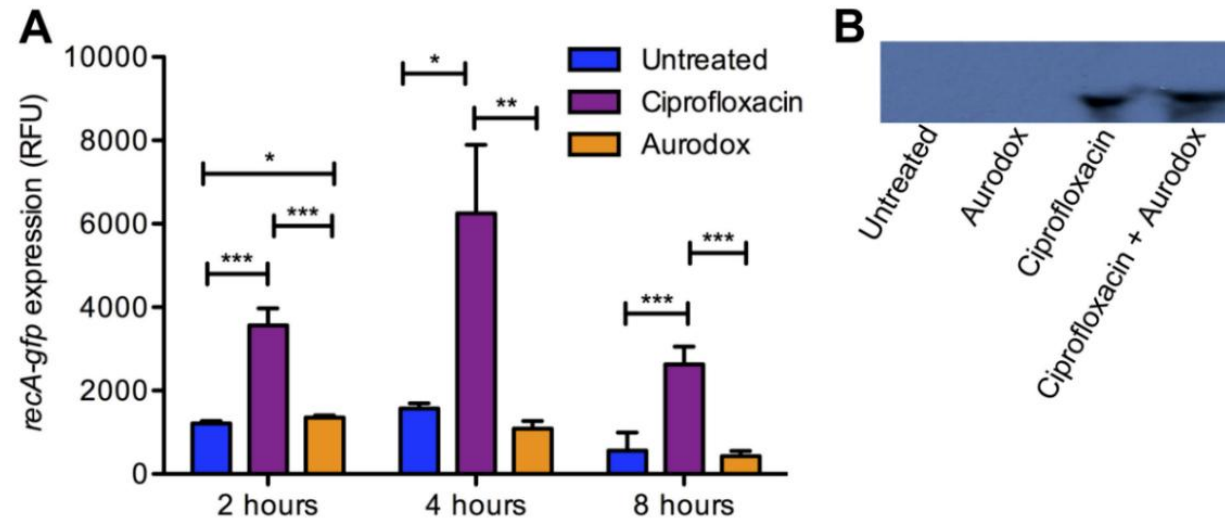


Figure 1.13: Aurodox treatment does not induce RecA-mediated Stx expression. Taken from McHugh et al., 2019. (A) Analysis of *in vitro* recA-gfp expression in Aurodox-treated EHEC. Aurodox and ciprofloxacin were added at 6 μ M. Error bars correspond to SDs (n = 4). P-values for Aurodox-treated versus ciprofloxacin-treated bacteria were 0.01. *, P 0.05; **, P 0.005; ***, P 0.001. (B) Immunoblot analysis of Stx expression in untreated, Aurodox-treated, ciprofloxacin-treated, and Aurodox- and ciprofloxacin-treated *C. rodentium* DBS100. Primary antibodies for Shiga toxin B subunit (6 kDa) were used.

1.7.4 Whole genome sequencing and mining of *S. goldiniensis*

McHugh *et al.*, (2022) sequenced the Aurodox producer, *S. goldiniensis*' genome using a combination of Illumina NovaSeq short reads, and both Oxford Nanopore MinION and PacBio long read sequencing. The genome was assembled using Spades and the draft genome scaffolded against the closest related strain using MeDuSa to provide a genome of nine contigs (McHugh *et al.*, 2022).

In order to comprehend the biosynthetic capabilities of *S. goldiniensis* and identify a putative aurodox gene cluster, AntiSMASH software was used. This analysis revealed 36 putative biosynthetic gene clusters in the *S. goldiniensis* genome which theoretically encode for both conserved and novel metabolites. Heterologous expression of the putative BGC responsible for the production of aurodox, from a clone in a genomic library (pAurl) in the *Streptomyces coelicolor* super-host, strain M1152 confirmed the biosynthetic origin of aurodox (Gomez-Escribano and Bibb, 2011; McHugh *et al.*, 2022). This work now enables the detailed characterisation of the biosynthesis of aurodox to be elucidated.

1.7.5 Deciphering the aurodox biosynthetic gene cluster

Analysis of the BGC responsible for aurodox production revealed a multi-modular polyketide synthase pathway similar to the closely related kirromycin BGC, with over 60% similarity of genes encoding aurodox biosynthesis to those encoding kirromycin biosynthesis. 23/25 genes on the aurodox BGC had functional homologs in kirromycin biosynthesis from *Streptomyces collinus*, and so functions for genes of the aurodox BGC were depicted from those of the kirromycin biosynthetic gene cluster (Weber *et al.*, 2008). McHugh *et al.* also characterised the biosynthesis of aurodox and the resistance profile of *tuf2* in *S. goldiniensis* facilitating aurodox production alongside the Major-Facilitator Superfamily protein (AurT), an efflux pump.

As both aurodox and kirromycin are Elfamycin antibiotics, looking to the BGCs responsible for the production of similar compounds can help to shed light on gene function and compound biosynthesis. This approach will be used during this study with the aim to further decipher the aurodox BGC through genetic manipulation of the cluster. One such Elfamycin producer is *Streptomyces ramocissimus* which has been shown to produce kirromycin and also possesses similar *tuf* genes used for Elfamycin resistance as *S. goldiniensis* (Vijgenboom et al., 1994) . The whole genome of *S. ramocissimus* has not yet been sequenced and so little is known about its kirromycin biosynthetic gene cluster or the resistance mechanisms (*tuf* genes) in which *S. ramocissimus* possesses to facilitate kirromycin production.

1.8 Rationale and specific aims

1.8.1 Rationale

The emergence of resistance to frontline antibiotics has resulted in an urgent need to develop new antimicrobials and new approaches to combat resistance. Interest has increased in AV compounds and molecules such as aurodox from *S. goldiniensis* represent a good starting point to approach this as it has proven safety in animal use and a novel mode of action, recently determined (McHugh et al. 2019, 2022).

It is hypothesised that deciphering the genomes of other Elfamycin producers and their BGCs, alongside genetic manipulation of the aurodox BGC may shed more light on the biosynthesis and resistance mechanisms required for elfamycin production and provide insight into our wider understanding of enzymatic evolution of antibiotic biosynthetic clusters.

1.8.2 Specific Aims

The thesis has the following specific aims:

- Determine the sequence of *S. ramocissimus* Kirromycin BGC, with a view to expand the knowledge of kirromycin-like Elfamycin biosynthesis and evolution of related BGCs.
- Dissect the biosynthesis of aurodox by finding roles for undefined key genes within the BGC through gene deletion and enzymatic characterisation.
- Determine the immunity mechanisms used by kirromycin-like Elfamycin producing strains and their effect on the antibiotic and anti-virulent activity.

Chapter 2: Materials and Methods

2.1 Chemicals and Reagents

Throughout this project, all chemicals used were of analytical grade and were purchased from Fischer Scientific, Invitrogen, Qiagen or Sigma-Aldrich, unless stated otherwise.

2.2 Growth, Maintenance of Bacteria and Media

2.2.1 Bacterial growth and Maintenance

Unless otherwise stated, *Streptomyces* species were grown at 30 °C, 200 rpm. Liquid cultures of bacteria were prepared in 50 mL of media in 250 mL Erlenmeyer flasks, When culturing *Streptomyces*, coiled springs were added to prevent pelleting. To prepare *Streptomyces* spore stocks, a single colony from a *Streptomyces* culture was used to inoculate a confluent lawn of growth on agar. After 7-10 days of growth and after the formation of spores, 2 mL of sterile 50% glycerol solution was applied to the plate and the spores were disturbed. The resulting spore solutions were passed through sterile 5 mL syringes containing cotton wool to remove cell debris. An equal volume of sterile dH₂O was added to the suspensions, resulting in a final glycerol concentration of 25%. Glycerol stocks were preserved at both – 20 °C and – 80 °C for long term storage.

Unless otherwise stated, all liquid media was prepared in 250 mL batches in 500 mL Duran bottles and sterilised by autoclaving at 121 °C at 100 kPa. Bacterial culture media is shown in Table 2C, which provides instructions for the creation of 1 L of liquid media. For solid media, 20 g/L of agar was added to prior to autoclaving. To prepare soft agar, agar component was reduced to 10 g/L. For EPEC and EHEC, MEM-HEPES was purchased from Sigma-Aldrich and L-glutamine levels were adjusted to 0.568 g L⁻¹ before use.

2.2.2 Strains and Plasmids

Table 2A: Strains used in this study with detailed description, genotype and source.

Strain	Description	Genotype	Reference
<i>Streptomyces goldiniensis</i> WT (ATCC 21386)	WT, aurodox producing strain	Wild-type	ATCC
<i>Streptomyces ramocissimus</i> WT (ATCC 27529)	WT, Kirromycin producing strain	Wild-type	Gift from Gilles van Weizel
<i>Streptomyces collinus</i> Tü 365	WT, Kirromycin producing strain	Wild-type	Gift from Wolfgang Wolheben
<i>S. coelicolor</i> M1152	<i>Streptomyces coelicolor</i> 'superhost'	$\Delta act \Delta red \Delta cpk \Delta cda \Delta rpoB$	(Gomez-Escribano and Bibb, 2012)
<i>S. coelicolor</i> M1152 + pESAC13-A	Superhost and Empty vector	<i>AprR</i>	(McHugh et al., 2022)
<i>S. coelicolor</i> M1152 + pESAC13-A- <i>AurI</i>	Superhost and aurodox cluster	<i>AprR</i>	(McHugh et al., 2022)
<i>S. coelicolor</i> M1152 + pESAC13-A +PMS82	Superhost, aurodox cluster and empty vector	<i>AprR HygR</i>	(McHugh, 2020)
<i>S. coelicolor</i> M1152 + pESAC13-A- <i>AurI</i> + PMS82- <i>tuf2</i>	Superhost, aurodox cluster and <i>tuf2</i> from <i>S. goldiniensis</i>	<i>AprR HygR</i>	(McHugh, 2020)
<i>S. coelicolor</i> M1152 + PMS82	Superhost, empty vector	<i>HygR</i>	(McHugh, 2020)
<i>S. coelicolor</i> M1152 + PMS82- <i>tuf2</i>	Superhost, and <i>tuf2</i> from <i>S. goldiniensis</i>	<i>HygR</i>	(McHugh, 2020)
<i>S. coelicolor</i> M1152 + pESAC13-A- <i>AurI</i> $\Delta aurAI$	Superhost and aurodox cluster, <i>AurAI</i> replaced with hygromycin resistance.	<i>AprR HygR</i>	(McHugh et al., 2022)
<i>S. coelicolor</i> M1152 + pESAC13-A- <i>AurI</i> $\Delta aurB$	Superhost and aurodox cluster, <i>AurB</i> replaced with hygromycin resistance.	<i>AprR HygR</i>	This Study
<i>S. coelicolor</i> M1152 + pESAC13-A- <i>AurI</i> $\Delta aurHV$	Superhost and aurodox cluster, <i>AurHV</i> replaced with hygromycin resistance.	<i>AprR HygR</i>	This Study
<i>S. coelicolor</i> M1152 + pESAC13-A- <i>AurI</i> $\Delta aurM^*$	Superhost and aurodox cluster, <i>AurM</i> * replaced with hygromycin resistance.	<i>AprR HygR</i>	This Study
<i>S. coelicolor</i> M1152 + pESAC13-A- <i>AurI</i> $\Delta aurQ$	Superhost and aurodox cluster, <i>AurQ</i> replaced with hygromycin resistance.	<i>AprR HygR</i>	This Study
<i>Enterococcus faecium</i> (ATCC 51299)	WT, clinical isolate	Wild-type	ATCC
<i>Staphylococcus aureus</i> (ATCC 43300)	WT, clinical isolate	Wild-type	ATCC
<i>Klebsiella pneumoniae</i> (ATCC 700603)	WT, clinical isolate	Wild-type	ATCC

<i>Acinetobacter baumannii</i> (ATCC 19606)	WT, clinical isolate	Wild-type	ATCC
<i>Pseudomonas aeruginosa</i> (ATCC 27853)	WT, clinical isolate	Wild-type	ATCC
<i>Escherichia coli</i> (ATCC 25922)	WT, clinical isolate	Wild-type	ATCC
<i>Bacillus subtilis</i> (ATCC 23857)	WT, clinical isolate	Wild-type	ATCC
<i>Escherichia coli</i> DH5α	<i>E. coli</i> K12 derivative	<i>huA2 (argF-lacZ)</i> U169 <i>phoA glnV44</i> 80 (<i>lacZ</i>)M15 <i>gyrA96 recA1</i> <i>relA1 endA1</i> <i>thi-1 hsdR17</i>	(Grant et al., 1990)
<i>E. coli</i> DH10β Top10 ©	<i>E. coli</i> K12 derivative	<i>mcrA</i> , Δ(<i>mrr-hsdRMS-mcrBC</i>), Φ <i>lacZ(del)</i> M15, Δ <i>lacX74</i> , <i>deoR</i> , <i>recA1</i> , <i>araD139</i> , Δ(<i>ara-leu</i>)7697, <i>galU</i> , <i>galK</i> , <i>rpsL</i> (SmR), <i>endA1</i> , <i>nupG</i>	Invitrogen
<i>E. coli</i> ET12567	<i>E. coli</i> K12 derivative	<i>dam13::Tn9</i> , <i>dcm6</i> , <i>hsdM</i> , <i>hsdR</i> , <i>recF143</i> , <i>zlj201::Tn10</i> , <i>galK2</i> , <i>galT22</i> , <i>ara14</i> , <i>lacY1</i> , <i>xylS</i> , <i>leuB6</i> , <i>thi-1</i> , <i>tonA31</i> , <i>rpsL136</i> , <i>hisG4</i> , <i>tsx78</i> , <i>mtli</i> , <i>glnV44</i> .	(MacNeil et al., 1992)
<i>E. coli</i> TUV93-0 + <i>ler-gfp</i>	WT, <i>ler-gfp</i> transcriptional fusion	CmR	(McHugh et al., 2019)
<i>E. coli</i> TUV93-0 + <i>rpsM-gfp</i>	WT, <i>rpsM-gfp</i> transcriptional fusion	CmR	(McHugh et al., 2019)
<i>E. coli</i> TUV93-0 + pAJR70	WT, Promotorless GFP	CmR, AmpR	(Roe et al., 2003)
<i>E. coli</i> BL21 (DE3)	<i>E. coli</i> BL21 derivative	<i>F</i> <i>ompT hsdS_B</i> (<i>r_B⁻</i> , <i>m_B⁻</i>) <i>galdcmrne131</i> (DE3) CmR, AmpR	(Studier and Moffatt, 1986)

Table 2B: Plasmids used in this study with detailed antibiotic selection and sources.

Plasmid Name	Description	Resistance	Reference
pUZ8002	non-transferable helper plasmid, used in intergenic conjugation.	Kanamycin	(Larcombe et al., 2024; Paget et al., 1999)
pESAC-13A	Phage Artificial Chromosome, Φ C31 integrase, <i>lacZ</i>	Apramycin, carbenicillin	(Sosio et al., 2001)
pESAC-13A- <i>Aurl</i>	Phage Artificial Chromosome, Φ C31 integrase, aurodox cluster	Apramycin	(McHugh, 2020)
pESAC13-A- <i>Aurl</i> _ Δ <i>aurAI</i>	Phage Artificial Chromosome, Φ C31 integrase, aurodox cluster	Apramycin, Hygromycin	(McHugh, 2020)
pESAC13-A- <i>Aurl</i> _ Δ <i>aurB</i>	Phage Artificial Chromosome, Φ C31 integrase, aurodox cluster	Apramycin, Hygromycin	This study
pESAC13-A- <i>Aurl</i> _ Δ <i>aurHV</i>	Phage Artificial Chromosome, Φ C31 integrase, aurodox cluster	Apramycin, Hygromycin	This study
pESAC13-A- <i>Aurl</i> _ Δ <i>aurM</i> *	Phage Artificial Chromosome, Φ C31 integrase, aurodox cluster	Apramycin, Hygromycin	This study
pESAC13-A- <i>Aurl</i> _ Δ <i>aurQ</i>	Phage Artificial Chromosome, Φ C31 integrase, aurodox cluster	Apramycin, Hygromycin	This study
pIJ10700	Re-direct template	Hygromycin	(Gust et al., 2003)
pIJ10790	λ -RED (<i>gam</i> , <i>bet</i> , <i>exo</i>), <i>cat</i> , <i>araC</i> , rep101ts	Chloramphenicol	(Gust et al., 2003)
pR9406	Driver plasmid during Tri-Parental Mating	Ampicillin, carbenicillin	(Jones et al., 2013)
pMS82	Φ BT1 integrase	Hygromycin	(Gregory et al., 2003)
pMS82_ <i>tuf2</i>	Φ BT1 integrase, <i>tuf2</i> from <i>S. goldiniensis</i>	Hygromycin	(McHugh, 2020)
pSET-AMP- <i>E.coli</i> 1_ <i>tuf2</i>	Synthetic vector from IDT	Ampicillin, carbenicillin	Integrated DNA Technologies
pVS45	Plasmid with arabinose inducible promoter	Ampicillin, carbenicillin	R. E. McHugh, Unpublished work.
pVS45_ <i>tuf2</i>	Plasmid encoding <i>tuf2</i> from <i>S. goldiniensis</i> with arabinose inducible promoter	Ampicillin, carbenicillin	R. E. McHugh, Unpublished work.
pSEVA238	Plasmid with benzoic acid inducible promoter	Kanamycin	(Gawin et al., 2017)
pSEVA238_ <i>tufB</i>	Plasmid encoding <i>tufB</i> from <i>S. goldiniensis</i> with benzoic acid inducible promoter	Kanamycin	(Gawin et al., 2017)
pSEVA238_ <i>tuf2</i>	Plasmid encoding <i>tuf2</i> from <i>S. goldiniensis</i> with benzoic acid inducible promoter	Kanamycin	(Gawin et al., 2017)
<i>ler</i> -gfp	<i>ler</i> -gfp transcriptional fusion	Chloramphenicol	(McHugh et al., 2019)
<i>rpsM</i> -gfp	<i>rpsM</i> -gfp transcriptional fusion	Chloramphenicol	(McHugh et al., 2019)

pAJR70	Promotorless GFP	Ampicillin	(Roe et al., 2003)
pET-21a(+)	Bacterial Expression vector with inducible T7 promotor	Ampicillin, carbenicillin	MilliporeSigma (Novagen)
pET-21a(+)_AurB	Bacterial Expression vector with inducible T7 promotor encoding expression of AurB	Ampicillin, carbenicillin	This study
pET-21a(+)_AurHV	Bacterial Expression vector with inducible T7 promotor encoding expression of AurHV	Ampicillin, carbenicillin	This study
pET-21a(+)_AurM*	Bacterial Expression vector with inducible T7 promotor encoding expression of AurM*	Ampicillin, carbenicillin	This study
pET-21a(+)_AurQ	Bacterial Expression vector with inducible T7 promotor encoding expression of AurQ	Ampicillin, carbenicillin	This study

2.2.3 Media and Antibiotics

Table 2C: Bacterial Culture Media used in this study. This table provides instructions for the creation of 1 L of liquid media. For solid media, 20 g/L of agar was added to prior to autoclaving. To prepare soft agar, agar component was reduced to 10 g/L.

Media Name	Recipe	pH
Glucose Yeast Malt Medium (GYM) (Kieser et al., 2000)	10 g malt extract, 4 g glucose extract, 4 g yeast extract, 2 g CaCO ₃ , dH ₂ O to 1 L	pH 7.2
Difco nutrient media (NA) (Difco)	15 g Difco Nutrient Broth powder, dH ₂ O to 1 L	pH 6.8
Soy Flour Mannitol (MS) (Hobbs et al., 1989)	20 g mannitol, 20 g soya flour tap H ₂ O to 1 L	NA
Lysogeny Broth (LB) (Sambrook et al., 1989)	10 g tryptone, 5 g NaCl 5 g yeast extract, dH ₂ O to 1 L	pH 7.2
2X Yeast Tryptone Media (2XYT) (Kieser et al., 2000)	16 g tryptone, 10 g yeast, 4 g NaCl, dH ₂ O to 1 L.	pH 7.2
Super Optimal Broth with Catabolite Repression Medium (SOC) (New England Biolabs)	20 g tryptone, 5 g yeast extract, 1 mL 1M NaCl, 0.25 mL 1M KCl, 1 mL 2M Mg ²⁺ stock, 1 mL 2M glucose, dH ₂ O to 1 L	pH 7.0
Modified Yeast Extract Malt Extract (YEME) (Hoskisson et al., 2001)	10 g glucose, 5 g Oxoid malt extract, 5 g Difco Bacto-peptone, 3 g yeast extract, dH ₂ O to 1 L	pH 7.3
Aurodox Production Media (AP) (Berger et al., 1973)	20 g glycerol, 1 g glucose, 5 g corn steep powder, 2 g meat extract, 1 g soybean flour, dH ₂ O to 1 L	pH 7.2
V6 Media (Marinelli, 2009)	10 g glucose, 5 g corn steep solids, 5 g yeast extract, 5 g peptone, 3 g casein hydrolysate, 1.5 g NaCl, dH ₂ O to 1 L	pH 7.5
ZY media	10 g tryptone, 5 g yeast extract, dH ₂ O to 1 L	NA
20x NPS	66 g (NH ₄) ₂ SO ₄ , 136 g KH ₂ PO ₄ , 142 g Na ₂ HPO ₄ , dH ₂ O to 1 L	NA
50x 5052	250 g Glycerol, 25 g D-Glucose, 100 g Lactose, dH ₂ O to 1 L	NA
Autoinduction medium (ZYP-5052) (Studier, 2005)	1 M MgSO ₄ , 20 mL 50x 5052, 50 mL, 20 x NPS, ZY media to 1 L	NA

Table 2D: Antibiotics and their working concentrations used throughout this study.

Antibiotic	Class	Working concentration	Storage Solvent
Aurodox	Elfamycin, binds to EF-Tu	100 µg/ mL	DMSO
Ampicillin	B-lactam	100 µg/ mL	H ₂ O
Apramycin	Aminoglycoside	50 µg/ mL	H ₂ O
Carbenicillin	B-lactam	100 µg/ mL	H ₂ O
Chloramphenicol	N-dichloroacylphenylpropanoid	25 µg/ mL	~98% EtOH
Hygromycin B	Substitute aminoglycoside	100 µg/ mL	H ₂ O
Kirromycin	Elfamycin, binds to EF-Tu	100 µg/ mL	DMSO
Kanamycin	Aminoglycoside	50 µg/ mL	H ₂ O
Nalidixic acid	DNA gyrase inhibitor antibiotic	25 µg/ mL	0.1M NaOH

2.2.4 Gravimetric Dry-Weight Analysis of *Streptomyces* Growth

Streptomyces spores were pre-germinated in GYM Media for 48 hours and inoculated 1/100 into Erlenmeyer flasks containing 50 mL GYM media. These were then incubated at 30 °C, 200 rpm, for twelve hours before 500 µL culture from three 'growth' flasks was removed and transferred on to a Whatman glass microfiber filter paper that had been previously dried in an oven at 55°C for 48 hours to remove moisture. A vacuum system was used to pull the culture through a Buchner funnel, leaving only cell mass on the filter paper. Filter papers were dried for 12 hours in a 55 °C oven before being weighed. Additionally, at each 12 hour time point, the same flask was removed from the incubator, centrifuged at 4000 $\times g$ to remove cells, and the supernatant subject to solvent extraction via chloroform for future LC-MS and bioactivity analysis (Kieser et al., 2000). This was then repeated every twelve hours for one week to establish stationary phase and the stage of Elfamycin production during the *Streptomyces* life cycle.



2.3 Molecular Biology

2.3.1 DNA Isolation

DNA was isolated from 2 x 10 mL GYM Media liquid culture of *Streptomyces* grown for 3 days in 30°C shaking incubator, 200 rpm. The following protocol was adapted from Actinobase, and uses a salting out method to isolate high molecular weight DNA (Feeney et al., 2022). The two cultures were centrifuged at top speed for 30 minutes and the media discarded. The pellets were resuspended in 3 mL TES Buffer (75 mM NaCl, 25 mM EDTA pH 8, 20 mM Tris-HCl pH 7.5) in 15 mL falcon tubes. Aliquots (150 µL) of lysozyme (20mg mL⁻¹) was added to lyse cells and the sample was incubated at 37°C for 3 hours. Aliquots (84 µL) of proteinase K (20mg mL⁻¹) solution were added alongside 360 µL of 10% SDS and the sample was mixed by inversion and incubated at 55°C for 2 hours, inverting occasionally. Aliquots (1.2 mL) of 5M NaCl was added and mixed by inversion before allowing the sample to cool to 37°C or lower. 3 mL chloroform was added and mixed by inversion before incubating for 30 minutes at 20°C. The sample was centrifuged at top speed for 15 minutes at 20°C. Next, the top layer of the sample was removed with a cut pipette tip and transferred into a new sterile 15 mL falcon tube. The solution was incubated on ice for 2 minutes before adding equal volume ice cold isopropanol and mixed by inversion then stored at -20°C overnight. The next day, DNA was spooled onto a sealed Pasteur pipette before storing in a sterile Eppendorf tube. The DNA was then rinsed in 1ml 70% ethanol and centrifuged at top speed for 10 minutes. Leftover ethanol was pipetted off leaving approximately 10 µL on the sample and was left to air dry. Finally, the DNA was resuspended in 500 µL of sterile TE buffer.

2.3.2 PCR Conditions

For diagnostic and confirmation PCRs, REDTaq DNA Polymerase (Sigma) was used according to manufacturer's instructions. For cloning applications, the proof-reading Q5 Polymerase (NEB) was used according to manufacturer's instructions.

A	Initial Denaturation	95° C	1 minute	
	25–35 Cycles	95° C	15 seconds	
		*55–72° C	15 seconds	
		72° C	20 seconds/kb	
	Final Extension	72°C	2 minutes	
	Hold	4–10° C	∞	
B	Initial Denaturation	98° C	30 seconds	
	25–35 Cycles	98° C	5-10 seconds	
		*50–72° C	10-30 seconds	
		72° C	20-30 seconds/kb	
	Final Extension	72°C	2 minutes	
	Hold	4–10° C	∞	

2.3.3 Oligonucleotide primer List

Table 2E: Oligonucleotide primers used in this study, designed on SnapGene™ synthesised by IDT.

Name	Sequence 5'-3'	Tm°	Description
16S_Foreward	AGAGTTTGGATCMTGGCTCAG	56.3	Primers for amplification of the 16S rRNA gene for sequencing.
16S_Reverse	CGGTTACCTTGTTACGACTT	52.3	
AurB_Deletion_Foreward	GGCGGACGTCTTGGCCGGCCCGACGGGAGACACG GCGTGATTCCGGGGATCCGTCGACC	78.0	Redirect primers for amplification of the hygromycin resistance cassette present on PIJ10700 with overhangs corresponding to <i>AurB</i> .
AurB_Deletion_Reverse	GAGGATTTCCATGGGGTCTCTCTTCCGGGTCC GTCATGTAGGCTGGAGCTGCTTC	72.6	
AurHV_Deletion_Foreward	GTGAATCACGTTCCGGCCCCGGATAGGGTGATCCA CATGATTCCGGGGATCCGTCGACC	76.7	Redirect primers for amplification of the hygromycin resistance cassette present on PIJ10700 with overhangs corresponding to <i>AurHV</i> .
AurHV_Deletion_Reverse	TTGTATCCCTATACGGTCTTGTAGCTGAAGCTGTGG TCATGTAGGCTGGAGCTGCTTC	77.1	
AurM*_Deletion_Foreward	CGGCTCGCCTGACGGACCCGGAAGAGAGAGACCC CCATGATTCCGGGGATCCGTCGACC	73.7	Redirect primers for amplification of the hygromycin resistance cassette present on PIJ10700 with overhangs corresponding to <i>AurM*</i> .
AurM*_Deletion_Reverse	AGCCCTGGCCCGCGAAGAGGAAGACCGGTGCGAG CATCATGTAGGCTGGAGCTGCTTC	70.0	
AurQ_Deletion_Foreward	CGAGCGGCGCCCCGGAACGACGACGGAACGGACA CCATGATTCCGGGGATCCGTCGACC	75.8	Redirect primers for amplification of the hygromycin resistance cassette present on PIJ10700 with overhangs corresponding to <i>AurQ</i> .
AurQ_Deletion_Reverse	CGGTGCGGGCATCGCCGGCCACGACGCGCACCAT CGTCATGTAGGCTGGAGCTGCTTC	75.7	
AurB_Deletion_Check_Foreward	GCGCCACGGTCATGACCTCC	63.5	Primers ~ 200 bp upstream and downstream of <i>AurB</i> to check re-direct.
AurB_Deletion_Check_Reverse	CCGGGGACGGTGAGCATCT	62.2	
AurHV_Deletion_Check_Foreward	TGGTGTGGTGGCGGCGTT	63.5	Primers ~ 200 bp upstream and downstream of <i>AurHV</i> to check re-direct.
AurHV_Deletion_Check_Reverse	CGCCAGGAGAAACAGCTGCC	61.4	
AurM*_Deletion_Check_Foreward	CACCGAACTGCTGGACCGTC	60.7	Primers ~ 200 bp upstream and downstream of <i>AurM*</i> to check re-direct.
AurM*_Deletion_Check_Reverse	CCGGCTGGGTGAGCGCGAA	66.0	
AurQ_Deletion_Check_Foreward	CCGACGTTGAGGATGACCGA	59.2	Primers ~ 200 bp upstream and downstream of <i>AurQ</i> to check re-direct.
AurQ_Deletion_Check_Reverse	GAATGCGCCGGGAGGAAG	59.1	
AurB_Restriction_Foreward	AAGAAGGAGATATACATATGGTGACACCCGGGCCA	66.2	Primers for the amplification of <i>AurB</i>

	CC		from synthesised pUC57 construct containing NdeI and HindIII restriction sites.
AurB_Restriction_Reverse	CTCGAGTGCGGCCGCAAGCTTGCCAGCCTTCTCA GGCG	74.9	
AurHV_Restriction_Forward	AAGAAGGAGATATACATATGATGCTTCAGGAAGTGA AAGGAACAC	62.9	Primers for the amplification of <i>AurHV</i> from synthesised pUC57 construct containing NdeI and HindIII restriction sites.
AurHV_Restriction_Reverse	CTCGAGTGCGGCCGCAAGCTTAGCCGCTCCTTCTG GCCA	66.2	
AurM*_Restriction_Forward	AAGAAGGAGATATACATATGATGGAAATATTAAC TAGCTGTATCAG	59.8	Primers for the amplification of <i>AurM*</i> from synthesised pUC57 construct containing NdeI and HindIII restriction sites.
AurM*_Restriction_Reverse	CTCGAGTGCGGCCGCAAGCTTGCTGGCACGCAGG	74.3	
AurQ_Restriction_Forward	AAGAAGGAGATATACATATGATGAATACAGCCCCTA TTGAGGACC	63.2	Primers for the amplification of <i>AurQ</i> from synthesised pUC57 construct containing NdeI and HindIII restriction sites.
AurQ_Restriction_Reverse	CTCGAGTGCGGCCGCAAGCTTAACCCGTTCATACA TGGTACCG	70.6	
PET-21a(+)_Seq_Check_Forward	ACCCGCCGCGCTTAATGCGC	66.6	Primers ~ 200bp upstream and downstream of the MCS of pET-21a(+) used for sequencing to confirm cloning.
PET-21a(+)_Seq_Check_Reverse	TCGAGATCTCGATCCCGCGA	60.0	

2.3.4 Gel electrophoresis

Unless otherwise stated, gels containing 1 % agarose were used for gel electrophoresis. Agarose concentration was increased to 1.5 % for PCR products smaller than 500 bp. Agarose was dissolved in TAE buffer (40 mM Tris-acetate, 1 mM EDTA) by boiling using a microwave. The gel mixture was then cooled before ethidium bromide was added to a final concentration of 100 µg/ mL and poured into a casting tray, sealed with rubber stoppers. DNA samples were mixed with 6x blue/orange loading dye (Promega), and relevant molecular weight markers were chosen according to band size (Promega). Throughout this project, agarose gels were run using Bio-Rad gel dock systems, with 1 x TAE used as the running buffer. In general, gels were run at 90 V for between 45 and 90 minutes, with the run time being increased for larger gels. DNA was visualised and imaged under UV excitation using Syngene Bioimaging Ingenius trans-illuminator. For extraction of DNA from the agarose gel, a UV trans-illuminator was used on low for minimal exposure time and a scalpel was used to cut the required band from the gel. DNA products were extracted using the Wizard® SV Gel and PCR Clean-Up kit (Promega Corporation, 2009).

2.3.5 Restriction digests

Restriction enzymes were sourced from Promega, and the appropriate digest conditions and buffers were determined via the Promega Restriction Enzyme Tool (<https://www.promega.co.uk/resources/tools/retool/>).

2.4 Sequencing, Genome Assembly and Annotation.

2.4.1 Whole genome sequencing using Illumina Technologies

Sequencing of *S. ramocissimus* was performed by Novogene on an Illumina NovaSeq 6000 sequencing platform, where the sequencing library was generated on-site from pre-supplied genomic DNA isolated as described in previous methods, generating 150 bp paired end reads.

2.4.2 Assembly of *S. ramocissimus* genome using Illumina Short Reads

The quality of sequencing reads were assessed using QUAST software (Gurevich et al., 2013; version 5.2.0) and assembled using Unicycler software (Wick et al., 2016; version 0.5.0). Putative assemblies were then submitted to AutoMLST software to identify the phylogenetically closest neighbouring organism, which was then used as a reference genome assembly to allow scaffolding of the *S. ramocissimus* genome using MeDuSa software (Alanjary et al., 2019; Bosi et al., 2015). The closest related organism to *S. ramocissimus* was *Streptomyces longwoodensis*. Assembly quality was assessed using Quast and the assembly annotated using PROKKA. The *de novo* assembly was visualised on Bandage by upload of GenBank files to provide contig number and length (Wick et al., 2015). All analysis was performed on the publicly available bioinformatic analysis server, Galaxy.au, with the exception of AutoMLST and MeDuSa which were performed on their respective servers. In all cases, default settings were used for analysis.

2.4.3 Bioinformatic analysis of *S. ramocissimus* genome

Taxonomy analysis: Preliminary multi-locus-sequence-analysis (MLSA) of *S. ramocissimus* was undertaken by uploading FASTA files of assembled contigs to the autoMLST server (Alanjary et al., 2019). Analysis conditions included DeNovo mode

with nearest organisms and MLST genes on default. The resultant phylogenetic tree allowed for placement of *S. ramocissimus* into a taxonomic clade with *Actinospica acidophila* automatically selected as an outlier. The phylogenetic tree was then edited and presented on Figtree for visualisation.

Identification of biosynthetic gene clusters: identification and preliminary annotation of biosynthetic gene clusters of *S. ramocissimus*, *S. goldiniensis* and *S. collinus* was performed using AntiSMASH 6.0.0. For maximum accuracy in BGC identification, the gene clusters of all 3 organisms were identified and counted using “strict” settings. Additional packages such as KnownClusterBlast, ClusterBlast, SubClusterBlast and MIBiG cluster comparison were also ran in parallel (Blin et al., 2021).

Comparison of Elfamycin biosynthetic gene clusters: to compare Elfamycin gene clusters of *Streptomyces* species, cluster sequences were downloaded from AntiSMASH as GenBank files (.gbk). Visual comparisons between gene clusters, including percentage similarity, were generated using Clinker and annotated manually for gene name and visualisation (Gilchrist and Chooi, 2021).

Comparison of biosynthetic genes within clusters: NCBI Basic Local Alignment Search Tool was used alongside AntiSMASH output of gene cluster to allow for analysis of gene function, naming and calculation of percentage similarity between genes of clusters (Altschul et al., 1990; Medema et al., 2011).

2.4.4 16S rRNA Sequencing

Purified PCR products were diluted to a concentration of 10 ng/μL and added to 15 μL of distilled water in duplicate. Concentration and quality of samples were calculated using a Nanodrop (Thermo Scientific). The DNA samples (with primers) were sequenced by Eurofins for 16S rRNA gene sequencing (sanger). Both forward and reverse 16S rRNA gene sequences were aligned and trimmed using BioLign software. The aligned contigs were input into BLAST software (NCBI) and FASTA

files for similar species were obtained (Altschul et al., 1990).

2.4.5 Phylogenetic analysis

FASTA sequences were aligned using Clustal Omega (Sievers et al., 2011). The evolutionary history were created using the Neighbour-Joining method (Saitou and Nei, 1987). The evolutionary distances were created using the Tamura-Nei method or the Jones-Taylor-Thornton method and evolutionary analysis was conducted in MEGA X (Kumar et al., 2018). All trees were run with 500 bootstraps and newick files exported to International Tree of Life (IToL) for annotation and editing.

2.4.6 MinION Sequencing of Aurodox Phage artificial chromosome pESAC13-A_pAur

The MinION plasmid DNA library was created according to Nanopore™ 1D ligation protocol using 1 µg plasmid DNA. From this, 75 µl was loaded into a MinION© flow cell and placed in the MinION sequencer. The sequencer was run for twelve hours, and the raw data was converted to sequence data by base calling via MinKnow base calling software, provided by Nanopore™

2.5 Assessing natural product production and bioactivity of *Streptomyces* strains

2.5.1 Solvent Extraction of aurodox from *Streptomyces* cultures

Liquid cultures of bacterial *Streptomyces* sp. were prepared by inoculating a single colony in 50 mL GYM liquid media in an Erlenmeyer shake flask with baffle, 200 rpm. Cultures were grown at 30 °C for one week. Cultures were aseptically transferred into 50 mL falcon tubes and centrifuged for 20 minutes at 4200 x g, separating cell debris from the supernatant. Culture supernatants were filter sterilised through a 0.2 µm Millipore™ filter. Using glass equipment throughout, the culture supernatants were mixed with equal volume of chloroform and a separation funnel was used to remove the lower, solvent phase which was stored in 50 mL Duran bottles. Samples were then dried under nitrogen gas or by use of the Rotavapor™ (Buchi) and extracts were dissolved in 500 µL of 100% DMSO and transferred into an Eppendorf. 10 µL of extract was diluted in 90 µL nuclease free water or ethanol and submitted for LC-MS analysis.

2.5.2 Liquid Chromatography Mass Spectrometry

LC-MS was carried out on an Agilent 1100 HPLC instrument in conjunction with a Waters Micromass ZQ 2000/4000 mass detector. Electrospray ionization (ESI) was used in all cases. The RP-HPLC analysis was conducted on a Zorbax 45 mm x 150 mm C18 column at 40 °C. Ammonium acetate buffers were used as follows: Buffer A (5 mM Ammonium acetate in Water) and Buffer B (5mM Ammonium acetate in acetonitrile). Positive and negative electrospray methods were applied with of 100 to 1000 AMU positive, 120-1000 AMU negative with a scanning time of 0.5 seconds. The UV detection was at a wavelength of 254 nm.

2.5.3 Agar Plug and disc diffusion Bioassays Against ESKAPE Pathogens

Strains were tested for bioactivity against clinically relevant ESKAPE Pathogens. ESKAPE strains were cultured overnight in 37 °C at 200 rpm in 10 mL of LB. Overnight cultures were diluted into 15 mL of soft nutrient agar to give a final OD₆₀₀ value of 0.01 and transferred onto square petri dishes containing 40 mL of LB agar. Agar plugs (6 mm diameter) from culture plates of streptomyces strains were placed onto the pathogen containing plates in triplicate. Negative controls were a media plug and positive controls were co-amoxiclav paper discs. Disc diffusion assays were carried out similarly with the use of paper discs containing 1 mg/ml crude extract from cell fermentation. Plates were incubated for 12 hrs at 37 °C then zones of inhibition and change colony morphology were observed (mm) with a ruler.

2.6 Generation of aurodox derivatives in the heterologous host using the re-direct method

2.6.1 Redirect-PCR targeting system in *Streptomyces* for lambda-red mediated gene deletions on Phage Artificial Chromosomes

Method detailed in (Gust et al., 2003). Redirect-PCR primers were designed for 4 key aurodox genes as according to PCR targeting system in *Streptomyces coelicolor* A3(2) (Gust et al., 2003, Datsenko and Wanner, 2000) on the aurodox PAC (pESAC13-A_pAur). pIJ10700 was used as a template for amplification of the hygromycin disruption cassette, purified from agarose gel electrophoresis. The resulting PCR product with overhangs of the gene to be replaced transformed *E. coli* Top10 + pIJ10790 + pESAC-13A-pAur cells, which had been induced by growth with 10 mM arabinose at 30 °C to induce lambda-red recombinase genes, by electroporation and plated LB agar with selection antibiotics hygromycin and apramycin and incubated at 37 °C overnight, where temperature change facilitates the loss of temperature-sensitive pIJ10790, the lambda-red recombinase plasmid. Transformed colonies were then selected and subject to tri-parental mating to facilitate transfer of the disrupted phage artificial chromosome (pESAC13-A_pAur_ΔX) to ET12567 for conjugation into *Streptomyces coelicolor* M1152 (Gust et al., 2003).

2.6.2 Preparation of electrocompetent *Escherichia coli*

A 10 mL overnight culture of *E. coli* was prepared in LB media with relevant antibiotics. The following day, cultures were diluted 1/50 and grown to an OD₆₀₀ of 0.6. The culture was chilled on ice for five minutes before being centrifuged at 4000 x g for five minutes. The cell pellet was then resuspended in 25 mL of sterile, ice cold 50 % glycerol solution and centrifuged at 4000 x g for five minutes. This washing procedure was

then repeated twice. The pellets were resuspended in 400 μ L of sterile water with 10% glycerol (Sambrook et al., 1989). Electroporation with the PCR product was carried out using BioRad GenePulser II set to 200 Ω , 25 μ F and 2.5Kv with the expected time constant as 4.5-4.9 ms.

2.6.3 Tri-Parental Mating

Method detailed in (Jones et al., 2013). Overnight cultures of *E. coli* DH10 β Top10 $\text{\textcircled{C}}$ (Invitrogen) containing the aurodox PAC pESAC13-A_pAur, *E. coli* Top10 + pR9604 and ET12567 with appropriate antibiotics (Table 2D), were used to inoculate fresh 50 mL cultures of *E. coli*. The cultures were grown at 37 $^{\circ}$ C at 250 rpm until the culture reached an OD₆₀₀ of 0.6, where cells were then washed three times in fresh, LB by centrifugation at 4000rpm to remove residual antibiotics. Cells were resuspended in 1 mL of LB media, where 20 μ L of each strain was spotted on top of the other in the centre of an LB media agar plate containing no antibiotics. The plate was grown at 37 $^{\circ}$ C overnight and the following day, the cell mass was re-streaked onto antibiotic selection plates to select for the presence of the conjugating plasmid in ET12567. Presence of the plasmid was confirmed by colony PCR.

2.6.4 Intergenic conjugation of integrating vectors into *Streptomyces*

Method detailed in (Kieser et al., 2000). Overnight culture of ET12567 + pUZ8002 inoculated 50 mL culture of LB media. Culture was grown to an OD₆₀₀ of 0.6 and washed twice with 10 mL LB media and centrifugation at 4000 \times g to remove any residual antibiotics before resuspension in 1 mL LB in a sterile Eppendorf tube. In parallel, approximately 10^6 *Streptomyces* spores were added to 500 μ L 2xYT media in an Eppendorf tube and subjected to heat-shock at 50 $^{\circ}$ C for ten minutes. Spores were recovered at room temperature for ten minutes before 500 μ L of ET12567 +pUZ8002 +plasmid was added to the spores and vortexed briefly before removing

most of the cell supernatant after centrifugation. The cells were then resuspended in the remaining supernatant and plated onto MS agar plates containing 10 mM MgCl₂ and incubated for 16 hours at 30 °C. Plates were then overlaid with 1 mL of sterile water containing 0.5 mg/mL nalidixic acid to kill the remaining *E. coli* cells. Plates were further incubated for 40 hours and exconjugant colonies were selected and patched onto MS agar containing selective antibiotics for the plasmid and nalidixic acid (Gust et al., 2003)

2.7 Cloning of key aurodox biosynthesis genes into pET-21a(+)

2.7.1 *In silico* cloning and plasmid construction

In silico cloning and plasmid construction was carried out using SnapGene [™] (Version 4.2.11). Plasmid maps were constructed and annotated using the 'show features' function and exported as tifs.

2.7.2 Plasmid construction using restriction cloning

pET-21a(+) overexpression constructs were created by restriction cloning where pUC57 (Genscript) vectors carrying a biosynthetic gene of interest from the aurodox BGC, codon optimised for *E. coli* expression were amplified by PCR to add both NdeI and HindIII restriction sites to the start and end of the gene respectively. The pET-21a(+) vector and amplified gene with restriction sites were digested with NdeI and HindIII by double digest to create compatible overhangs allowing binding by T4 DNA Ligase. Appropriate concentrations, determined by the NEBioCalculator from New England Biolabs (accessed at <https://nebiocalculator.neb.com/#!/ligation>), of digested pET-21a(+) (vector) and digested PCR product with compatible overhangs were incubated at 4 °C overnight with T4 DNA ligase (New England Biolabs) to allow ligation both fragments together to form the pET-21a(+)_AurX overexpression vector. Correct orientation and reading frame of plasmid was determined by PCR, digest sanger sequencing (Eurofins).

2.8 Overexpression, identification and purification of Key aurodox biosynthesis genes in *E. coli* BL21 DE3

2.8.1 Hexa-His-tag protein expression using autoinduction media

Colonies from fresh *E.coli* BL21 (DE3) transformations containing pET-21a(+) overexpression plasmids with the biosynthesis gene of interest were picked and inoculated in 10 mL overnights containing LB with 100 µg/mL of carbenicillin. *E. coli* BL21 (DE3) colonies containing only pET-21a(+) were used as the negative control. 1 mL aliquot of overnight was spun down and used as an uninduced control. 50 mL ZY-5052 autoinduction media was inoculated in Erlenmeyer 250 mL flasks with a 500 µL aliquot of the BL21 overnight cultures and grown at 18 °C for 72 hours, 26°C for 48 hours and at 37 °C for 24 hours, all with shaking at 200 rpm. Cultures were pelleted by centrifugation at 4000 x *g* for 20 minutes.

2.8.2 Identification and purification of protein

Pellets were weighed and resuspended in BugBuster® Master Mix (MM) (Merck Millipore Novagen™) at 5 mL BugBuster® MM per mg pellet concentration. The serine protease inhibitor PMSF was added to a concentration of 1mM and the BugBuster® MM was incubated at room temperature until the lysate was clear. Lysate was centrifuged at max RPM for 20 minutes at 4 °C to remove cell debris and supernatant was retained for SDS-PAGE analysis and ran as documented previously in these methods.

2.8.3 Inclusion body solubilisation

Pellets were weighed and resuspended in BugBuster® MM. To determine presence or absence of inclusion bodies in the overexpression cultures grown at 37 °C, the cultures were spun down at 4200 x *g* for 20 minutes at 4° C and the pellet was retained

and washed three more times with 1:10 diluted BugBuster® MM. Finally, the pellet was resuspended in 1:10 diluted BugBuster® MM and quantified using a Bradford Protein Assay. The remaining resuspended pellet was boiled at 95 °C in 5x SDS sample loading dye and stored at -20 °C for SDS-PAGE analysis and ran as documented previously in these methods.

2.8.4 SDS – PAGE and Coomassie brilliant blue staining

The remaining cell supernatant from both secreted and cellular proteins was discarded and proteins resuspended in 100 µL Nu Page LDS Sample Buffer (Invitrogen). SDS load dye was added to each sample at 1:4 ratio and boiled at 95 °C for 10 minutes. To 4 to 12% NuPAGE Bis-Tris Gels (Invitrogen), 10 µL of sample and 7 µL of Blue Prestained Protein Standard Broad Range (11-250 kDa) (New England Biolabs) was added and ran at 140 V for 1 hour. SDS-Page gels were stained for 1 hour with Coomassie brilliant blue (Novex) and destained using a solution of detain solution (40% Methanol, 10% acetic acid, 50% dH₂O) and stored in water overnight before imaging.

2.8.5 Protein Transfer, Wash and Antibody Treatment

The nitrocellulose transfer membrane was prepared according to BioRad BlotModule II instructions using a wet-sandwich transfer system and run at 25 V, 100 mA for 1.45 hours. Following transfer, membrane was washed 4 times in deionised water for 5 minutes each time to remove residual transfer buffer. The membrane was incubated for one hour in blocking solution at room temperature. All membrane incubations and washed were set up with agitation. Primary 6x Anti-His-Mouse antibody (ThermoFisher) was diluted 1:1,000 in the blocking solution. Following the blocking, the membrane was incubated with the primary antibody in blocking solution overnight

at 4 °C. The next day, the nitrocellulose membrane was washed 3x for 10 minutes in wash buffer. The membrane was incubated in a 1:50,000 dilution of the secondary Anti-Mouse-Goat-HRP antibody (ThermoFisher) in blocking solution for one hour at room temperature and washed 6 times with washing buffer for 5 minutes each to remove unbound secondary antibody.

2.8.6 Chemiluminescent detection of aurodox biosynthesis proteins

A 1:1 working solution of the SuperSignal West Pico Plus (ThermoFisher) chemiluminescent substrate was pipetted into a square plate and the membrane was incubated in the substrate for 4 minutes. The blot was removed, drained, and kept in a plastic seal for imaging with the ChemiDocMP Imaging System (BioRad).

2.8.7 Protein preparation of aurodox biosynthesis proteins via French pressure cell

Prior to purification, the *E. coli* BL21 DE3 cells first had to be lysed and proteins isolated. This was achieved via the French press: a hydraulic pump system that places cells under high pressure and forces them to rupture, thus fragmenting the membrane (Simpson et al., 1963). Cells were harvested by centrifugation and immediately cooled on ice and resuspended in solubilisation buffer. The solubilised cells were then broken by three passages through a French Press maintained at 20,000 psi. Remaining intact cells were pelleted by centrifugation at 23,000 x g, 4 °C for 30 minutes (JA 25-50, Beckman Avanti JXN-26). The supernatant was retained for analysis.

2.8.8 Protein purification via Immobilised Metal Affinity Chromatography

The protein solution was passed through 1 ml HisTrap FF crude (Cytiva) using the ÄKTA Pure FPLC platform (GE Healthcare). The column had previously been loaded with cobalt and equilibrated in IMAC A buffer. The hepta-his-tag on pET-21a(+) has

affinity to the cobalt bound to the resin, whilst other proteins within the solution flow through the column freely. After sample loading was complete, non-specifically bound proteins were eluted by washing the column in 10 column volumes (CV) of IMAC A containing 20 mM imidazole. AurM* was eluted from the column using an imidazole gradient, gradually increasing from 20 mM to 500 mM over 20 column volumes. The eluent was collected in a 96-well deep well plate in 2 mL fractions. Protein size and purity was verified via SDS-PAGE electrophoresis. Elution fractions containing AurM* were identified and stored for future use.

2.9 Overexpression and identification of EF-Tu2/EF-TuB in EHEC

2.9.1 Overexpression of *tuf2/tufB* in EHEC and gathering of Secreted proteins

Tuf2/ TufB overexpression strains were grown overnight at 37 °C, 250 rpm, in LB media. Fresh LB media containing appropriate antibiotic selection was inoculated to an OD₆₀₀ of 0.05 from the overnight culture and grown for 1.5 hours at 37 °C, 250 rpm. Protein expression was induced by the addition of arabinose or benzoic acid to a total volume of 2% or 2.0 mM respectively. The culture was left to grow for a further 4-6 hours or until the OD₆₀₀ reached 0.6. Cultures were centrifuged at 4000 x g.

2.9.2 Harvesting of cell lysate and secreted proteins

To the cell cultures, trichloroacetic acid was added to a final concentration of 10% culture volume to extract secreted proteins from cell supernatant. The remaining cell pellet was dried and stored at – 20 °C overnight. Cell supernatant with TCA was centrifuged at 4000 x g for 20 minutes the next day to collect secreted proteins and the cell pellet resuspended and treated with Bug Buster (Merck) at a volume of 5 mL/g of cell mass for 1 hour and centrifuged at 4000 x g for 20 minutes to collect proteins.

2.9.3 Western blotting for EF-Tu2

Proteins requiring analysis by western blotting were run as previously described on a 4 to 12% NuPAGE Bis-Tris Gel (Invitrogen) and transferred to ECL nitrocellulose membrane (GE Healthcare) using a Nupage Novex gel transfer system (Invitrogen). Proteins were blocked by submerging the membrane in 5% skimmed milk powder in PBS-Tween (PBST) for one hour. Incubation with primary antibody took place overnight in fresh 1% milk powder buffered in PBS at a 1:1,000 dilution. The next day, the membrane was washed 5 times with PBST for 5 minutes at a time before incubating for 1 hour with anti-mouse horseradish peroxidase (HRP)-conjugated

secondary antibody at a dilution of 1:2,000 in PBST-1% milk. The membrane was then washed in PBST as before and imaged.

2.10 Experimental assays in this study

2.10.1 Analysis of the effect of Elfamycins and aurodox derivatives on *in vitro* growth and cell viability

Overnight culture of EHEC (TUV93-0), was used to inoculate 200 ml Erlenmeyer flasks containing 50 ml of LB broth with or without 5 µg/ mL of aurodox and kirromycin to an initial OD₆₀₀ of 0.05. This was carried out in triplicate. At each time point, 100 µL of culture was removed and diluted 1/10 in LB medium, and the OD₆₀₀ was measured by spectrophotometry. The standard error mean of optical densities was calculated, and a standard curve was plotted using R Studio. The trendlines were fitted by joining the points and error bars were plotted as standard deviations from the means. P-values were determined using an unpaired t-test.

2.10.2 *In vitro* GFP fusion reporter assays

E. coli strains were grown in 5 mL MEM-HEPES and treated with 5 µg/ mL aurodox/kirromycin/aurodox derivative or 100% DMSO. Strains containing pSV45_*tuf2* or pSEVA238_*tuf2*/ pSEVA238_*tufB* were supplemented with 100 µg/ mL ampicillin or kanamycin respectively. *tuf2/tufB* expression was induced with the addition of arabinose (for pSV45) to a final concentration of 2 % with dH₂O as a control and benzoic acid (for pSEVA238) to a final concentration of 2.0 mM. Optical density was measured at 600 nm and fluorescence at 485/20 nm using a FLUOstar Optima Microplate Reader System (BMG Labtech) over 8 hours.

2.10.3 Enzymatic methylation assay (AurM*)

The methyltransferase assay was based on that developed by McKean et al., (2019). Briefly, to a 1.5 mL Eppendorf tube, AurM* (varied concentrations), SAM (S-Adenosylmethionine, varied concentrations), Kirromycin in 100% DMSO (varied

concentrations), DTT (1.00 mM) and BSA (1.00 mg/mL) (all final concentrations) in potassium phosphate buffer (100 mM, pH 6.8). Reactions were incubated using a Thermomixer at 37 °C for 1 h or 24 h at 500 rpm (or on the bench) before analysis by RP-HPLC and LCMS to confirm product identity. Aurodox (dissolved in DMSO) was used as a positive control for the presence of a peak on the spectra and DMSO used as a negative control. For more in-depth detail as to experimental conditions and development is provided in Chapter 4.

Chapter 3: Expanding the knowledge of kirromycin-like elfamycin biosynthesis and enzyme evolution within biosynthetic gene clusters.

3.1 Introduction

The Elfamycins are a group of structurally diverse antibiotic compounds that target Elongation Factor Thermo unstable (EF-Tu), disrupting the role of EF-Tu in translation during prokaryotic protein synthesis. Elfamycin compounds have been shown to be produced from multiple species of Actinobacteria, where kirromycin has found to be produced by both *Streptomyces collinus* and *Streptomyces ramocissimus*. As shown previously in this thesis, elfamycin antibiotics can be classified into two groups, based on the stage at which they effect protein synthesis via EF-Tu. The kirromycins act on EF-Tu after it has formed the ternary complex with aa-tRNA, preventing ribosome dissociation and stalling protein synthesis (S. M. Prezioso et al., 2017). The kirromycins are a class of molecules that can be sub-divided based on their chemical structure into kirromycin-like, L-681,217-like, and factumycin-like, though they all possess the similar function (Table 3A). The kirromycin-like subgroup is determined by the presence of an intramolecular ketal group called goldinonic acid, the L-681,217-like subgroup is characterised by the lack of the terminal pyridone ring, and the factumycin-like subgroup contains a terminal pyridone ring but lacks the central furan ring (Fig. 3.1; Prezioso et al., 2017). Though much is known about the structure of the kirromycin-like elfamycins, there is a gap in knowledge surrounding the biosynthesis of kirromycin-like Elfamycins, the structure of the BGCs and enzyme evolution among similar BGCs.

Table 3A: Elfamycin antibiotics can be produced by many strains, including *Streptomyces*.

Elfamycin compounds and their producing strains, kirromycin-like compounds and their producers as discussed in Chapter 1 of this thesis, are shown in red.

Elfamycin	Producing Strains	Reference
Aurodox	<i>Streptomyces goldiniensis</i>	(Berger et al., 1973)
Kirromycin	<i>Streptomyces collinus</i>	(Wolf et al., 1972)
Kirromycin	<i>Streptomyces ramocissimus</i>	(Vijgenboom et al., 1994)
Kirrothricin	<i>Streptomyces cinnemoneus</i>	(Cappellano et al., 1997)
Efrotomycin	<i>Nocardia lactamdurans</i>	(Dewey et al., 1985)
GE2770A	<i>Planobispora roaea</i>	(Selva et al., 1991b)
Pulvomycin	<i>Streptoverticillium mobaraense</i> , <i>Streptomyces albosporeus</i> var. <i>labilomyceticus</i> .	(Assmann and Wolf, 1979)
Pulvomycin	<i>Streptoverticillium netropsis</i>	(Zief et al., 1957)
Factumycin	<i>Kitasatospora setae</i>	(Ichikawa et al., 2010)
Factumycin	<i>Streptomyces</i> sp. WAC5292	(Thaker et al., 2012)
L-681,217	<i>Streptomyces cattleya</i>	(Kempf et al., 1986)
Enacyloxin II a	<i>Frateuria</i> sp. W-315	(Watanabe et al., 1992)
Phenelfamycins A and B	<i>Streptomyces sulphureus</i>	(Yarlagadda et al., 2020)
Phenelfamycins A - F	<i>Streptomyces violaceoniger</i>	(Hochlowski et al., 1988)
Phenelfamycins G and H	<i>Streptomyces albospinus</i>	(Brötz et al., 2011)

3.2 Results

3.2.1 Kirromycin-like elfamycin biosynthetic gene clusters share a conserved structure.

To expand knowledge of kirromycin-like Elfamycin biosynthesis and enzyme evolution among similar BGCs, the core BGCs of elfamycins must first be explored. Genome sequences from kirromycin-like elfamycin producers; *Streptomyces collinus*, *Kitasatospora setae* and *Streptomyces cattleya* were retrieved from NCBI. The core elfamycins produced from these strains and their associated references were analysed (Table 3A). Genomes of the three kirromycin-like producing strains were analysed on AntiSMASH (Blin et al., 2021) using 'strict' parameters to mine the genome for its biosynthetic potential. These strict parameters instruct AntiSMASH software only to detect well-defined clusters containing all required parts, increasing the likelihood of retrieving the full elfamycin BGC from these strains. For all three *Streptomyces* strains, a kirromycin-like BGC was found when AntiSMASH utilised the MIBiG Database for known cluster comparisons (Blin et al., 2021; Medema et al., 2015). The model kirromycin producer, *Streptomyces collinus*, possess the BGC kirromycin BGC with the MIBiG database (cluster number BGC0001070). The genomes of *Kitasatospora setae* and *Streptomyces cattleya* were also found to possess kirromycin-like BGCs with an 84% and 42% gene similarity respectively, to the kirromycin BGC from *S. collinus* on the MIBiG database. It is important to note that this gene similarity value considers coverage of the query sequence with respect to the reference BGC from MIBiG. Therefore, if a query BGC putatively encoding production of a natural product is part of a larger supercluster, the gene similarity score can be much lower than expected, even if all components of the putative BGC are present compared to the reference cluster. This is because only one part of the

supercluster may encode the BGC identified on MiBIG. This has been observed for the BGCs of other kirromycin-like elfamycins such as that of aurodox.

The aurodox BGC forms part of a biosynthetic supercluster, which also possesses the gene clusters of bottromycin A2 and concanamycin was found to be 40% similar to the BGC of kirromycin from *S. collinus* (McHugh, 2020). Upon dissection of the boundaries of the aurodox biosynthesis genes, however, this gene similarity of the two BGCs was found to be >60% (McHugh et al., 2022).

The structural similarity of the kirromycin-like elfamycin molecules is reflected in the biosynthetic genes encoding their production. Using clinker.pi, a visual representation of the architecture of the related BGCs was created. This allows visualisation of not only genes responsible for biosynthesis of the kirromycin-like elfamycins, but also the architecture of the BGC and gives an indication homology that may occur between gene clusters. All three known producers possess a NRPS/PKS arrangement of six genes which is highly conserved (Fig. 3.1). These six multimodular megasynthases (KirAI-AVI/FactAI-FactAVI) are the core genes responsible for the synthesis of the backbone of the kirromycin-like elfamycins, where additional tailoring enzymes drive their structural diversity (Thaker et al., 2012; Weber et al., 2008). The architecture of the BGCs varies between the three producing strains. Where the kirromycin and L-681,217 BGCs follow a PKS/NRPS arrangement followed by the tailoring genes, the factumycin gene cluster is inverted with the tailoring genes being upstream of the PKS/NRPS genes of FactAI-AVI, shown in the architectural inversion (Fig. 3.1).

Examination of the homology between the BGCs, and subsequently the function of genes in relation to structure (Table 3B) shows percentage amino acid similarity of the BGCs of L-681,217 and factumycin to kirromycin. The first gene in the kirromycin BGC is *KirP*, this encodes the biosynthesis of a Phosphopantetheinyl transferase (shown in red, Fig. 3.1). These enzymes are usually required to attach a phosphopantetheine prosthetic group to carrier proteins of PKS and NRPS enzymes,

which would fit with its location before the NRPS/PKS cascade of KirAI-AVI (Lambalot et al., 1996). KirP has a homolog in the L-681,217 BGC, with a % amino acid similarity of 31.28%. there is, however, no PPTase present on the BGC of factumycin (Fig. 3.1, Table 3B). Pavlidou et al., (2011) demonstrated that an inactivation of KirP led to the reduction of kirromycin produced by 19% (Pavlidou et al., 2011), this suggests that *K. setae* may not be producing factumycin to its full potential and that complimenting the strain with a further PPTase may result in greater factumycin production.

Two other genes from the kirromycin BGC do not have orthologs in the factumycin BGC. These are KirHVI and KirE, located at the end of the kirromycin BGC (shown in grey in Fig. 3.1, and red in Table 3B). These genes are proposed to encode a phytanoyl-CoA hydroxylase and an acetyltransferase belonging to the GNAT family (Weber et al., 2008). When compared to the kirromycin BGC, the factumycin BGC contains one additional gene absent from the kirromycin BGC, *FacMIII*. This was predicted to encode a methyltransferase and is consistent with the requirement for N-methylation of the pyridone ring in factumycin (shown in grey in Fig. 3.1 and green in Table 3B).

When compared to kirromycin, the BGC of L-681,217 is missing a number of homologous genes including all the ORFS annotated as encoding hypothetical proteins present on the kirromycin BGC, KirHI-HVI, the crotonyl CoA reductase encoded by *KirN*, the GNAT family acetyltransferase encoded by *KirE*, and most structurally important, KirB and KirD, the NRPS and aspartate 1-decarboxylase precursor responsible for the cyclisation of the terminal pyridone ring of kirromycin (Weber et al., 2008) and factumycin (FacB and FacD). Remarkably, it was shown that the presence of pyridone ring in elfamycins does not contribute to the antimicrobial activity of the molecule (Hall et al., 1989).

L-681,217 has additional genes not present in the other two BGCs. Both kirromycin and factumycin BGCs lack a thioesterase, required for cleaving the molecule from the

protein complex, a thioesterase is present on the BGC of L-681,217 at gene position three, named for the purposes of this study as L-T, (Fig. 3.1 and Table 3B). The kirromycin and Factumycin BGCs were found to lack a thioesterase, however bioinformatic analyses suggested that KirHI and FacHI were putative Dieckmann cyclases that drive tetramic acid and pyridone scaffold biosynthesis (Gui et al., 2015). These act as an alternative to a thioesterase and allow the biosynthesis of kirromycin and factumycin to continue. Weber et al., (2008) hypothesised that in the case of kirromycin biosynthesis, the aspartate-1-decarboxylase, KirD, was able to provide the non-proteogenic amino acid β -alanine precursor which was required for the closure of the pyridone ring and the final step of condensation, catalysed by the NRPS KirB (Weber et al., 2008). Later work from Thaker et al., (2012) suggested that similar to this, the formation of the pyridone ring in factumycin achieves cleavage of the molecule from the NRPS/PKS complex without the requirement for a thioesterase such as L-T. The presence of L-T and absence of a homolog to Kir/FacD and B in the gene cluster of L-681,217 correlates with the lack of the terminal pyridone ring in this compounds structure. Though there is no thioesterase present on the kirromycin or factumycin BGCs, more recent studies suggest that Kir/FacHI has the ability to act as a thioesterase alternative by facilitating Dieckmann cyclisation during kirromycin and factumycin biosynthesis (Gui et al., 2015). This action is likened to Kir/FacB, where the conserved gene cassette enables the formation of the pyridone rings present in both structures. Other additional genes of L-681,217 include *l-sam*, a S-adenosylmethionine synthase and a second LuxR family transcriptional regulator, *l-RII*. Where a role of these genes could be responsible for producing and regulating the provision of methyl-donors for each of the methylation steps required for biosynthesis on the backbone of the elfamycins.

Finally, towards the end of the L-681,217 BGC, there is a gene which is predicted by BLASTp to encode an exported protein of unknown function, L-HI. Not only does this

gene have no homolog in either of the kirromycin-like BGCs compared to kirromycin and factumycin, but it also retrieves no hits from the NCBI BLASTp database. The FASTA amino acid sequence of L-HI was subject to further analysis to determine if the protein is likely to be destined towards the secretory pathway. Signal peptides are short amino acid sequences in newly synthesised proteins that target proteins into, or across, membranes. Using SignalP (version 5.0, accessible at <https://services.healthtech.dtu.dk/services/SignalP-5.0/>), the presence of signal peptides and the location of their associated cleavage sites were analysed for L-HI (Almagro Armenteros et al., 2019). L-HI was predicted to contain a TAT signal peptide, used to direct proteins to the Tat translocon. This is supported by the presence of the characteristic twin-arginine motif in the N-region (Berks, 1996). The hidden Markov model calculates the probability of whether the submitted sequence contains a signal peptide or not, where probability values close to 1.0 have a high probability (Eddy, 2004). SignalP predicted the probability of the presence of a TAT signal peptide was 0.4036, a value which is low confidence. The cleavage site for the signal peptide was predicted to be between position 30 and 31 of the peptide at a probability score of 0.0875, also low confidence. Given the nature of the protein and the low confidence in the SignalP values, it is unlikely this is a secreted protein.

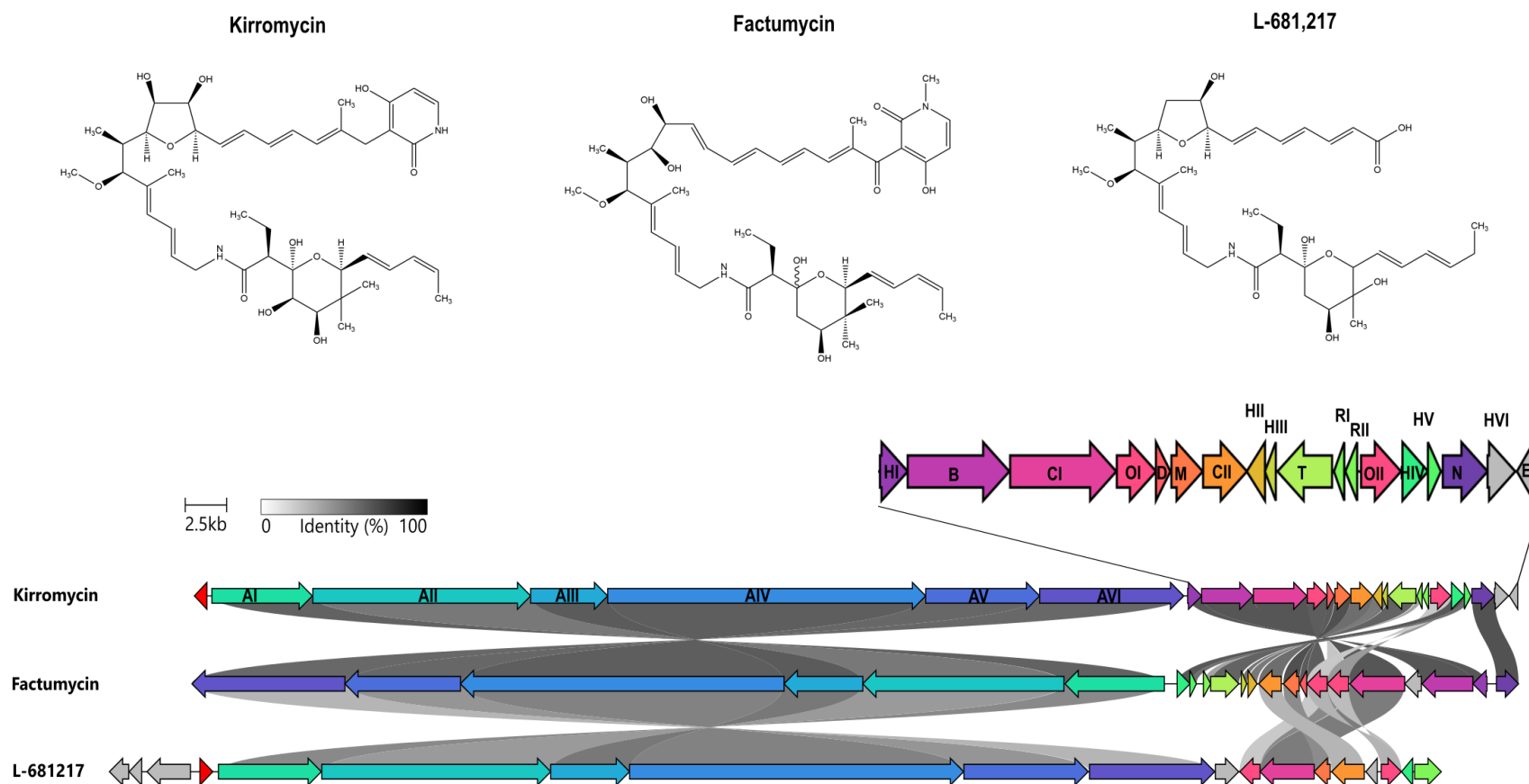


Figure 3.1: Elfamycin chemical structure is similar, while the architecture of the biosynthetic gene clusters encoding their production is highly dynamic. Adjoining lines represent amino acid similarity according to scale. Grey genes represent those with no homolog in other kirromycin-like BGCs. Figure generated by clinker.py using FASTA files of the elfamycin BGC's.

Table 3B: Percentage amino acid similarity of Elfamycin biosynthesis genes.

Factumycin from *K. setae* and L-681217 from *S. cattleya* were compared to kirromycin from *S. collinus* by BLASTp to determine % similarity. Red indicates the absence of gene from a cluster, green indicate the addition of the gene to the cluster.

Gene function	% AA similarity		
	<i>S. collinus</i> (Kirromycin)	<i>K. setae</i> (Factumycin)	<i>S. cattleya</i> (L-681,217)
S-adenosylmethionine synthetase			L-Sam
Alpha/beta fold hydrolase			L-T
LuxR family transcriptional regulator			L-RII
Phosphopantetheinyl transferase	KirP		31.28
Trans-AT type PKS	KirAI	69.42	52.31
Trans-AT type PKS	KirAII	67.27	51.98
Hybrid NRPS/PKS	KirAIII	71.13	59.29
Trans-AT type PKS	KirAIV	69.82	56.10
Trans-AT type PKS	KirAV	67.41	49.88
Cis-AT type PKS	KirAVI	70.13	42.27
Asp-tRNA(Asn)/Glu-tRNA(Gln) amidotransferase subunit GatA			L-Gat
Hypothetical protein (Dieckmann cyclase)	KirHI	74.82	
Nonribosomal peptide synthase	KirB	73.75	
N-methyltransferase		FacII	
Acyltransferase	KirCI	73.81	59.47
Cytochrome P450 hydroxylase	KirOI	73.28	48.86
Aspartate 1-decarboxylase precursor	KirD	74.10	
Methyltransferase	KirM	75.32	53.77
Acyltransferase	KirCII	65.19	52.55
Exported protein of unknown function			L-HI
Hypothetical protein	KirHII	61.67	
Hypothetical protein	KirHIII	61.82	
Major facilitator superfamily transporter N-terminus	KirTII/ KirTII	69.77	47.73
Transcriptional regulatory protein, TetR family, N-terminus	KirRI	65.18	62.38
Transcriptional regulatory protein, TetR family, C-terminus	KirRII		
Cytochrome P450 hydroxylase	KirOII	52.15	40.98
Hypothetical protein	KirHIV	72.94	
Hypothetical protein	KirHV	64.62	
Crotonyl CoA reductase	KirN	79.68	
Hypothetical protein (phyH)	KirHVI		
Acetyltransferase, GNAT family	KirE		

3.2.2 Characterisation of key kirromycin-like Elfamycin producing strains.

Elfamycin molecules have been found to be produced by more than one strain. This has been shown for *Streptomyces collinus* and *Streptomyces ramocissimus* which both produce kirromycin (Vijgenboom et al., 1994; Wolf et al., 1972).

Similar to these kirromycin BGCs, the aurodox BGC of *Streptomyces goldiniensis*, is highly homologous to the BGC responsible for the production of kirromycin, sharing 23/25 genes although different final products are produced. The BGC for aurodox possesses an additional hypothetical protein, AurQ and an additional Sam dependant methyltransferase, AurM* which was shown to methylate the pyridone ring of aurodox, responsible for the only structural difference from kirromycin (McHugh et al., 2022).

To further understand the production and evolution of kirromycin-like elfamycins, three bacterial species, *S. collinus*, *S. ramocissimus* and *S. goldiniensis* are further characterised below.

To characterise the gross morphology of these three *Streptomyces* species, they were grown on Mannitol Soya Flour (MS) agar for 10 days (Fig. 3.2). MS medium is a complex medium used for the routine cultivation of *Streptomyces* sp. As most species have been documented to sporulate well on this medium (Kieser et al., 2000). Following incubation, colonies were observed, and the presence of mature spores evaluated.

The strains possess a pale grey spore colouration, forming ‘volcano-like’ colonies. Upon analysis of the plate, it is also apparent that the strains are all producing a golden-brown pigment which can be observed in the area surrounding a single colony of each *Streptomyces* strain present in the agar. Much like other Elfamycin producing strains, it is often observed that gold pigments are produced due to the goldinonic acid component of the molecules the strain produces (Vogelely et al., 2001, Fig. 1.11). Here, the pigment being produced could be the elfamycin compound kirromycin, in

the case of *S. collinus* and *S. ramocissimus*; or aurodox, in the case of *S. goldiniensis*, where both compounds contain goldinonic acid. Finally, the spores of *S. collinus*, when plated with *S. ramocissimus* and *S. goldiniensis*, are much darker than that when it is clustered alone, suggesting that a pigment such as melanin could be produced. The genome of *S. collinus* possesses a BGC responsible for the production of melanin alongside other spore pigments and so activation of this BGC in this case is likely (Iftime et al., 2016).

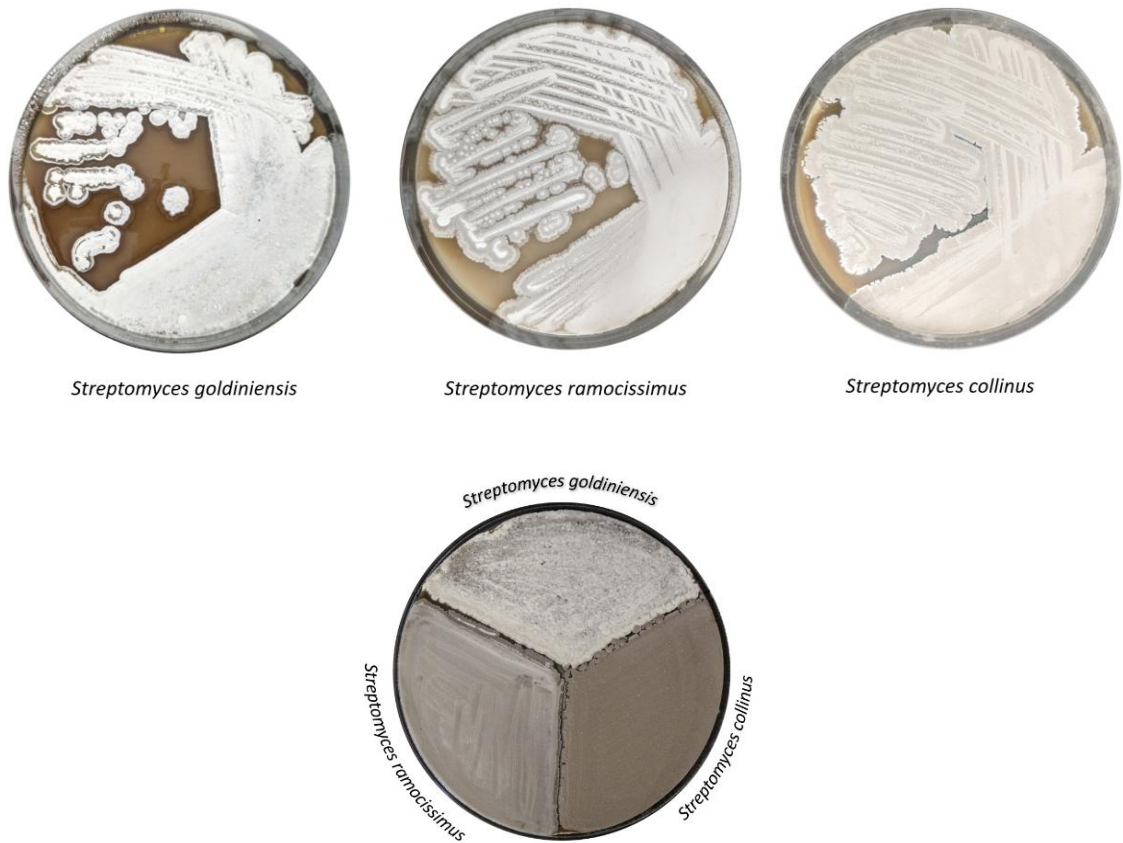


Figure 3.2: A gold pigment can be observed around colonies of *Streptomyces goldiniensis*, *Streptomyces collinus* and *Streptomyces ramocissimus* when grown on MS agar. Strains were grown on MS agar for 10 days at 30 °C until sporulation was achieved, and the plate imaged.

To determine whether the gold-brown pigments produced by the strains were elfamycin antibiotic compounds, the bioactivity of these strains on MS agar was assessed by agar plug bioassays of the three strains against the six clinically relevant ESKAPE pathogens, *Enterococcus faecium*, *Staphylococcus aureus*, *Klebsiella pneumoniae*, *Acinetobacter baumannii*, *Pseudomonas aeruginosa*, and *Enterobacter spp.* (Mulani et al., 2019). At the time of study, *Enterobacter spp.* were not available and so *Escherichia coli* was used instead.

Of the six ESKAPE pathogens tested against, bioactivity of the three *Streptomyces* strains was observed against *Staphylococcus aureus* and *Klebsiella pneumoniae*, when the strains were grown on MS agar (Fig. 3.3).

Zones of inhibition were observed in *S. aureus* growth surrounding MS agar plugs of *S. goldiniensis* ($P = 0.038$), *S. collinus* ($P = 0.001$), and *S. collinus* ($P = 0.014$), when compared to the MS agar media control. The same was observed for *S. aureus*, where zones of growth inhibition were observed for *S. goldiniensis* ($P = 0.019$) and *S. ramocissimus* ($P = 0.035$), when compared to the MS agar media control. No bioactivity was observed from *S. collinus* against *S. aureus*, suggesting that insufficient quantities of bioactive compounds were produced by *S. collinus* on MS agar for the inhibition of *S. aureus* growth (Fig. 3.3).

Due to their susceptibility to metabolites produced by these organisms, *S. aureus* and *K. pneumoniae* will be used through the duration of this thesis as the bacterial indicator organisms when assessing the bioactivity of elfamycin producing strains.

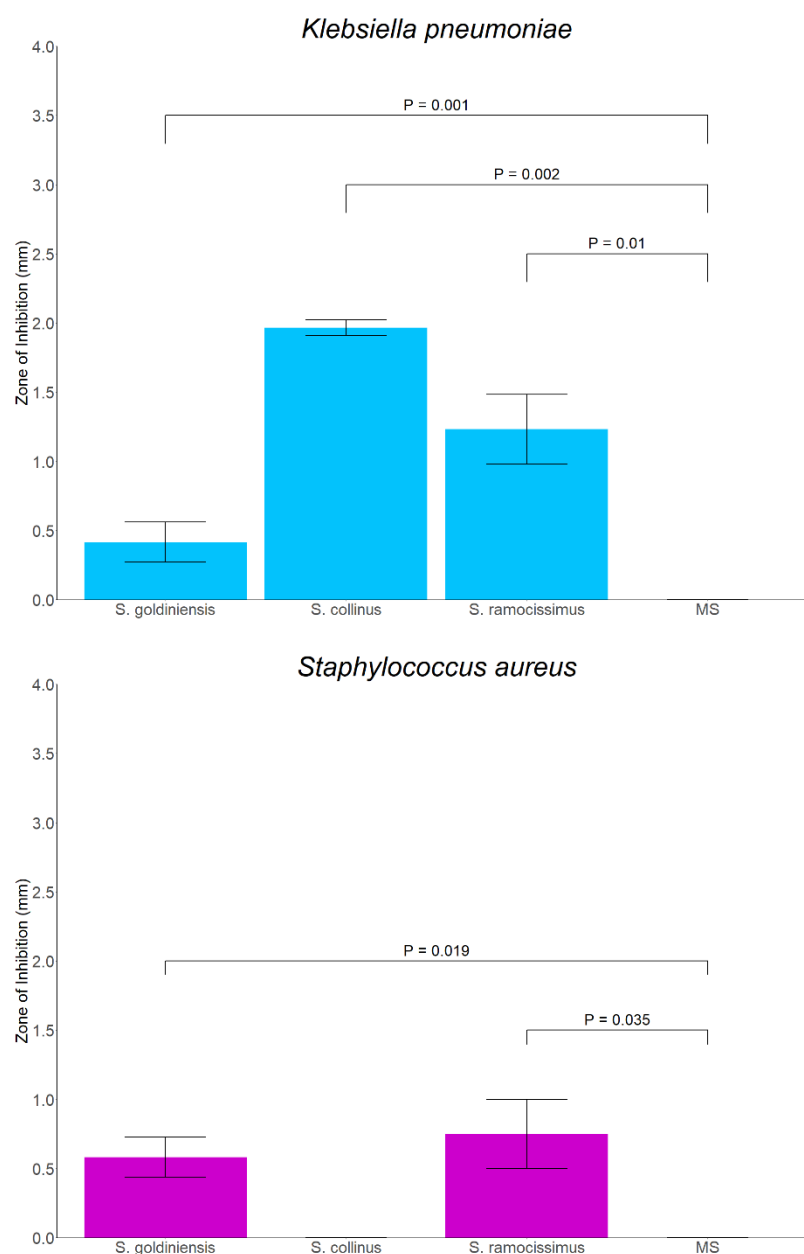


Figure 3.3: Elfamycin-producing *Streptomyces* inhibit the growth of both Gram-positive and Gram-negative pathogens. *Streptomyces* strains were grown for 10 days on MS agar at 30°C until sporulated. Agar plugs of each strain were plated on indicator strains, *Staphylococcus aureus* ATCC 43300 and *Klebsiella pneumoniae* ATCC 700603, which were normalised to an OD₆₀₀ of 0.01 in soft nutrient agar. Assay plates were grown for 12 hours at 37°C and zones of inhibition were measured in mm with a ruler.

To understand the growth of the bacteria strains in liquid culture, the three strains were grown in liquid GYM medium, a yeast and malt based medium supplemented with glucose, which is commonly used for the cultivation of *Streptomyces* species (Feeney et al., 2022). McHugh et al.,(2020) showed that *S. goldiniensis* was able to grow successfully in GYM liquid culture and so it was hypothesised that the other elfamycin producing *Streptomyces* species may grow in a similar fashion. Cell dry weight (mg/ mL) was measured to assess the growth of *Streptomyces* in liquid culture due to the 'gold standard' optical density measurement being inaccurate (Hobbs et al., 1989). As *Streptomyces* exhibit mycelial growth, and liquid culture is not always homogenous, therefore a representative sample of culture is weighed, and dry cell mass is assessed over triplicate samples in triplicate bacterial cultures.

It can be seen that in GYM liquid medium, *S. goldiniensis* and *S. ramocissimus* reach stationary phase at approximately 48 hours (Fig. 3.5 & Fig. 3.6), whereas *S. collinus* is much faster, reaching stationary phase at approximately 36 hours (Fig. 3.4). This is incredibly important as the data gathered here is used to assess the *Streptomyces* strains growth cycle, and in turn at which point during fermentation the strain reaches stationary phase, predicting the activation of secondary metabolism-linked gene expression. This onset of specialised metabolism occurs during the secondary metabolism phase of growth and is linked to the expression of specialised metabolite BGCs (de Lima Procópio et al., 2012).

During fermentation in GYM, the specific growth rates of the three *Streptomyces* strains were calculated based on the exponential growth phases, where the specific growth rate of *S. collinus* was found to be more than three-fold that of *S. goldiniensis* and 12-fold that of *S. ramocissimus* (Table 3C).

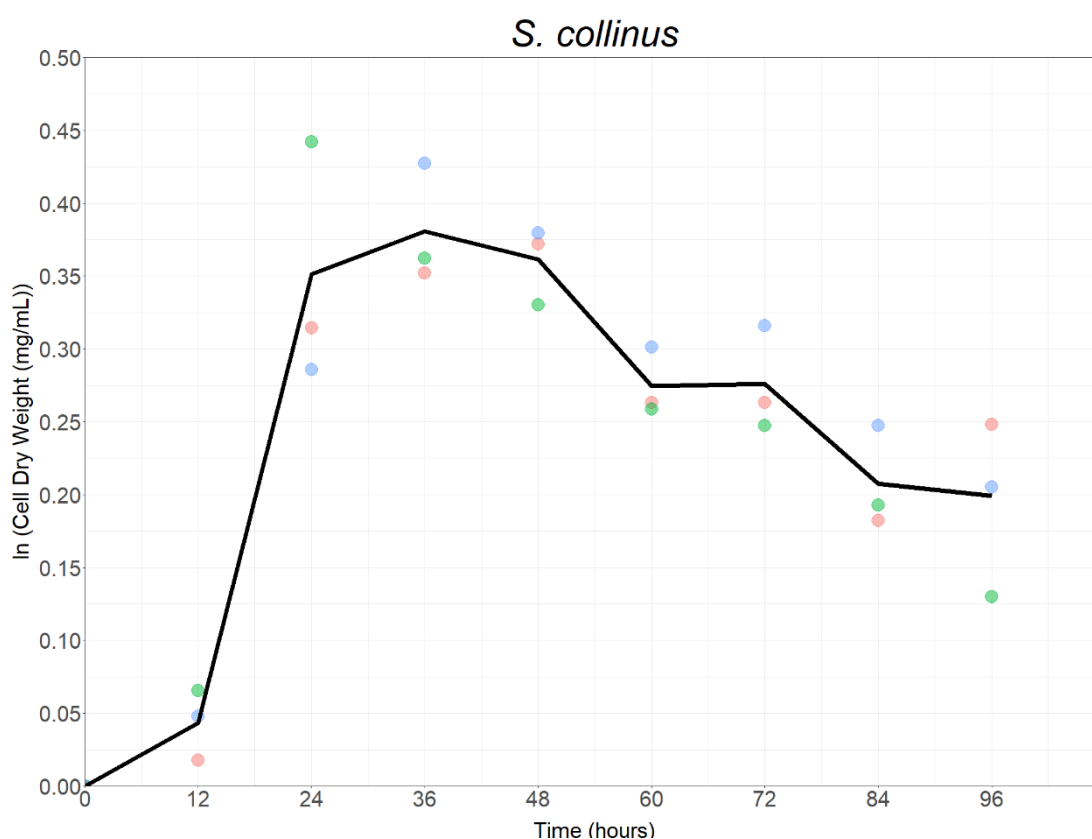


Figure 3.4: Gravimetric dry weight analysis of *Streptomyces collinus* growth in GYM liquid medium. Dry weight was determined through gravimetric separation of cell mass from media. The three strains were grown in triplicate flasks (200 rpm, 30 °C) from three separate bacterial colonies for biological replicates represented by red, blue and green dots. For each of the three strains, three technical representative samples were taken from each of three biological replicate flasks three flasks at each timepoint, where averages of these three technical replicates are plotted on this semi-log plot. Trendlines are indicated by the average of biological replicates.

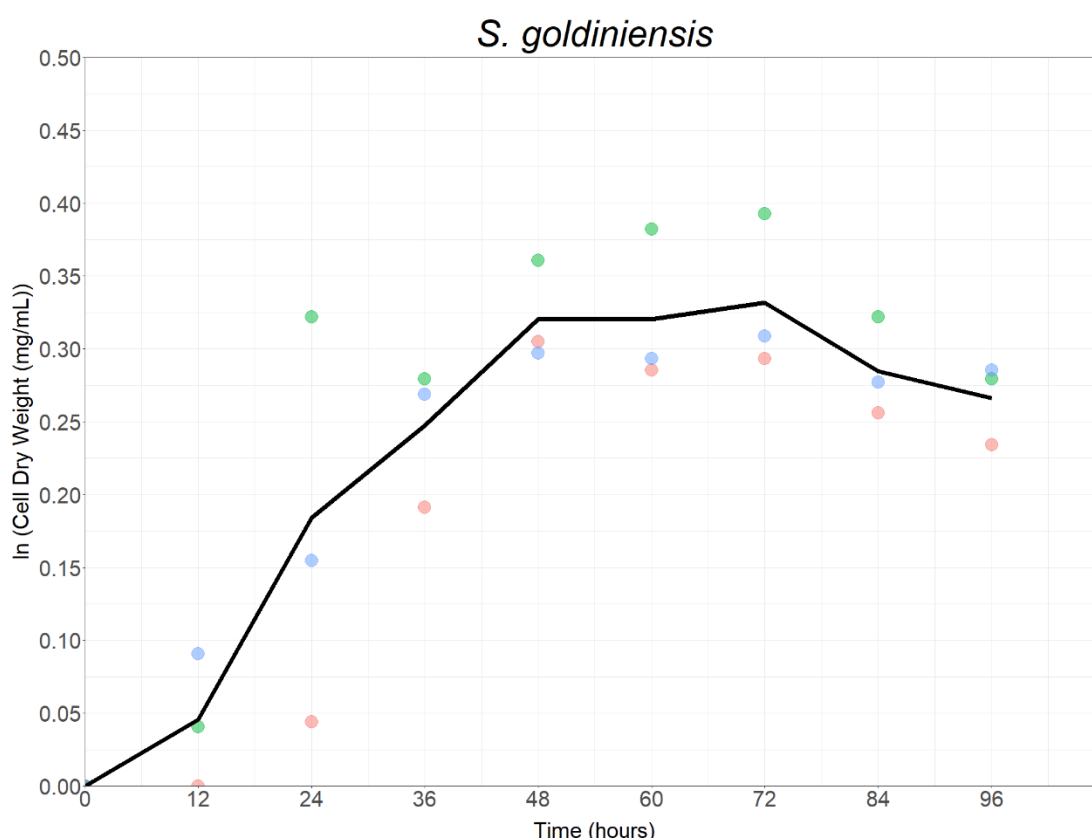


Figure 3.5: Gravimetric dry weight analysis of *Streptomyces goldiniensis* growth in GYM liquid medium. Dry weight was determined through gravimetric separation of cell mass from media. The three strains were grown in triplicate flasks (200 rpm, 30 °C) from three separate bacterial colonies for biological replicates represented by red, blue and green dots. For each of the three strains, three technical representative samples were taken from each of three biological replicate flasks three flasks at each timepoint, where averages of these three technical replicates are plotted on this semi-log plot. Trendlines are indicated by the average of biological replicates.

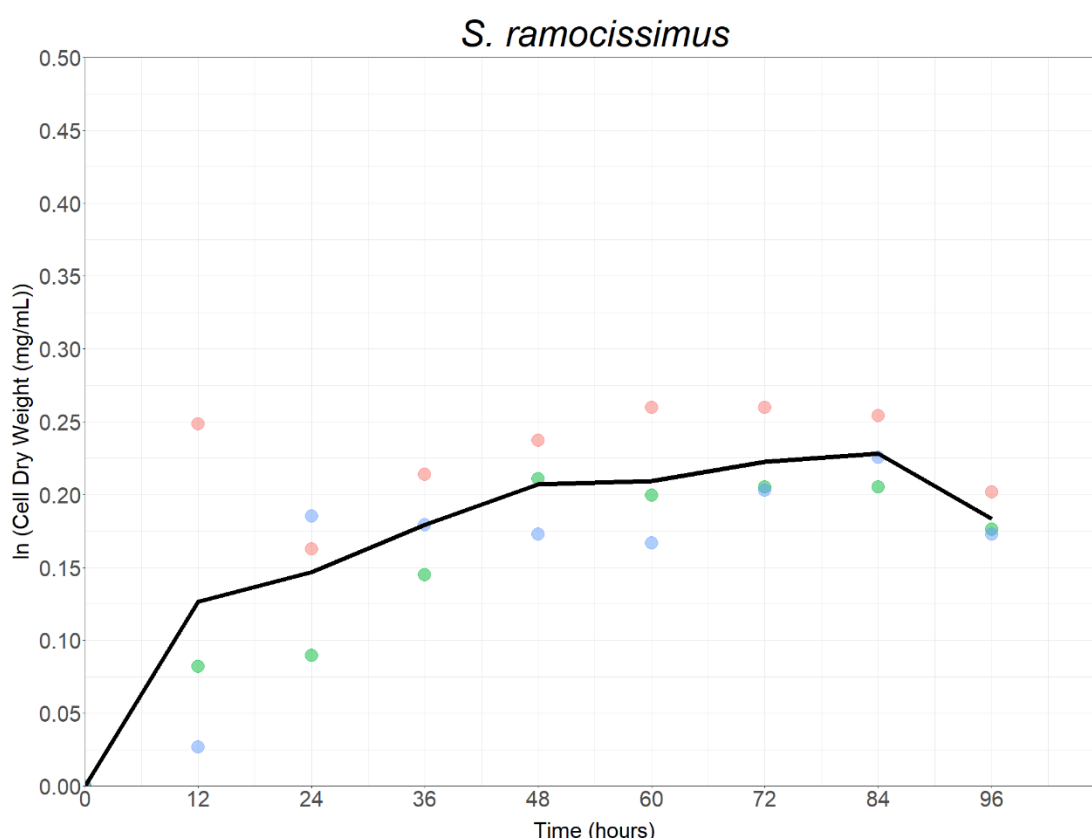


Figure 3.6: Gravimetric dry weight analysis of *Streptomyces ramocissimus* growth in GYM liquid medium. Dry weight was determined through gravimetric separation of cell mass from media. The three strains were grown in triplicate flasks (200 rpm, 30 °C) from three separate bacterial colonies for biological replicates represented by red, blue and green dots. For each of the three strains, three technical representative samples were taken from each of three biological replicate flasks three flasks at each timepoint, where averages of these three technical replicates are plotted on this semi-log plot. Trendlines are indicated by the average of biological replicates.

Table 3C: *Streptomyces collinus* has a higher specific growth rate than that of *Streptomyces goldiniensis* or *Streptomyces ramocissimus*. Specific growth rate was calculated based on the slope of the exponential growth phases of *Streptomyces* strains (Fig. 3.4, 3.5 & 3.6)

Strain	Specific growth rate (hour ⁻¹)
<i>Streptomyces goldiniensis</i>	0.05
<i>Streptomyces collinus</i>	0.17
<i>Streptomyces ramocissimus</i>	0.01

Culture supernatants from each of the *Streptomyces* strains after 3 days of growth were subject to solvent extraction with chloroform. The resulting extracts were prepared and analysed through bioassays and LC/MS and compared to authentic standards of aurodox and kirromycin (Hello Bio).

Aurodox was detected in the fermentation of *S. goldiniensis* in GYM, confirmed by the characteristic presence of a LC trace peak at approximately 7.7 minutes, in line with that of the aurodox standard (Fig. 3.8). The same can be observed when looking at the M/Z ratio of the *S. goldiniensis* fermentation in GYM compared to that of the aurodox standard which both possess a M/Z ratio of 793.4 (Fig. 3.8). *S. ramocissimus* and *S. collinus*, possess the same characteristic peak at a retention time of 7.5 minutes is comparable to that of the kirromycin standard, however only the fermentation of *S. ramocissimus* in GYM showed a corresponding peak from mass spectrometry with an M/Z ratio of 779.4 (Fig. 3.7 & Fig. 3.9).

Analysis of the bioactivity of the *Streptomyces* fermentation extracts in GYM media after 3 days was carried out against *S. aureus* and *K. pneumoniae* (Fig. 3.10). *S. goldiniensis*, the aurodox producer, showed bioactivity against both organisms, where the authentic aurodox standard (concentration of 1 mg/mL) was found to have more activity than the fermentation extract of *S. goldiniensis* against both *K. pneumoniae* ($P = 0.001$) and *S. aureus* ($P = 0.009$, Fig. 3.10).

For the kirromycin producer *S. ramocissimus* fermentations in GYM media, bioactivity was observed, but again the concentration produced in the fermentation broth was found to be lower than the authentic kirromycin standard (concentration of 1 mg/mL) from the fermentation extracts against *K. pneumoniae* ($P = 0.01$). In bioactivity assays with *S. aureus*, there was no significant difference in the bioactivity of the *S. ramocissimus* GYM fermentation extract when compared to the kirromycin standard ($P = 1.000$), suggesting that they inhibit the growth of *S. aureus* at a comparable level.

Though no kirromycin equivalent mass was detected in the extract of *S. collinus*, a peak at the correct retention time of approx. 7.5 minutes was shown (Fig. 3.7). In addition to this, bioactivity was observed from GYM fermentation extracts of *S. collinus* against both ESKAPE pathogens. The kirromycin standard (1 mg/mL) had greater bioactivity against *K. pneumoniae* ($P = 0.002$) and *S. aureus* ($P = 0.002$) than the *S. collinus* fermentation extract, even though bioactivity was observed (Fig. 3.10). Both LC/MS and bioactivity assays were performed using the same fermentation extracts, therefore it is unusual to observe bioactivity against the ESKAPE pathogens from *S. collinus* which seemingly does not produce kirromycin under these fermentation conditions. One explanation for this could be that due to the specific growth rate of *S. collinus* being higher than that of the other two strains, kirromycin within the fermentation may start to degrade over time. During this analysis, bioactivity analysis was carried out the same day as solvent extraction however the extracts for LC/MS were stored prior to analysis and so degradation of the sample could be likely here. Another explanation could be that the BGC of kirromycin is not activated under these fermentation conditions, and that another BGC present of the genome of *S. collinus* may be accounting for the strain's bioactivity against the ESKAPE pathogens after solvent extraction. Another interpretation could be that chloroform extraction at a different pH could allow for the kirromycin to be detected and that in this case, perhaps a sub optimal pH was used causing the kirromycin to remain within the aqueous phase. Of the 32 BGCs present on the genome of *Streptomyces collinus*, one is responsible for the production of pentalenolactone, a sesquiterpene antibiotic that exhibits various biological activities which include diverse antibacterial and antifungal activity, as well as potent inhibitory activity toward the glycolytic enzyme glyceraldehyde 3-phosphate dehydrogenase (Iftime et al., 2016). The activation this BGC and production of this sesquiterpene antibiotic could be responsible for the bioactivity observed, other than that from the kirromycin BGC.

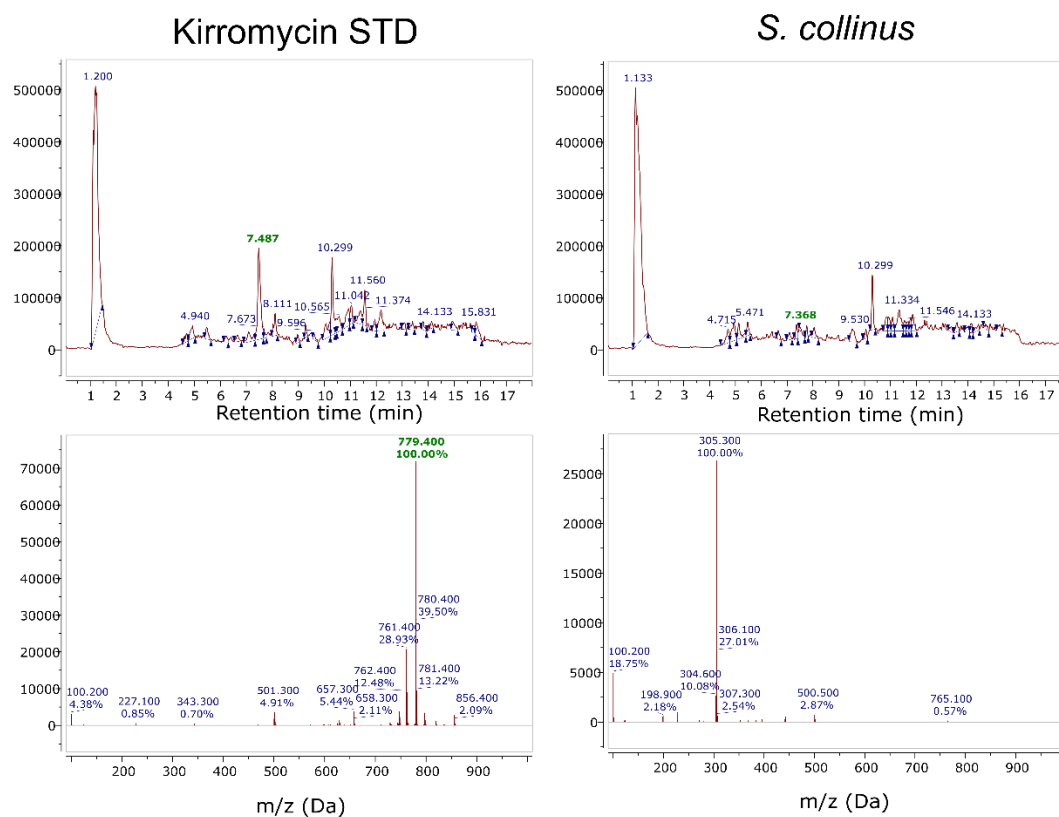


Figure 3.7: Total ion Chromatograms from HPLC indicate the correct retention time of kirromycin present in fermentation extracts of *Streptomyces collinus*. Culture supernatants from *Streptomyces collinus* were subject to solvent extraction with chloroform after 3 days of growth (200 rpm, 30 °C). Kirromycin standard was purchased from Hello Bio, diluted to 1 mg/ mL and has a retention time of approx. 7.5 minutes, and a corresponding M/Z ratio of 779.4.

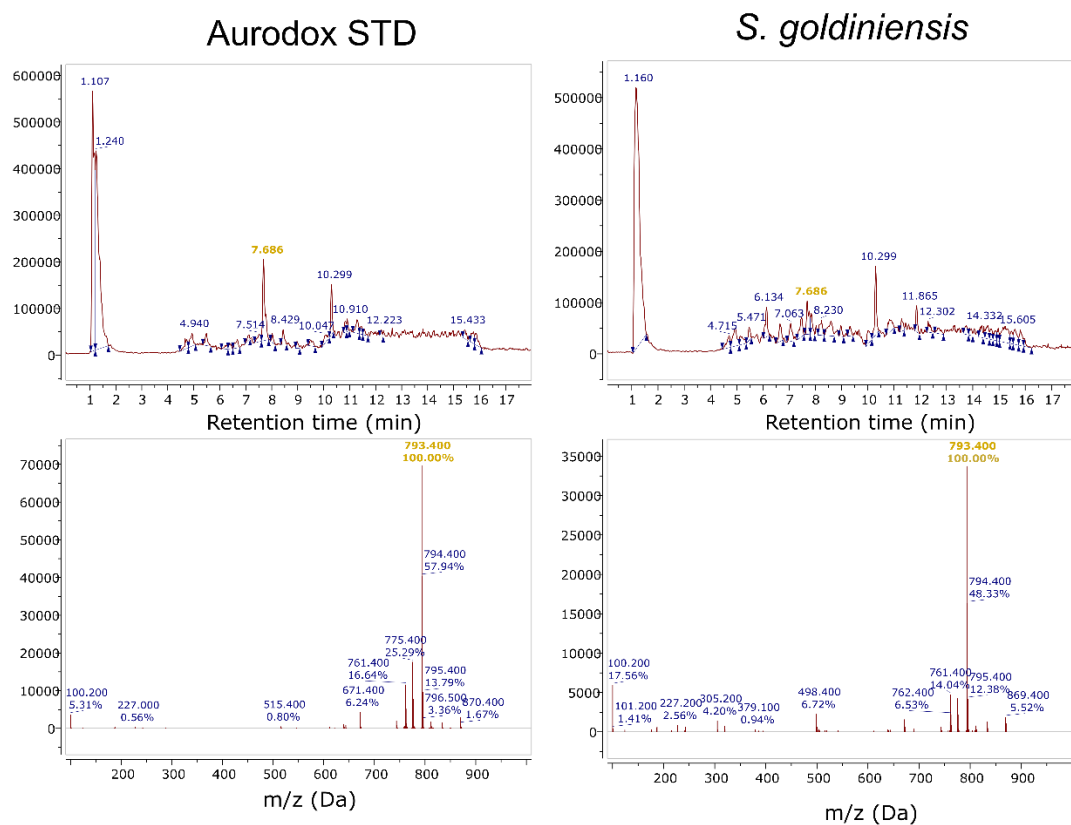


Figure 3.8: Total ion Chromatograms from HPLC indicate the presence of aurodox in fermentation extracts of *Streptomyces goldiniensis*. Culture supernatants from *Streptomyces goldiniensis* were subject to solvent extraction with chloroform after 3 days of growth (200 rpm, 30 °C). Aurodox standard was purchased from Hello Bio, diluted to 1 mg/ mL and has a retention time of approx. 7.7 minutes, and a corresponding M/Z ratio of 793.4.

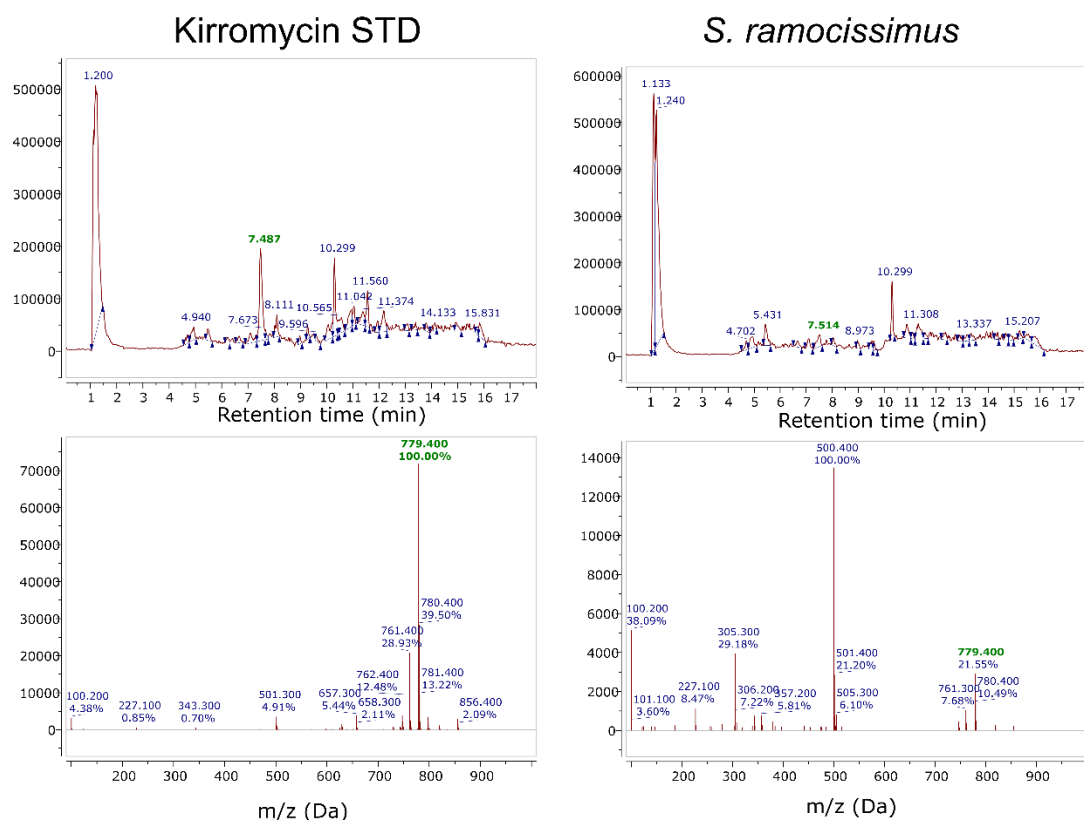


Figure 3.9: Total ion Chromatograms from HPLC indicate the presence of kirromycin in fermentation extracts of *Streptomyces ramocissimus*. Culture supernatants from *Streptomyces ramocissimus* were subject to solvent extraction with chloroform after 3 days of growth (200 rpm, 30 °C). Cultures were centrifuged at 4200 x g for 20 minutes, and the supernatant was filter-sterilized. The supernatant was mixed with chloroform, and the lower solvent phase was collected and dried under nitrogen or with a Rotavapor™. Extracts were dissolved in 100% DMSO and analysed by LC-MS using an Agilent 1100 HPLC system and Waters Micromass ZQ 2000/4000 mass detector. RP-HPLC was performed on a Zorbax C18 column, with ammonium acetate buffers and UV detection at 254 nm. Electrospray ionization (ESI) was used for both positive and negative modes (100-1000 AMU positive, 120-1000 AMU negative). Kirromycin standard was purchased from Hello Bio, diluted to 1 mg/ mL, retention time of approx. 7.5 minutes, and a corresponding M/Z ratio of 779.4.

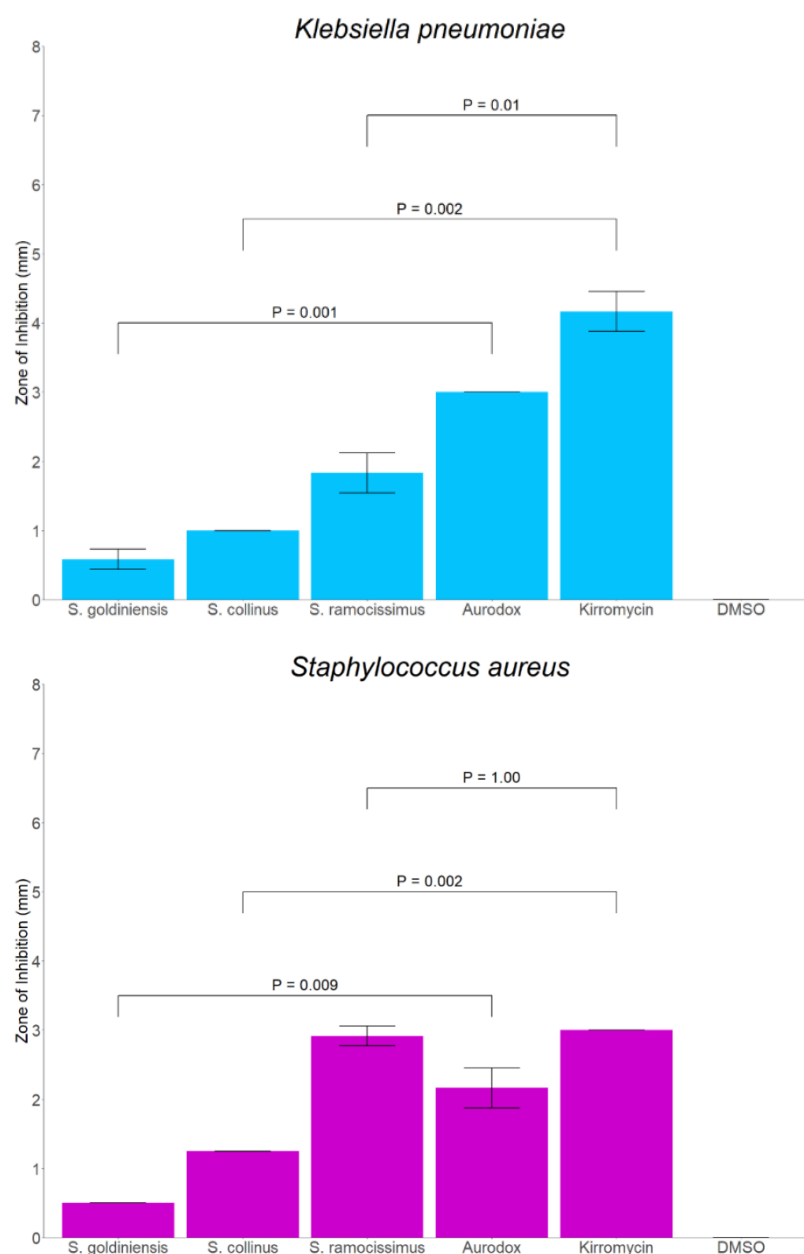


Figure 3.10: Disc diffusion bioassays against Gram-positive and Gram-negative pathogens indicate the production of elfamycins in fermentation extracts from elfamycin producing *Streptomyces*. *Streptomyces* fermentation extracts (GYM liquid media, 30°C, 3 days, 200 rpm) were added to paper discs and plated on indicator strains, *Staphylococcus aureus* ATCC 43300 and *Klebsiella pneumoniae* ATCC 700603, which were normalised to an OD₆₀₀ of 0.01 in soft nutrient agar. Assay plates were grown for 12 hours at 37°C and zones of inhibition were measured in mm with a ruler.

For *Streptomyces goldiniensis* and *Streptomyces collinus*, production of their Elfamycin compounds is well documented. McHugh et al., (2020) showed that in extracts taken from 50 mL *S. goldiniensis* shake-flask cultures, aurodox was not detected until 154 hours of growth in GYM liquid media. This was confirmed by a characteristic 7.2 minute peak in the HPLC trace, in addition to detection of the aurodox mass in the negative and positive scans from Mass Spectrometry and the onset of bioactivity (McHugh, 2020). Similarly, *Streptomyces collinus* was found to produce kirromycin after two days of growth in pre-culture medium (TSB) then subsequent passage 5 mL of the pre-culture into kirromycin production medium and grown for six days prior to a 1:1 ethyl acetate extraction. The corresponded retention time of kirromycin in this study was 12.2 minutes due these authors using a different LC-MS set up, and an M/Z ratio for kirromycin (795.4) was obtained (Robertsen et al., 2018). With a M/Z ratio of 779.4, it is likely that the kirromycin detected here has lost a neutral fragment, such as a methyl group, resulting in a lower M/Z ratio.

Remarkably, the production of kirromycin from *S. ramocissimus* is not widely documented. The growth phases and specific growth rate of *S. ramocissimus* in GYM are shown (Fig. 3.6, Table 3C, Fig. 3.9). Chloroform extraction throughout growth of *S. ramocissimus* were prepared and analysed through bioassays and LC-MS in order to establish the kirromycin production phase. During analysis of the fermentation extracts, the mass for kirromycin (779.4) was first detected in the fermentations of *S. ramocissimus* in GYM media at 48 hours, with the greatest production of the compound and the highest HPLC peak obtained at 72 hours (Fig. 3.11). These data correspond to the bioactivity of the fermentation extracts, where inhibition of *K. pneumoniae* begins at 48 hours (Fig. 3.12). For both *K. pneumoniae* and *S. aureus*, the greatest inhibition of growth was during 72 hours, where according to the mass spectrometry data (Fig. 3.11), production of kirromycin peaked.

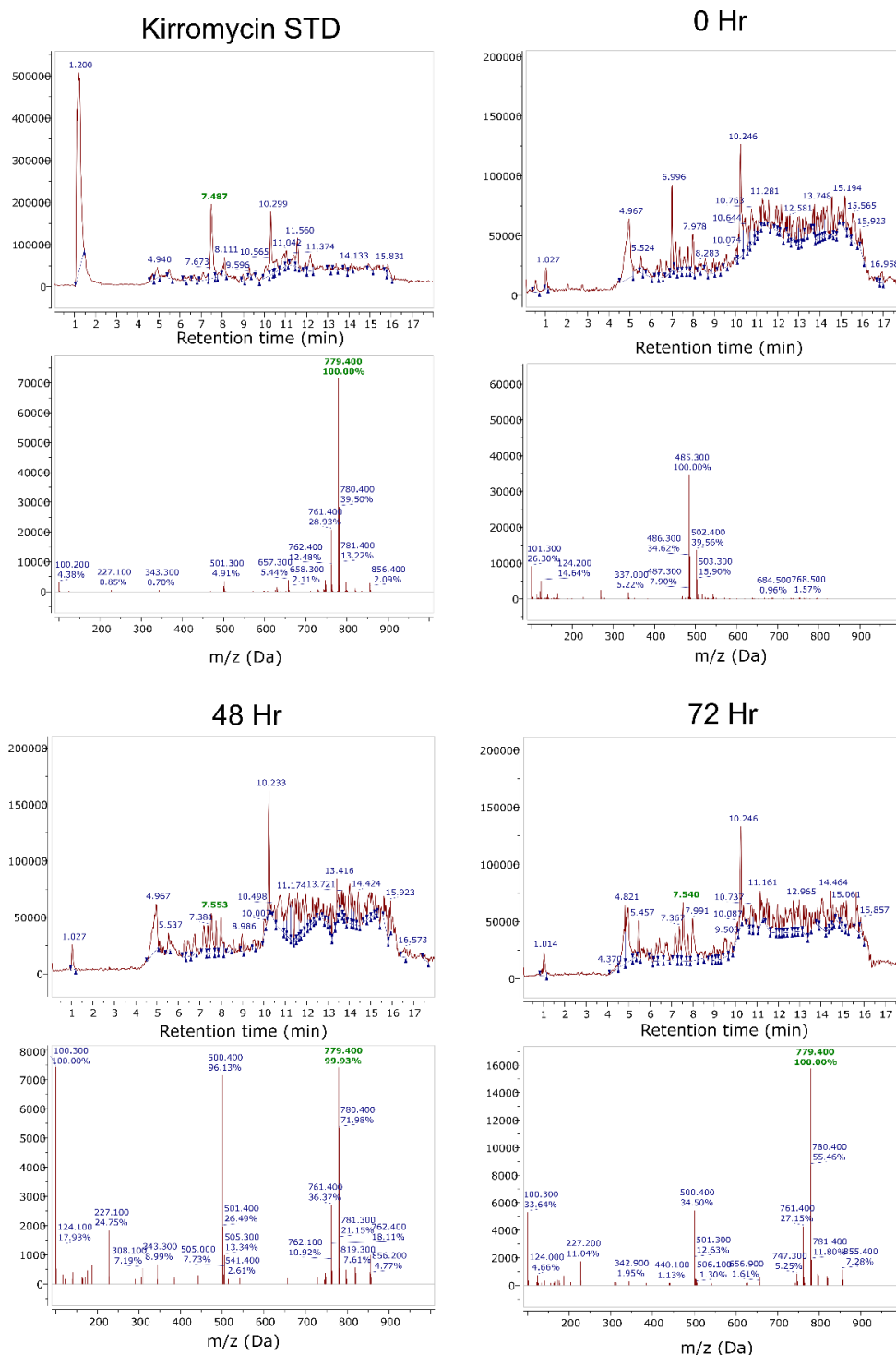


Figure 3.11: Total ion Chromatograms from HPLC indicate the production of kirromycin at 48 hours of growth, with the highest production at 72 hours. Cultures were processed for analysis as per methods (2.5.2 & 2.5.2) Kirromycin standards were purchased from Hello Bio, diluted to 1 mg/ mL and have a retention time of 7.5 minutes, and a corresponding M/Z ratio 779.4.

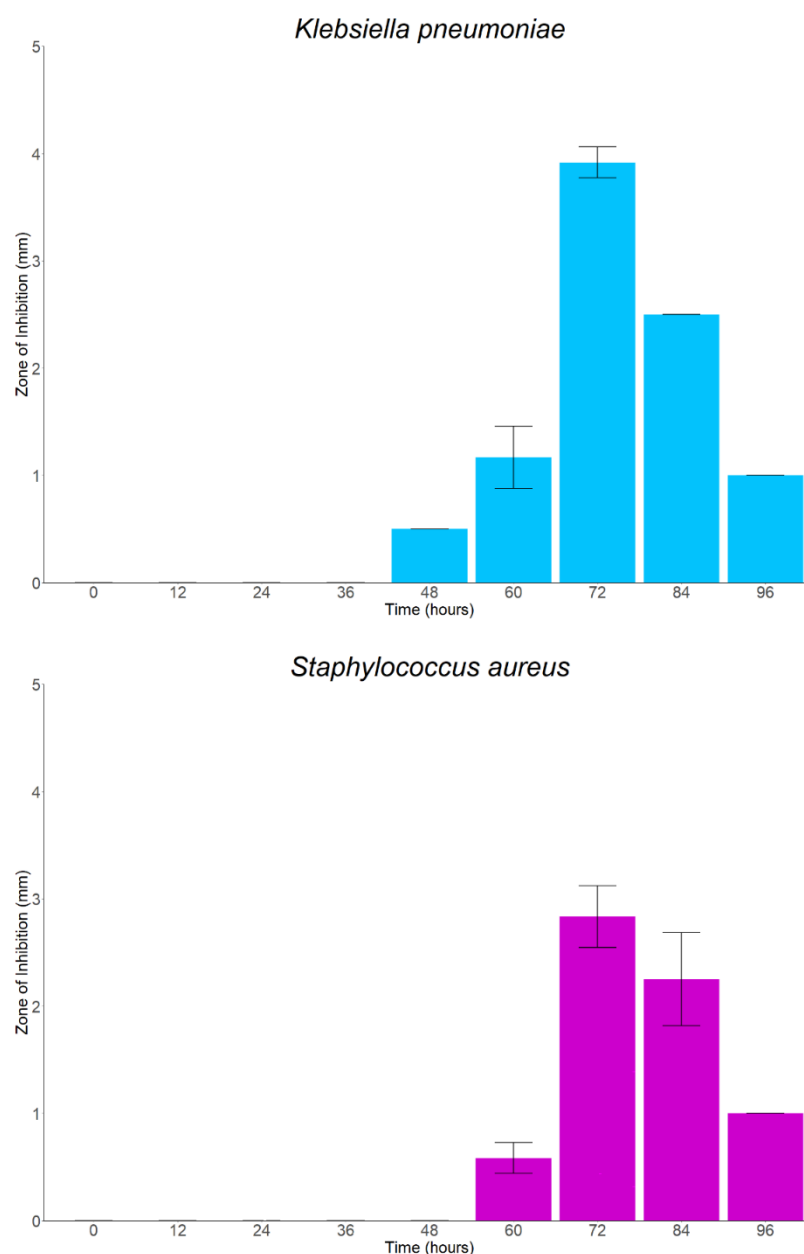


Figure 3.12: Bioactivity of fermentation extracts against Gram-positive and Gram-negative pathogens indicate that kirromycin production peaks at 72 hours of *S. ramocissimus* growth in GYM liquid media. *Streptomyces* fermentation extracts (GYM liquid media, 30°C, 200 rpm) were added to paper discs and plated on indicator strains, *Staphylococcus aureus* ATCC 43300 and *Klebsiella pneumoniae* ATCC 700603, which were normalised to an OD₆₀₀ of 0.01 in soft nutrient agar. Assay plates were grown for 12 hours at 37°C and zones of inhibition were measured in mm with a ruler.

Though both aurodox and kirromycin were detected in the fermentation of *S. goldiniensis* and *S. ramocissimus*, it was hypothesised that fermentation of the strains in different media could increase elfamycin yield from the cell culture. In the literature, strains have been optimised for elfamycin production in kirromycin production medium for *S. collinus* (Robertsen et al., 2018) and aurodox production medium for *S. goldiniensis* (Berger et al., 1973). Both media contain soya flour, which can cause issues downstream during analysis as separation of biomass from media can prove difficult, hindering processes such as DNA or RNA extraction which require cell mass separation from the medium.

To address this, a range of media were evaluated to ascertain which was optimal for production of elfamycins by *Streptomyces* strains with little effect on downstream processing. Batch fermentations (50 mL) in shake flasks were set up in several media. All media were chosen due to their utility as media for elfamycin production, but also for the amenability to downstream processing of biomass and metabolites. Lysogeny broth (LB) used as a control given *Streptomyces* rarely reach high biomass levels when grown in this medium (Kieser et al., 2000). The media chosen were Nutrient Broth (NB; Oxoid), Lysogeny Broth (LB, Sambrook et al., 1989), Aurodox Production medium (AP, Berger et al., 1973), V6 media (v6, Marinelli, 2009) and Glucose, yeast and malt media (GYM, Kieser et al., 2000)

Strains were grown in each medium for three days and culture supernatants were harvested and extracted in chloroform. LC-MS analysis of the extracts shows aurodox to be present in fermentation extracts from AP, V6 and GYM with a corresponding retention time of approximately 7.7 minutes. Corresponding M/Z ratio is also 793.4, consistent with the aurodox standard. No aurodox was detected in fermentation in NB, although a small amount of aurodox detected in the fermentation of *S. goldiniensis* in LB (Fig. 3.13 & Fig. 3.14).

Though aurodox was detected within the fermentation extracts of *S. goldiniensis* cultured in AP, V6, GYM and LB, bioactivity was observed against Gram-positive ($P = 0.005$) and Gram-negative bacteria ($P = 0.009$) for the extracts of *S. goldiniensis* cultured in GYM media, where the activity was found to be less than the aurodox standard (Fig. 3.15). When compared to the mass spectrometry data, the absorbance value in the HPLC is highest in that for GYM suggesting a greater signal and detection of aurodox (Fig. 3.14).

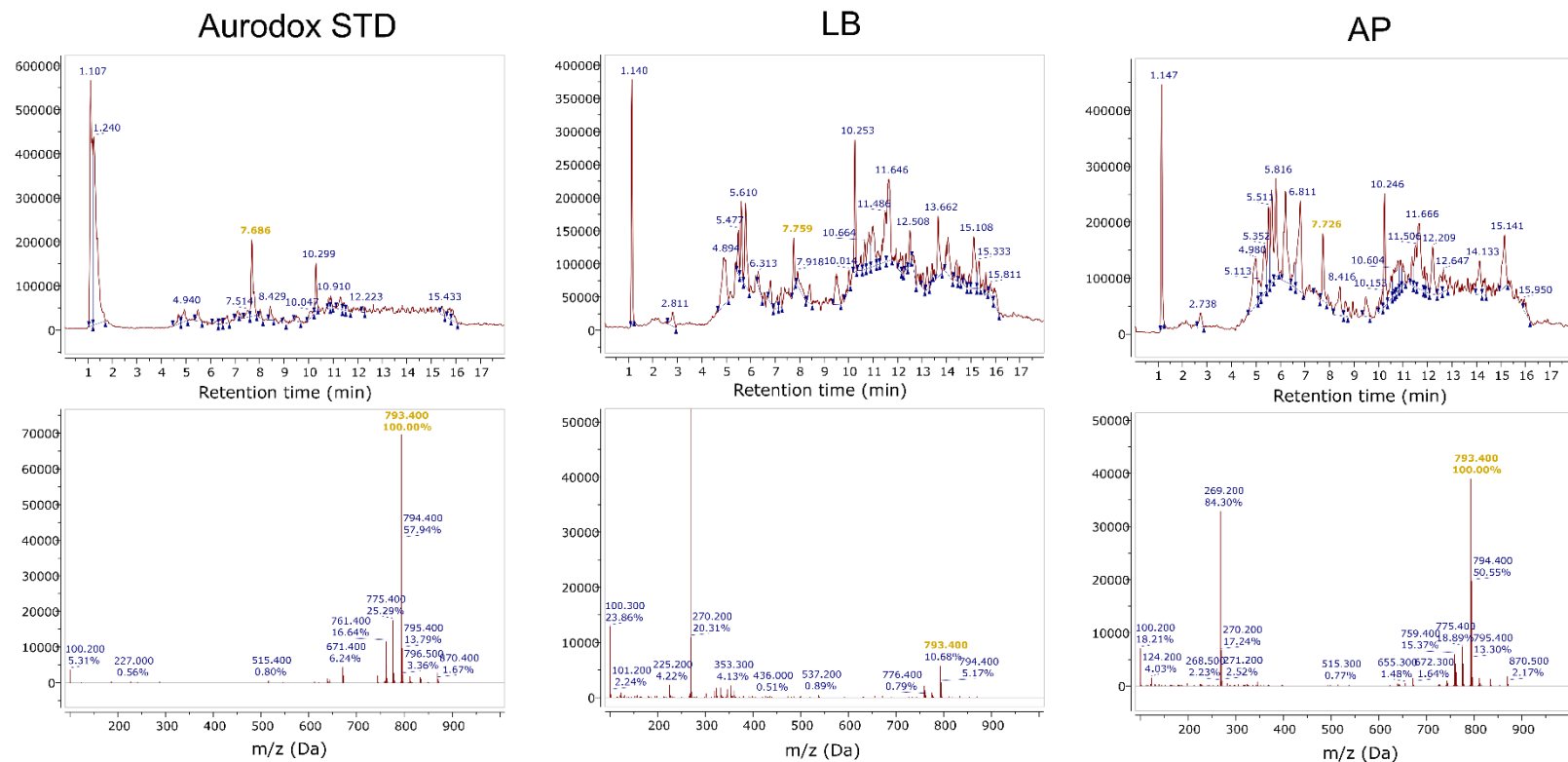


Figure 3.13: Aurodox is produced during fermentation of *S. goldiniensis* in LB and AP liquid media. Cultures were processed for analysis as per methods (2.5.2 & 2.5.2). Aurodox standard sample concentration was 1 mg/ml (Total Ion Chromatograms (TICs) from LCMS analysis of culture supernatants from *S. goldiniensis* in varied media. Gold labelled retention times and M/Z indicate that of aurodox. Complementary Mass Spectrometry data is shown, where an M/Z ratio of 793.4 indicates aurodox is present.

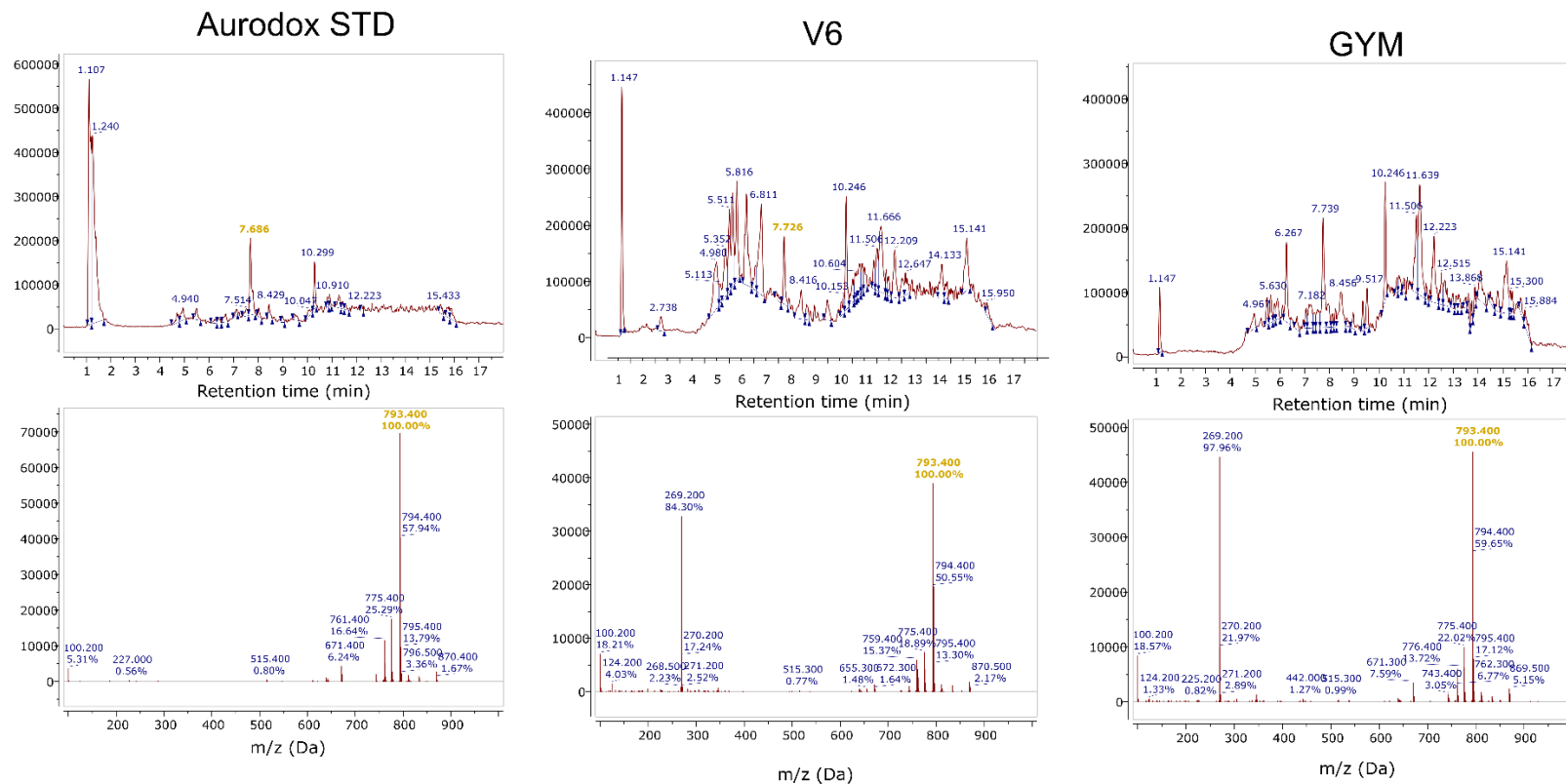


Figure 3.14: Aurodox is produced during fermentation of *S. goldiniensis* in V6 and GYM liquid media. Cultures were processed for analysis as per methods (2.5.2 & 2.5.2). Aurodox standard sample concentration was 1 mg/ml (Total Ion Chromatograms (TICs) from LCMS analysis of culture supernatants from *S. goldiniensis* in varied media. Gold labelled retention times and M/Z indicate that of aurodox. Complementary Mass Spectrometry data is shown, where an M/Z ratio of 793.4 indicates aurodox is present.

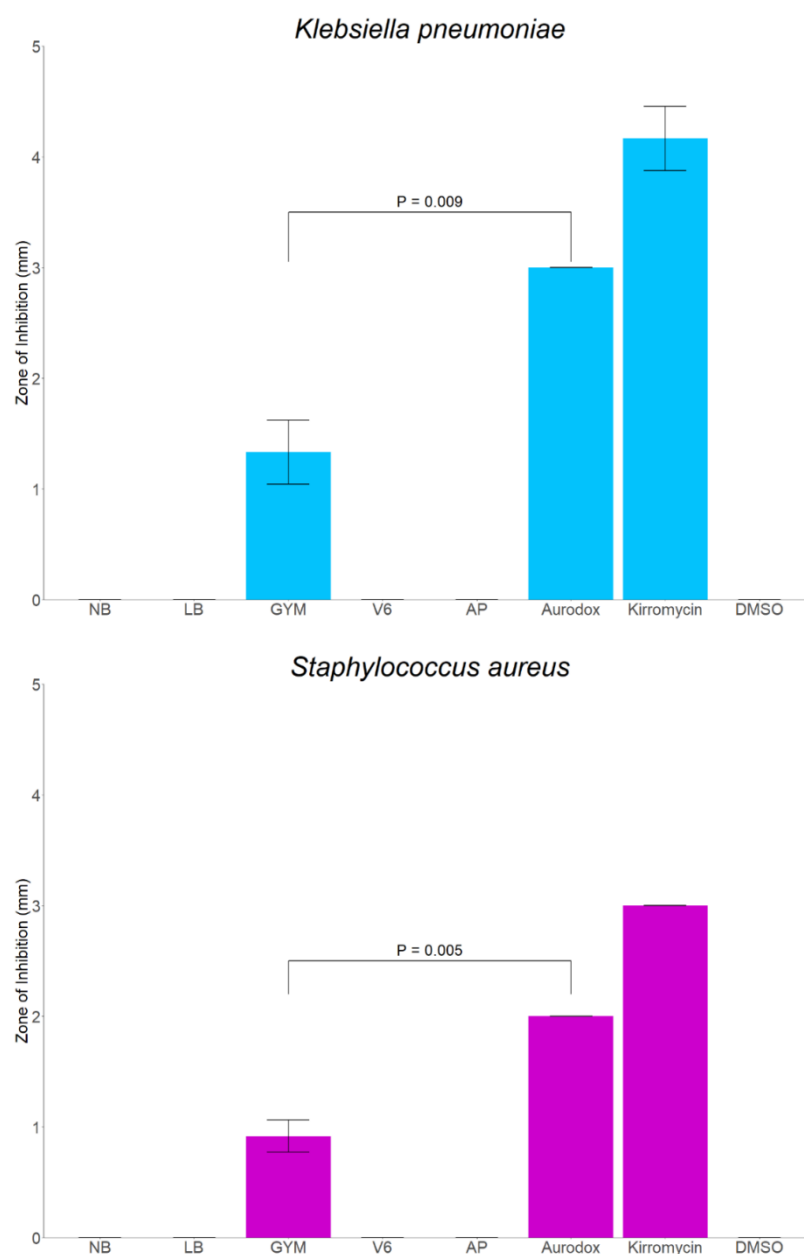


Figure 3.15: Bioactivity of fermentation extracts against both Gram-positive and Gram-negative pathogens indicate GYM is the optimum media for aurodox production during fermentation of *S. goldiniensis*. *Streptomyces goldiniensis* fermentation extracts (liquid media, 30°C, 3 days, 200 rpm) were added to paper discs and plated on indicator strains, *Staphylococcus aureus* ATCC 43300 and *Klebsiella pneumoniae* ATCC 700603, which were normalised to an OD₆₀₀ of 0.01 in soft nutrient agar. Assay plates were grown for 12 hours at 37°C and zones of inhibition were measured in mm with a ruler.

Similar results were obtained from the fermentations of *S. ramocissimus*, where kirromycin was found to be produced in fermentations in LB and GYM media, all possessing a retention time of ~7.5 minutes and a m/z ratio of 779.3 (Fig. 3.16). No mass corresponding to that of kirromycin was found in fermentations in NB, AP, or V6 medium, but, like aurodox, kirromycin was detected in fermentations in LB. Though kirromycin was also detected within the fermentation extracts of *S. ramocissimus* cultured in AP, GYM and LB, bioactivity was observed against Gram-positive ($P = 0.005$) bacteria, though less than that of the kirromycin standard. For Gram-negative bacteria, the extracts of *S. ramocissimus* cultured in GYM media was found to have comparable bioactivity to the kirromycin standard ($P = 0.741$, Fig. 3.17). When compared to the mass spectrometry data, mAu value is highest in that for GYM suggesting a greater signal and detection of kirromycin (Fig. 3.16).

For both *S. goldiniensis* and *S. ramocissimus*, HPLC analysis revealed GYM to be the best media for fermentations of Elfamycins. The extracts appear to be free from contaminating metabolites/media extracted components. Therefore, for future work in this study, GYM will be used for liquid culture of *Streptomyces*.

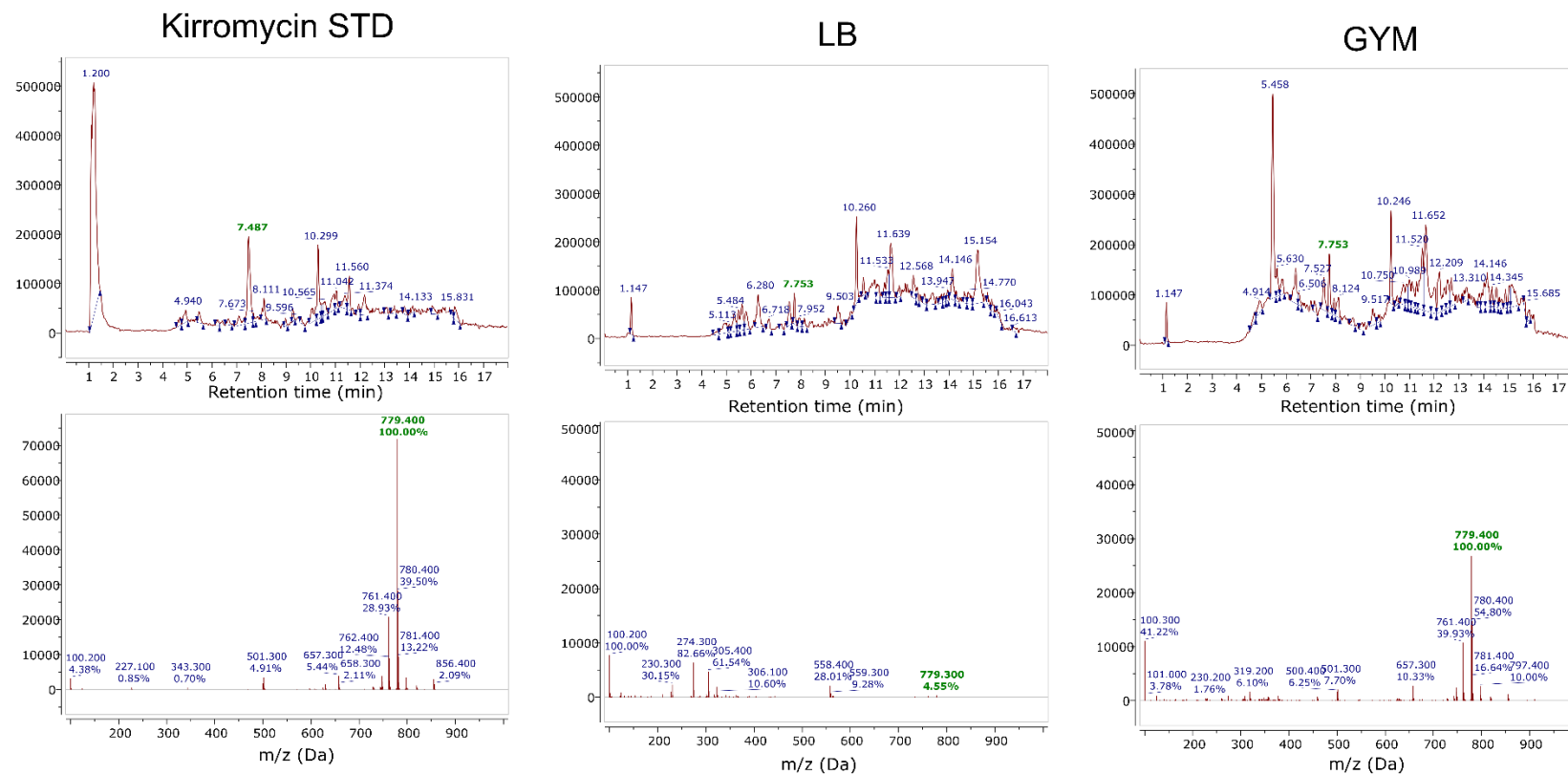


Figure 3.16: Kirromycin is produced during fermentation of *S. ramocissimus* in LB and GYM liquid media. Cultures were processed for analysis as per methods (2.5.2 & 2.5.2). Kirromycin standard sample concentration was 1 mg/ml (Total Ion Chromatograms (TICs) from LCMS analysis of culture supernatants from *S. ramocissimus* in varied media. green labelled retention times and M/Z indicate that of kirromycin. Complementary Mass Spectrometry data is shown, where an M/Z ratio of 779.3 indicates kirromycin is present.

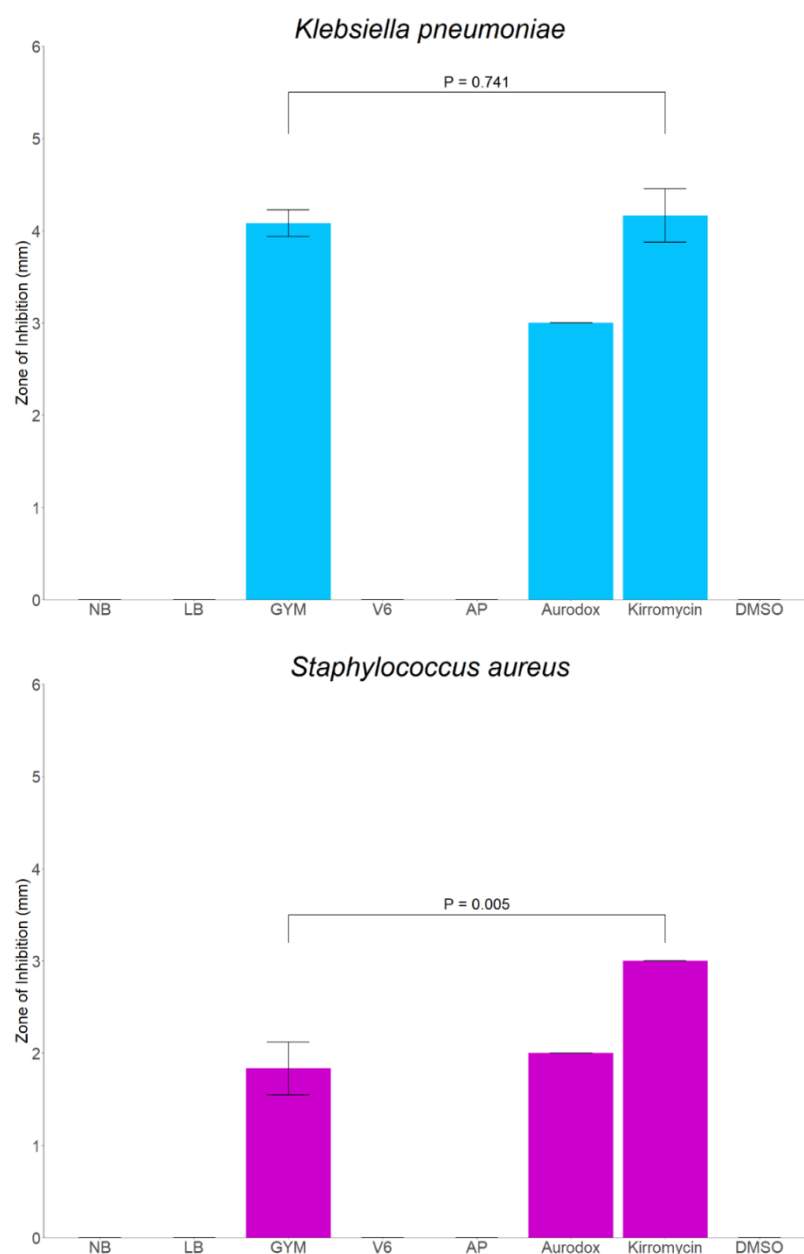


Figure 3.17: Bioactivity of fermentation extracts against both Gram-positive and Gram-negative pathogens indicate GYM is the optimum media for kirromycin production during fermentation of *S. ramocissimus*. *Streptomyces ramocissimus* fermentation extracts (GYM liquid media, 30°C, 3 days, 200 rpm) were added to paper discs and plated on indicator strains, *Staphylococcus aureus* ATCC 43300 and *Klebsiella pneumoniae* ATCC 700603, which were normalised to an OD₆₀₀ of 0.01 in soft nutrient agar. Assay plates were grown for 12 hours at 37°C and zones of inhibition were measured in mm with a ruler.

3.2.3 Sequencing of the *S. ramocissimus* genome

The genome sequences of *S. goldiniensis*, *S. collinus* and their elfamycin biosynthetic gene clusters are published (McHugh et al., 2021, 2022; Rückert et al., 2013; Weber et al., 2008). Though many of the genes *S. ramocissimus* possesses have been discussed in great detail in the literature, including the *tuf* genes 1-3, and the *ssgA* gene, the genome sequence of *Streptomyces ramocissimus* has not been determined (Olsthorn-Tieleman et al., 2002; Tieleman et al., 1997; Vijgenboom et al., 1994).

It is hypothesised that identifying the BGC for kirromycin in *S. ramocissimus* may enable a deeper understanding of kirromycin biosynthesis and more widely other Elfamycin compounds and provide insight into our understanding of evolution of antibiotic BGCs.

GYM broth cultures of *S. ramocissimus* were grown for three days at 30° C, shaking at 200 RPM. Prior to DNA extraction, the two cultures of *S. ramocissimus* were subjected to rigorous quality control checks to ensure the extracted DNA was of *S. ramocissimus* alone and free of contamination, and that the DNA extracted was of sufficient quality for DNA for sequencing. Samples of the two cultures of *S. ramocissimus* were taken after 2 days of growth and plated onto nutrient agar. The plates were grown at 37° C overnight to determine the absence of contaminants.

DNA was extracted from the two 50 mL *S. ramocissimus* cultures in accordance to the 'Salting Out Genomic DNA Extraction Method' on Actinobase (Feeney et al., 2022). After extraction of the DNA, the quality of each DNA sample was evaluated spectrophotometrically and the 260:280 ratio was confirmed as approximately 1.8, indicating no protein or RNA contamination of the preparation. DNA was quantified by Qbit, with the concentrations of DNA samples being 101 ng/μL and 95 ng/μL respectively for sample one and two. DNA was run on a 2% agarose gel at 90V for 60 minutes to confirm the integrity of the DNA (Fig. 3.18).

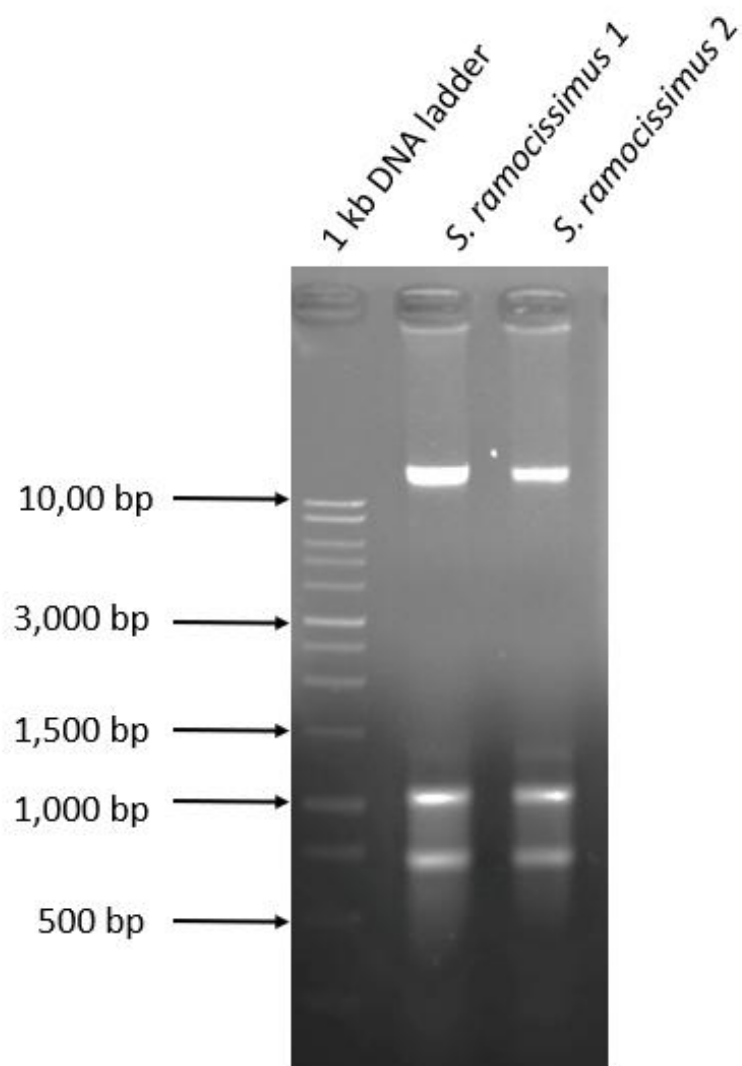


Figure 3.18: Quality assurance of extracted *Streptomyces ramocissimus* DNA.

Extracted *S. ramocissimus* DNA samples were run on a 2% agarose gel, 90 V for 60 minutes.

Amplification of the 16S rRNA gene of the extracted *S. ramocissimus* DNA was performed using polymerase chain reaction with the conditions outlined in Chapter 2. The resulting PCR product was then run on a 1% agarose gel for 60 minutes at 90 V. Amplification of the 16S rRNA gene of both samples was successful and the amplicon was the same size (1500bp) as the positive control which was the 16S rRNA gene of *S. coelicolor* (Fig. 3.19).

The resulting PCR products were sequenced (Sanger sequencing, Eurofins) in both the forward and reverse direction and the sequences combined using BioLign software using CAP Contig assembly program to form one aligned contig (*S.ramocissimus_16S_Aligned*). The resulting contig was subjected to Basic Local Alignment Search Tool (BLAST; NCBI) using the nucleotide blast setting to identify bacterial strains with similar 16S rRNA nucleotide sequences (Altschul et al., 1990). The results for the BLAST of *S. ramocissimus* 16S rRNA gene are outlined (Table 3D).

S. ramocissimus 16S rRNA was most similar to *Streptomyces gilvifuscus* (percentage similarity 98.94%). The majority of 16S rRNA sequences of strains which were identified as being >98% similar belong to Streptomycetes, highlighting the difficulty in using 16S rRNA as a discriminatory marker in this genus (Kiepas et al., 2023; Labeda et al., 2012).

Interestingly however, when the 16S rRNA sequences are aligned using Clustal Omega software (Sievers et al., 2011), sequence similarity is present through the majority of the aligned 16S rRNA genes of those identified by NCBI BLAST, apart from one main region of variability (highlighted in Fig. 3.20, with a red box) appearing on each 16S rRNA sequence between nucleotides 100-250 of the given sequence. There are 9 variable regions within the 16S rRNA sequence which can be used for identification of species (Abellan-Schneyder et al., 2021). In this case, the variable region of these *Streptomyces* falls between regions one and two (shown in green, Fig.

3.20). Often two or more regions, or the sequence between the variable regions, are analysed for greater analysis depth. In this case, there is a clear region of variability present within the V1-V2 boundaries. This region has been historically termed the α region and has shown to be most effective for analysis of the 16S rRNA gene within *Streptomyces* (Kataoka et al., 1997; Stackebrandt et al., 1991).

From the closely related species identified by BLAST, the phylogeny of the 16S rRNA genes of these strains, plus that of *S. goldiniensis*, *S. collinus* and the type strain, *S. coelicolor* is shown (Fig. 3.21), where *S. ramocissimus* (blue) is shown to clade alongside other *Streptomyces*.

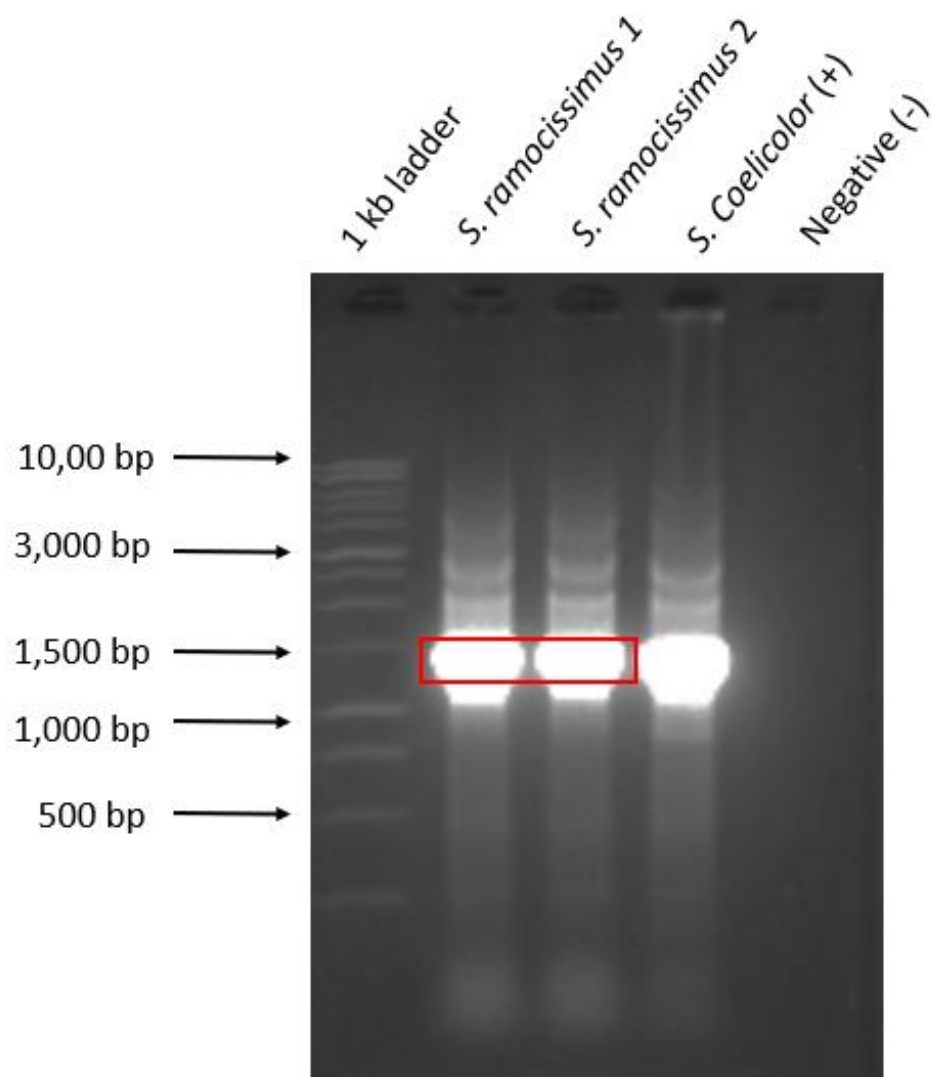


Figure 3.19: Amplification of the 16S rRNA gene from extracted *Streptomyces ramocissimus* DNA. Agarose gel of amplified 16S rRNA gene from *S. ramocissimus* using 16S primers, red box indicates the 16S rRNA gene present at approximately 1500 bp. Positive control is *Streptomyces coelicolor* extracted DNA, negative control is Nuclease free water. 2% agarose gel, ran at 90 V for 60 minutes

Table 3D: NCBI Basic Local Alignment Search Tool results for 16S rRNA gene sequences of similar species to *S. ramocissimus.**

Strain	% similarity	GenBank Accession Number
<i>Streptomyces gilvifuscus</i>	98.94%	OP114768.1
<i>Streptomyces panaciradicis</i>	98.85%	MK519192.1
<i>Streptomyces recifensis</i>	98.85%	EU216596.1
<i>Streptomyces ginsengisoli</i>	98.76%	KF649337.1
<i>Streptomyces olivoviridis</i>	98.76%	LC033613.1
<i>Streptomyces durhamensis</i>	98.59%	KT961129.1
<i>Streptomyces novaecaesareae</i>	98.59%	KF772673.1
<i>Streptomyces echinatus</i>	98.59%	NR112264.1
<i>Streptomyces triostinicus</i>	98.50%	MN548370.1
<i>Streptomyces miharaensis</i>	98.50%	KY569410.1
<i>Streptomyces plumbidurans</i>	98.50%	MW526995.1

* Forward, reverse 16S rRNA sequences were provided by Eurofins Genomics using Sanger Sequencing. Forward and reverse reads were aligned using the CAP Contig assembly program via the BioLign desktop platform. 16S rRNA gene of *S. ramocissimus* was run through nucleotide BLAST via the NCBI online server, where the program was selected for highly similar sequences (megablast).

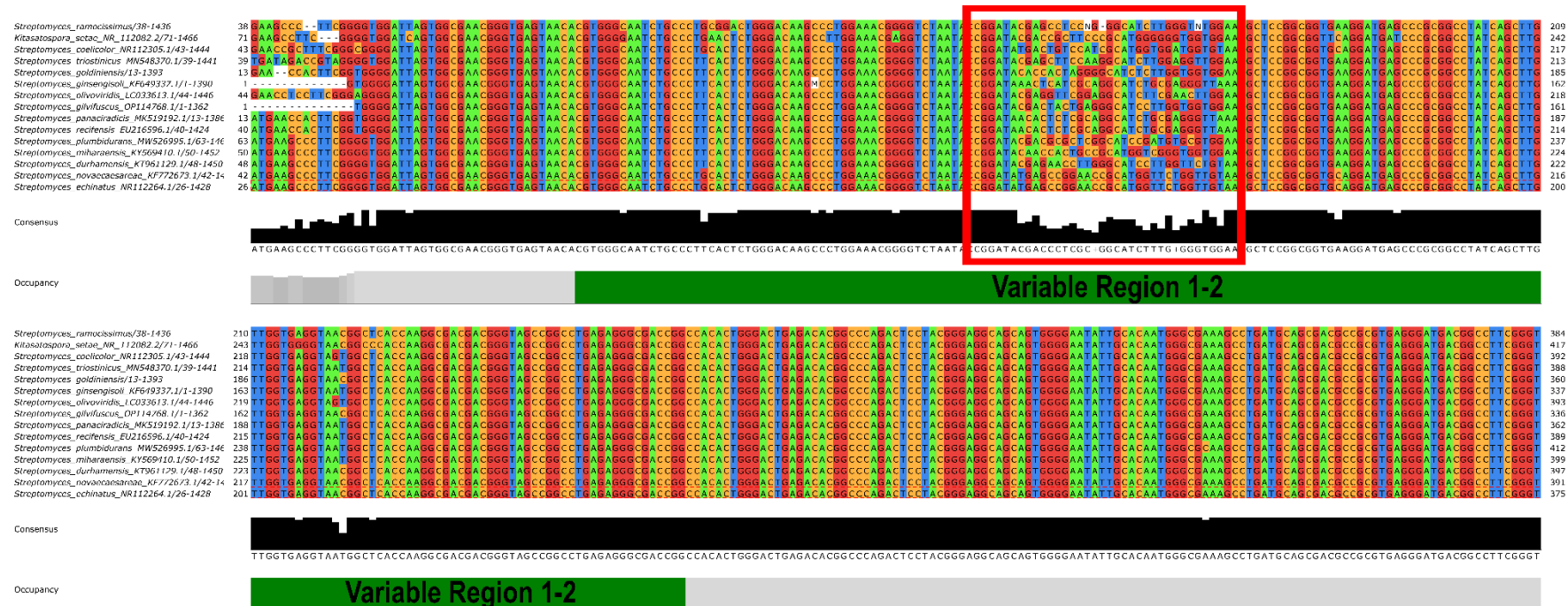


Figure 3.20: The 16S rRNA gene of *Streptomyces ramocissimus* contains variable regions 1-2 like other *Streptomyces*. Similar sequences previously identified by NCBI BLAST software were input and aligned using Clustal Omega online server and visualised on Jalview software. Regions of variability 1-2 within 16 genes are shown in green with the hypervariable α region shown in red box. *S. coelicolor* and *K. setae* were used as comparison strains.

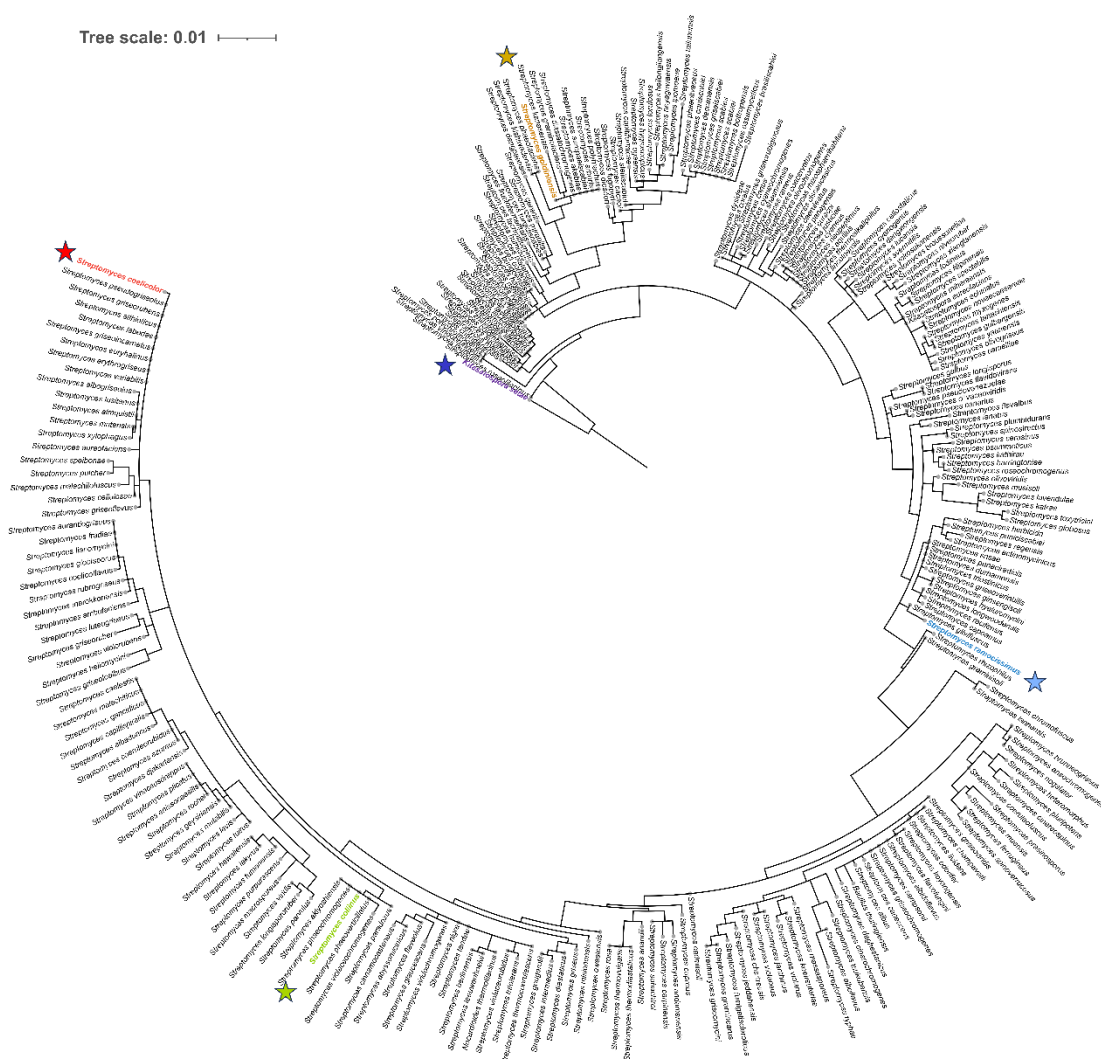


Figure 3.21: Maximum likelihood tree of *S. ramocissimus* and other elfamycin producing strains. 16S sequences of similar species to *S. ramocissimus* (blue) were obtained from BLAST search of the 16S sequence with standard parameters. 16S sequences of *S. goldiniensis* (gold), *S. collinus* (green) and *S. coelicolor* A3(2) (red) were also included with *Kitasatospora setae* (purple) used as an outgroup. Sequences were aligned using Clustal Omega software and used to form a maximum likelihood tree with 500 bootstraps. The tree was exported to ITOL for formatting and analysis and rooted at *Kitasatospora setae*.

The 16S rRNA gene has allowed for characterisation of bacterial species based on single nucleotide polymorphisms, where now, 16S rRNA gene sequencing is the most dominant method of primary phylogenetic identification of bacterial species (Tringe et al., 2008). The 16S rRNA gene is useful and often accurate at genus level identification of bacterial species. However, there has been the suggestion that the 16S rRNA gene alone, is not sufficient evidence to identify or define *Streptomyces* species. This is due to many *Streptomyces* species having high sequence similarity within their 16S genes causing low taxonomic resolution (Kiepas et al., 2023). This can be observed during our analysis of the 16S gene of *S. ramocissimus*, where many strains appear to be identical to others according to their 16S rRNA phylogeny. This can be seen for *S. coelicolor* (red, Fig. 3.21), causing an obstacle during the identification of species with just one gene.

To solve this, in addition to the 16S rRNA gene, multiple *Streptomyces* conserved genes such as *ssgA* and *ssgB* have been sequenced in addition to the 16S rRNA gene to facilitate easier and more reliable identification and classification of *Streptomyces* species (Girard et al., 2013). Both genes are involved in the *Streptomyces* life cycle, where *ssgB* encodes a product which is involved in the cessation of growth prior to sporulation-specific cell division, and *ssgA* is involved in the stimulation of septum formation of the spore forming cell (Keijser et al., 2003; van Wezel et al., 2000).

Superseding this, it is widely regarded that for accurate phylogenetic analysis for *Streptomyces* species, the recommended workflow is to undertake robust whole genome analysis to elucidate the taxonomy, phylogeny and detailed genomic information about the nature of the *Streptomyces* species (Kiepas et al., 2023). To combat issues with high GC content and repetitive sequences in *Streptomyces* genomes, hybrid approaches to genome sequencing is often used, where multiple sequencing platforms are used to provide both long and short sequencing reads. This

is especially useful for elucidating the highly repetitive PKSs and NRPSs present on BGCs (Heng et al., 2023) Illumina NovaSeq 6000 (Novogene) was used to generate paired-end sequencing reads of length PE150bp. Once obtained, the reads were processed through the Quality assessment Tool for Genome Assemblies (QUAST) (Version 5.2.0) server through the Galaxy.au online server where default settings were used throughout (Fig. 3.22, Gurevich et al., 2013).

Illumina only sequencing revealed that *S. ramocissimus* genome has approximately 71.14% GC content as with other *Streptomyces* species. The genome assembly is comprised of 142 contigs, with an estimated genome size of approximately 8.382 Mbp. Assembly through Unicycler software (Version 0.5.0) provided an N50 score of 215985 and an L50 score of 13 (Wick et al., 2016). The N50 and L50 values and the high contig number suggest that assembly from, Illumina sequencing alone results in a highly fragmented genome assembly (Fig. 3.22).

To improve the assembly of the *S. ramocissimus* genome, MeDuSa (Version 1.6), was employed (Bosi et al., 2015). This Multi-Draft Based Scaffolder uses a closed genomic sequence of a related species to bridge gaps between contigs and also to orientate contigs into the correct conformation. In more recent years, the addition of multi-locus sequence typing analysis to whole genome analysis, has proven beneficial in deciphering the complex *Streptomyces* genus. By example AutoMLST software uses an Automated Multi Locus Species Tree approach to determine phylogenetic and evolutionary relatedness among Actinobacteriota species (Alanjary et al., 2019). To identify the closest relative with an assembled genome, the provisional genome assembly of *S. ramocissimus* was run through AutoMLST (Alanjary et al., 2019). The phylogenetic tree corresponding to the AutoMLST output for *S. ramocissimus* (Fig. 3.23), where other important Elfamycin and well-studied strains such as *S. goldiniensis* (Maehr et al., 1979), *S. collinus* (Laiple et al., 2009) and *S. coelicolor* M145 (Feeney et al., 2022) have also been added into this analysis.

AutoMLST identified *Streptomyces longwoodensis* DSM 41677, type strain (Nouioui et al., 2018; Prosser and Palleroni, 1976), as the closest related strain to *S. ramocissimus*. *S. longwoodensis* was identified during our analysis of the 16S phylogeny of *S. ramocissimus*, and clades closely to *S. ramocissimus*. The complete, annotated genome of *S. longwoodensis* (Prosser and Palleroni, 1976) was used to scaffold the *S. ramocissimus* Illumina reads using Unicycler (Version 0.5.0). The assembly following scaffolding was then run through QUAST to determine any changes in the quality of the assembly. It was found that the number of contigs had reduced from 142 to 75 (Fig. 3.24) by a bandage plot (Wick et al., 2015). The predicted genome size, based on the assemble reduced in size from 8.382 to 8.379 Mbp. This suggests that scaffolding had identified overlaps in contigs. The N50 and L50 values also improved with the N50 increasing from 215985 to 626623 and the L50 decreasing from 13 to 6, indicating that scaffolding to the *S. longwoodensis* genome has improved assembly quality (Fig. 3.24).

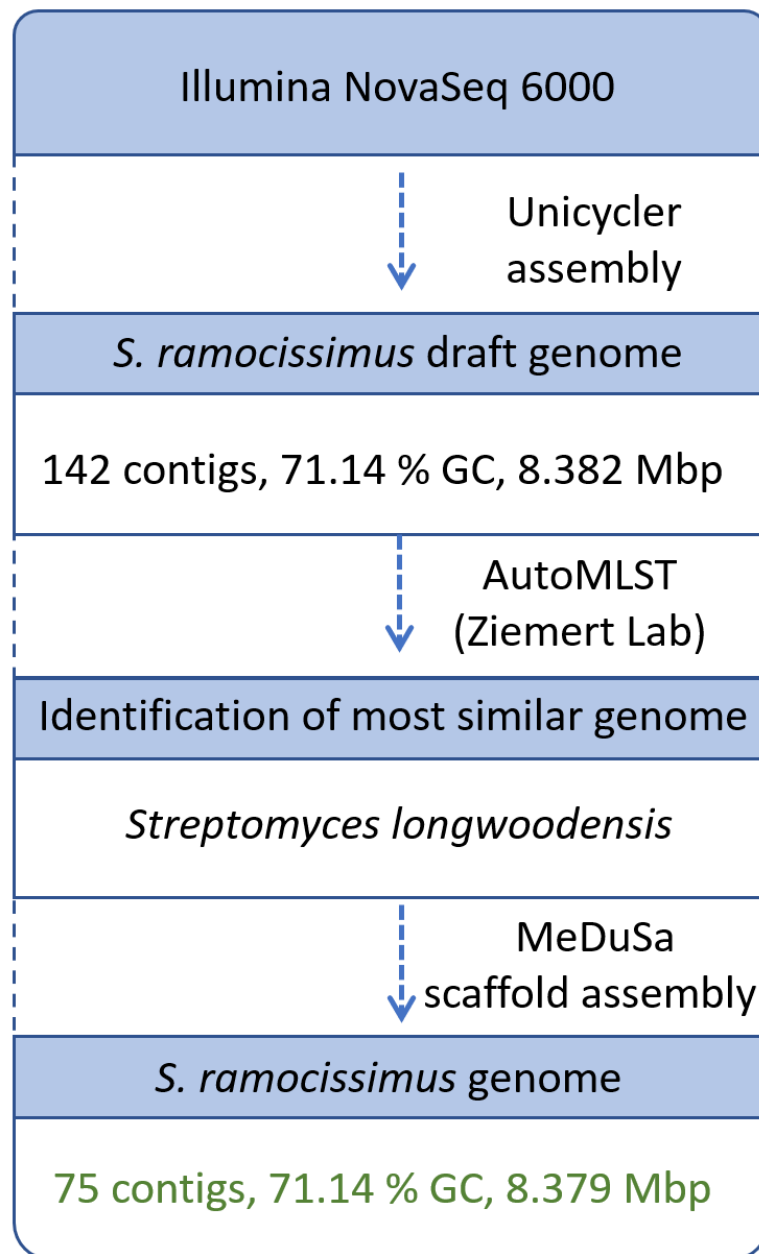
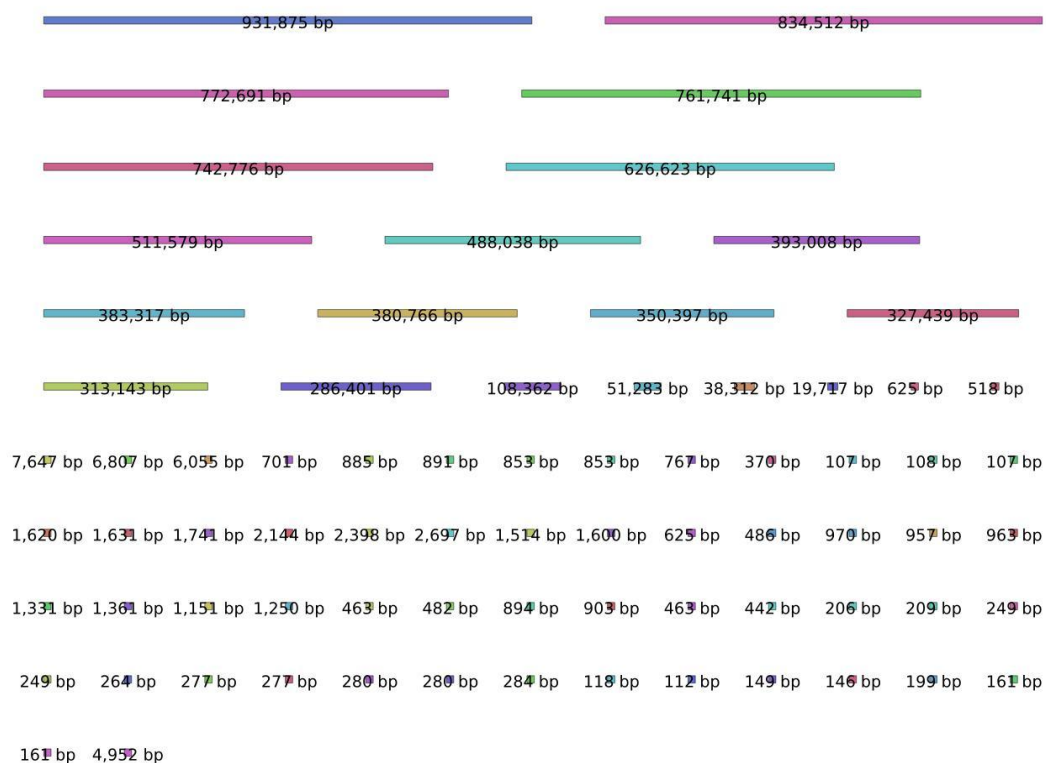


Figure 3.22: Workflow used in the assembly of the *S. ramocissimus* genome.



Genome Size (bp)	8379284
% GC Content	71.14
N50	626623
L50	6
Number of Contigs	75
Neighbour	<i>Streptomyces longwoodensis</i>

Figure 3.24: Summary of final *S. ramocissimus* genome assembly. (A) Bandage graphical representation of the contigs contributing to the final assembly and their relative size (Galaxy.au) (B) QUAST summary from final *S. ramocissimus* assembly.

During the course of this work, a further kirromycin producing strain was published as part of a metagenomic study (Maza et al. 2019). This *Streptomyces*, ISL094, was isolated from the Atacama desert, Chile, in a study to expand the knowledge of the Altiplano landscape and to obtain a better representation of its microbiome (Maza et al., 2019). Analysis of the resulting metagenomes indicated the presence of a kirromycin-like elfamycin cluster within the genome of the *Streptomyces* ISL094 strain.

Upon comparison of the assembly statistics for the four genomes of the kirromycin/aurodox producing *Streptomyces* (*Streptomyces* ISL094, *S. ramocissimus*, *S. collinus* and *S. goldiniensis*; Fig. 3.25), several observations can be made. Firstly, all four strains possess characteristic *Streptomyces* genomes, greater than 7 Mb. The genome of *S. goldiniensis* appears to be ~10 Mb, (Fig. 3.25, A). The genome of *S. collinus* is the best resolved genome, in three contigs closely followed by *S. goldiniensis* with 9. The *Streptomyces* ISL094 and *S. ramocissimus* both have large numbers of contigs from their assemblies (Fig. 3.25, B). Upon assessment of the contigs, it reflects the L50 and N50 scores for all the genomes (Fig. 3.25, C&D). All four genome assemblies possess a GC content (%) of greater than 71% (Fig. 3.25, E), typical of *Streptomyces*, a trait which can make genomic sequencing of the species difficult (Gomez-Escribano et al., 2015).

Though the genome assemblies of both *S. ramocissimus* and *Streptomyces* ISL094 are not of the same quality as *S. collinus* and *S. goldiniensis*, it was hypothesised biosynthetic gene cluster responsible elfamycin biosynthesis could be identified from the contigs, this would enable comparisons of the individual BGCs.

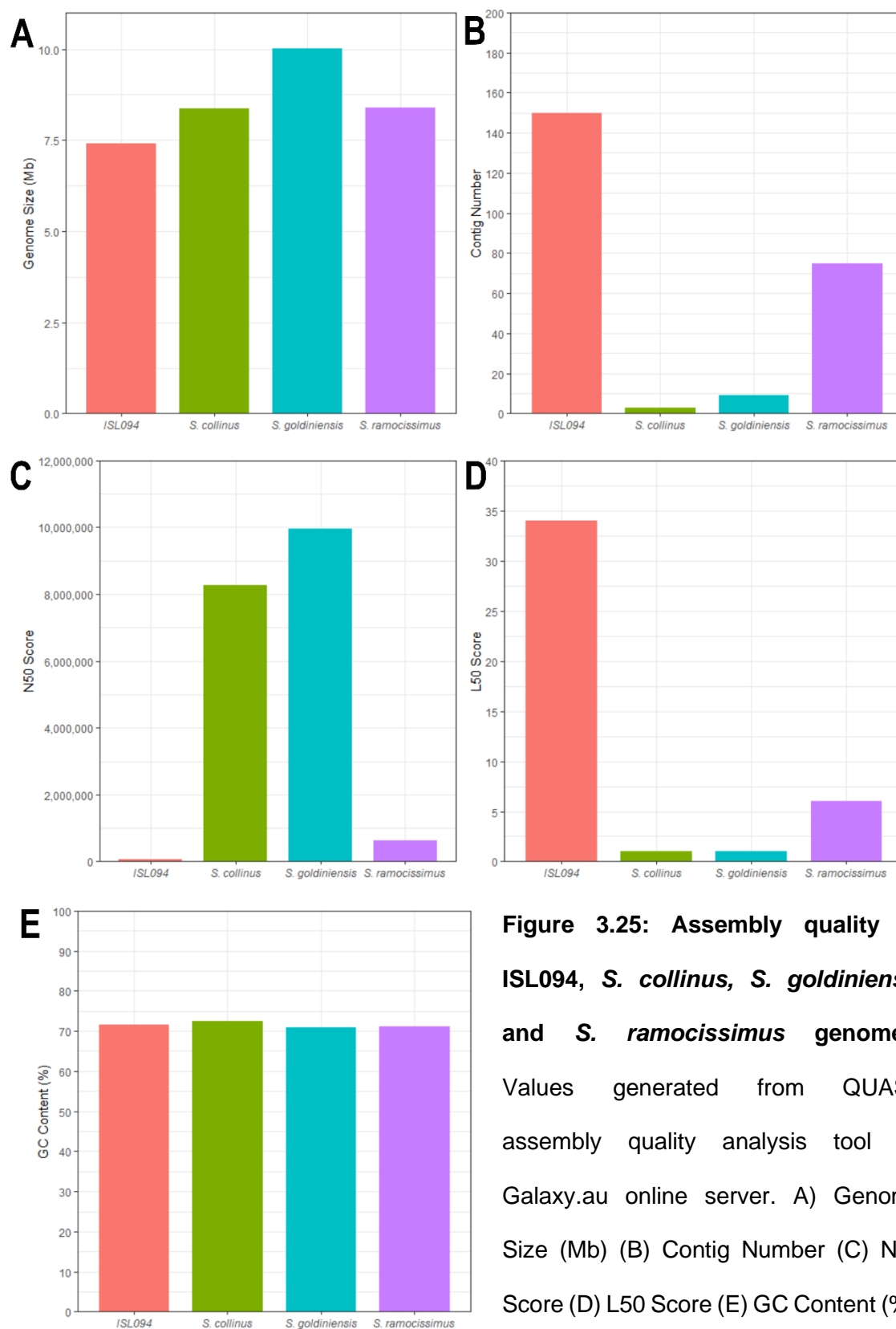


Figure 3.25: Assembly quality of ISL094, *S. collinus*, *S. goldiniensis* and *S. ramocissimus* genomes. Values generated from QUAST assembly quality analysis tool on Galaxy.au online server. A) Genome Size (Mb) (B) Contig Number (C) N50 Score (D) L50 Score (E) GC Content (%).

3.2.4 Assessing the biosynthetic potential of Elfamycin-producing strains.

Streptomyces species are well known for their high biosynthetic potential (Lee et al., 2021). They are capable of producing a range structurally and functionally diverse natural products which have been exploited for a range of clinical uses, representing 75% of clinically useful antibiotics presently available (Janardhan et al., 2014). Since the genomes of both *Streptomyces coelicolor* and *Streptomyces avermitilis* were sequenced and completed in 2002-2003, the 'genomics age' of antibiotic discovery began. Sequencing of the *Streptomyces coelicolor* genome revealed that the genome encoded a further 18 biosynthetic gene clusters than the four previously identified under laboratory conditions. This observation has been consistently repeated in every *Streptomyces* genome subsequently sequenced and is therefore regarded as a widespread phenomenon, rather than being unique to *S. coelicolor* (Ikeda et al., 2014; Ohnishi et al., 2002).

The increase in sequencing platform power and a lowering of genome sequencing cost (Moore's law, Muir et al., 2016; Moore., 2006) has led to the mass sequencing of many bacterial species genomes. This abundance of genomic data has driven the development of computational methods to mine bacterial genomes for BGCs such as AntiSMASH (Blin et al., 2021) and PRISM (Skinnider et al., 2020) to name a few. To understand the biosynthetic potential of the four elfamycin-producing *Streptomyces* strains and to identify the BGCs responsible for the elfamycin, the genome assemblies of all four strains were subjected to AntiSMASH (V6.0) analysis.

The biosynthetic potential of the *S. goldiniensis* and *S. collinus* genomes have been well documented by McHugh et al., (2021) and Weber et al.,(2013). Their findings are consistent with the literature in terms of the number of putative biosynthetic gene clusters found in *Streptomyces* genomes, with *S. goldiniensis* predicted to encode 35 BGCs in its genome and *S. collinus* predicted to encode 32. These data were found

to be largely similar upon reanalysis using AntiSMASH version 6.0. It was predicted *S. collinus* possessed 36 BGCs, four more than first thought (Fig. 3.26). This is likely reflective of the development of the AntiSMASH algorithms which may be better at BGC cluster production when compared to the original version of 2.0 analysis of Weber et al., (2013). The genomes of *S. collinus* and *S. goldiniensis* were found to possess diverse BGCs, including Type I, II and III polyketide, non-ribosomal peptide, and siderophore encoding BGCs were identified as well as the presence of BGCs that are highly conserved across the genus such as those encoding geosmin, desferrioxamine and melanin (Akbarzadeh et al., 2007; Polapally et al., 2022; Zaroubi et al., 2022, Fig. 3.26).

The genome of *S. ramocissimus* was predicted to possess 23 distinct natural product BGCs. The distribution of BGCs within the *S. ramocissimus* genome was as expected with products predicted such as non-ribosomal peptides (NRPs) and Types I & II polyketides were identified in addition to the conserved *Streptomyces* BGCs encoding products such as pigments (melanin) and siderophores such as desferrioxamine.

The genome of *Streptomyces* ISL094 was predicted to encode 33 BGCs in total, similar to the number possessed by *S. collinus* and *S. goldiniensis*, though the genome is not high-quality AntiSMASH was still able to predict BGCs from the genome assembly, with the *Streptomyces* ISL094 strain possessing BGCs encoding PKs, NRPs, terpenes and other compounds such as the lanthipeptide, sapB and desferrioxamine.

The circos plot (Fig. 3.26) indicates that BGCs encoding polyketides are of highest abundance within these four *Streptomyces* strains, closely followed by NRPs and terpenes. The genome assembly of *S. collinus* was found to encode the largest number of BGCs, 36, when compared to the smallest of *S. ramocissimus* only possessing 23. Given *S. ramocissimus* is a known kirromycin producer, and that *Streptomyces* ISL094 has previously been identified as possessing a kirromycin-like

BGC, it is unsurprising that an Elfamycin-like biosynthetic gene cluster was identified in both genome assemblies, which are thought to encode kirromycin-like BGCs. In addition, kirromycin-like BGCs were found in the genome assemblies of *S. goldiniensis* and *S. collinus*. Whilst the genome assemblies of *S. ramocissimus* and *Streptomyces* ISL094 are not of sufficient quality to draw conclusions about their overall genome structure, and the occurrence of plasmids as in *S. collinus* (Rückert et al., 2013). It did allow the identification of complete kirromycin-like BGCs.

AntiSMASH predicted the kirromycin biosynthesis genes of *S. ramocissimus* to be 92% similar to the kirromycin-like BGC of *Streptomyces collinus* Tü 365. The same similarity can be observed for *S. goldiniensis*, where 92% of genes from the kirromycin-like cluster of *S. goldiniensis* were found to be similar to the kirromycin-like BGC of *Streptomyces collinus* Tü 365. The genes of ISL094's kirromycin-like BGC were found to be 88% similar to the kirromycin BGC of *S. collinus*, indicating the presence of BGCs which could be responsible for the production of kirromycin-like elfamycins in all four strains. These data are outlined where the AntiSMASH outputs for known cluster comparisons to the kirromycin-like BGCs of all four strains are shown (Fig. 3.27).

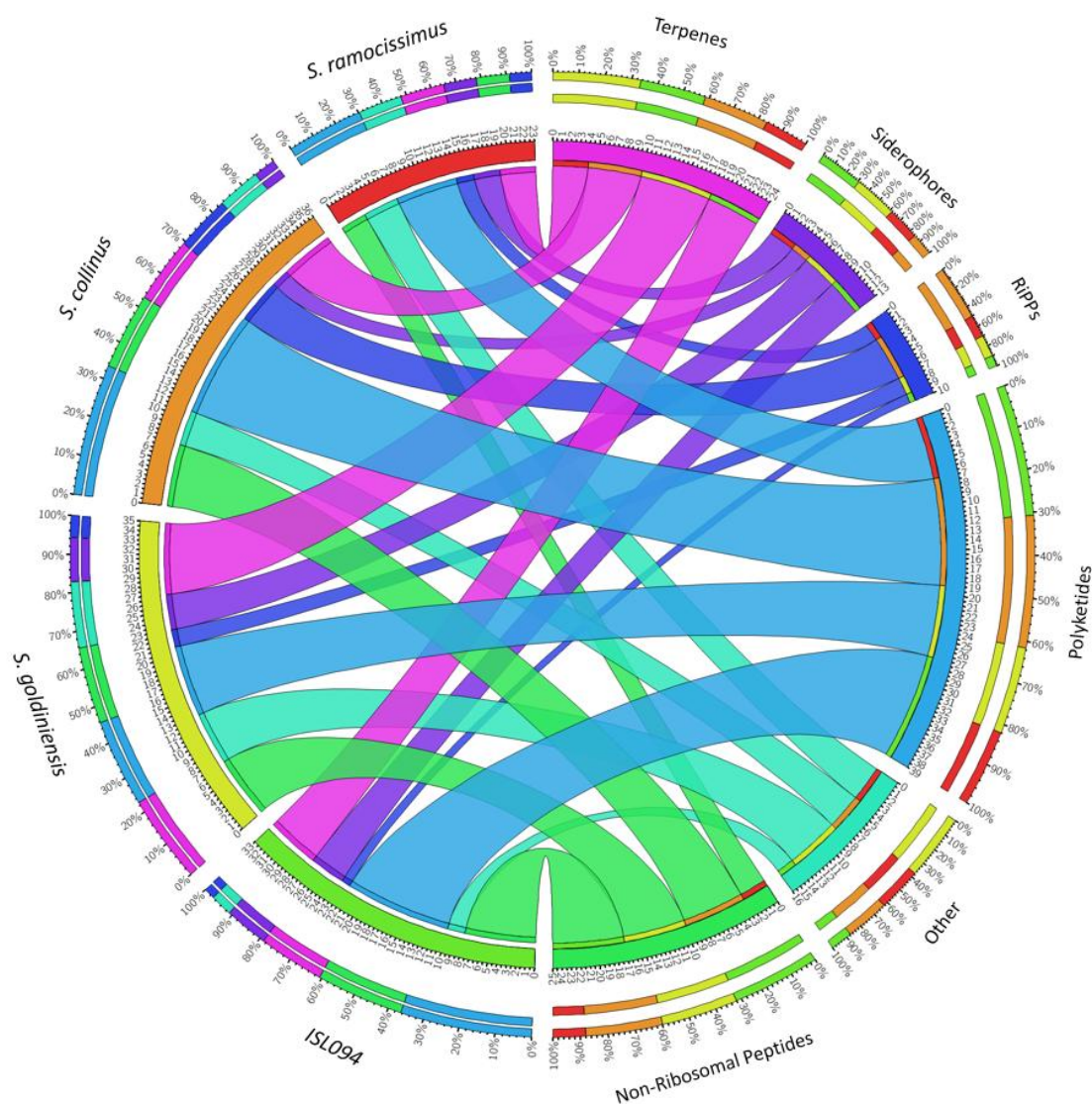


Figure 3.26: *S. ramocissimus*, *S. collinus*, *S. goldiniensis* and ISL094 genomes are predicted to encode large biosynthetic potential. BGC type predicted by AntiSMASH software (Version 6.0), where the given percentages indicate the proportion of each class of BGC encoded for by each strain. Circos plot was generated using 'Circos Table viewer – Circular Visualisation of Tabular Data' accessible at <http://mkweb.bcgsc.ca/tableviewer/>.

Query sequence

 BGC0001070: kirromycin (92% of genes show similarity), NRP+Polyketide:Modular type I polyketide+Polyketide:Trans-A

Query sequence
BGC0001070: kirromycin (100% of genes show similarity), NRP+Polyketide.Modular type I polyketide+Polyketide:Trans-

Query sequence
BGC0001070: kirromycin (92% of genes show similarity), NRP+Polyketide:Modular type I polyketide+Polyketide:Trans-A

Query sequence
BGC0001070: kirromycin (88% of genes show similarity), NRP+Polyketide:Modular type I polyketide+Polyketide:Trans-A

Figure 3.27: *S. ramocissimus*, *S. goldiniensis* and ISL094 all possess a biosynthetic gene cluster which shows similarity of the kirromycin BGC of *S. collinus*. Top hit for BGC similarity was kirromycin for all showing 92%, 100%, 92% and 88% respectively. ‘Strict’ parameters were used throughout.

3.2.5 Deciphering the biosynthetic gene clusters of Elfamycins.

To compare the kirromycin-like elfamycin BGCs sequences from *S. goldiniensis*, ISL094, *S. collinus* and *S. ramocissimus* at the nucleotide level, the genomes were compared using clinker.pi (Gilchrist and Chooi, 2021, Fig. 3.28). This allowed the overall architecture of the four BGCs to be compared. It was apparent that the kirromycin-like elfamycin clusters of the four exhibit re-arrangements that result in different gene orders. The kirromycin-like elfamycin BGCs of *S. collinus* and *S. ramocissimus* share a similar overall structure, with the core-PKS/NRPS units at one end of the BGC, downstream of the tailoring genes (Weber et al., 2008). When compared to the kirromycin-like elfamycin BGCs of *S. goldiniensis* and *Streptomyces* ISL094, the PKS/NRPS genes appear to be inverted in these clusters, with the tailoring genes upstream of the PKS/NRPS genes (McHugh et al., 2022) This plotting of the four BGCs against each other highlights the genetic inversion of the tailoring genes (Fig. 3.28). Previously shown in this Chapter, the elfamycin BGCs of Factumycin, from *Kitasatospora setae*, and L-681,217 from *S. cattleya* share a similar PKS/NRPS architecture with tailoring genes (Fig. 3.1, Table 3B). Comparison of these with the kirromycin producers *S. collinus* and *S. ramocissimus* kirromycin BGCs follow the same structure of PKS/NRPS cascade with the tailoring genes upstream, whereas the L-681,217 BGC from *S. cattleya*'s tailoring genes are found both upstream and downstream of the NRPS/PKS genes (Fig. 3.1 & Fig. 3.28). It was also observed that structurally the BGCs of *Streptomyces* ISL094 and *S. goldiniensis* are most similar to that of the factumycin BGC from *K. setae*, where structurally tailoring genes are found upstream of the PKS/NRPS genes (Ichikawa et al., 2010; Thaker et al., 2012).

Given the kirromycin-like elfamycin BGCs of *S. collinus* and *S. goldiniensis* have previously been characterised (McHugh et al., 2022; Weber et al., 2008), the identification of likely kirromycin-like BGCs in *Streptomyces* ISL094 and *S. ramocissimus* was previously unknown. Sequence similarity analysis using BLASTp was performed on each gene within these kirromycin-like BGCs to identify homologues and to assign putative functions to genes using the best characterised kirromycin cluster from *S. collinus*, where extensive mutant and biochemical analysis has been performed (Laiple et al., 2009; Pavlidou et al., 2011, 2011, 2011; Robertsen et al., 2018; Weber et al., 2008).

BLASTp analysis of *S. ramocissimus* and *Streptomyces* ISL094 reveals the kirromycin BGC of *S. ramocissimus* is most similar to the kirromycin BGC of *S. collinus* enabling the gene nomenclature and function to be assigned (Tables 3E & 3F). The only difference between the kirromycin clusters possessed by both organisms is that in *S. ramocissimus*, the TetR/AcrR family transcriptional regulator KirR is present as a single ORF and not split into the N and C termini as was proposed with *S. collinus* (Tilman Weber et al., 2008), this is also found to be the case for the MFS transporter, KirT, both of which will be discussed later in this thesis.

For the kirromycin-like elfamycin BGC of *Streptomyces* ISL094, it is observed that the BGC is more similar architecturally and in sequence to the aurodox BGC of *S. goldiniensis* (Fig. 3.28). Notably, the BGC contains a second methyltransferase, denoted here as KirM*, homologous to the SAM-dependant methyltransferase AurM* in the aurodox cluster. This suggests that the kirromycin-like elfamycin BGC of *Streptomyces* ISL094 has the potential to be an aurodox BGC. In addition, the BGC contains a 4'-phosphopantetheinyl transferase, something which the aurodox BGC does not possess but is present in the kirromycin BGCs of *S. collinus* and *S. ramocissimus*.

Further analysis of homology between the clusters will be carried out in remainder of this Chapter, where the results from these BLASTp tables act as a source for reference when discussing gene function.

Table 3E: Putative kirromycin biosynthesis genes from *S. ramocissimus*. Genes are named according to their kirromycin homolog and function predicted based on their closest hit via NCBI BLAST.

<i>Streptomyces ramocissimus</i>			
Gene	Function	Closest Blast Hit	AA similarity (%)
<i>KirP</i>	4'-phosphopantetheinyl transferase	<i>Streptomyces</i> sp. ADI98-12	93.94%
<i>KirAI</i>	beta-ketoacyl synthase N-terminal-like domain-containing protein	<i>Streptomyces viridosporus</i>	96.46%
<i>KirAII</i>	SDR family NAD(P)-dependent oxidoreductase	<i>Streptomyces</i> sp. CA-210063	92.38%
<i>KirAIII</i>	non-ribosomal peptide synthetase	<i>Streptomyces viridosporus</i>	97.26%
<i>KirAIV</i>	L-histidine N(alpha)-methyltransferase	<i>Streptomyces anulatus</i>	95.22%
<i>KirAV</i>	SDR family NAD(P)-dependent oxidoreductase	<i>Streptomyces anulatus</i>	96.08%
<i>KirAVI</i>	type I polyketide synthase	<i>Streptomyces anulatus</i>	95.35%
<i>KirHI</i>	hypothetical protein	<i>Streptomyces</i> sp. CA-210063	97.87%
<i>KirB</i>	amino acid adenylation domain-containing protein	<i>Streptomyces viridosporus</i>	96.88%
<i>KirCI</i>	ACP S-malonyltransferase	<i>Streptomyces viridosporus</i>	97.12%
<i>KirOI</i>	cytochrome P450	<i>Streptomyces viridosporus</i>	96.24%
<i>KirD</i>	Aspartate 1-decarboxylase 1 precursor	<i>Streptomyces</i> sp. ADI98-12	96.58%
<i>KirM</i>	class I SAM-dependent methyltransferase	<i>Streptomyces</i> sp. CA-210063	97.17%
<i>KirCII</i>	acyltransferase domain-containing protein	<i>Streptomyces</i> sp. NBRC 110035	94.38%
<i>KirHI</i>	DUF2087 domain-containing protein	<i>Streptomyces</i> sp. AC627_RSS907	91.89%
<i>KirHIII</i>	DUF6204 family protein	<i>Streptomyces</i> sp. AC627_RSS907	97.27%
<i>KirTI/TII</i>	MFS transporter	<i>Streptomyces spongiicola</i>	92.42%
<i>KirRI/RII</i>	TetR/AcrR family transcriptional regulator	<i>Streptomyces</i> sp. NBC_01571	97.81%
<i>KirOII</i>	cytochrome P450	<i>Streptomyces</i> sp. S6	99.27%
<i>KirHIV</i>	hypothetical protein	<i>Streptomyces</i> sp. AC627_RSS907	97.68%
<i>KirHV</i>	DUF3037 domain-containing protein	<i>Streptomyces viridosporus</i>	98.47%
<i>KirN</i>	crotonyl-CoA carboxylase/reductase	<i>Streptomyces</i> sp. NBC_01571	97.58%
<i>KirHVI</i>	phytanoyl-CoA dioxygenase family protein	<i>Streptomyces</i> sp. CA-210063	97.51%
<i>KirE</i>	hypothetical protein AQJ91_46245	<i>Streptomyces dysideae</i>	96.12%

Table 3F: Putative kirromycin-like elfamycin biosynthesis genes from ISL094.

Genes are named according to their kirromycin homolog and function predicted based on their closest hit via NCBI BLAST.

<i>Streptomyces</i> ISL094			
Gene	Function	Closest Blast Hit	AA similarity (%)
<i>KirHI</i>	hypothetical protein	<i>Streptomyces</i> sp. G-G2	94.01%
<i>KirB</i>	non-ribosomal peptide synthetase	<i>Streptomyces</i> sp. CB00455	95.45%
<i>KirM*</i>	methyltransferase	<i>Streptomyces kronopolitis</i>	97.30%
<i>KirCI</i>	ACP S-malonyltransferase	<i>Streptomyces kronopolitis</i>	95.63%
<i>KirOI</i>	cytochrome P450	<i>Streptomyces</i> sp. CB00455	98.09%
<i>KirOII</i>	cytochrome P450	<i>Streptomyces kronopolitis</i>	94.51%
<i>KirD</i>	aspartate-1-decarboxylase	<i>Streptomyces</i> sp. CB00455	96.38%
<i>KirM</i>	class I SAM-dependent methyltransferase	<i>Streptomyces</i> sp. CB00455	96.55%
<i>KirCII</i>	acyltransferase domain-containing protein	<i>Streptomyces kronopolitis</i>	96.21%
<i>KirII (x)</i>	DUF2087 domain-containing protein	<i>Streptomyces</i> sp. CB00455	93.48%
<i>KirHIII</i>	DUF6204 family protein	<i>Streptomyces</i> sp. CB00455	97.30%
<i>KirT/TII</i>	MFS transporter	<i>Streptomyces</i> sp. CB00455	96.95%
<i>KirR/RII</i>	TetR/AcrR family transcriptional regulator	<i>Streptomyces</i> sp. CB00455	96.44%
<i>KirNI</i>	crotonyl-CoA carboxylase/reductase	<i>Streptomyces</i> sp. G-G2	92.90%
<i>KirNII</i>	crotonyl-CoA carboxylase/reductase	<i>Streptomyces globosus</i>	88.89%
<i>KirHVI</i>	DUF3037 domain-containing protein	<i>Streptomyces</i> sp. WAC05292	94.66%
<i>KirHIV</i>	hypothetical protein	<i>Streptomyces</i> sp. CB00455	95.75%
<i>KirP</i>	4'-phosphopantetheinyl transferase	<i>Streptomyces kronopolitis</i>	92.02%
<i>KirAI</i>	SDR family NAD(P)-dependent oxidoreductase	<i>Streptomyces kronopolitis</i>	93.57%
<i>KirAII</i>	SDR family NAD(P)-dependent oxidoreductase	<i>Streptomyces kronopolitis</i>	93.93%
<i>KirAIII</i>	non-ribosomal peptide synthetase	<i>Streptomyces kronopolitis</i>	97.24%
<i>KirAIV</i>	L-histidine N(alpha)-methyltransferase	<i>Streptomyces</i> sp. CB00455	92.26%
<i>KirAV</i>	SDR family NAD(P)-dependent oxidoreductase	<i>Streptomyces kronopolitis</i>	94.21%
<i>KirAVI</i>	type I polyketide synthase	<i>Streptomyces kronopolitis</i>	94.16%

3.2.5.1 PKS/NRPS (KirAI-KirAVI)

In the original study of Weber et al., (2008), names were assigned to each of the genes within the kirromycin BGC which have been used to inform the naming of other elfamycin BGCs such as the aurodox BGC from *S. goldiniensis*, the factumycin BGC from *Streptomyces* spp. WAC5292 and the kiromycin and kirromycin-like BGC of *S. ramocissimus* and *Streptomyces* ISL094 from this study. As observed in all of the elfamycin BGCs elucidated in this study, and reflected structurally in the elfamycin compounds themselves, there is a homologous polyketide synthase (PKS)/ Non-Ribosomal Peptide Synthase (NRPS) cascade consisting of both cis and trans-acetyltransferases and trans-malonyl and ethylmalonyl transferase docking domains present. These genes have been termed *kirAI-kirAVI* and show homology to the *aurAI-aurAVI* and *facAI-facAVI* genes from other elfamycin producers (Gui et al., 2015; McHugh et al., 2022; Weber et al., 2008).

Using AntiSMASH ClusterTools software to annotate PKS/NRPS modularity, the PKS/NRPS modules of KirAI-KirAVI were predicted for both *S. ramocissimus* (Fig. 3.29) and *Streptomyces* ISL094 (Fig. 3.30) as was done with Aurodox and Kirromycin previously. It is predicted that the modular nature of KirAI-KirAVIs catalytic domains permit the enzymatic extension of an acetyl-CoA molecule, with KirI and KirII extending the acetyl-CoA molecule via Claisen condensation reactions, as seen in kirromycin and aurodox biosynthesis (McHugh et al., 2022; Robertsen et al., 2018). Based on the AntiSMASH ClusterTools output and cross-referencing with the corresponding modules of KirAI-KirAVI enzymes from *S. collinus*, it can be predicted that AurIII is a hybrid PKS/NRPS enzyme with catalytic activity enabling condensation of glycine and incorporation of an amide bond. This process is conserved in the pathway of kirromycin biosynthesis in *S. collinus*, where KirAIII contains consecutive condensation and adenylation domains. Finally, KirAIV-KirAVI are predicted to extend the kirromycin backbone in all four kirromycin-like elfamycin encoding BGCs.

When the domain structure from kirromycin biosynthesis genes from *S. ramocissimus* was compared to KirAI-KirAVI from *S. collinus*, an additional dehydratase domain (DH) was present on KirAII from *S. ramocissimus*, the location of which has been added to the proposed kirromycin biosynthesis pathway for *S. ramocissimus* (Red box, Fig. 3.29). When compared to *Streptomyces* ISL094, the trans-AT docking domain from KirAIV in *S. collinus* has been replaced by a dehydratase domain, shown by a red box (Fig. 3.30), and may represent an alternative mechanism for double bond formation in these molecules (Barajas et al., 2019; Nair et al., 2020; Yin and Dickschat, 2021).

3.2.5.2 Malonyl and ethylmalonyl transferase (KirCI and KirCII)

As observed in both kirromycin biosynthesis from *Streptomyces collinus*, and aurodox biosynthesis from *S. goldiniensis*, it is predicted that the genes from *S. ramocissimus* and *Streptomyces* ISL094 encode homologs of KirCI and KirCII, trans-acting malonyl and ethylmalonyl transferase enzymes which function, in conjunction with the cis-AT domains within KirAVI is to supply the extender units of the extending polyketide chain successively via KirAI-KirAV (McHugh et al., 2022; Robertsen et al., 2018; Weber et al., 2008, Fig. 3.29 and Fig. 3.30).

3.2.5.3 Aspartate-1-decarboxylase and NRPS (KirD and KirB)

The non-ribosomal peptide synthetase KirB catalyses the incorporation of β -alanine into the growing polyketide chain. The β -alanine for this provided through the action of the aspartate-1-decarboxylase, KirD, a homolog of the primary metabolic enzyme PanD, required for pantothenate biosynthesis. KirAIV-KirAI are proposed to extend the kirromycin backbone further, before KirB, which contains the conserved DTLQLGVIWK motif, a sequence indicative of alanine accepting active sites (Rausch et al., 2005), catalyses the incorporation of β -alanine. This has been shown in both

kirromycin and aurodox biosynthesis and is comparable to the BGC architecture of *S. ramocissimus* and *Streptomyces* ISL094 (Laiple et al., 2009; McHugh, 2020; McHugh et al., 2022; Fig. 3.29 and 3.30).

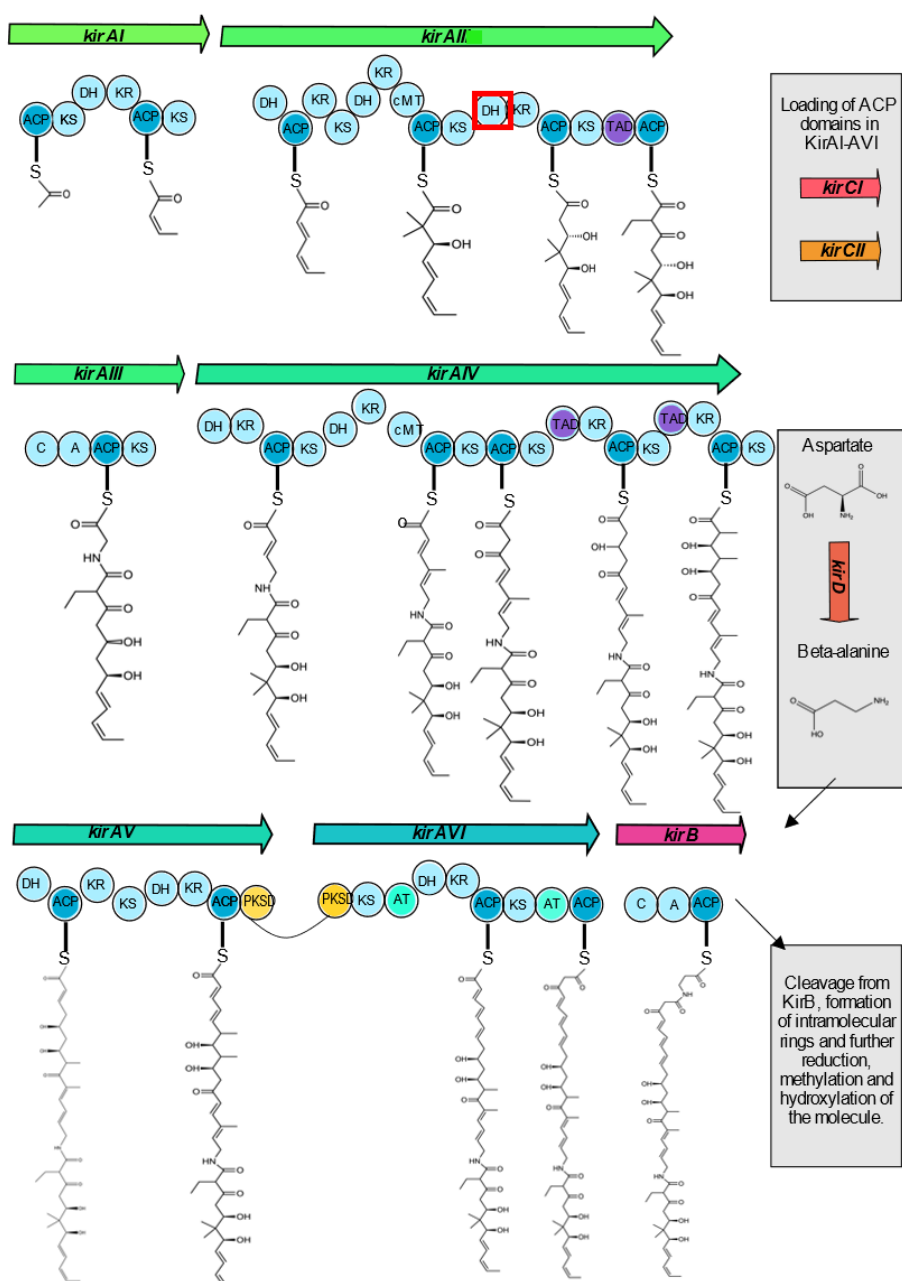


Figure 3.29: Proposed biosynthesis of kirromycin backbone from *S. ramocissimus* by the enzymes KirAI-KirAVI. ACP: acyl carrier protein; AT: acyltransferase domain; C: condensation domain; DH: dehydratase domain ER: enoyl reductase domain; KR: keto reductase domain; KS: keto synthase domain; MT: methyl transferase domain; PKP: peptidyl carrier protein; TAD: trans-AT docking domain. Compared to kirromycin biosynthesis in *S. collinus*, additional DH domain is shown in red box. Figure created on InkScape.

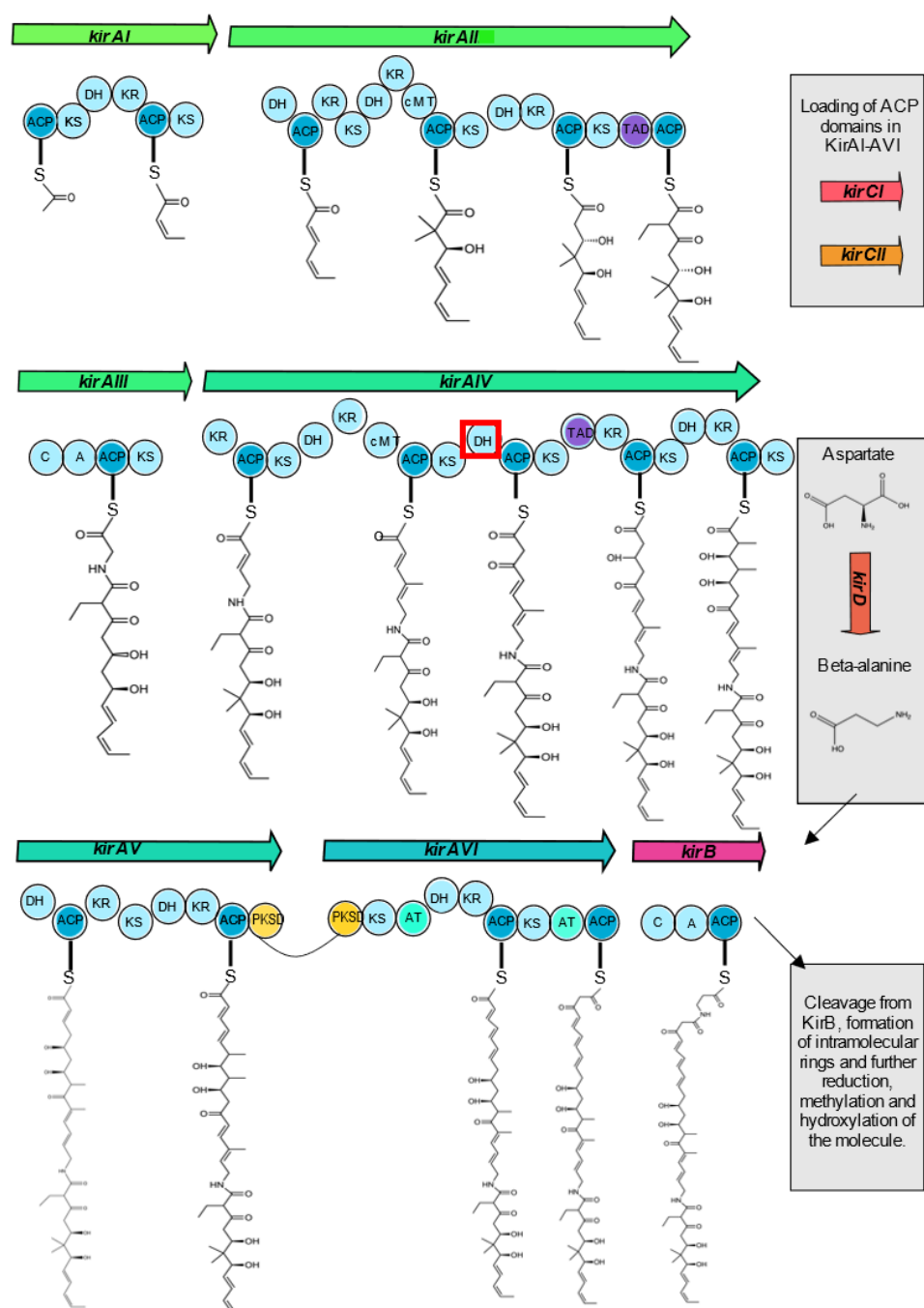


Figure 3.30: Proposed biosynthesis of kirromycin-like elfamycin backbone from *Streptomyces* ISL094 by the putative enzymes KirAI-KirAVI. ACP: acyl carrier protein; AT: acyltransferase domain; C: condensation domain; DH: dehydratase domain ER: enoyl reductase domain; KR: keto reductase domain; KS: keto synthase domain; MT: methyl transferase domain; PCP: peptidyl carrier protein; TAD: trans-AT docking domain. Figure created on InkScape.

Given the kirromycin BGC from *S. collinus* possesses two genes (*kirP* and *kirE*) that are absent from the aurodox BGC from *S. goldiniensis*, and that *S. goldiniensis* possesses two additional genes (AurQ and AurM*) not present in the kirromycin BGC, it is also known that different molecules are produced, although structurally AurM* is responsible for the only difference in the final product. This logic could be applied to all four BGCs responsible for the kirromycin-like elfamycin production (Discussed above), and whilst there is great similarities between the BGCs responsible for production of kirromycin-like elfamycins from the four producers, there are regions of dissimilarity which may provide insight into the type of molecule produced by *Streptomyces* ISL094.

3.2.5.4 Phosphopantetheinyl transferase (PPTase, KirP)

Firstly, when compared to the three other kirromycin-like BGCs, the aurodox BGC does not possess a gene encoding a phosphopantetheinyl transferase (PPTase, Fig. 3.28). Commonly, in BGCs encoding the production of PKS/NRPSs, PPTases are present to facilitate post-translational activation of acyl carrier proteins (ACPs) in PKSs and peptidyl carrier proteins (PCPs) in NRPSs (Owen et al., 2011). Pavlidou et al., (2011) showed that in the biosynthesis of kirromycin, the PPTase, encoded by *kirP*, catalysed the activation of ACPs and PCPs during biosynthesis via transfer of the phosphopantetheinyl arm, which is required for attachment of intermediates. Given that two of the three known kirromycin-like BGCs (exception is aurodox) also possesses PPTases (Fig. 3.28 & Table 3E, 3F, 3G). It is hypothesised that there is likely a promiscuous PPTase present elsewhere within the genome of *S. goldiniensis* which may catalyse this activity. The PPTase has been postulated to be essential (Thaker et al., 2012), as deletion of the PPTase from the kirromycin BGC in *S. collinus* resulted in a 90% decrease in kirromycin production (Pavlidou et al., 2011). As the kirromycin-like elfamycin BGCs from *S. goldiniensis* and *S. ISL094* are similar, it was

proposed that using amino acid sequence of the PPTase on the BGC from *Streptomyces* ISL094 may help identify potential PPTases present elsewhere in the genome of *S. goldiniensis* which act on the aurodox. BLAST analysis of the amino acid sequence of the *S. ISL094* PPTase against the *S. goldiniensis* genome showed that there were two PPTases present within the genome. One of these PPTases is located within a Type-2-polyketide synthase BGC with a 60% similarity to fluostatins M-Q (found on region 1.22 of the *S. goldiniensis* genome, Fig. 3.31, gold), and the other is located within a Type-1-polyketide synthase BGC, where the cluster has a 40% gene similarity to that of a marineosin A/B polyketide (found on region 1.33, Fig. 3.31, gold). Phylogenetic analysis of these two potential PPTases with those found on the other kirromycin-like BGCs indicates that those which are present on kirromycin-like BGCs clade together, as seen for *S. ramocissimus* (Fig. 3.31, Blue), *S. collinus* (Green) and *S. ISL094* (Red). The two PPTases present elsewhere in the *S. goldiniensis* genome (Fig. 3.31, shown in gold) are less similar. One hypothesis proposed is that the hypothetical protein that lacks a homolog in the kirromycin BGC, AurQ is an uncharacterised protein with PPTase-like activity (McHugh, 2020), which is investigated in Chapter 4 of this thesis.

3.2.5.5 Phytanoyl-CoA hydroxylase (PhyH, KirHVI)

The second observation that can be made is that *Streptomyces* ISL094 lacks a phytanoyl-CoA hydroxylase (PhyH, Table 3G) encoded for by Kir/AurHVI. PhyH catalyses the 2-hydroxylation of 3-methyl-branched acyl-CoAs (Croes et al., 2000). The role of KirHVI was elucidated to function as a hydroxylase, as a mutant in *kirHVI* lack a hydroxyl group at the C-30 position in the furan moiety of kirromycin (Robertsen et al., 2018). This could potentially deliver a final molecule without the C-30 hydroxylation.

3.2.5.6 Crotonyl CoA (KirN)

Several genes within the four clusters, such as the crotonyl CoA (KirN) appear to be duplicated, with two copies of each gene annotated. KirN appears to have two copies of the same gene (KirNI and KirNII) in *Streptomyces* ISL094 (Table 3G). Due to the amino acid sequence lengths of KirNI and KirNII being much shorter than that of the other KirN homologs and both genes situated beside each other in the BGC, it was predicted that both KirNI and KirNII are misannotated and make up a full length KirN from *Streptomyces* ISL094 is due to an error in sequencing. To test this, an amino acid alignment was generated (ClustalOmega) and the domain structures of KirNI and KirNII against AurN from the BGC of aurodox was performed on InterPro (Paysan-Lafosse et al., 2022), to resolve domain architecture (Fig. 3.33). These analyses show that KirNI from *Streptomyces* ISL094 encodes the N terminus of the protein KirN/AurN as seen in other kirromycin-like elfamycin BGCs and KirNII encodes the C terminus (Fig. 3.33) suggesting KirNI/KirNII is mis-annotation of genes.

3.2.5.7 TetR family transcriptional regulator (KirR)

The same can be observed when trying to resolve the TetR family transcriptional regulator KirRI/KirRII from *S. collinus*. Three of the kirromycin-like BGCs encode one regulator, KirR/AurR, where same is not true for *S. collinus* which possesses two, located beside each other on the BGC (Table 3G). The same phenomenon of shorter genes was observed and so similar amino acid alignment (ClustalOmega) and domain elucidation by InterPro was carried out. From the amino acid alignment, it seems KirRII from *S. collinus* is responsible for the encoding of the N terminus of KirR, when compared to that from *S. ramocissimus*, this was validated by the domain output by InterPro showing similar protein domains in KirRII from *S. collinus* at the beginning of KirR from *S. ramocissimus* (Fig. 3.34). The C terminus of KirR from *S.*

ramocissimus was shown to correspond to KirRI from *S. collinus*, further confirming this hypothesis (Table 3G; Fig. 3.34, Weber et al., 2008).

3.2.5.8 Cytochrome p450 (KirO)

Finally, the BGC of *Streptomyces* ISL094 possesses an additional cytochrome p450 in comparison to the kirromycin-like BGCs of the other three strains, termed KirO0 (Table 3G). Given the BGC of aurodox exists as part of a 'supercluster' encoding other compounds such as bottromycin and concanamycin A, other additional cytochrome P450s were also identified on this BGC upstream of the aurodox coding region with homology to that of KirO0, termed AurO0 for the purpose of this analysis. Phylogenetic assessment of all cytochrome P450s present in these BGCs was performed to understand the distribution of these in the kirromycin-like clusters (Fig. 3.32). It was found that KirO0 (Red) was closely related to AurO0 (Gold) compared to the cytochrome P450s present in the coding region of the other kirromycin-like BGCs (blue, green). (Fig. 3.32) This was unexpected due to the similar structure of the aurodox BGC of *S. goldiniensis* and kirromycin-like BGC from *Streptomyces* ISL094 both possessing a cytochrome P450 at the end of each cluster. This suggests that this additional cytochrome P450 of *Streptomyces* ISL094 may either be replacing the missing hydroxylation reaction (from PhyH), which is well established in natural products (Rudolf et al., 2017) maybe involved in biosynthesis of other compounds such as Type-1 polyketides as indicated by the antiSMASH output. Further analysis shows that the other two cytochrome P450s of *Streptomyces* ISL094 have distinct homologs in the other kirromycin-like elfamycin BGCs and are termed KirOI and KirOII in line with their homology. Interestingly, however, with this nomenclature in mind, it can be seen that the cytochrome P450s of *Streptomyces* ISL094 have undergone a re-arrangement when compared to that of the aurodox BGC of *S. goldiniensis*, where the AurOI homolog of KirOI is situated directly after KirOII instead of at the beginning

of the BGC (Fig. 3.28) This maybe a direct example of gene displacement and should be investigated further with the context of BGC evolution in mind.

Table 3G: Analysis of the genes present of kirromycin-like elfamycin BGCs reveals gene loss, duplication and addition. In comparison to the kirromycin BGC of *S. collinus*, genes missing from other elfamycin BGCs are highlighted in red, additional genes are shown in green and genes which appear to be additional but are through to be one gene split into two, encoding two components of the same protein are shown in yellow.

Gene function		Gene name	<i>S. collinus</i>	<i>S. ramocissimus</i>	<i>S. goldiniensis</i>	ISL094
4'-phosphopantetheinyl transferase (PPTase)		KirP	1	1	0	1
phytanoyl-CoA dioxygenase family protein (PhyH)		KirHVI	1	1	1	0
Crotonyl CoA carboxylase/reductase		KirN/KirNII	1	1	1	2
TetR family transcriptional regulator		KirR/KirRII	2	1	1	1
Cytochrome P450		KirOI & KirOII	2	2	2	3

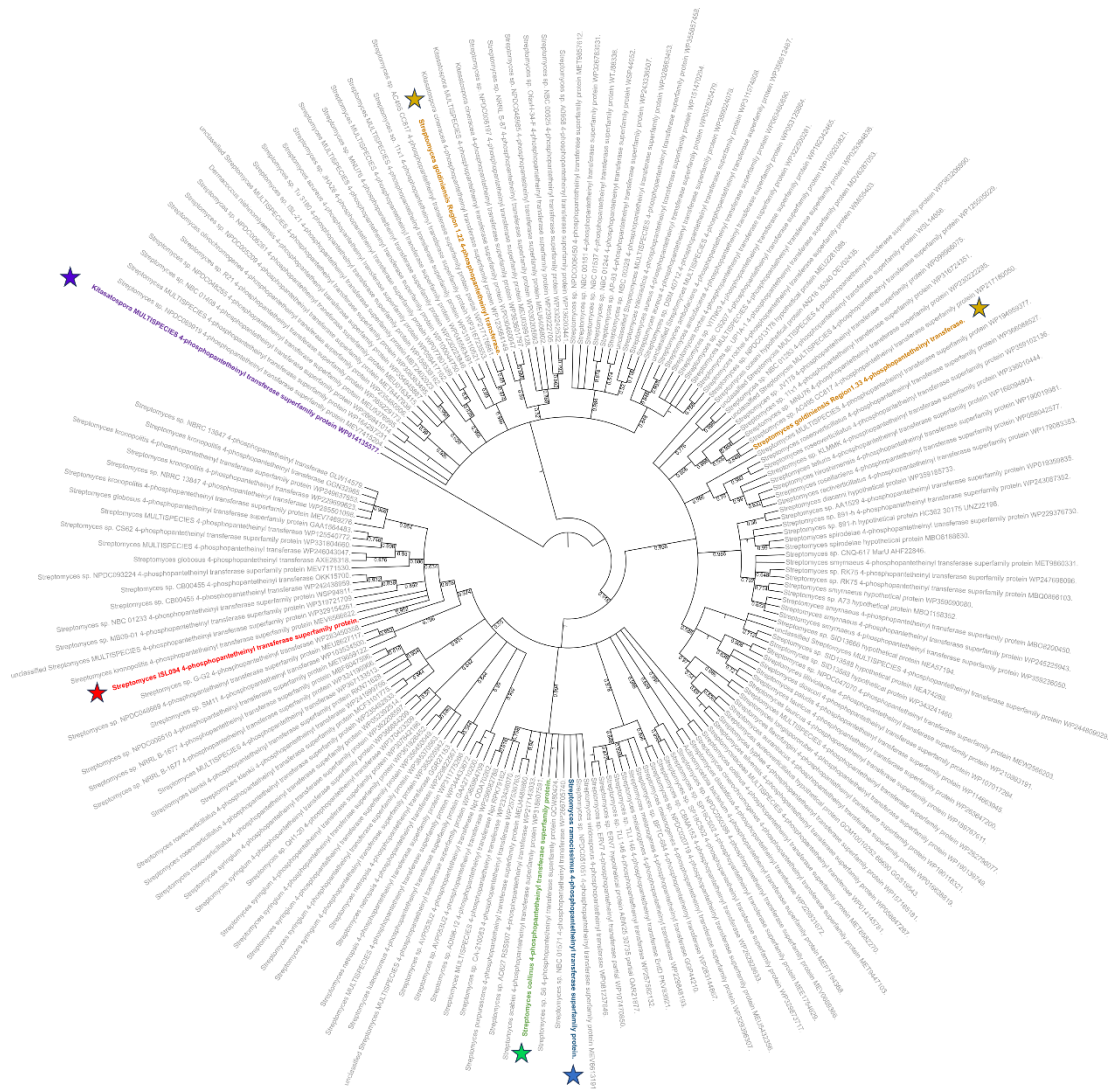


Figure 3.31: Phylogenetic analysis of phosphopantetheinyl transferase superfamily protein (KirP) from *S. collinus*, *S. ramocissimus* and the putative PPTases from *S. goldinensis* and *S. ISL094*. Amino acid sequences from similar phosphopantetheinyl transferases were subject to alignment via clustal omega. Evolutionary history was inferred by using the Maximum Likelihood method and JTT matrix-based model. The bootstrap consensus tree inferred from 500 replicates was generated on MegaX and nwk file visualised on ITOL.

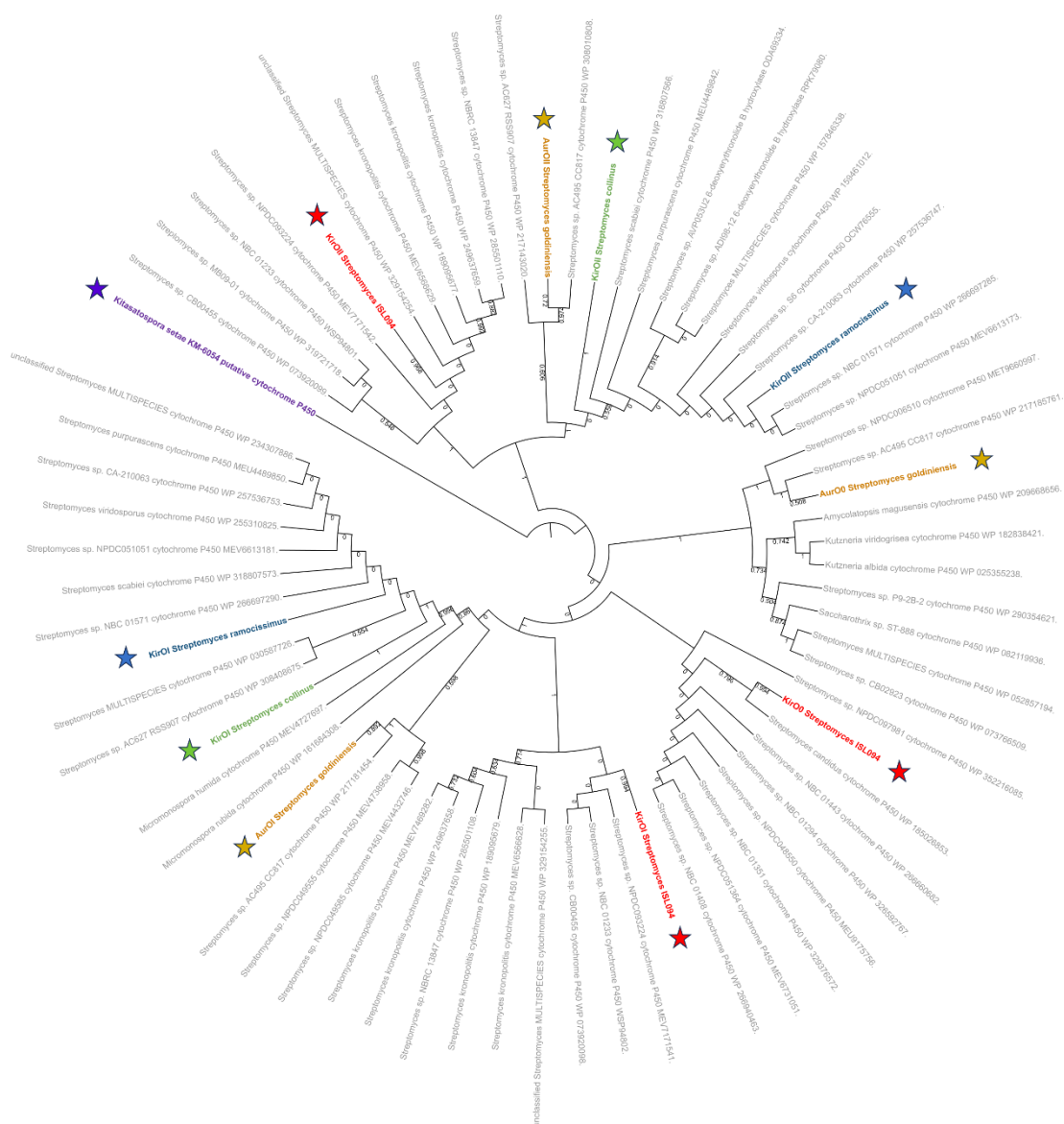


Figure 3.32: Phylogenetic analysis of cytochrome P450s from four kirromycin-like elamycin BGCs from *S.ramocissimus*, *S. collinus*, *S.goldinensis* and *S. ISL094*. Amino acid sequences from similar cytochrome P450s were subject to alignment via clustal omega. Evolutionary history was inferred by using the Maximum Likelihood method and JTT matrix-based model. The bootstrap consensus tree inferred from 500 replicates was generated on MegaX and nwk file visualised on iTOL.

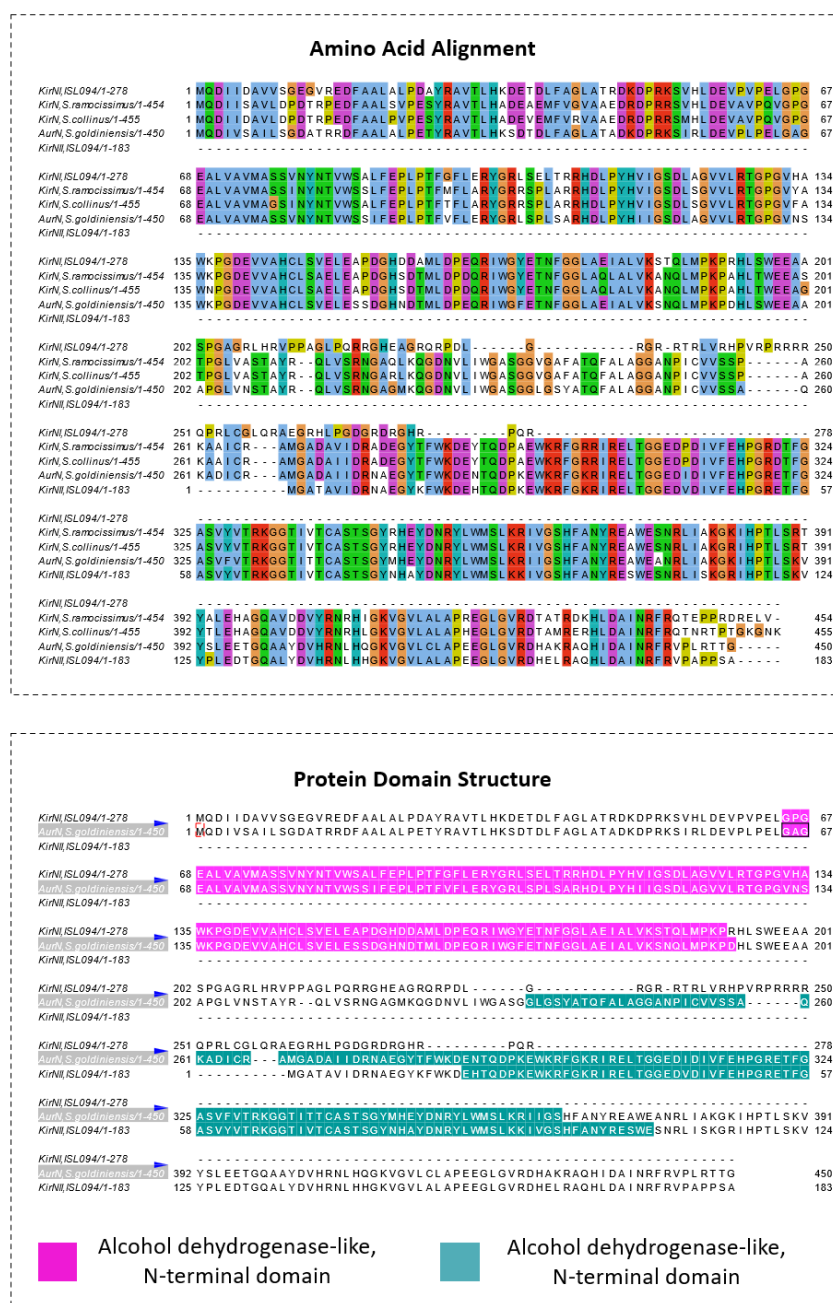


Figure 3.33: Solving the domain structures of the Crotonyl CoA carboxylase/reductase from ISL094. Amino acid alignments were generated on Clustal Omega and visualised on Jalview. FASTA sequences of Crotonyl CoA carboxylase/reductase from ISL094 and *S. goldiniensis* elfamycin BGCs were input to InterPro and protein domain structures identified and mapped onto amino acid alignment. Alcohol dehydrogenase-like, C-terminal shown in cyan, Alcohol dehydrogenase-like, N-terminal domain shown in pink.

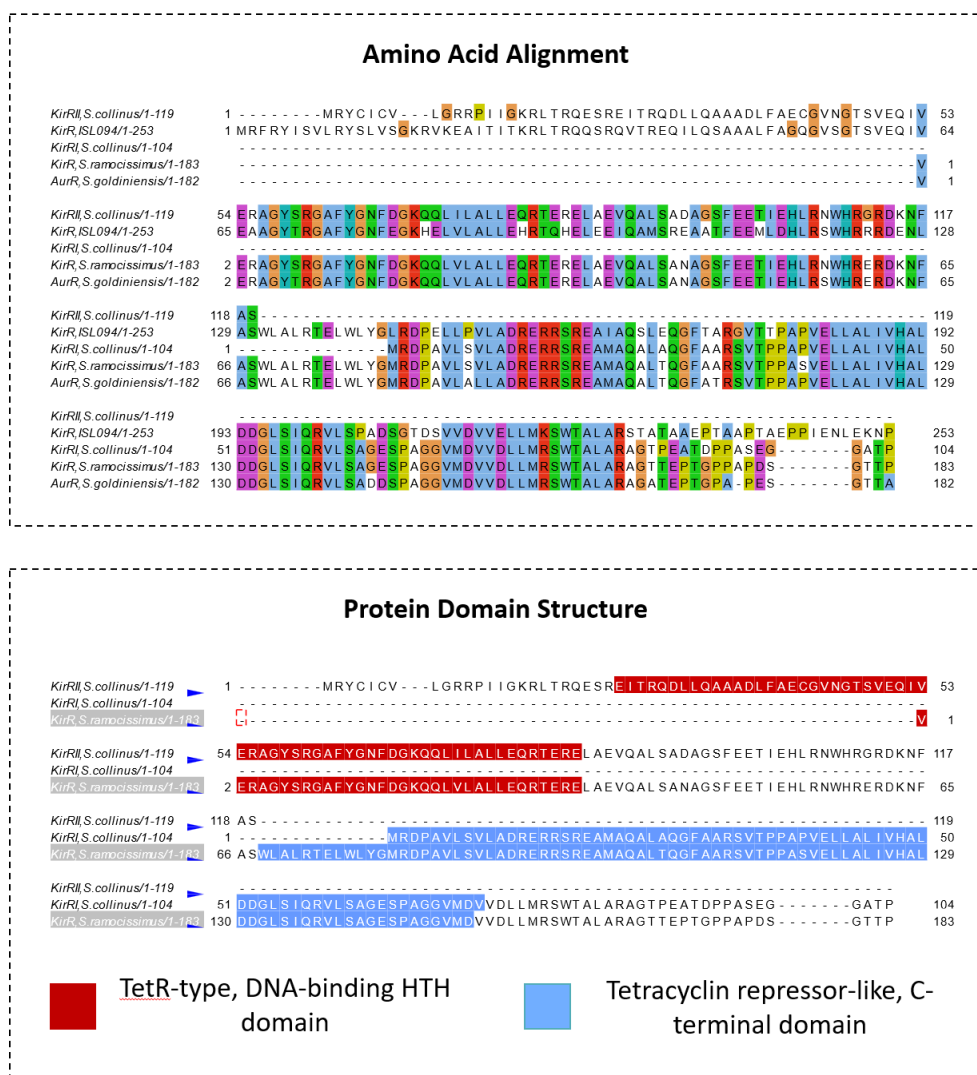


Figure 3.34: Solving the domain structures of the TetR family transcriptional regulator from *S. collinus*. Amino acid alignments were generated on Clustal Omega and visualised on Jalview. FASTA sequences of Crotonyl CoA carboxylase/reductase from ISL094 and *S. goldiniensis* elfamycin BGCs were input to InterPro and protein domain structures identified and mapped onto amino acid alignment. TetR-type, DNA-binding HTH domain shown in red, Tetracycline repressor-like, C-terminal domain shown in blue.

3.2.5.9 Methyltransferase (KirM*/AurM*)

When the genes responsible for the tailoring of the elfamycin molecular are examined (Fig. 3.35), the kirromycin-like clusters from ISL094 and *S. goldiniensis* are the only two of the four BGS to contain an additional methyltransferase (AurM* and KirM*). The absence of a second methyltransferase in the BGC of the known kirromycin producers *S. collinus* and *S. ramocissimus* is no surprise when the absence of methylation on the pyridone ring of kirromycin is considered (Fig. 3.28). The methyltransferase, AurM*, of the aurodox BGC of *S. goldiniensis* was found to be responsible for the conversion of kirromycin to aurodox during the last step of biosynthesis (McHugh et al., 2022). This, coupled with the elfamycin BGC of ISL094 showing most genetic similarity to that of the aurodox BGC of *S. goldiniensis* (Fig. 3.28), suggests that the elfamycin BGC of ISL094 could contain the genetic potential for aurodox production.

When the protein alignment structure of the two methyltransferases AurM* and KirM* is compared, they are found to be highly similar (81.08% amino acid similarity). Interestingly, while not identical, the proteins are very closely related, each contains 332 amino acid residues, with no gaps (Fig. 3.36, A). Additionally, when the predicted protein structure (AlphaFold) is analysed the 3D models are congruent (Fig. 3.36 B). when both 3D structures of AurM* and KirM* were aligned, the RMSD (root mean square deviation) was computed between aligned pairs of the backbone C-alpha atoms in superposed structures. The superposed structure of AurM*/KirM* had a low RMSD score of 0.561, indicating the two structures had little deviation from each other. Secondly, the TM-score (template modelling score) was calculated as a measure of topological similarity between the template (AurM*) and model structures (KirM*). The TM-score ranges between 0 and 1, where 1 indicates a perfect match and 0 is no match between the two structures. In this case, a score of 0.81 is a

remarkably close match, indicating topological similarity between the proteins AurM* and KirM*.

One of the most studied families of methyltransferases is the S-adenosyl-L-methionine (SAM) dependent family, of which AurM* belongs. The first SAM dependant methyltransferase structure to be identified was catechol O-MTase (COMT): an enzyme involved in the metabolism of neurotransmitters in the central nervous system (Vidgren et al., 1994) The structure of COMT consists of eight alpha-helices and one beta-sheet to form the characteristic Rossman fold arrangement of the B-E helices and the 1-5 strands. This structural fold is highly conserved across all known SAM methyltransferases, despite the SAM binding domain varying greatly over the family (Martin and McMillan, 2002). The methyltransferases of AurM* and KirM* adopt this same structure which is unsurprising given the known conserved structural fold of the SAM dependant methyltransferases.

These similarities between KirM* from *Streptomyces ISL094* and AurM* from *S. goldiniensis* continue to be observed when phylogeny is analysed. All methyltransferases present on the kirromycin-like elfamycin clusters of *S. goldiniensis*, *S. ISL094*, *S. collinus* and *S. ramocissimus*, were analysed in a maximum likelihood tree alongside their closest hits from NCBI BLAST (Fig. 3.37). The results show a distinct split in how related the methyltransferases are, with Aur/KirM methyltransferases sitting firmly on the opposite clades of the tree from Aur/KirM*. As KirM* from *S. ISL094* is more related to AurM* than that of the other methyltransferases, this continues to support the argument that KirM* could have a role in the biosynthesis of Aurodox, similar to that which AurM* has in aurodox biosynthesis.

Though similar, AurM* and KirM* sit further from each other than first expected. It can be seen that KirM* did not evolve from AurM*, therefore suggesting that a recruitment event of AurM* to the kirromycin-like BGC of *S. ISL094* is unlikely. Instead, KirM* and

AurM* are evolutionary cousins and share a recent common ancestor which likely lead to the diversification of both. Evolutionary, this suggests that two independent recruitment events occurred in the kirromycin-like BGCs of *S. goldiniensis* and *S. ISL094* resulting in the formation of aurodox BGCs in both.

This recruitment of M* to two individual kirromycin-like BGCs suggests that the same may be happening in other kirromycin-like elfamycin clusters. Potentially indicating the presence of other aurodox producers.

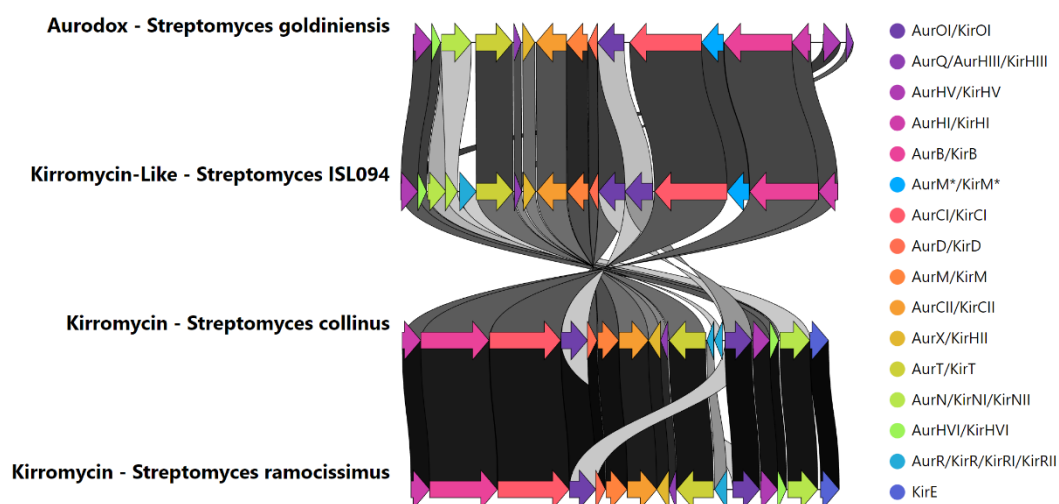


Figure 3.35: Comparison of gene similarity of the tailoring genes present on elfamycin gene clusters. Adjoining lines represent amino acid similarity according to scale. Figure generated by clinker.py. Light blue genes highlight the additional methylation of aurodox, encoded by the SAM-dependant *N*-methyltransferase and the putative SAM-dependant Methyltransferase of KirM*.

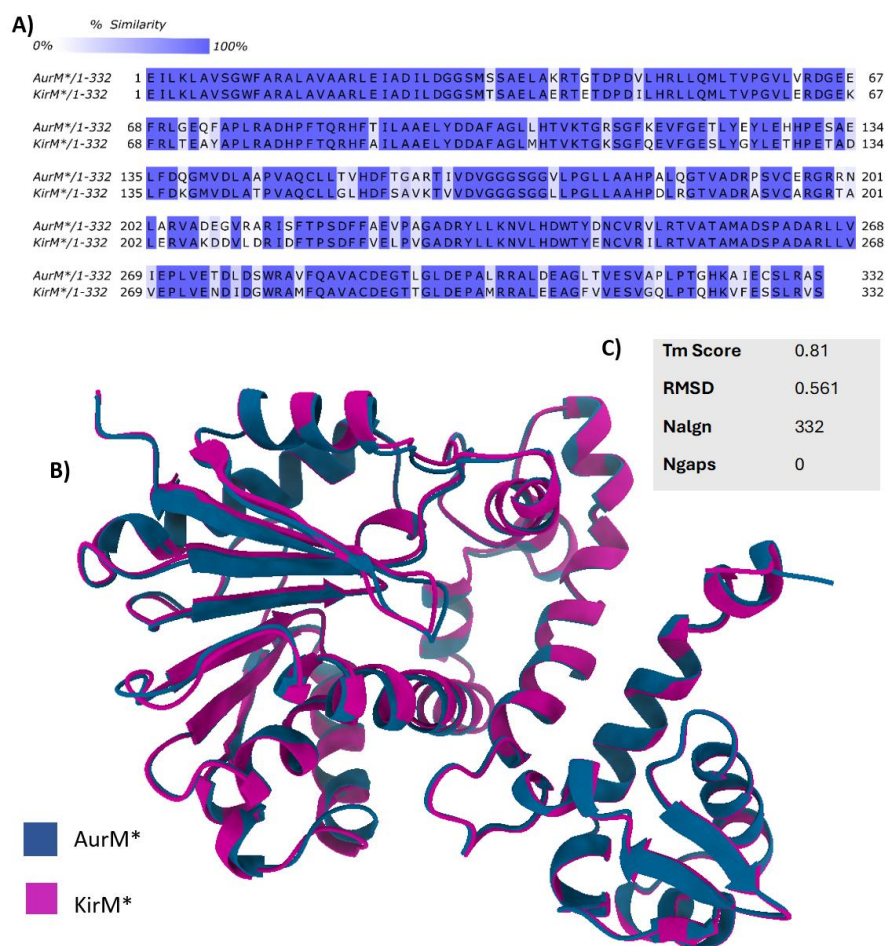


Figure 3.36: AurM* and KirM* share a high Amino acid similarity and predicted protein structure. (A) Amino acid alignments were generated on Clustal Omega and visualised on Jalview. (B) Protein structures generated on AlphaFold software (accessible at https://colab.research.google.com/github/sokrypton/ColabFold/blob/main/beta/AlphaFold2_advanced.ipynb#scrollTo=Riekgf0KQv_3). Five iterations of protein structure were run for maximum accuracy and structure consensus. Output PDB files were input into PDBE Fold (accessed at www.rcsb.org/alignment, Bittrich et al., 2024)) and aligned using jFATCAT (Z. Li et al., 2020) with 'rigid parameters'. The superposed structures were viewed and images edited on ChimeraX software (version 1.6.1). (C) PDBE superposed protein structure statistics are given indicating structural similarity.

3.2.6 Discovery of other potential kirromycin-like biosynthetic gene clusters.

Since the protein structures and topology of AurM* and KirM* are so well conserved (Fig. 3.36), and the BGC architecture of Aurodox from *S. goldiniensis* and the putative BGC of kirromycin/Aurodox from *Streptomyces* ISL094 is similar (Fig. 3.28), it was thought that the conservation of these SAM dependant methyltransferases may be useful in the exploration for more putative aurodox BGCs with similar structure to the Aurodox in addition to that of *Streptomyces* ISL094.

The amino acid sequence of AurM* was subject to NCBI BLAST against the refseq_protein database and accession numbers from the top 100 hits were used for input into FlaGs (Saha et al., 2021) FlaGs, name meaning flanking genes, can be used to analyse the conservation of gene neighbourhoods from a given query gene or gene sequence. FlaGs reveals 123 different homologous groups of flanking genes. These are mostly *Streptomyces* species with exception of some, for example: *Kitasatospora Spp.*, *Pectobacterium Spp.* and *Micromonospora Spp.* (Fig. 3.38).

From the analysis, several BGCs were identified with similar structure to that of Kirromycin/aurodox. Of the 123 different homologous groups of flanking genes, groups 1-5 were of particular interest in this analysis. These groups are as follows; 1- Non-Ribosomal Peptide synthetase/Acyltransferase, 2 - Cytochrome P450, 3 - Hypothetical protein, 4 - Class I SAM-dependent methyltransferase, 5 – Aspartate 1-decarboxylase. Within the species that contain this particular sequence of genes (Fig. 3.39), six of the species contained polyketide synthases/ non-ribosomal peptide synthetase upstream of the sequence. As shown previously in this Chapter (Fig. 3.28) this is the case for the Aurodox and Kirromycin encoding BGCs. The species were *Amycolatopsis magusensis* (one duplicate), *Amycolatopsis cihanbeyliensis*, *Micromonospora humida*, *Micromonospora rubida* and *Saccharopolyspora sp. NFXS83*.

WP_141561066.1:751Mycocystis aeruginosa BAWA0137a
 WP_159474402.1:193Mycobacterium thermophilum
 WP_180743138.1:84Pectobacterium carotovorum
 WP_214145413.1:95Pectobacterium carotovorum subsp. carotovorum
 WP_141512816.1:83Pectobacterium actinodorum
 WP_224010911.1:89Pectobacterium actinodorum
 WP_318493156.1:89Pectobacterium actinodorum
 WP_240348310.1:83Pectobacterium polium
 WP_214525442.1:89Pectobacterium polium
 WP_240604818.1:87Pectobacterium polium
 WP_217108211.1:89Pectobacterium polium
 WP_240315841.1:89Pectobacterium polium
 WP_216518414.1:87Pectobacterium polium
 WP_217003181.1:89Pectobacterium polium
 WP_215925549.1:89Pectobacterium polium
 WP_174873323.1:89Pectobacterium polium
 WP_142401817.1:87Mycobacterium sp. J2208.183
 WP_235404385.1:76Thiobacillus bogovici
 WP_097124222.1:73Thiobacillus maritima 3111
 WP_275420212.1:43Thiobacillus thiooxidans
 WP_245318128.1:100Streptomyces griseochromogenes
 WP_047942441.1:41Streptomyces griseochromogenes
 WP_184147346.1:40Streptomyces olivaceus/oblivus
 WP_245215444.1:57Streptomyces sp. B000.15.9
 WP_215480687.1:56Streptomyces olivaceus/oblivus
 WP_120386609.1:45Streptomyces sp. 12
 WP_187145812.1:43Streptomyces sp. Scl3.3
 WP_144281544.1:40Streptomyces sp. B011.188
 WP_240274371.1:31Streptomyces sp. B09.87
 WP_277444025.1:45Streptomyces sp. S0042
 WP_248881815.1:43Streptomyces sp. ST13.2.2
 WP_042488181.1:43Streptomyces sp. C04
 WP_248393774.1:41Streptomyces sp. B0C.01275
 WP_248881815.1:43Streptomyces olivaceus/oblivus
 WP_267481318.1:38Streptomyces sp. B1
 WP_148131121.1:35Streptomyces sp. CCM.002014
 WP_150171510.1:31Streptomyces tendae
 WP_189744419.1:38Streptomyces tendae
 WP_247498827.1:37Streptomyces sp. B023
 WP_234380214.1:40Streptomyces tendae
 WP_264316105.1:36Streptomyces sp. B023
 WP_23774244.1:79Oncobasella coenobacterae
 WP_043451841.1:41Streptomyces sp. 2114.4
 WP_177144889.1:41Streptomyces sp. 2113.5
 WP_188237333.1:44Actinobacteria subsp.
 WP_178918189.1:42Actinobacteria subsp.
 WP_235977446.1:77Streptomyces parvus/parvus
 WP_125644444.1:74Streptomyces chrysomycetoides KCM.4735
 WP_26845738.1:78Streptomyces chrysomycetoides
 WP_56781748.1:68Streptomyces griseochromogenes
 WP_171008111.1:73Actinobacteria sp. B002.109
 WP_230158615.1:80Actinobacteria subsp.
 WP_114017393.1:39Streptomyces tendae/oblivus
 WP_07784414.1:27Streptomyces tendae/oblivus
 WP_17673414.1:38Streptomyces sp. OryM.343
 WP_265289713.1:43Streptomyces sp. B01
 WP_248927097.1:44Streptomyces sp. B0C.00654
 WP_148413615.1:40Streptomyces sp. B01.1
 WP_138441872.1:47Streptomyces subsp.
 WP_14134487.1:76Streptomyces chrysomycetoides
 WP_161952211.1:46Streptomyces tendae/oblivus
 WP_161952211.1:46Streptomyces tendae/oblivus
 WP_048781313.1:32Cyanobacteria sp.
 WP_097784446.1:44Streptomyces sp. B018
 WP_122447385.1:33Streptomyces tendae/oblivus
 WP_25649522.1:33Streptomyces tendae/oblivus
 WP_07899997.1:30Streptomyces tendae/oblivus
 WP_077844442.1:44Streptomyces tendae/oblivus
 WP_077844442.1:44Streptomyces tendae/oblivus
 WP_105971843.1:21Streptomyces tendae
 WP_154444446.1:26Streptomyces sp. B01.2.36
 WP_110066163.1:28Streptomyces tendae/oblivus
 WP_141310880.1:31Streptomyces tendae/oblivus
 WP_14198738.1:23Streptomyces tendae/oblivus
 WP_240273874.1:21Streptomyces tendae/oblivus
 WP_208644802.1:20Streptomyces tendae/oblivus
 WP_246877945.1:23Streptomyces tendae/oblivus
 WP_141684112.1:19Streptomyces tendae/oblivus
 WP_24945144.1:17Streptomyces tendae/oblivus
 WP_215431271.1:18Streptomyces sp. AC49.0C817
 WP_214144891.1:13Streptomyces sp. B01787
 WP_114059181.1:13Streptomyces tendae/oblivus
 WP_13154782.1:19Streptomyces sp. WAC0393
 WP_181214481.1:18Streptomyces sp. B011
 WP_283418121.1:18Streptomyces sp. G.03
 WP_07892101.1:40Streptomyces sp. CCM.015
 WP_215019231.1:73Streptomyces sp. B01.14
 WP_248877441.1:18Streptomyces tendae/oblivus
 WP_18981871.1:18Streptomyces tendae/oblivus
 WP_138818124.1:18Streptomyces tendae/oblivus
 WP_209317891.1:18Streptomyces tendae/oblivus
 WP_015392512.1:18Streptomyces tendae/oblivus
 WP_23448242.1:11Streptomyces tendae/oblivus
 WP_18474548.1:11Streptomyces tendae/oblivus
 WP_184941818.1:14Streptomyces sp. B001.8.1677
 WP_27715222.1:24Streptomyces sp. AAB
 WP_254780181.1:14Streptomyces sp. AAB

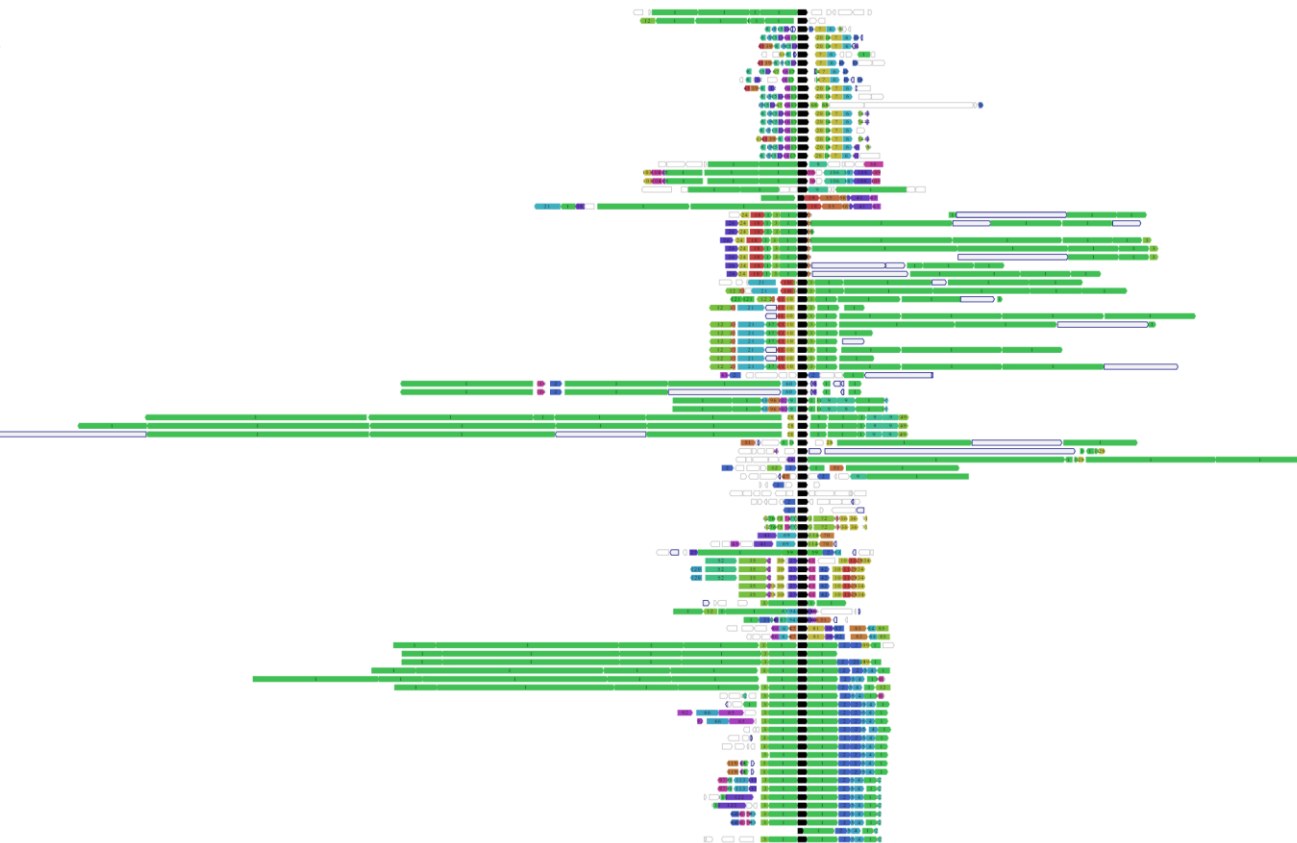


Figure 3.38: FlaGs identified gene clusters with similar methyltransferases to AurM*. Top 100 NCBI BLAST hits for similar amino acid sequences to AurM* were included in the FlaGs analysis. To-scale figure of flanking genes is shown. Empty genes with grey borders are not conserved in the dataset, and grey genes with blue borders are pseudogenes. FlaGs reveals 123 different homologous groups of flanking genes.



Black **SAM-dependant methyltransferase (AurM* query)**

1	Non-Ribosomal Peptide synthetase/Acyltransferase
2	Cytochrome P450
3	Hypothetical protein
4	Class I SAM-dependent methyltransferase
5	Aspartate 1-decarboxylase

Figure 3.39: Schematic of the FlaGs groups of flanking genes corresponding to that of the Aurodox and Kirromycin BGCs (1-5). Homologous group number and predicted gene function are shown for groups 1-5.

The genomes of the five species were used as a query in AntiSMASH (V6) using 'strict' parameters to mine the genome for their biosynthetic potential, instructing AntiSMASH software only to detect well-defined clusters containing all required parts. Four of the five *Streptomyces* strains (excluding *Micromonospora humida*), contained a kirromycin-like BGC was found when the genomes were mined on AntiSMASH utilising the MIBiG Database for known cluster comparisons (Blin et al., 2021; Medema et al., 2015).

On the kirromycin-like BGC of *Amycolatopsis magusensis*, 53% of genes show similarity to that of the kirromycin BGC from *S. collinus*. The same 53% gene similarity was found in the kirromycin-like BGC of *Amycolatopsis cihanbeyliensis*. *Micromonospora rubida* contained a kirromycin-like BGC with 73% gene similarity to *S. collinus*' Kirromycin BGC and finally, *Saccharopolyspora sp. NFXS83* possessed a BGC with 57% gene similarity.

Similar to the Aurodox BGC from *S. goldiniensis*, both *M. rubida* and *S. spp. NFXS83* possess other biosynthetic genes on their 'superclusters' in which their kirromycin-like elfamycin BGC genes are found. Both *M. rubida* and *S. spp. NFXS83* were found to encode the putative production of bottromycin (Fig. 3.40), like the aurodox supercluster of *S. goldiniensis*. Genes encoding Bottromycin A2 – an anti-MRSA compound- can be found beside of the aurodox region of the supercluster and can also be found in *Streptomyces. bottropensis*, a closely related strain to *S. goldiniensis* (McHugh, 2020; McHugh et al., 2022). Bottromycin A2 is an anti-MRSA compound, whose gene cluster was re-defined in 2012 to contain only 12 genes (Crone et al., 2012), all of which are present in the superclusters containing kirromycin-like elfamycin BGCs of *S. goldiniensis*, *M. rubida* and *S. sp. NFXS83*.

Though further dissection of each of the biosynthesis genes within these clusters will be necessary to determine if they have the potential for kirromycin-like elfamycin production, all contain the characteristic SAM-dependent methyltransferase between

a Non-Ribosomal Peptide synthetase and Acyltransferase. This suggests that it is not only *Streptomyces* ISL094 which could be a putative aurodox producer, but also *A. magusensis*, *A. cihanbeyliensis* and *M. rubida*, *Saccharopolyspora* sp. NFXS83.

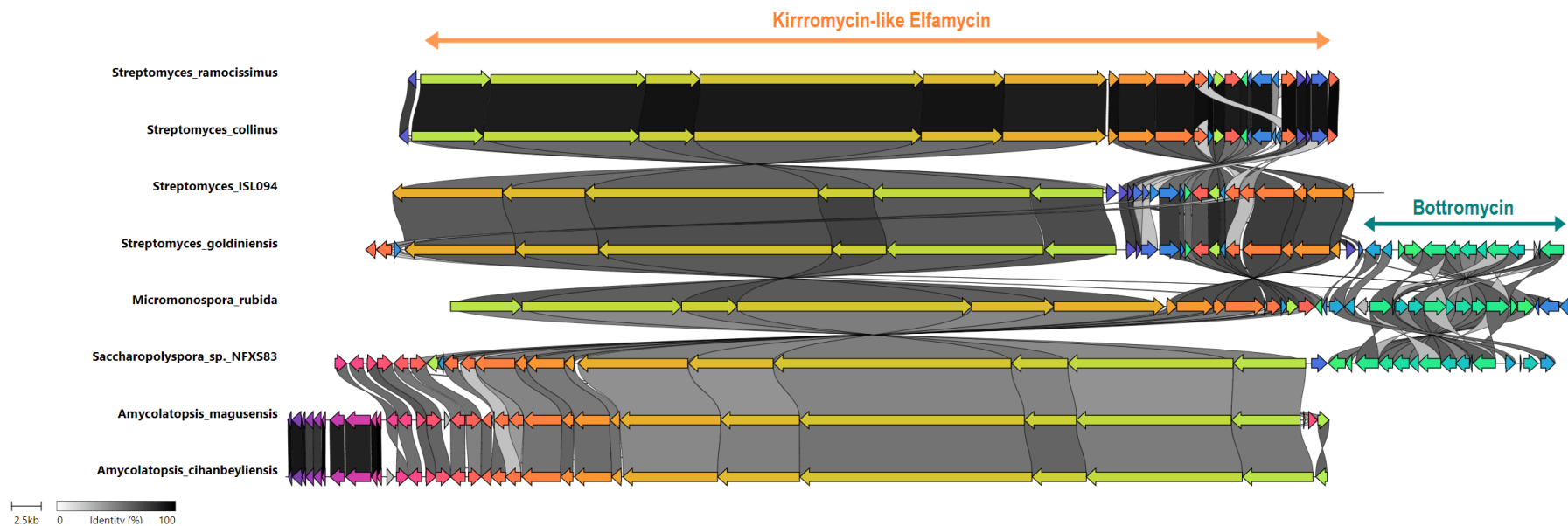


Figure 3.40: FlaGs analysis of SAM-dependant *N*-methyltransferase AurM* identified other BGC;s with a similar structure to those that are known kirromycin-like elfamycin producers. Adjoining lines represent amino acid similarity according to scale. Figure generated by clinker.py using FASTA sequences of BGCs. Kirromycin-like elfamycin region is shown in orange and Bottromycin encoding region is shown in teal.

3.3 Summary

Chapter 3 saw the introduction of the three classes of elfamycins, kirromycin, Factumycin and L-681,217, and the architecture of the biosynthetic gene clusters that encode their production (Table 3A & Fig. 3.1). Having previously investigated the architecture of the BGCs responsible for production of Factumycin and L-681,217, this work built upon that by Thaker et al., (2012) where the architecture of the kirromycin BGC from *S. collinus* was compared too. This work found additional links between the BGCs responsible for kirromycin-like elfamycin production and help to further annotate the potential roles for unannotated genes within the BGCs (Fig. 3.1 & Table 3B).

This Chapter also saw the characterisation of three kirromycin-like elfamycin producing strains *S. goldiniensis*, *S. collinus* and *S. ramocissimus*. For each of the three strains, their morphology (Fig. 3.2), specific growth rate (Table 3C), bioactivity (Fig. 3.3 & 3.10) and elfamycin production (Fig. 3.7, 3.8 & 3.9) were analysed under various conditions. For *S. goldiniensis*, our results supported the findings of R. E. McHugh across multiple studies (2020 and 2019), where the growth rate, bioactivity and production of elfamycins were found to be similar to the previous work. Building on this, it was found that aurodox was produced by *S. goldiniensis* in both AP and V6 media too, not just in LB and GYM, which is different from the findings of R.E. McHugh (2020; Fig. 3.14). Unfortunately, no production of kirromycin from *S. collinus* was observed during this initial study. As the production of kirromycin from *S. collinus* has been well documented, it was not deemed necessary for this study to explore the production under laboratory conditions further (Weber et al., 2008). However, should this work be replicated and production of kirromycin from *S. collinus* be required, the strain should be cultivated in production medium, as described by Weber et al.,

(2008), consisting of soybean flour (10 g/L⁻¹), mannite (10 g/L⁻¹), CaCO₃ (5 g/L⁻¹), and tap water, an adapted version of SFM media (Table 2C).

For *S. ramocissimus*, the production of kirromycin during fermentation is not documented like *S. collinus*, which is surprising given the wealth of literature that exists about its EF-Tu copies (Olsthooorn-Tieleman et al., 2002, 2007). During this study, kirromycin was found to be produced in LB and GYM media (Fig. 3.16). during fermentation in GYM media, it was found to be produced at approximately 48 hours (Fig. 3.11), which has not been before documented. These data support work from Schniete et al., (2018) who suggest that stationary phase of growth is linked to antibiotic production, this is observed for the strain when grown in GYM media (Fig. 3.6).

Sequencing of the *S. ramocissimus* genome using Illumina sequencing alone resulted in a fragmented assembly, which could be improved by the addition of long read sequences (Fig. 3.24). Despite the assembly quality, the BGC of kirromycin from *S. ramocissimus* was found to remain intact, therefore was fully annotated with comparison to the kirromycin BGC from *S. collinus* (Table 3E).

Alongside this work, a second kirromycin-like elfamycin BGC was identified in *S. ISL094* during a metagenomic study by Maza et al., (2019), which was also fully annotated, this time based upon the aurodox BGC of *S. goldiniensis* due to their nucleotide similarity. The kirromycin-like elfamycin biosynthesis genes of each of these strains was investigated, where comparison between the BGCs helped to resolve key genes within the clusters. The four kirromycin-like elfamycin producers identified as being phylogenetically distant (Fig. 3.21) it may be interesting to see that they are capable of production of such similar elfamycin molecules. Additionally, these molecules are produced from BGCs which have structural and architectural changes, yet similar molecules are produced (Fig. 3.28). As the clusters possess several structural differences, several recombination events could have occurred to drive the

evolution of the order of these clusters, which may explain their presence in such phylogenetically distant *Streptomyces*.

Finally, the methyltransferase AurM* was investigated alongside its homolog in the BGC of *S. ISL094*, termed KirM*. It was thought that due to the similarity between the methyltransferases (Fig. 3.36) and their presence in the BGC of aurodox but not kirromycin (Fig. 3.28) that the BGC of *S. ISL094* could be a second known aurodox producer.

Chapter 4: Elucidating gene function within the aurodox biosynthetic gene cluster.

4.1 Introduction

In the previous Chapter, the differences in BGC architecture, and the associated differences in elfamycin molecule structure were investigated. Through this analysis, the function of key genes and their products within these elfamycin BGCs was proposed. However, to elucidate the role of these genes in the biosynthesis of elfamycins, and importantly kirromycin-like elfamycins such as aurodox and kirromycin, molecular and biochemical analysis is required.

In the previous Chapter, the BGC of aurodox was identified and five genes, *aurAI*, *aurB*, *aurHV*, *aurM** and *aurQ*, were assigned putative roles during the analysis of other kirromycin-like BGCs. *aurAI* is thought to encode a polyketide synthase, while *aurB* a non-ribosomal peptide synthetase, where AurB catalyses the incorporation of β -alanine in to the growing polyketide chain, much like KirB from kirromycin biosynthesis (Weber et al., 2008). *aurHV* and *aurQ* are predicted to encode hypothetical proteins with no function assigned in other kirromycin-like elfamycin BGCs and finally, *aurM**, hypothesised to encode AurM*, a SAM dependant methyltransferase, shown to methylate pyridone ring of aurodox, and responsible for the only structural difference from kirromycin (McHugh et al., 2022). These genes are predominantly located at the beginning of the aurodox BGC, located amongst other 'tailoring' genes used to decorate the PKS cascade, with the exception of the polyketide synthase encoding *aurAI* (Fig. 4.1, McHugh et al., 2022)

To manipulate these genes genetically there must be a suitable expression system for the production of aurodox and its derivatives. McHugh et al., (2022) used a phage artificial chromosome (PAC) library, which was constructed from *S. goldiniensis* genomic DNA, to generate a heterologous expression vector for expression of the aurodox BGC. This model will be validated in this Chapter and used for further genetic

manipulation of the aurodox BGC for the elucidation of the role of these key aurodox biosynthesis genes.

To compliment these data, the role of these aurodox gene encoded proteins, will be analysed, through overexpression, purification and enzymatic analysis of protein function. Particular attention will be paid to the role of AurM* in the conversion of kirromycin to aurodox during aurodox biosynthesis, to further the knowledge on the differences between these kirromycin-like elfamycin compounds.

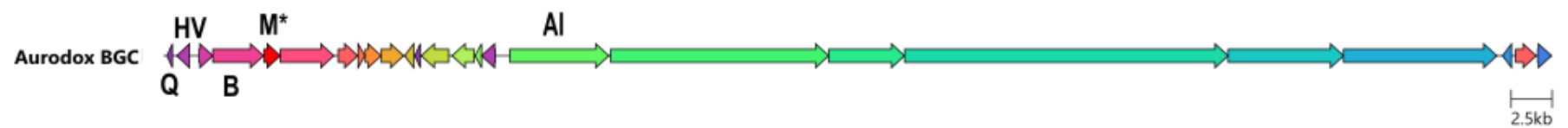


Figure 4.1: Genes of interest on the aurodox biosynthetic gene cluster. Figure generated by clinker.py using the FASTA sequence of the aurodox BGC. *aurAI*, *aurB*, *aurHV*, *aurM** and *aurQ* are labelled and their location on the aurodox BGC is shown.

4.2 Results

4.2.1 Sequencing of pESAC-13A_Aurl.

Having an appropriate expression system for aurodox production is essential in order to decipher the biosynthesis of the molecule. In order to establish if the putative aurodox BGC that was identified in the genome of *S. goldiniensis* was responsible for aurodox biosynthesis, A phage artificial chromosome (PAC) library was constructed from *S. goldiniensis* genomic DNA, and the resulting pESAC-13A vectors screened by PCR for the presence of the putative aurodox cluster (Bio S&T, Canada) (McHugh et al., 2022). After identification of clones containing the entire aurodox BGC, the clones were subject to pulse field gel electrophoresis (PFGE) to confirm the size of the insert and one clone was taken forward to further study (pESAC-13A_Aurl).

Though pESAC-13A_Aurl was confirmed to contain the putative aurodox cluster, the sequence of this PAC was unknown. Work during this thesis sought to sequence the complete aurodox, PAC pESAC-13A_Aurl, using both Illumina and Oxford Nanopore sequencing technologies.

The PAC was completely sequenced via short read Illumina NovaSeq sequencing provided by Novogene. and the Oxford Nanopore long read sequencing was done in-house to help scaffold the short read sequences from Illumina. Short sequencing reads provided by the Illumina platform provide high accuracy coverage and sequencing the depth of the genome with long reads from MinION enables scaffolding of the Illumina reads. Knowing the full sequence of the PAC is essential during the dissection of aurodox biosynthesis using this expression system and allows for molecular manipulation of the aurodox BGC present on the PAC to occur.

The aurodox PAC pESAC-13A_Aurl was found to contain a 129Kbp insert, of which contains the 87kb aurodox BGC present on the genome of *S. goldiniensis* (Fig. 4.2).

Also present on the aurodox PAC was a ϕ C31 integrase, a site-specific bacteriophage recombinase, which is able to catalyse chromosomal transgene insertion under a diverse range of experimental conditions (Sosio et al., 2001). The enzyme recognizes and catalyses unidirectional recombination between attachment motifs found in phage and bacterial genomes, attP and attB sites, respectively. During cloning, the ampicillin resistance gene was replaced by *S. goldiniensis* gDNA at BamHI sites, with the apramycin gene still present and acting as the resistance marker for selection of the PAC. Also contained on the pESAC-13A_AurI PAC are genes predicted to be involved in bottromycin biosynthesis. This concurs with the architecture of the aurodox supercluster, where bottromycin genes are found to flank aurodox genes on the aurodox BGC found in *S. goldiniensis*, the native producer (McHugh et al., 2021). Also identified are miscellaneous genes which have no obvious association to specialised metabolite production. All genes found to be involved in aurodox biosynthesis were manually annotated and confirmed by BlastP (Fig. 4.2).

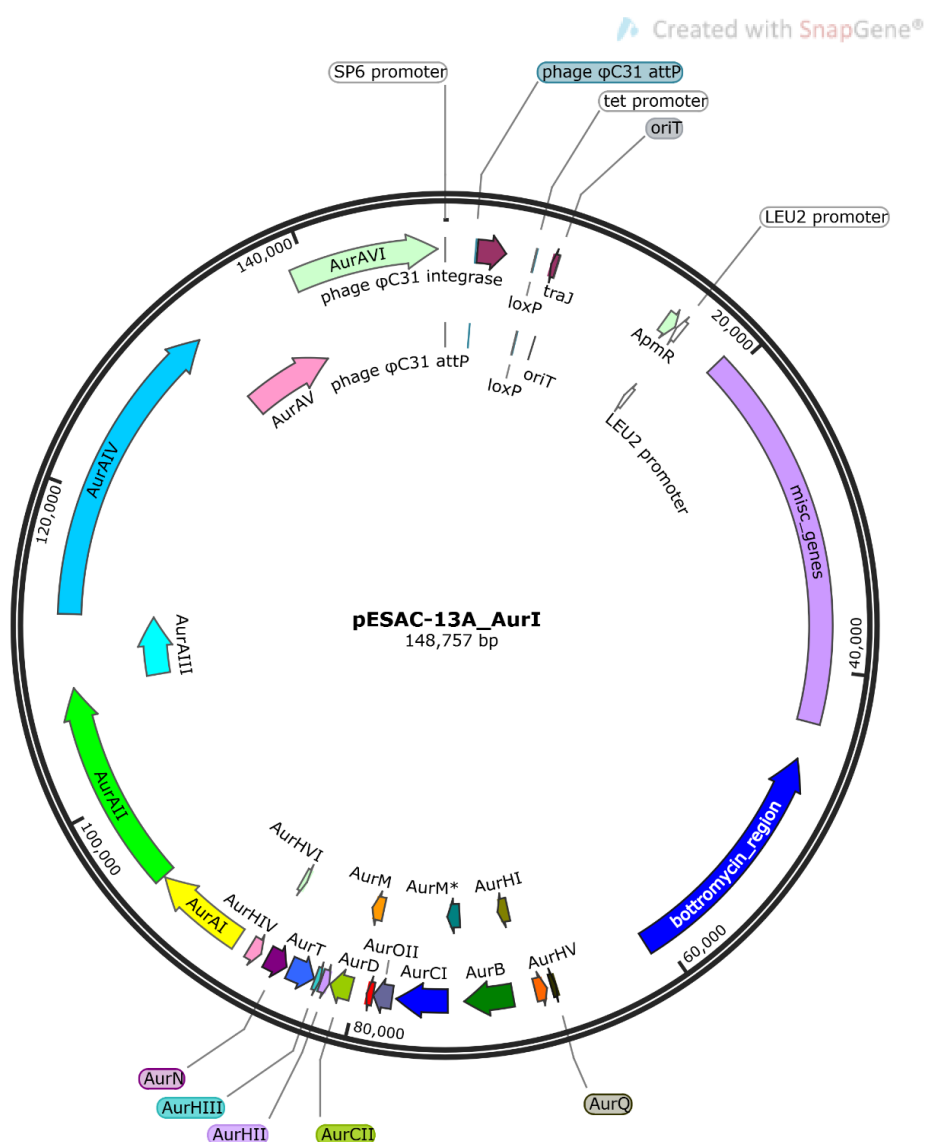


Figure 4.2: Annotated plasmid map of the pESAC-13A_AurI aurodox heterologous expression vector using Snapgene. Aurodox biosynthesis genes were manually annotated according to the sequence in the *S. goldiniensis* genome. Vector encodes φC31 integrase, ampicillin resistance gene (replaced by gDNA at BamHI sites during PAC construction) and apramycin resistance gene. Predicted bottromycin genes which flank aurodox-encoding genes in the native producer, *S. goldiniensis*, are shown in blue. Genes in the lilac region encode miscellaneous proteins with no obvious association to specialised metabolite production. Figure created in SnapGene.

4.2.2 Validation of *S. coelicolor* M1152 + pESAC-13A_AurI as a suitable heterologous expression system for aurodox biosynthesis.

Heterologous expression (HE) is widely considered to be the robust method of validating a specific BGCs involvement in the biosynthesis of specialised metabolites. In more recent years, the method has been used not only to express known BGCs but also those which can be termed 'silent' that are not expressed under laboratory conditions (Hoskisson and Seipke, 2020; Liu et al., 2021). Many *Streptomyces* heterologous hosts have been investigated over the years for the expression of natural product biosynthetic gene clusters, where as expected, some were found to be more successful than others (Baltz, 2010; Hwang et al., 2021). These strains include, the well documented heterologous host, *Streptomyces albus*, known for its ability to heterologously express not only *Streptomyces* BGCs such as that of steffimycin, but also BGCs from other species such as the thiocoraline BGC from *Micromonospora* (Gullón et al., 2006; Lombó et al., 2006). Several other strains such as *S. venezuelae*, *S. lividans* and *S. rimosus* have also been used to heterologously express BGCs (Liu et al., 2021).

In more recent years, an adoption of a more targeted approach to heterologous expression has been taken, where strains are generated and engineered for the purpose of heterologous expression of natural product gene clusters (Nepal and Wang, 2019). The well documented heterologous host, *Streptomyces coelicolor* M1152, is one example of this. As a derivation of *S. coelicolor* M145, the strain has been subject to the deletion of four of its BGCs. These BGCs were responsible for the production of actinorhodin (Δ act), undecylprodigiosin (Δ red), the Type I PKS coelimycin C1 (Δ cpk) and finally, the calcium dependant antibiotic (Δ cda). Deletion of these BGCs resulted in a much simpler Chromatogram during liquid chromatography, with fewer peaks, and a lower and more stable baseline for the analysis of MS data

(Gomez-Escribano and Bibb, 2011). In addition to the deletion of four BGCs, and the smaller genome size associated, point mutations were also introduced into *rpoB* and *rpsL* to pleiotropically increase the level of secondary metabolite production (Gomez-Escribano and Bibb, 2012). This increased secondary metabolite yield as a result of point mutations in *rpoB* and *rpsL* and has been observed widely among *Streptomyces* species (Shentu et al., 2018; Tanaka et al., 2013). As a result, the strain is often termed 'superhost' due to its affinity for heterologous expression of BGCs and specialised metabolite biosynthesis (Lopatniuk et al., 2014; McHugh et al., 2022; Sidda et al., 2016; Zettler et al., 2014)

Once validated as containing the aurodox BGC, the aurodox PAC pESAC-13A was introduced into *Streptomyces coelicolor* M1152 'superhost' at the ϕ C31 integration site. This was achieved via tri-parental mating and subsequent conjugation from the non-methylating ET12567/pR9604 to avoid the methyl-specific restriction system (Zhou et al., 2012). These processes of tri-parental mating and conjugation will be outlined further through the duration of this thesis.

Exconjugants containing the aurodox BGC were screened via PCR to confirm the presence of the PAC and used to confirm that the aurodox BGC does, in fact produce aurodox (McHugh et al., 2022).

In this study, the resulting strains were cultured in liquid GYM media alongside *S. goldiniensis*, the native aurodox producer, and grown at 30 °C, 200rpm for 7 days. Culture supernatants were extracted with equal volumes of chloroform and the extracts resuspended in ethanol and subject to Liquid Chromatography-Mass Spectrometry (LC-MS) analysis and compared to an authentic aurodox standard (HelloBio, Fig. 4.3). Aurodox was found to have a retention time of 7.21 minutes, with a corresponding M/Z ratio of 793.4 (Fig. 4.3 A). In fermentation extracts of *S. goldiniensis*, aurodox is also found at 7.21 mins with a M/Z ratio of 793.4 (Fig. 4.3 B). Extracts of the *S. coelicolor* M1152 + pESAC-13A empty vector control did not show

any evidence of aurodox production (Fig. 4.3 C), whereas fermentations of the strain containing the heterologously expressed aurodox BGC, *S. coelicolor* M1152 + pESAC-13A_AurI, exhibited the characteristic peak of aurodox at 793.4 M/Z at 7.21 minutes (Fig. 4.3 D). This indicated that the putative aurodox BGC in *S. goldiniensis*, was in fact responsible for the production of aurodox, and that the heterologous expression system of *S. coelicolor* M1152 + pESAC-13A_AurI is effective for the study of aurodox production. (McHugh et al., 2022)

In parallel, analysis of the bioactivity of the native and heterologous aurodox producer were analysed against the ESKAPE pathogens. Fermentation extracts of both *S. goldiniensis* and *S. coelicolor* M1152 + pESAC-13A_AurI exhibited bioactivity against *Klebsiella pneumoniae* and *Staphylococcus aureus*. Interestingly, heterologous expression of the aurodox biosynthetic gene cluster via the PAC pESAC-13A_AurI in *S. coelicolor* M1152 has greater bioactivity against both Gram-positive and Gram-negative bacteria than the native producer, *S. goldiniensis* (Fig. 4.4). This is consistent with the findings from other studies, where specialised metabolite production via this heterologous system was increased in *S. coelicolor* M1152 versus the native producer (Lopatniuk et al., 2014; McHugh et al., 2022; Sidda et al., 2016; Zettler et al., 2014). In summary, the heterologous expression of the pESAC-13A_AurI in *S. coelicolor* M1152 is a robust heterologous host for the expression and production of aurodox and can be used throughout this study for a model to base genetic manipulation upon to dissect aurodox biosynthesis, independent of the native producer, *S. goldiniensis*.

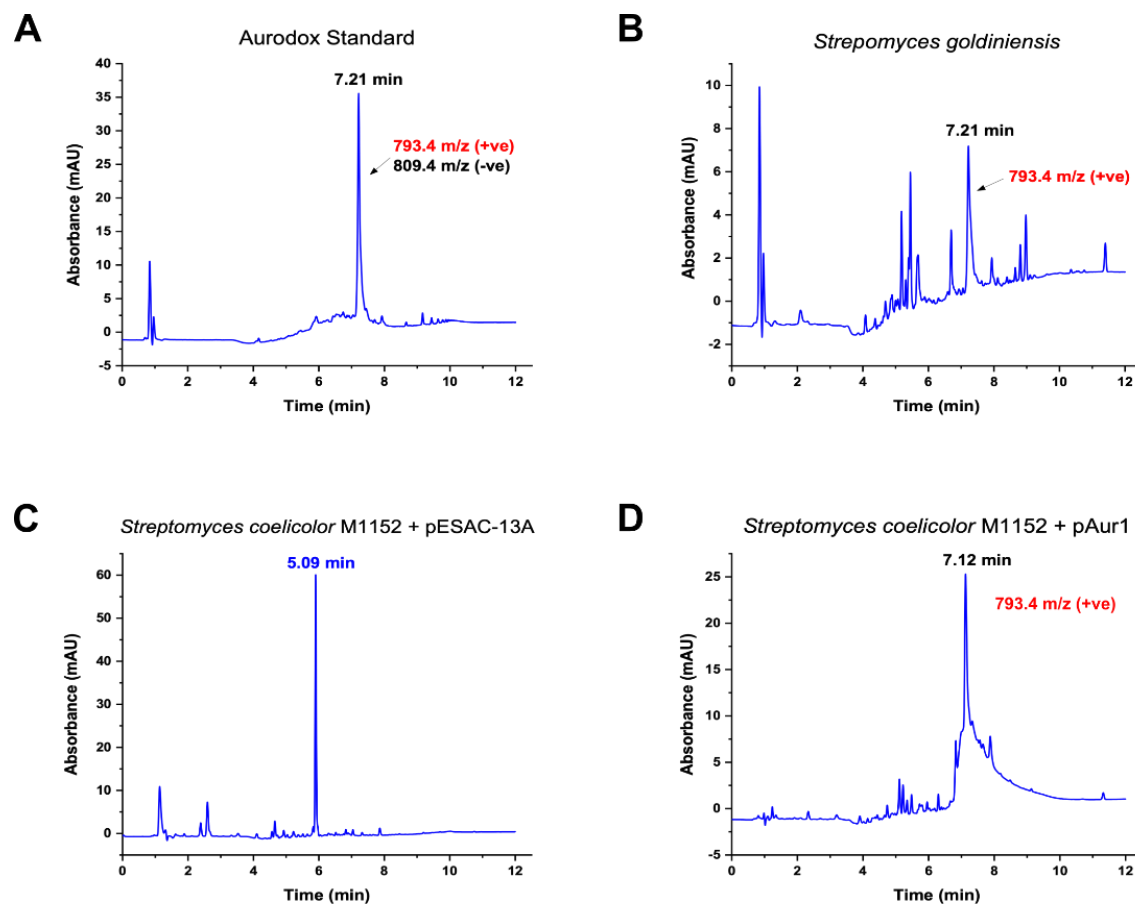


Figure 4.3: Aurodox can be heterologously expressed in *Streptomyces coelicolor* M1152. Cultures for chloroform extraction were prepared as in methods (2.5.1 & 2.5.2). Chromatograms of aurodox standard (HelloBio; 254 nm) A). The peak at aurodox retention time is indicated. (B) Chromatogram from wild-type *S. goldiniensis* indicating aurodox production. (C) Chromatogram from the empty vector (pESAC-13A) control strain *S. coelicolor* M1152, indicating the absence of an aurodox-associated peak. (D) Chromatogram of extract from the growth of *S. coelicolor* M1152/pAur1. The aurodox peak is visible at 7.21 min, MS data indicate the presence of aurodox (McHugh et al., 2022).

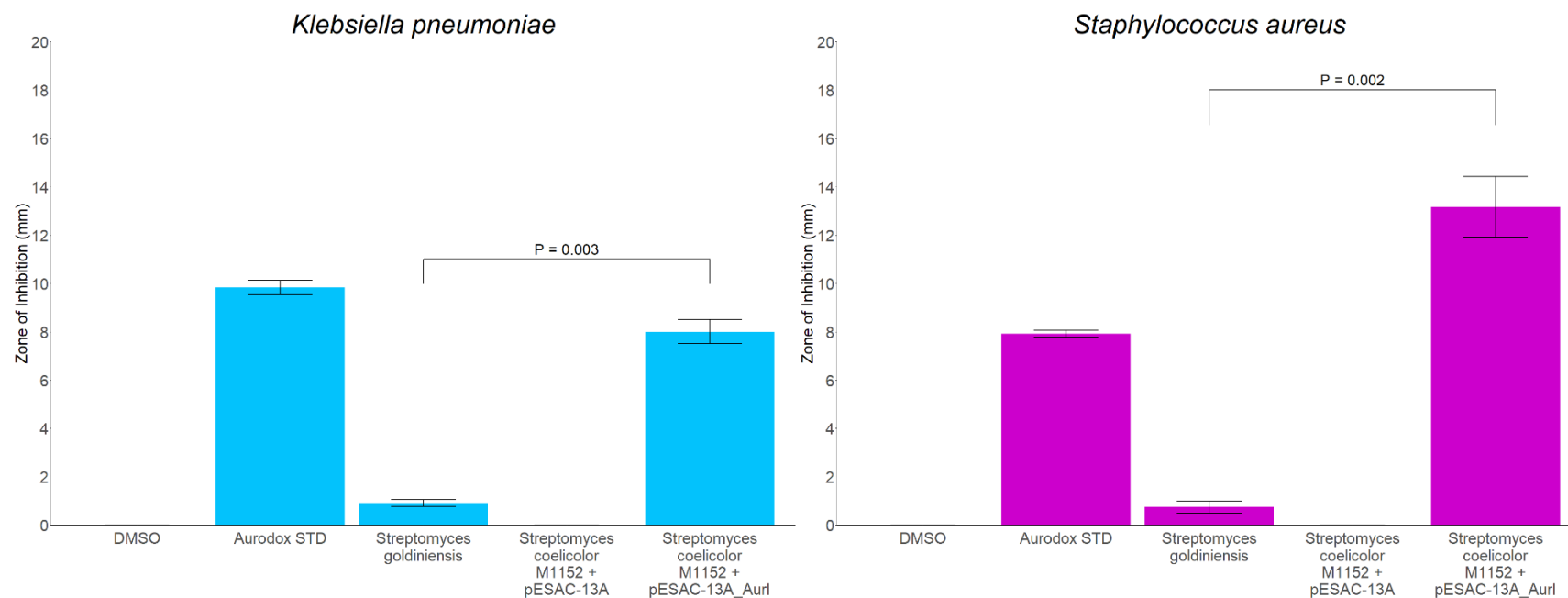


Figure 4.4: Heterologous expression of the aurodox biosynthetic gene cluster via the phage artificial chromosome pESAC-13A_AurI in *S. coelicolor* M1152 has greater bioactivity against both Gram-positive and Gram-negative bacteria than the native producer, *S. goldiniensis*. *Streptomyces* fermentation extracts (GYM liquid media, 30°C, 7 days, 200 rpm) were added to paper discs and plated on indicator strains, *Staphylococcus aureus* ATCC 43300 and *Klebsiella pneumoniae* ATCC 700603, were normalised to an OD₆₀₀ of 0.01 in soft nutrient agar. Assay plates were grown for 12 hours at 37°C and inhibition zones were measured in mm with a ruler.

4.2.3 Generation of mutant PACs using the pESAC-13A_AurI aurodox BGC expression vector and the Streptomyces re-direct protocol.

To help decipher the biosynthesis of aurodox, and in turn other kirromycin-like elfamycin molecules, key genes within the aurodox BGC were deleted in the PAC pESAC-13A_AurI. Using a modified version of redirect PCR targeting of Streptomyces method (Gust et al., 2003), the protocol was used to construct pESAC-13A_AurI_Δaur(x), mutant versions of the PAC, where key aurodox biosynthesis genes, for example *aurM*^{*} were replaced by a hygromycin resistance gene, (*hygR*, Fig. 4.5).

Firstly, *aurAI* was investigated. It has been shown by sequencing that the aurodox biosynthesis encoding region is flanked by other PKS genes other than *aurAI*. These additional PKS genes could have an effect on the aurodox PAC, and could belong to the bottromycin BGC found on part of the PAC. As further evidence is needed to associate the PKS genes of the aurodox BGC with the enzymatic biosynthesis of aurodox, other than just sequencing alone, the first PKS gene of the aurodox BGC, *aurAI*, was replaced with *hygR* via the re-direct protocol (Gust et al., 2003).

The next to be investigated were *aurHV* and *aurQ*, genes which encode hypothetical proteins and have no depicted functional homolog in other kirromycin-like elfamycin biosynthesis in the literature.

The gene *aurB* was also investigated, encoding a non-ribosomal peptide synthetase, KirB, which catalyses the incorporation of β-alanine in to the growing polyketide chain during kirromycin biosynthesis (Laiple et al., 2009; Weber et al., 2008).

Finally, *aurM*^{*}, a gene hypothesised to be responsible for the production of AurM^{*}, a SAM-dependant methyltransferase, during the biosynthesis of aurodox from kirromycin. It was hypothesized that AurM^{*} catalyses the conversion of kirromycin to aurodox and may be the last step in aurodox biosynthesis. Previously, to test this,

*aurM** from *S. goldiniensis* was cloned into an integrating vector (pIJ6902) and introduced into *Streptomyces collinus* Tü 365, a natural kirromycin producer, where *AurM** was expressed. Solvent extracts from supernatants of fermentations of *Streptomyces collinus* Tü 365 + pIJ6902_*aurM** were found to contain characteristic peaks corresponding to both that of aurodox and kirromycin (McHugh et al., 2022). It is thought that deletion of *aurM** in pESAC-13A_AurI will result in kirromycin production.

With use of a λ -red recombinase-based system in the *Streptomyces* re-direct protocol, pIJ790 (cat), containing the λ -red, was introduced into *E. coli* Top10 containing pESAC-13A_aurI. In parallel, the hygromycin resistance gene (*hygR*) was isolated via restriction digest (Fig. 4.6) amplified from pIJ10700 with overhangs which have sequence homology to flanking regions of each gene of interest, before the arabinose induction of the λ red recombinase, and electroporation of the mutant PAC was carried out to facilitate heterologous recombination (Fig. 4.7). This was done for *aurB*, *AurHV*, *aurM** and *aurQ*, where pESAC-13A_AurI_ Δ *aurAI* mutant PAC had been generated in a previous study (McHugh et al., 2022).

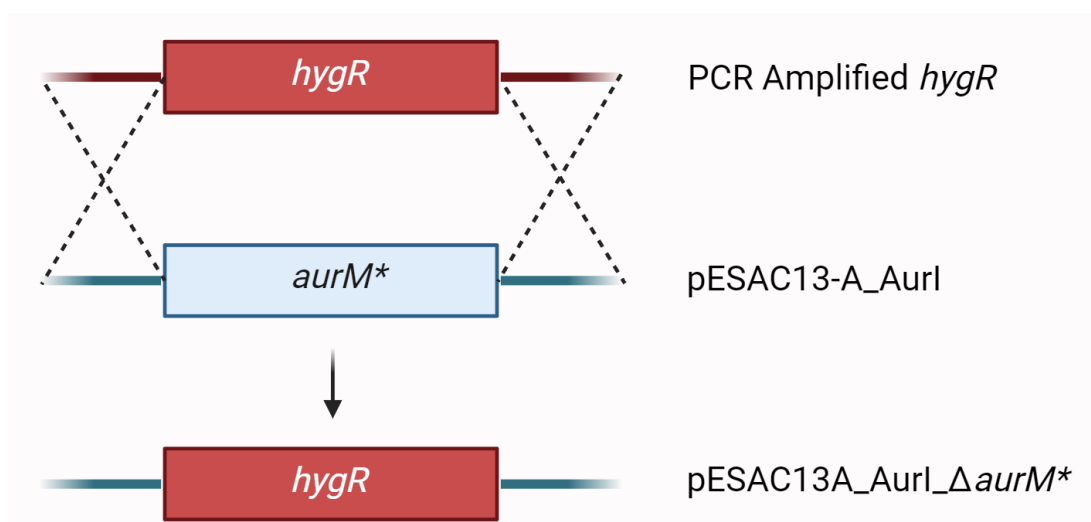


Figure 4.5: Aurodox biosynthesis genes of interest can be replaced with a hygromycin resistance cassette. Disruption via PCR-targeting method which harnesses *E. coli* BW25113 with pIJ790, a λ RED recombination plasmid. Protocol accessible at (https://streptomyces.org.uk/redirect/protocol_V1_4.pdf). Blue lines are the pESAC13-A_AurI PAC and red lines are the pIJ10700 vector.

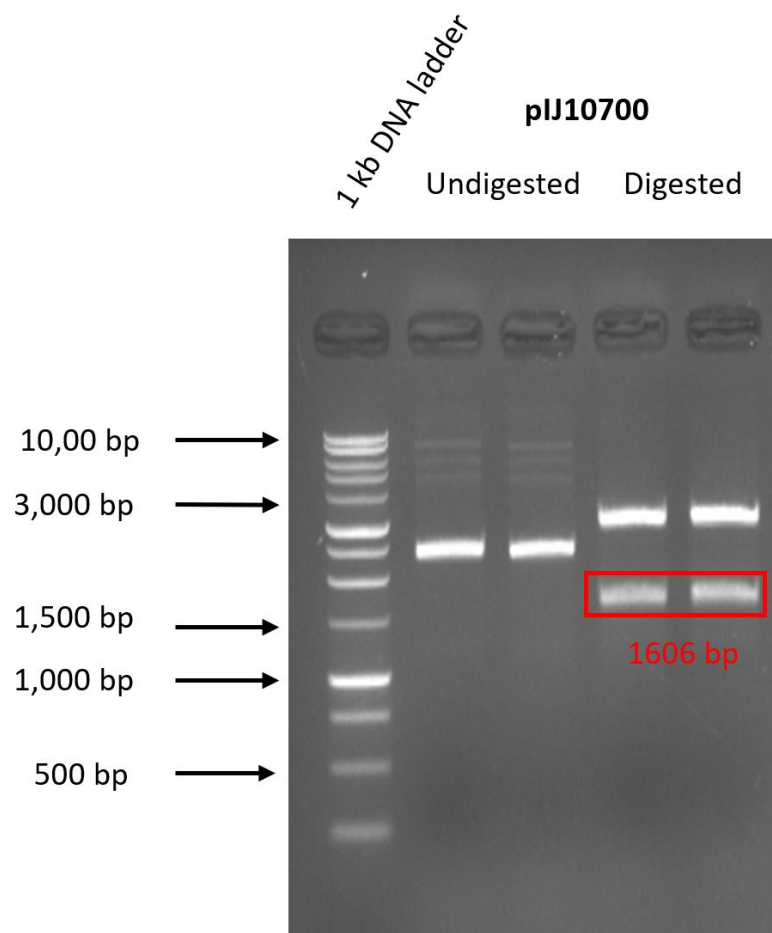


Figure 4.6: The plasmid pIJ10700 undergoes digestion via restriction enzymes, HindIII and SmaI to release hygromycin resistance cassette. Hygromycin resistance cassette can be visualised on agarose gel with a band at approximately 1606 bp, as shown in red. 1% agarose gel, ran for 90 V for 1 hour .

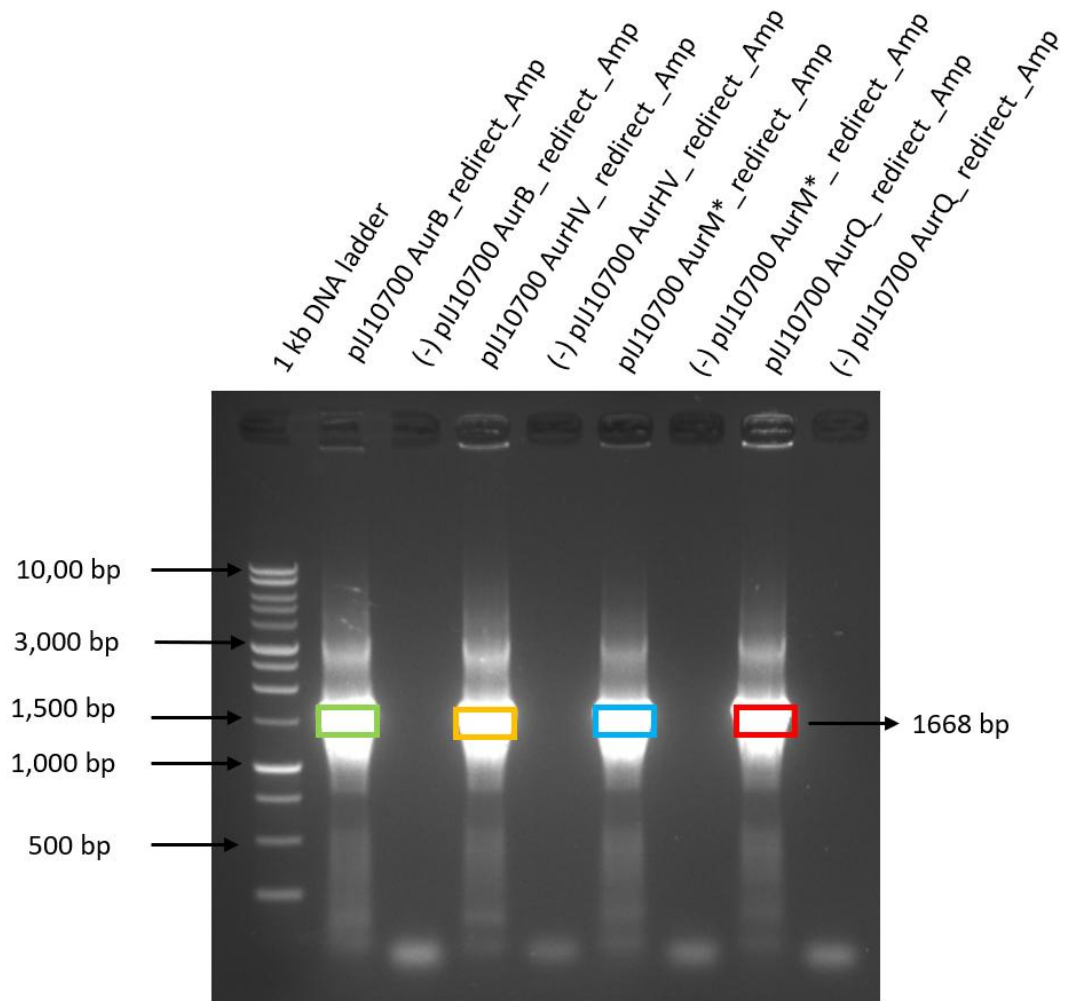


Figure 4.7: PCR amplification of the isolated hygromycin resistance cassette from plJ10700 with ‘long PCR primers’ designed according to the Disruption via redirect PCR-targeting method. Primers contain nucleotides flanking the genes of interest, where the hygromycin resistance cassette amplified with genes flanking AurB is shown in green, AurHV is shown in orange, AurM* is shown in blue and AurQ is shown in red respectively, all at approximately 1668bp. 1% agarose gel, ran at 90 V for 1 hour.

Typically, a conjugative approach would be taken to facilitate the transfer of mobile genetic elements into *Streptomyces*. Typically, this requires transformation of *E. coli* ET12567 + pUZ8002 with a chosen vector, where pUZ8002 encodes transfer machinery assisting in the transfer of vectors from *E. coli* to *Streptomyces* (Kieser et al., 2000; Larcombe et al., 2024; Zhou et al., 2012). In the case of the aurodox PAC, however, the large size of the vector made it impossible to transform *E. coli* ET12567 + pUZ8002 with the PAC. After investigation into other methods of conjugation, tri-parental mating was attempted to facilitate the transformation of *E. coli* ET12567, which was cured of the plasmid pUZ8002 (Larcombe et al., 2024), with pESAC-13A_Aurl mutants. To achieve this, the driver plasmid pR9604 (carbR) is contained within an *E. coli* Top10 strain and cultured on an antibiotic free agar plate alongside *E. coli* ET12567 and another *E. coli* Top10 strain containing the large vector of interest, the PAC mutants (Qin et al., 2017). During this stationary growth on solid media, horizontal gene transfer is facilitated between the three strains, all of which carrying different antibiotic resistance markers. After overnight growth, resulting colonies can be streaked onto fresh agar containing hygromycin, apramycin, carbenicillin, and chloramphenicol to select for the mutant aurodox PAC (*hygR ampR*), pR99604 (*carbR*), ET12567 (*cmR*), respectively. The resulting strain should be *E. coli* ET12567 with the mutant PAC and pR9604. To confirm this integration, colony PCRs were performed on *E. coli* ET12567 transformants after tri-parental mating, where compared to pESAC-13A_Aurl, which primers 200 bp upstream and downstream of each key gene amplified fragments corresponding to the size of the aurodox gene +~400 bp, all mutant PACs amplified bands at approximately 2000 bp (Fig. 4.8).

Vector maps for the final mutant PACs were generated, by using the original pESAC-13A_Aurl vector and sequencing overhangs of the mutated genes. These sequencing reads were combined, and it can be observed that for pESAC-13A_Aurl_ Δ *aurB*, that *aurB* has been replaced with a hygromycin resistance cassette (Fig. 4.9).

Once the *E. coli* ET21567 strains had been transformed with the mutant PAC and pR9604 generated from tri-parental mating, conjugation into *S. coelicolor* M1152 could occur.

After standard conjugation protocol was followed, 3 primary exconjugants were patched onto MS agar containing hygromycin, apramycin and nalidixic acid to screen for mutant PACs. Of the strains which showed resistance, one exconjugant lineage of each mutant PAC and controls were carried forward for analysis.

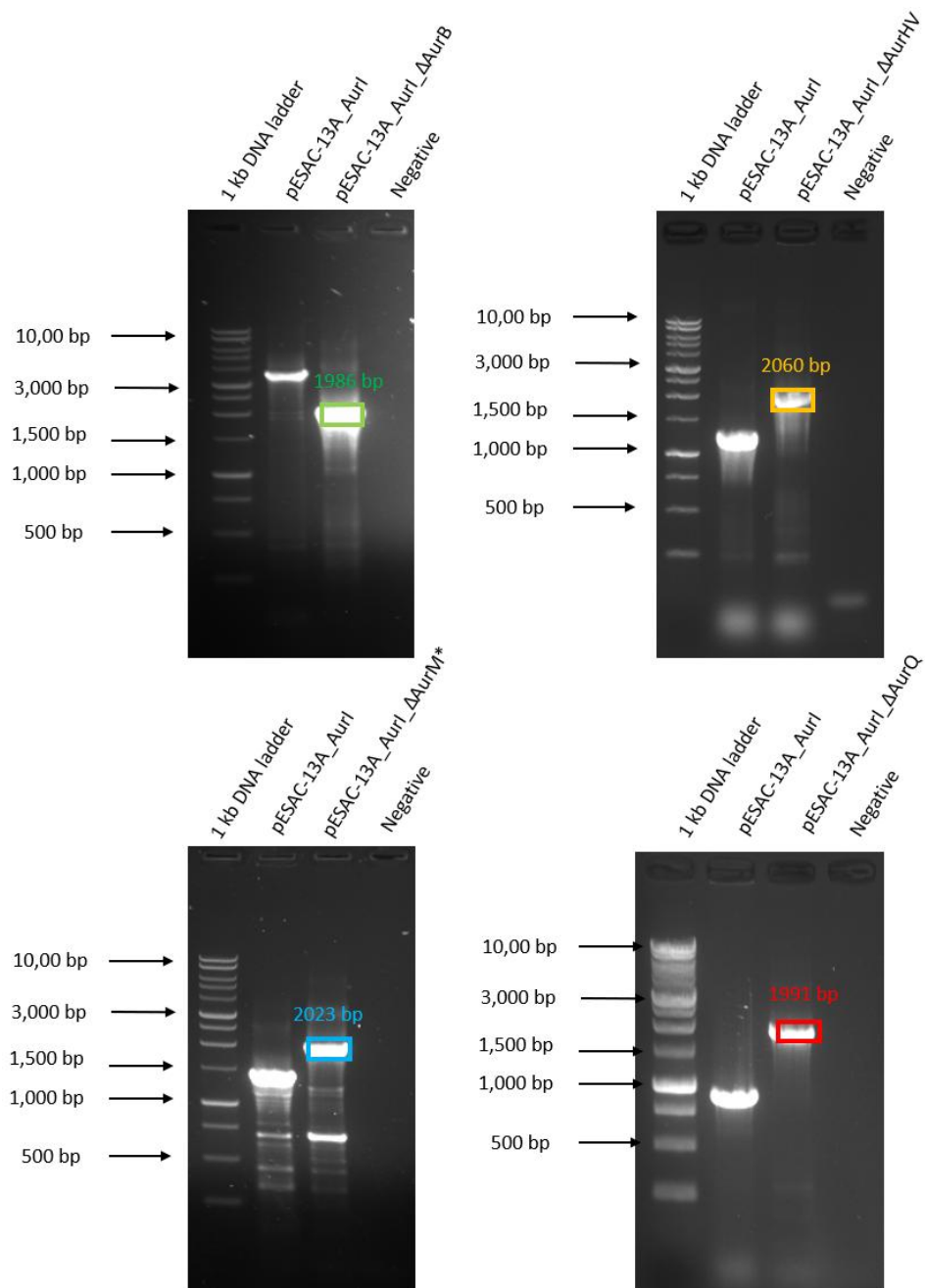


Figure 4.8: Confirmation of gene replacement with the hygromycin resistance cassette using colony PCR. Primers for each gene to be replaced are located approximately 200 bp upstream and downstream of the gene of interest to allow for accurate amplification and sequencing. AurB is shown in green (1986 bp), AurHV is shown in orange (2060 bp), AurM* in blue (2023 bp) and AurQ in red (1991 bp). 1% agarose gel ran for 90 V for 1 hour.

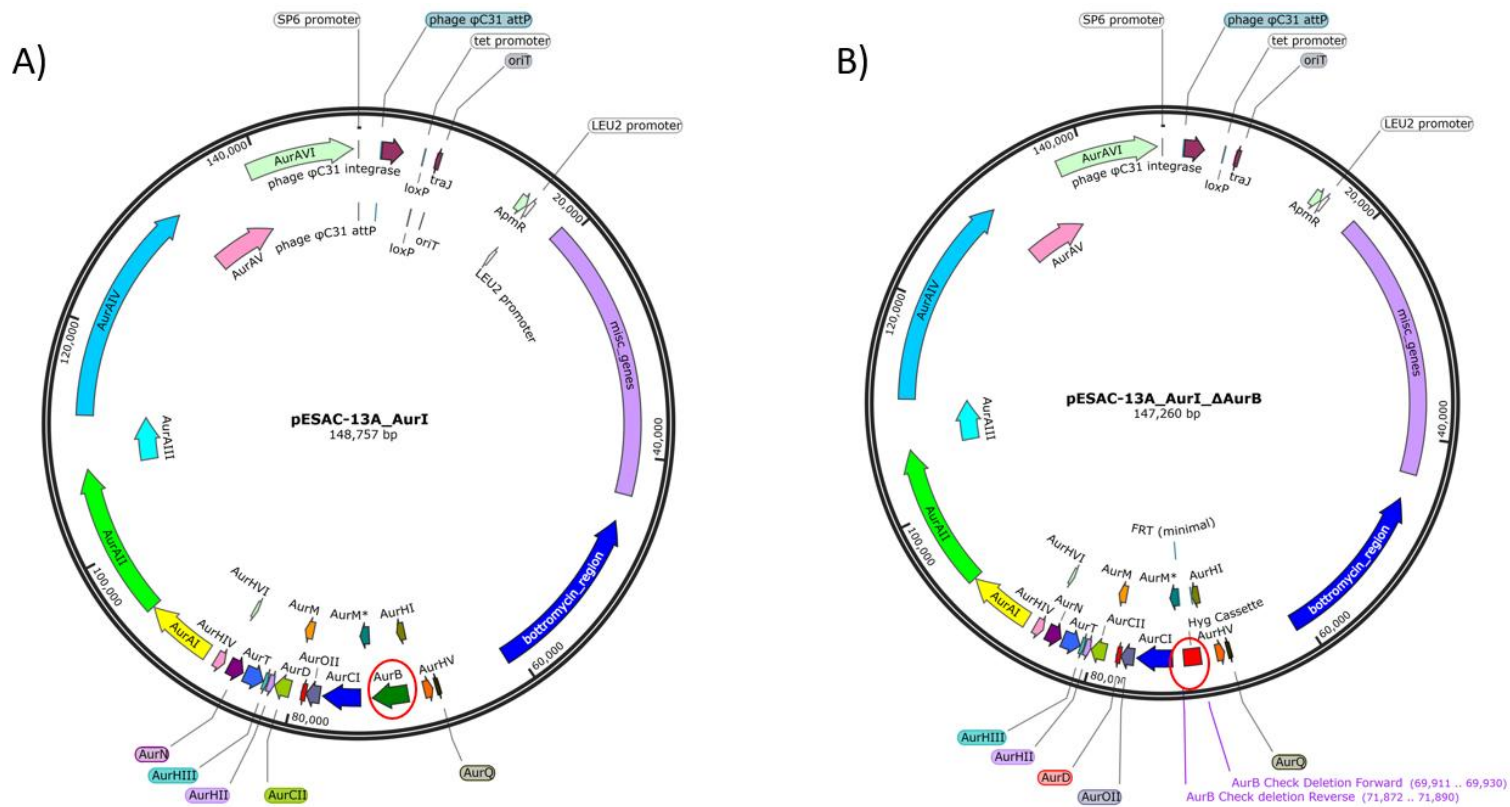


Figure 4.9: Plasmid map of the original aurodox phage artificial chromosome (PAC, A) and the altered PAC, where AurB has been replaced by a hygromycin resistance cassette B). Gene replacement circled in red. Plasmid maps generated on SnapGene.

4.2.4 Phenotypic and biochemical characterisation of the effect of key genes during aurodox biosynthesis using the *S. coelicolor* M1152 with pESAC-13A_AurI heterologous expression system.

When grown adjacent to each other on agar plates, phenotypic characterisation of the *S. coelicolor* M1152 heterologous expression and mutant PAC strains shows interesting phenotypes (Fig. 4.10) Firstly, *S. coelicolor* M1152 carrying the WT PAC and the $\Delta aurAI$ PAC appears to inhibit the sporulation of the other strains on the plate. This is apparent on GYM and MS agar. It can also be observed that these zones of sporulation cessation are larger on GYM agar. These suggest that the *S. coelicolor* strain containing the PAC gains the ability to produce a specific molecule, which is medium dependant. A similar observation was made in Chapter 3 of this thesis when investigating the different media aurodox is produced in (Fig. 3.13 & 3.14). The empty vector control of *S. coelicolor* M1152 + pESAC-13A shows little growth compared to the other strains and sporulation is retarded (evidenced by the lack of a powdery grey spore layer on the surface of the culture). When the agar culture plates of the heterologous expression vectors are viewed from the underside of the plates it is observed that on GYM and MS agar, both *S. coelicolor* M1152 with pESAC-13A_AurI and pESAC-13A_AurI_ ΔAI produce the characteristic kirromycin-like gold haze around the colonies, indicative of the goldinonic acid moiety of the kirromycin molecules. One final observation is that on the underside of MS plates, all strains, excluding the WT PAC and $\Delta aurAI$ PAC are producing a pink pigment in what looks to be response to those strains.

Using MS agar plugs of cultures strains, an assessment of the bioactivity of mutant PAC strains on solid agar, showed that *Streptomyces coelicolor* M1152 + pESAC-13A_AurI_ $\Delta aurAI$ is less bioactive than *Streptomyces coelicolor* M1152 + pESAC-13A_AurI against Gram-positive and Gram-negative bacteria (Fig. 4.11). No

bioactivity was observed on solid media against Gram-positives and Gram-negatives for *S. coelicolor* M1152 + pESAC-13A_AurI Δ B, Δ HV, Δ M* and Δ Q.

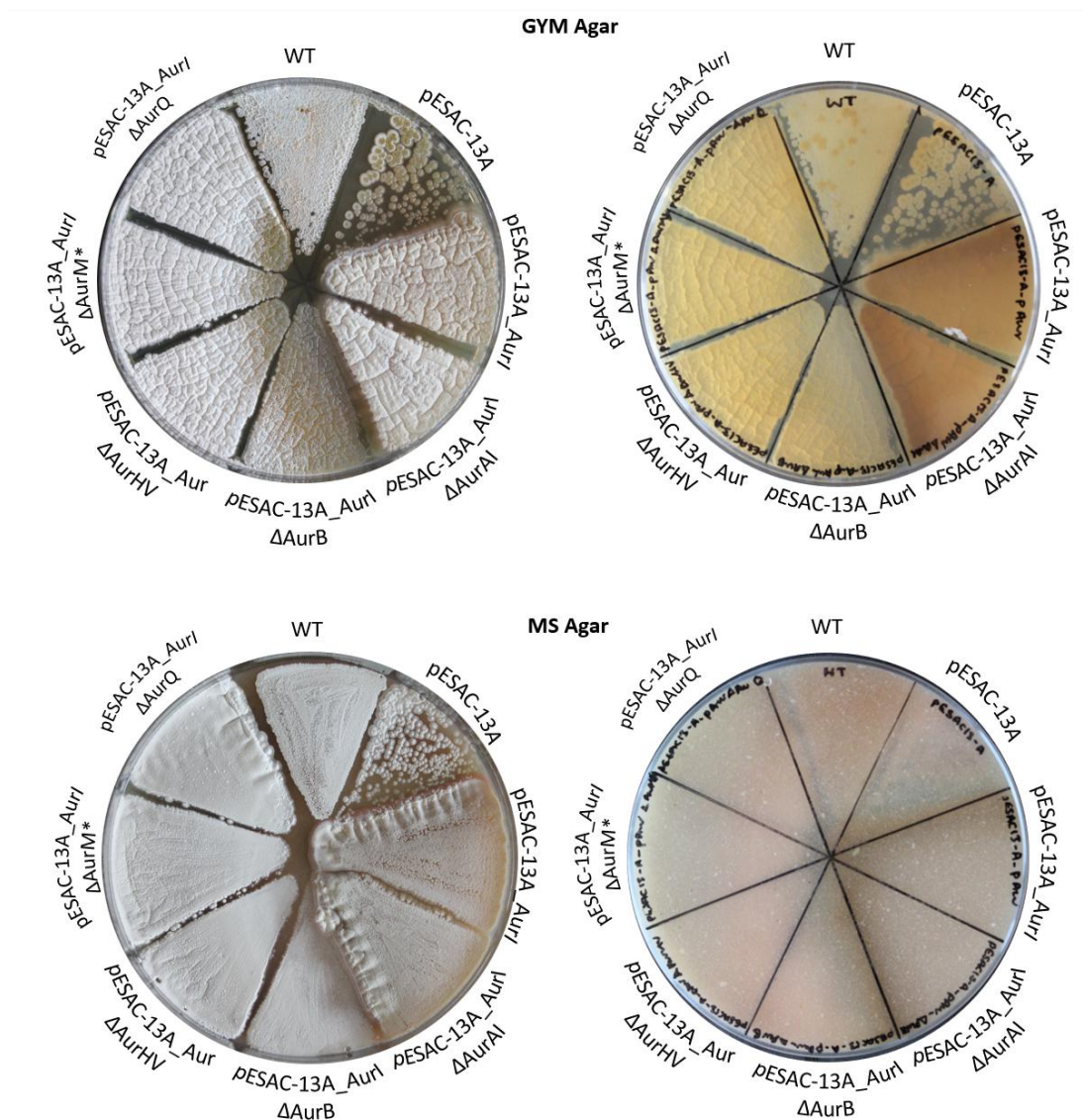


Figure 4.10: Phenotypic characterisation of heterologous expression strains and re-direct mutants. *Streptomyces* strains were grown on both GYM and MS agar for 10 days at 30 °C until sporulation was achieved. Strains used: *S. coelicolor* M1152 (WT), with pESAC-13A (empty vector), with pESAC-13A_AurI (aurodox BGC) and then the re-direct mutants of *S. coelicolor* M1152 + pESAC-13A_AurIΔB, ΔHV, ΔM* and ΔQ.

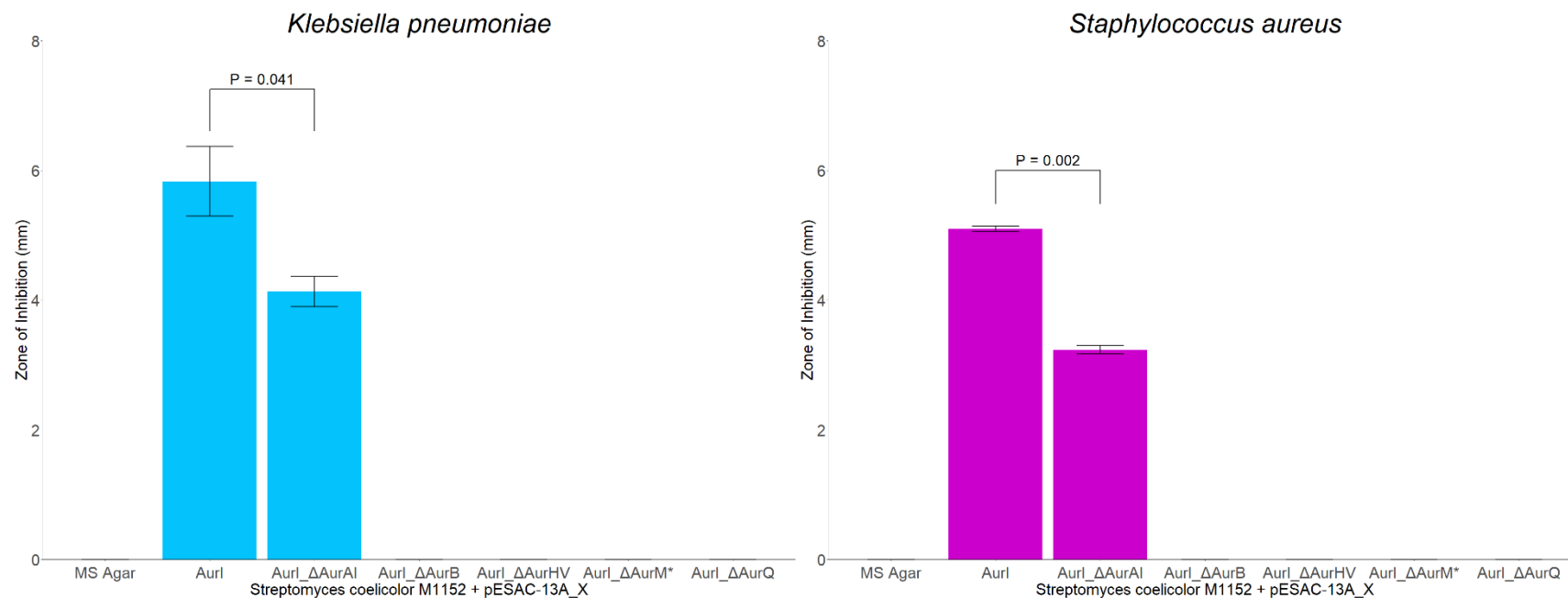


Figure 4.11: An assessment of the bioactivity of mutant strains on solid agar against Gram-positive and Gram-negative bacteria, where *Streptomyces coelicolor* M1152 + pESAC-13A_Aurl_ΔaurAI is shown to be less bioactive than *Streptomyces coelicolor* M1152 + pESAC-13A_Aurl. No bioactivity was observed in other deletion mutants. Negative controls were an MS agar plug. *Streptomyces* agar plugs (MS agar, 30°C, 7 days) were plated on indicator strains, *Staphylococcus aureus* ATCC 43300 and *Klebsiella pneumoniae* ATCC 700603, which were normalised to an OD₆₀₀ of 0.01 in soft nutrient agar. Assay plates were grown for 12 hours at 37°C and zones of inhibition were measured in mm with a ruler.

Given that deletion of *aurAI* results in less bioactivity than the WT, this strongly suggests that the PKS encoded for by *aurAI* plays a role in the biosynthesis of aurodox. This can be confirmed by solvent extraction of *Streptomyces* culture supernatants and looking to see the presence of a mass corresponding to aurodox or kirromycin-like derivatives in fermentation extracts.

Bacterial growth cultures of the 5 deletion strains and the WT, *S. coelicolor* M1152 + pESAC-13A_AurI, were grown at 30 °C, 200 rpm, for seven days and culture supernatants were extracted using chloroform. As described previously. The extracts were diluted in 100% EtOH and subject to LC/MS analysis (Fig. 4.12 & Fig. 4.13).

Aurodox was detected in the fermentation extracts of *S. coelicolor* M1152 + pESAC-13A_AurI at a retention time of approx. 8.0 minutes and possessed a mass of 793.40 indicating the production of aurodox when compared to the aurodox standard (Fig. 4.12).

For the deletion strains, a peak was found in the fermentation of *S. coelicolor* M1152 + pESAC-13A_AurI_ Δ *aurM*^{*}. At a retention time of 8.0 and a M/Z ratio of 779.40, the molecule identified is suspect to be kirromycin. When compared to the kirromycin STD, the *S. coelicolor* M1152 + pESAC-13A_AurI_ Δ *aurM*^{*} fermentation both contain a molecule with a mass of 779.40, suggesting that this could be kirromycin. This supports the findings of previous work by our group, where we found that the last step in aurodox biosynthesis is likely N-methylation from kirromycin to aurodox by AurM^{*} (McHugh et al., 2022). In the study, *aurM*^{*} from the native aurodox producer, *S. goldiniensis*, was introduced into *Streptomyces collinus* Tü 365, a native kirromycin producer, via pIJ6902 (integrating vector). LCMS analysis of solvent extracts from *S. collinus* Tü 365 + pIJ6902_aurM^{*} revealed the presence of both aurodox and kirromycin in the fermentation, suggesting the partial conversion of kirromycin to aurodox by the N-methylation facilitated by AurM^{*} (McHugh et al., 2022). These data

suggests the absence of AurM*, does not allow the N-methylation of the kirromycin molecule, preventing the production of aurodox.

For the subsequent gene deletions, *aurAI*, *aurB*, *AurHV* and *aurQ*, no characteristic peaks corresponding to that of aurodox or kirromycin were found (Fig. 4.13). This indicated that these genes are essential in the biosynthesis of the kirromycin-like elfamycin compound and are important for both aurodox and kirromycin biosynthesis as neither have been produced and are visible in the fermentation extracts.

When bioactivity of these fermentation extracts was assessed for the deletion strains, it was found that the compounds produced by *S. coelicolor* M1152 + pESAC-13A_AurI_Δ*aurAI* were still bioactive against both Gram-positive and Gram-negative bacteria, though less than the wild-type PAC ($p=0.005$, $p=0.002$, Fig. 4.14). Even though neither aurodox nor kirromycin were produced during the fermentation (Fig. 4.13), it is hypothesised that an intermediate molecule during the biosynthesis of aurodox is bioactive. This is because no bioactivity was found in the fermentation extracts of *S. coelicolor* M1152 + pESAC-13A vector alone, suggesting the bioactivity is linked to the biosynthesis of the aurodox molecule on the AurI PAC.

Secondly, the fermentation extract of *S. coelicolor* M1152 + pESAC-13A_AurI_Δ*aurM** also showed bioactivity, though less than the WT PAC ($p=0.001$, $p=0.005$, Fig. 4.14). There is molecule with a mass charge ratio (m/z) of 779.4 indicating that a small amount of kirromycin is produced following the deletion of *aurM**. This, coupled with the likelihood that kirromycin is being produced, suggested that the deletion of *aurM** from the aurodox PAC, and therefore the production of the methyltransferase protein AurM*, results in the production of kirromycin.

Given that a kirromycin-like molecule with bioactivity is produced from the deletion strains, it was hypothesised that these compounds, and/or their intermediates, may be active against the T3SS of EHEC, much like aurodox was found to be (McHugh et al., 2019).

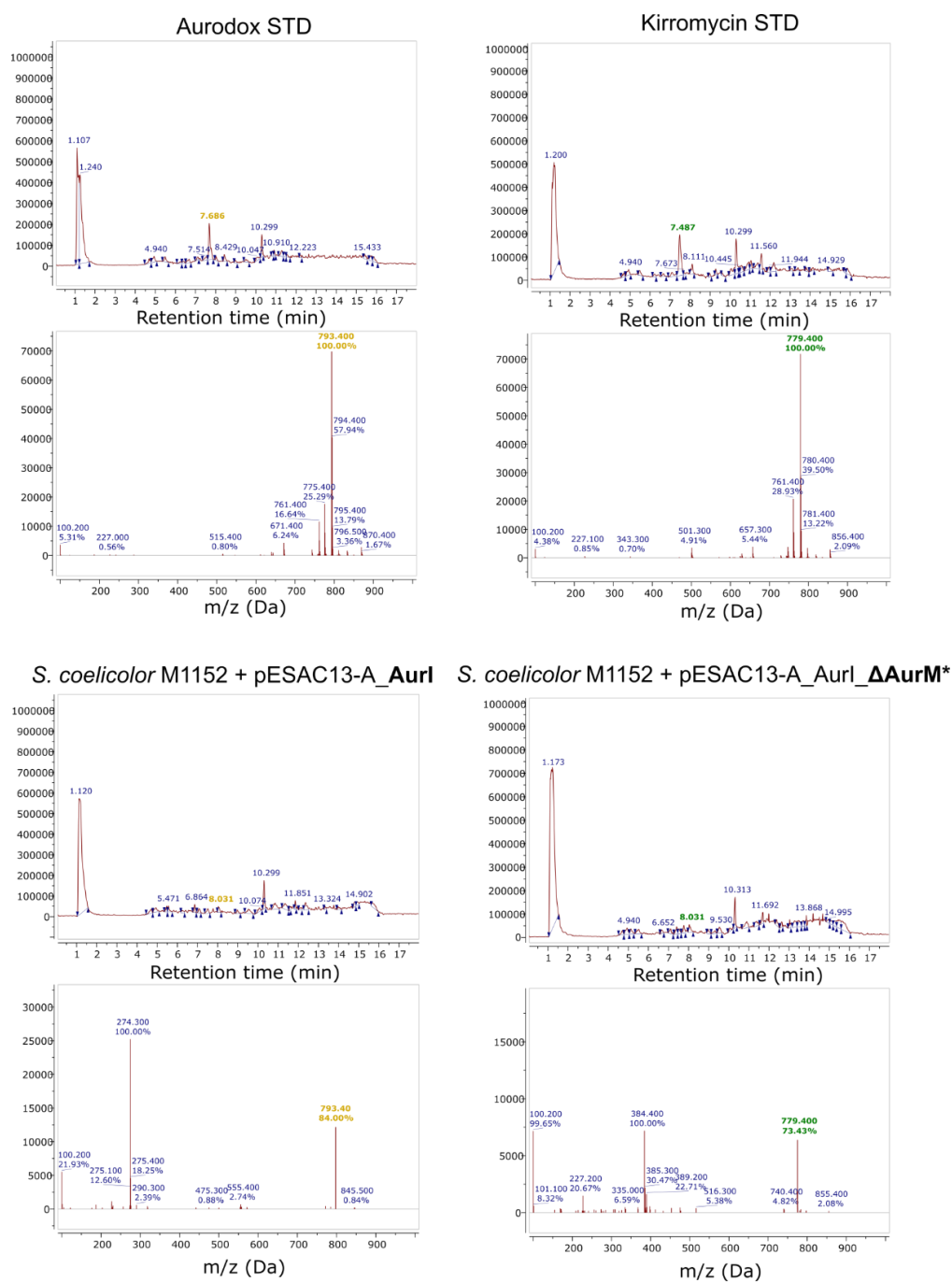
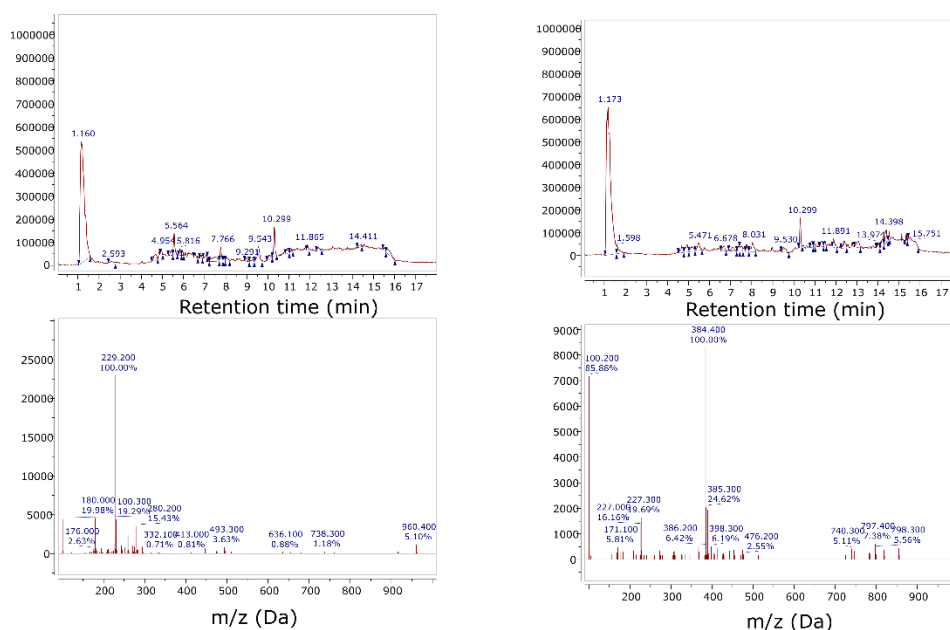


Figure 4.12: Total ion Chromatograms from HPLC indicate that gene deletion of *aurM from *S. coelicolor* M1152 + pESAC13-A_AurI results in production of a kirromycin-like molecule (m/z 779.40). Cultures were prepared for analysis as per methods (2.5.1 & 2.5.2). Aurodox and kirromycin standards were purchased from Hello Bio, diluted to 1 mg/ mL and have a retention time of approx. 7.7 and 7.5 minutes, and a corresponding M/Z ratio of 793.4 and 779.4, respectively.**

S. coelicolor M1152 + pESAC13-A_AurI_ΔAurAI *S. coelicolor* M1152 + pESAC13-A_AurI_ΔAurB



S. coelicolor M1152 + pESAC13-A_AurI_ΔAurHV *S. coelicolor* M1152 + pESAC13-A_AurI_ΔAurQ

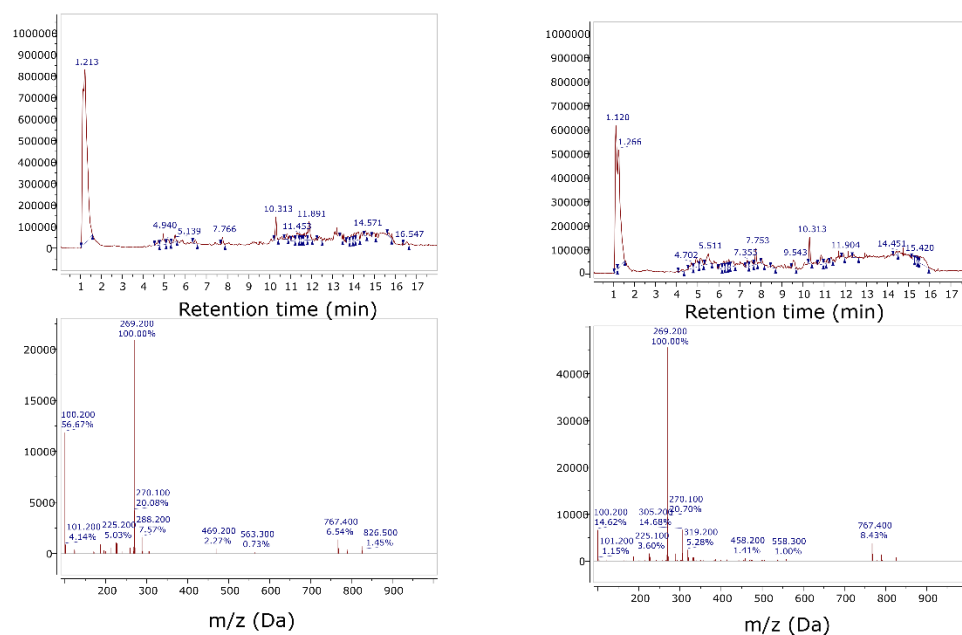


Figure 4.13: Total ion Chromatograms from HPLC indicate that *aurAI*, *aurB*, *AurHV* and *aurQ* are essential in the formation of kirromycin-like elfamycin molecule. Cultures were prepared for analysis as per methods (2.5.1 & 2.5.2). Aurodox and kirromycin standards can be seen in Figure 4.12 and were purchased from Hello Bio, diluted to 1 mg/ mL and have a retention time of approx. 7.7 and 7.5 minutes, and a corresponding M/Z ratio of 793.4 and 779.4, respectively

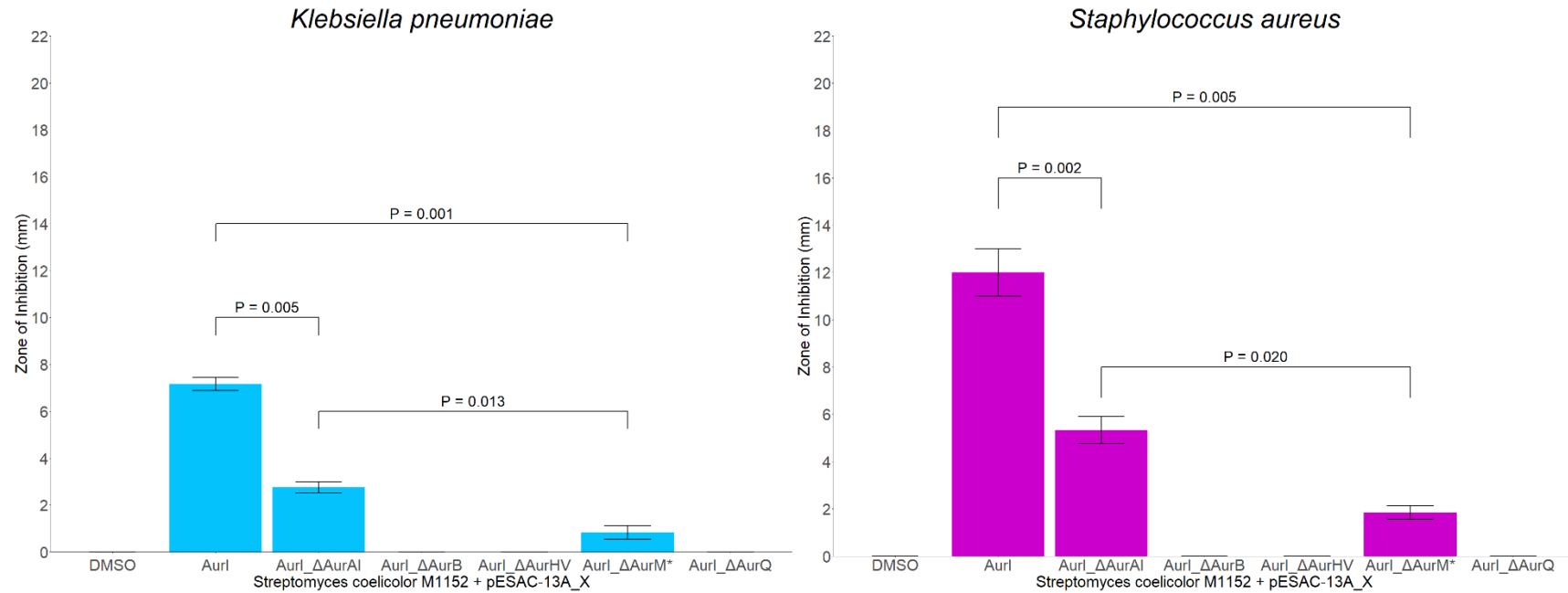


Figure 4.14: Bioactivity against both Gram-positive and Gram-negative bacteria was found in culture supernatant of *Streptomyces coelicolor* M1152 + pESAC-13A_Aurl, and the AurAl and AurM* mutants via disc diffusion assay. No bioactivity was observed in other deletion mutants. Fermentation extracts of strains were harvested (GYM liquid media, 30°C, 7 days, 200 rpm) with chloroform and resuspended in DMSO. Negative controls were DMSO. *Streptomyces* fermentation extracts were added to paper discs and plated on indicator strains, *Staphylococcus aureus* ATCC 43300 and *Klebsiella pneumoniae* ATCC 700603, which were normalised to an OD₆₀₀ of 0.01 in soft nutrient agar. Assay plates were grown for 12 hours at 37°C and zones of inhibition were measured in mm with a ruler.

4.2.5 Analysis of the effect of aurodox derivatives from the *S. coelicolor* M1152 pESAC-13A_AurI_ΔX heterologous expression system on the T3SS of Enterohaemorrhagic *E. coli*.

In both published and unpublished work, aurodox and kirromycin have been shown to downregulate the expression of key genes within the T3SS of Enterohaemorrhagic *E. coli* (McHugh et al., 2019, McHugh et al., Unpublished). As both deletion mutants *S. coelicolor* M1152 + pESAC-13A_AurI_ΔaurM* and *S. coelicolor* M1152 + pESAC-13A_AurI_ΔaurAI were shown to produce aurodox derivatives with bioactivity against Gram-positive and Gram-negative bacteria, the effect that these derivatives may have on the downregulation of the T3SS of Enterohaemorrhagic *E. coli* was investigated. The bacterial strain *E. coli* TUV93-0 is a well described strain of EHEC, which has been shown to initiate T3S under specific laboratory conditions (Cieza et al., 2015; Girard et al., 2007; Hews et al., 2017; McHugh et al., 2019; Shaw et al., 2008). This was confirmed during this study, where *E. coli* TUV93-0 was cultured under these T3SS inducing conditions (Roe et al., 2003). Strains were grown overnight in LB liquid media and then diluted 1:40 in fresh MEM-Hepes medium, typically this was done in volumes of 15 mL in Erlenmeyer flasks shaken at 200 rpm, 37°C. Once the cells had reached an OD₆₀₀ of 0.6, the cells were harvested by centrifugation and the cell lysate and supernatant containing secreted proteins were harvested as described in Chapter 2 of this thesis (Fig. 4.15).

It can be seen from the secreted proteins that both EspB/D and Tir are present as key proteins within the T3SS of EHEC, these indicate the induction of T3S under these conditions, confirming the method of Roe et al., (2003; Fig. 4.15).

Aurodox has been shown previously that it does not significantly affect the growth of *E. coli* TUV93-0 during T3SS inducing conditions (aurodox concentration of 5 µg /mL; McHugh et al., 2019). That was found in this study too, after treating TUV93-0 with

aurodox after 3 hours of growth. Interestingly, kirromycin to date had not yet been investigated. Unlike aurodox, kirromycin was shown to affect the growth of TUV93-0 under T3SS Inducing conditions (Fig. 4.16).

The TUV93-0 strains have been used as reporter strains under these T3SS inducing to analyse the effect that compounds have on the expression of the T3SS. These have been well documented in previous studies and so will not be validated further here (McHugh et al., 2019; Roe et al., 2003). These reporter strains are *E. coli* TUV93-0 *rpsM:gfp* and TUV93-0 *Ler:gfp*. GFP gene reporter assays were used to observe changes in gene expression of *ler* and the housekeeping gene *rpsM*. As described in Chapter 1 of this thesis, *ler* is the master regulator of the LEE pathogenicity island, responsible for the initiation of the T3SS in EHEC. If *ler* is downregulated, as is the expression of the T3SS in EHEC (McHugh et al., 2019; Shin, 2017). These GFP reporter strains were used to analyse the effect that aurodox had on the T3SS (McHugh et al., 2019). Additionally, in this study, aurodox, kirromycin and the potential derivatives produced in this thesis were also investigated to establish the effect these have on the expression of *ler*, and in turn, the T3SS of EHEC too.

When the growth (OD₆₀₀) of *E. coli* TUV93-0 was analysed in response to treatment with aurodox, kirromycin and the potential aurodox derivatives, similar results were observed for kirromycin, where a decrease in growth relative to the DMSO control was found (Fig. 4.17). The growth of *E. coli* TUV93-0 in response to aurodox treatment increased and that for the aurodox derivative Aurl_ Δ aurM* and Aurl_ Δ aurI were similar to that of the DMSO control.

To analyse gene expression, the fluorescence of the cells treated with aurodox, kirromycin and the derivatives was measured and normalised based on the OD₆₀₀ of the cells at that same time interval. This prevents bias associated with denser cultures having a greater fluorescence and is reported in relative fluorescence units (RFU). Analysis of the expression of the T3SS reveals that compared to the DMSO control,

expression of *ler* is reduced in response to all treatments (Fig. 4.18). Aurodox and the biosynthesised aurodox from the heterologous host expressing the aurodox BGC (Aurl) have the greatest reduction in *ler* expression, closely followed by the derivative Aurl_ Δ *aurAI*. The lowest effective observed to reduce *ler* expression was from kirromycin and the aurodox derivative resulting from the Aurl_ Δ *aurM*^{*} mutant, thought to produce kirromycin. This suggests that even though kirromycin can reduce the expression of *ler*, Aurodox and the molecule resulting from the deletion of *aurM*^{*} leads to greater activity.

When the housekeeping gene *rpsM* is analysed, relative fluorescence was comparable to the DMSO control for molecules produced from the WT cluster (Aurl) and the mutant Aurl_ Δ *aurAI* (Fig. 4.18). However, relative fluorescence was reduced in response to aurodox, kirromycin and Aurl_ Δ *aurM*^{*}. Based on the outlier present in the dataset for Aurodox, it is hypothesised that re-running the experiment will show a lesser reduction of *rpsM* gene expression.

These data not only confirm that Aurodox and kirromycin can downregulate the T3SS of EHEC, but also that the derivatives of the aurodox molecule generated in this study also possess this activity, suggesting other possible antivirulence compounds for the treatment of EHEC infections.

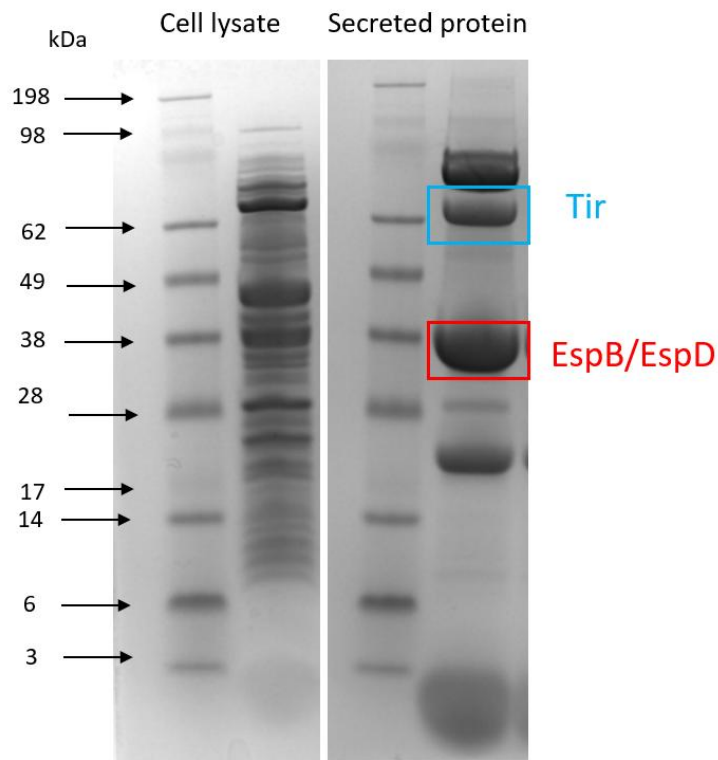


Figure 4.15: SDS-PAGE analysis of cell lysates and secreted proteins indicate that *E. coli* TUV93-0 produces T3S related proteins under T3SS inducing conditions. *E. coli* TUV93-0 cultured in T3S inducing medium (MEM-Hepes, 37 °C, 200 rpm) till OD₆₀₀ 0.6 was reached before harvesting protein. Both cell lysate and secreted proteins are shown. The location of EspB/EspD is shown in red at 34/39.5 kDa and Tir is shown in blue at 78 kDa.

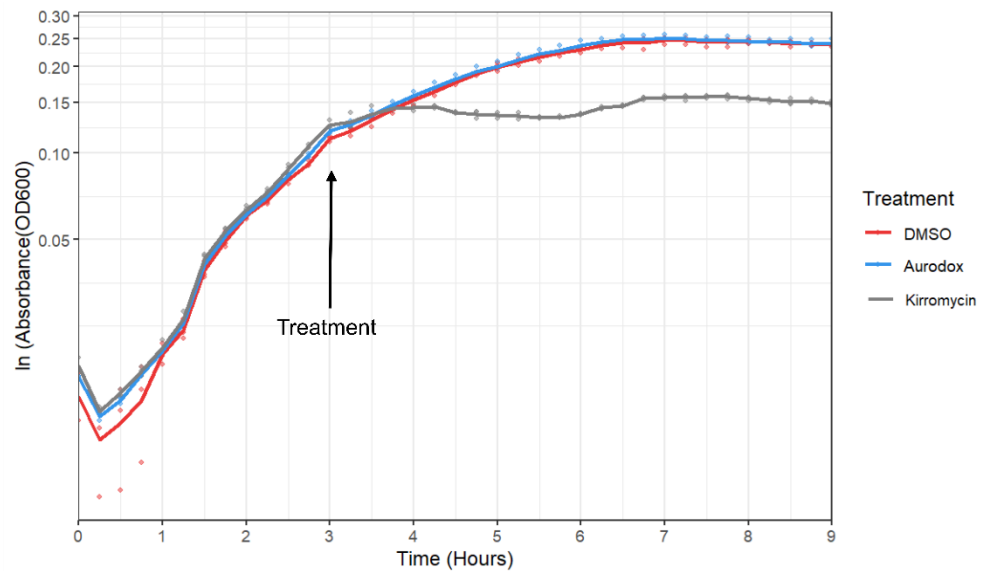


Figure 4.16: Unlike aurodox, kirromycin affects the growth of EHEC . *E. coli*

TUV93-0 was grown under T3SS inducing conditions (MEM-Hepes, 37 °C, 200 rpm) for 3 hours and then treated with 5 µg/ mL aurodox, kirromycin or DMSO as a control. OD₆₀₀ was measured every 15 minutes for the course of 9 hours using a the FLUOstar Optima Microplate Reader System (BMG Labtech). Strains were grown in triplicate wells from three separate overnight cultures for biological replicates represented by red, blue and grey dots. For each of the three biological replicates, three technical representative wells were used where averages of these three technical replicates are plotted on this semi-log plot. Trendlines are indicated by the average of biological replicates.

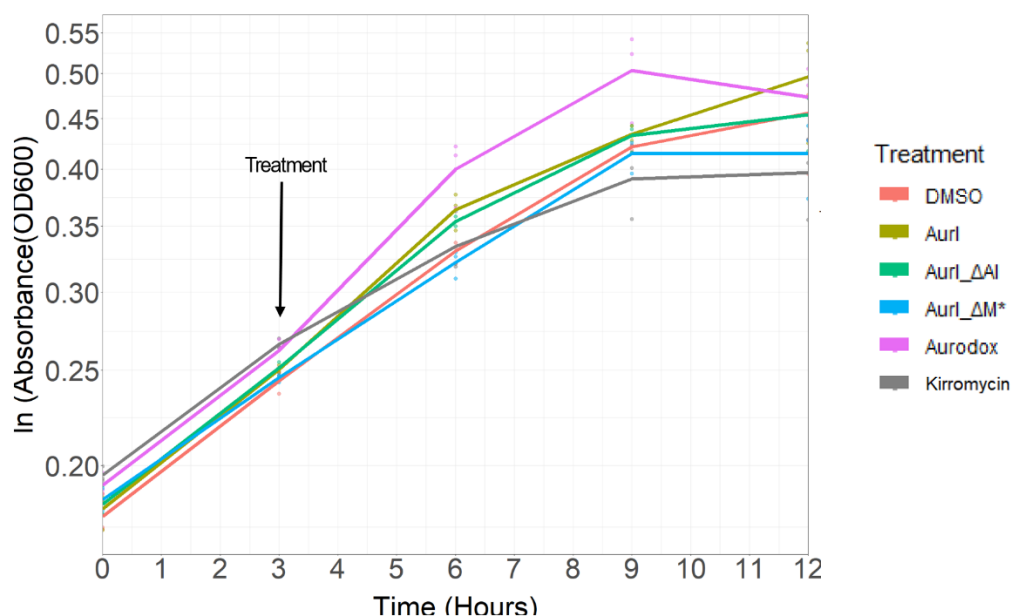


Figure 4.17: Analysis of the effect of Aurodox derivatives on the growth of EHEC. *E. coli* TUV93-0 was grown under T3SS inducing conditions (MEM-Hepes, 37 °C, 200 rpm) for 3 hours and then treated with 5 µg/ mL aurodox, kirromycin or 50 µg/ mL of aurodox derivate extract, with DMSO as a control. OD₆₀₀ was measured every 3 minutes for the course of 12 hours using a the FLUOstar Optima Microplate Reader System (BMG Labtech). Strains were grown in triplicate wells from three separate overnight cultures for biological replicates represented by coloured dots. For each of the three biological replicates, three technical representative wells were used where averages of these three technical replicates are plotted on this semi-log plot. Trendlines are indicated by the average of biological replicates.

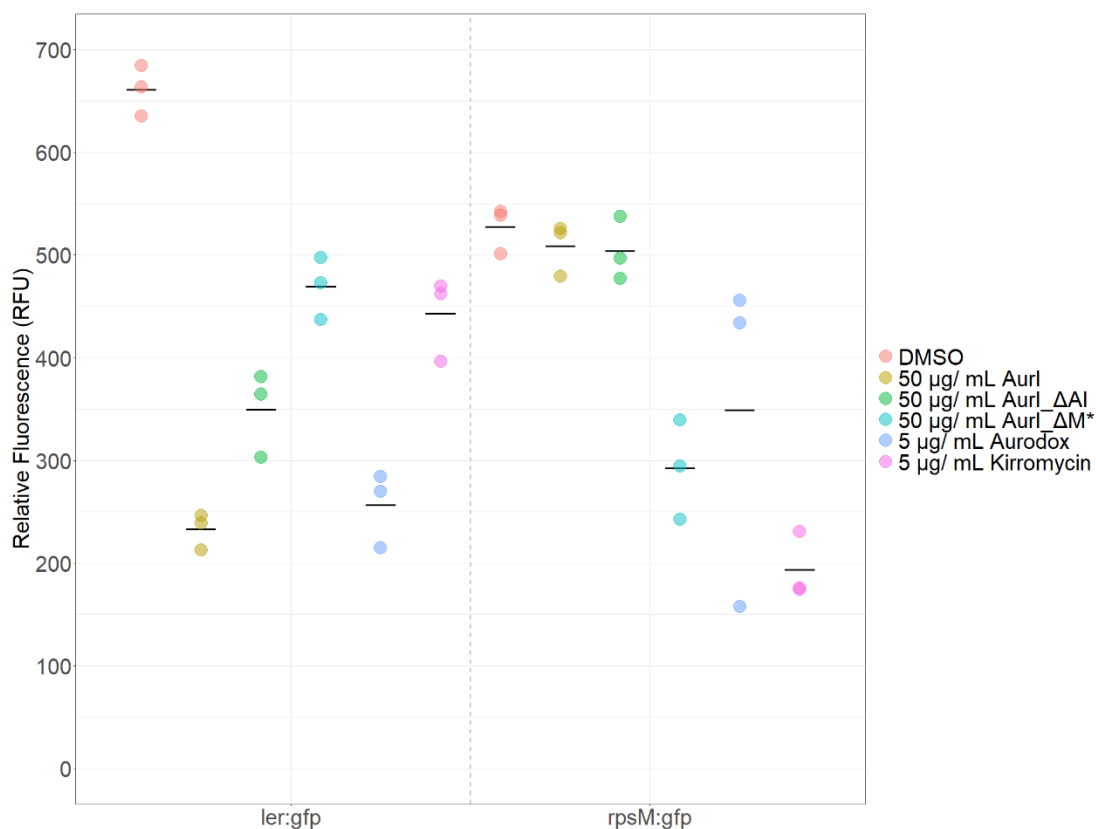


Figure 4.18: Like aurodox, its derivatives also downregulate the T3SS of *E. coli* TUV93-0. Relative fluorescence of *E. coli* TUV93-0 GFP-tagged strains in response to treatment with aurodox, kirromycin and molecules derived from the WT PAC (Aurl), Aurl_ Δ aurAI, Aurl_ Δ aurM* at 6hrs growth. *E. coli* TUV93-0 *rpsM:gfp* and *ler:gfp* reporter strains were grown under T3SS inducing conditions (MEM-Hepes, 37 °C, 200 rpm) for 3 hours and then treated with 5 µg/ mL aurodox, kirromycin or 50 µg/ mL of aurodox derivate extract, with DMSO as a control. OD₆₀₀ was measured every 3 minutes for the course of 12 hours using a the FLUOstar Optima Microplate Reader System (BMG Labtech). Data shown here is after 3 hours of treatment.

4.2.6 Creation of hexahistidine tagged aurodox biosynthesis genes

The four aurodox biosynthesis enzymes chosen for further study were cloned and recombinantly expressed with an aim to decipher their function in the biosynthesis of aurodox. To facilitate purification of the four aurodox biosynthesis enzymes using affinity chromatography (IMAC) the genes were cloned incorporating a hexa-histidine tag in the constructs of AurB, AurHV, AurM* and AurQ. The hexahistidine tag also facilitates detection of the tagged protein using Western Blot through anti-6x His antibodies.

To enable this, the nucleotide sequence of the chosen aurodox biosynthesis genes were retrieved from the aurodox BGC on the *S. goldiniensis* genome. After retrieval, the sequences were subject to codon optimisation via the GenSmart™ online codon optimisation tool (GenScript) for optimal expression in *E. coli* hosts. Due to high GC content and divergence in codon usage between species, often *Streptomyces* proteins can be difficult to express in *E. coli* hosts. Codon optimisation may improve the enzymatic yield in subsequent expression studies (Edison et al., 2020). Following codon optimisation, the stop codon of each gene was removed to facilitate overexpression. The resulting sequences were generated on pUC57 vectors by GenScript.

Once the pUC57 constructs were received, PCR amplification of the key aurodox biosynthesis genes was carried out. To allow efficient sub-cloning into different bacterial expression vectors, restriction enzyme sites (*NdeI* and *HindIII*) were added to either side of the sequence using PCR primers (Fig. 4.19). After agarose gel electrophoresis, bands corresponding to the size of each key gene were excised and subject to gel extraction (Promega).

The bacterial expression vector pET-21a(+) was chosen for overexpression (Fig. 4.20). This bacterial expression vector can be used for the inducible expression of N-terminally His-tagged proteins through an inducible T7 promoter.

Both the protein overexpression vector, pET-21a(+) and the PCR amplified aurodox genes were subject to restriction digestion with NdeI and HindIII (Fig. 4.21) and ligated via T4 ligase to form final overexpression constructs. Due to trouble with cloning, the bacterial expression vector pET-21a(+)_AurHV could not be cloned and this gene was abandoned to focus on the remaining three constructs.

These three constructs (pET-21a(+)_AurB, pET-21a(+)_AurM* and pET-21a(+)_AurQ) were tested via restriction digest with NdeI and HindIII to release the aurodox biosynthetic gene from the vector and via PCR to confirm the increased size of the insert in the multiple cloning site of pET-21a(+) when compared to the empty vector (Fig. 4.21). These primers were located approximately 200 bp upstream and downstream of the gene of interest on pET-21a(+) constructs, allowing the confirmation of insertion of the insert into pET-21a(+) and the infame nature of the His-tag via sanger sequencing (Eurofins). Plasmids were also subject to full plasmid sequencing (Plasmidsaurus) to confirm integrity of open reding frames and that no mutations had arisen during cloning (Fig. 4.22, 4.23 4.24).

The *E. coli* pET-21a(+) bacterial expression vectors containing the aurodox biosynthetic gene overexpression constructs were introduced into *E. coli* BL21 (DE3) strains by transformation to enable overexpression via a T7 promotor and purification from *E. coli*.

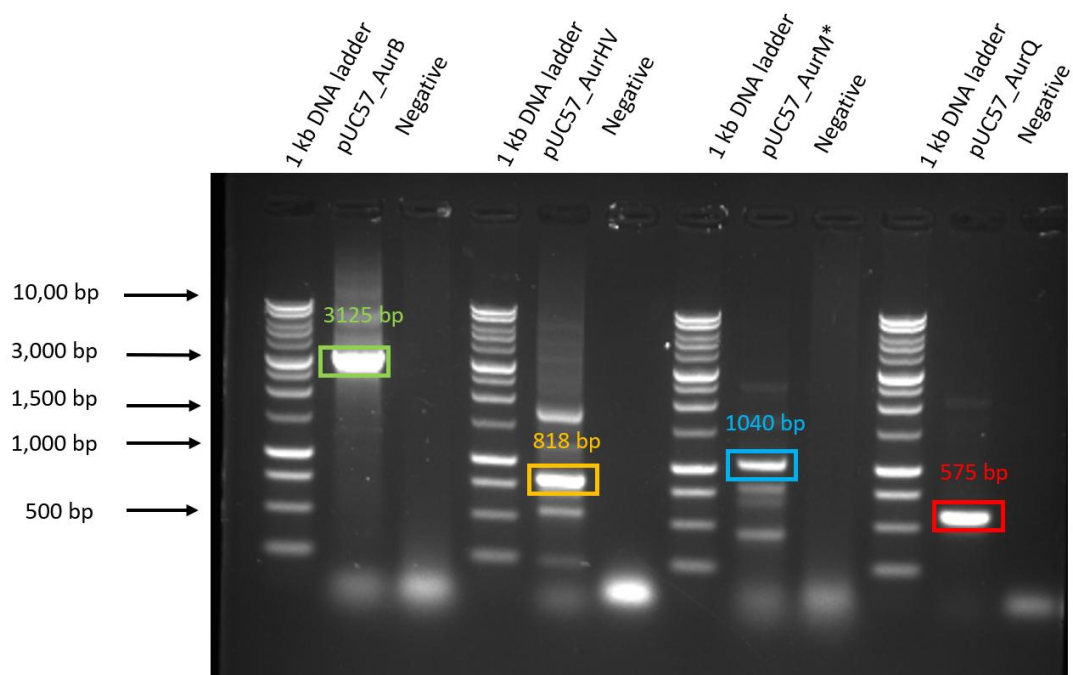


Figure 4.19: Agarose gel depicting the PCR amplification of codon optimised aurodox genes with primers containing HindIII and NdeI restriction sites from pUC57 constructs supplied by Genscript. Aurodox genes are as follows: AurB, shown in green at 3125 bp; AurHV, shown in orange at 818 bp; AurM*, shown in blue at 1040 bp; and AurQ, shown in red at 575 bp. Negative controls were ran with nuclease free water.

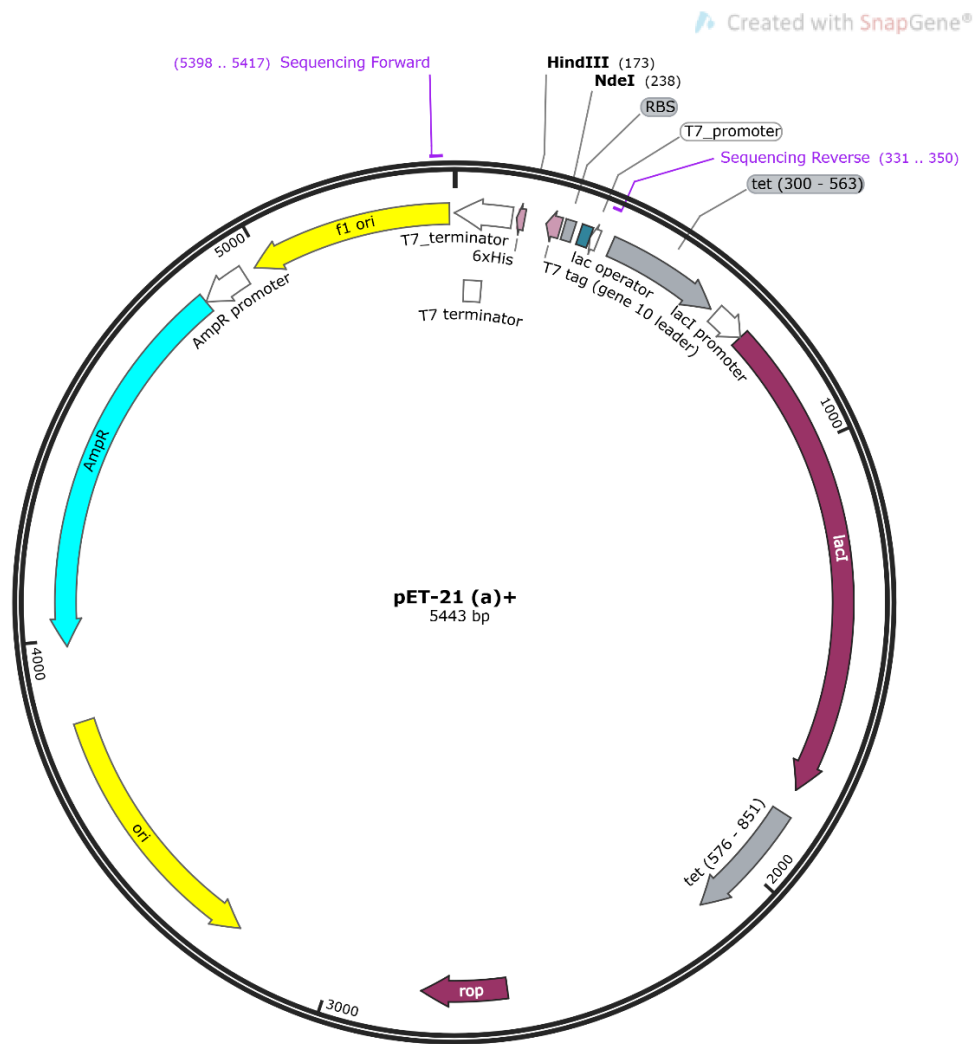


Figure 4.20: Annotated plasmid map of pET-21a(+). Features were annotated using SnapGene, where the ampicillin resistance gene is shown in cyan, the T7 promotor and terminators are shown in white and HindIII and NdeI restriction sites indicate the multiple cloning site for integration of key aurodox biosynthesis genes. Also shown are the sequencing primers used for validation of correct incorporation into the vector.

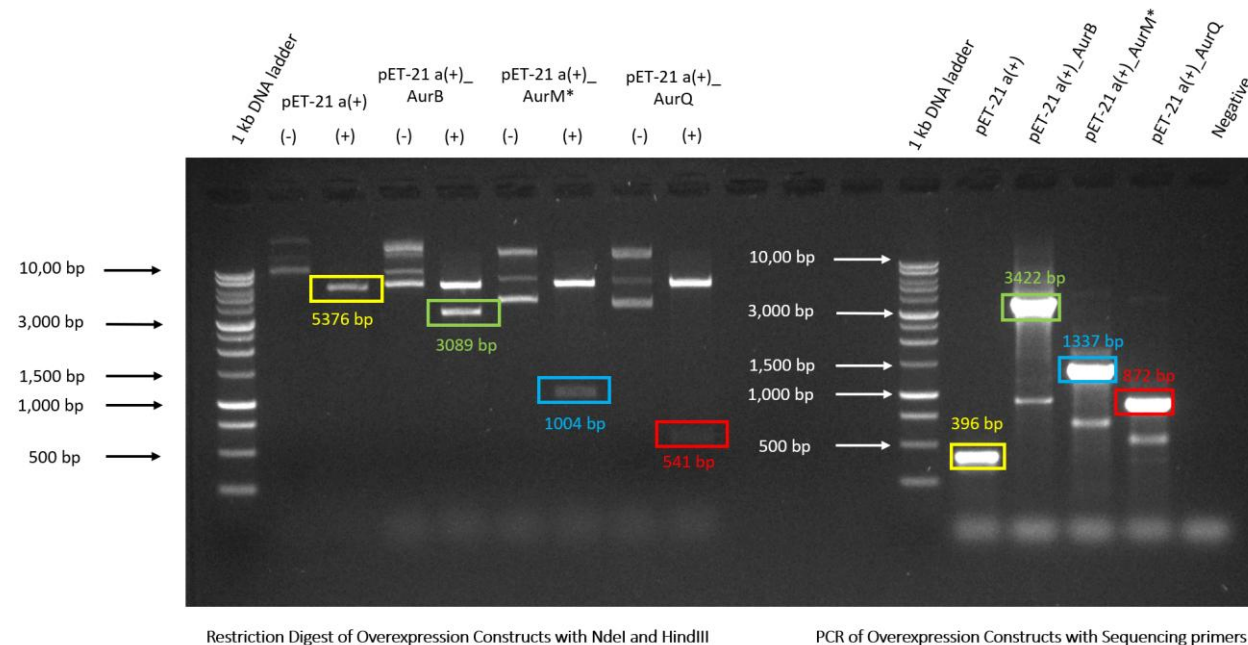


Figure 4.21: Agarose gel showing validation of pET-21 a(+) aurodox gene overexpression constructs via restriction digests and PCR. Overexpression constructs were digested with SmaI and HindIII to release aurodox genes at 3089 bp in green for AurB, 1004 bp in blue for AurM* and 541 bp in red for AurQ with the digested empty vector of pET-21 a(+) as a control. PCR amplification of the Aurodox genes within pET-21 a(+) vectors were done with sequencing primers approximately 200bp upstream and downstream of the aurodox gene on the pET-21 a(+) construct. Bands at 3422 for AurB in green, 1337 bp for AurM* in blue, and 872 bp for AurQ in red indicate successful gene integration. Amplification using these primers for pET-21 a(+) is at 396 bp shown in yellow as a control.

245

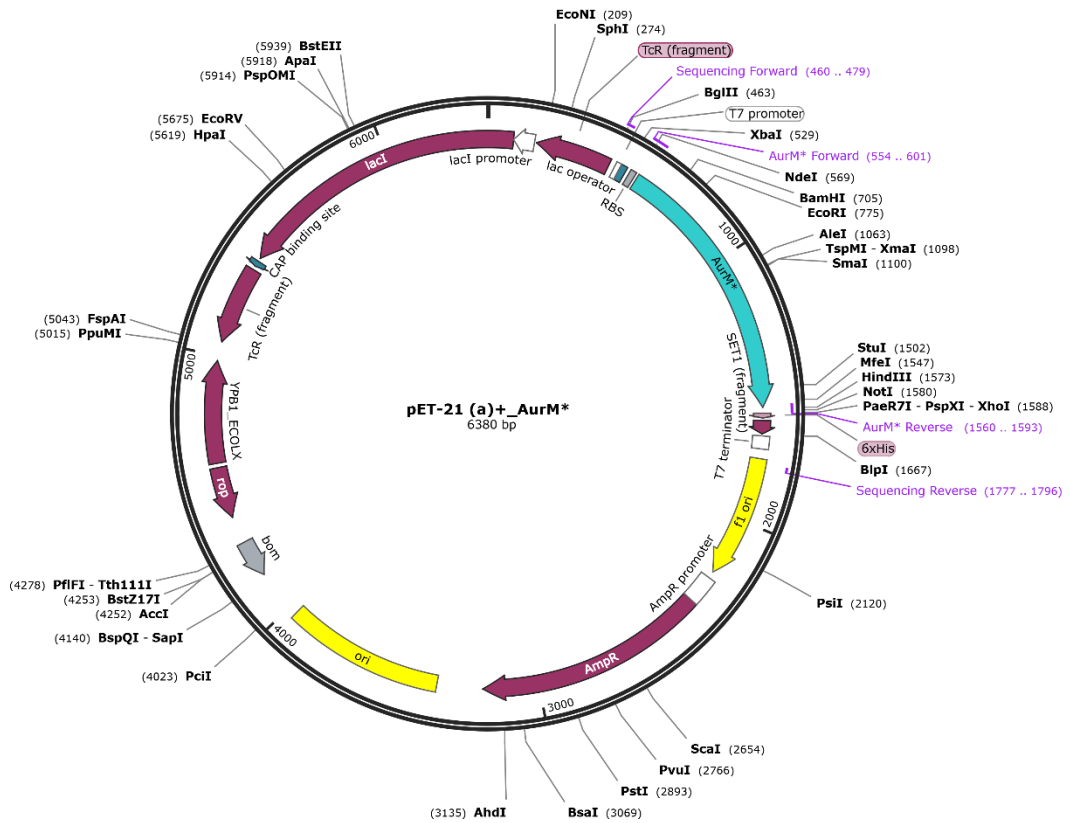


Figure 4.23: Plasmid map of pET-21a(+)_AurM* from whole plasmid sequencing of final overexpression constructs with Plasmidasaurus. *aurM is shown in cyan.**

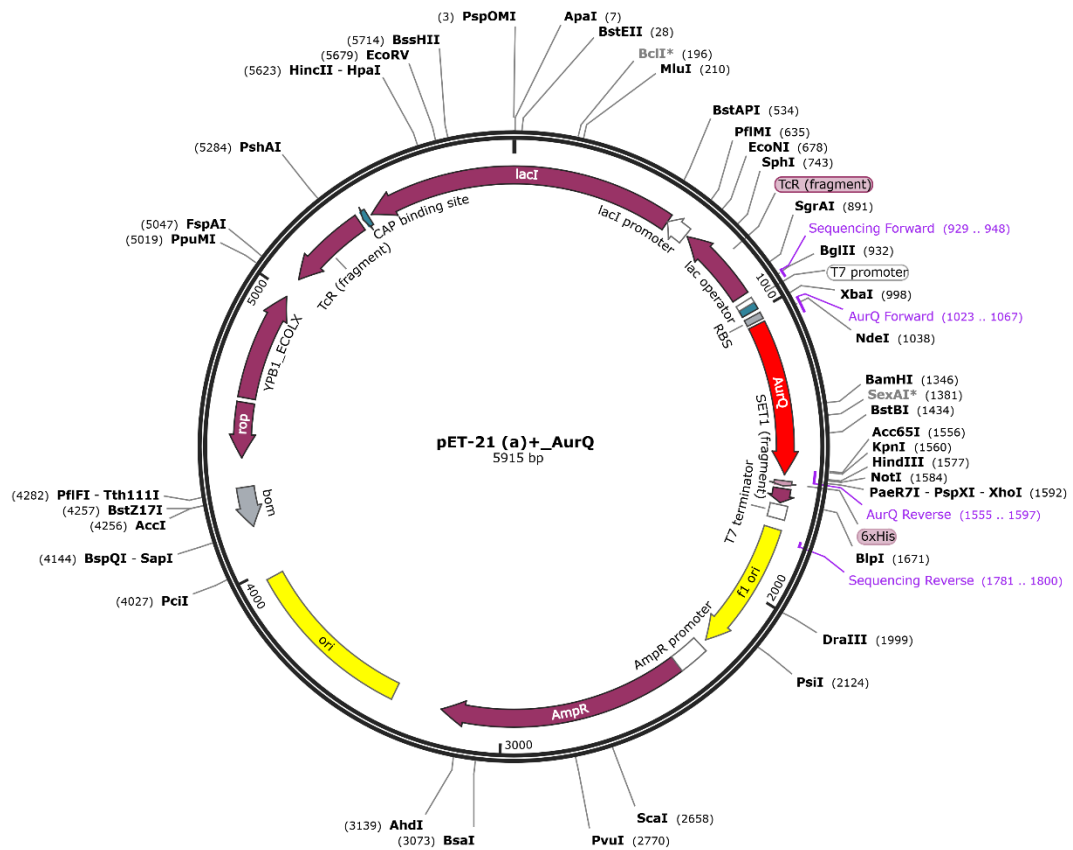


Figure 4.24: Plasmid map of pET-21a(+)_aurQ from whole plasmid sequencing of final overexpression constructs with Plasmidasaurus. *aurQ* is shown in red.

4.2.7 Optimising hexahistidine tagged protein overexpression and detection by Western Blot in *Escherichia coli* BL21

The *E. coli* strain BL21 was used for expression of aurodox biosynthesis proteins via the pET-21a(+) vector. BL21 contains the λ DE3 lysogen, used to carry the gene encoding T7 RNA polymerase, which is governed by the lacUV5 promoter. Induction of expression of this promoter can be via IPTG or another induction system, such as the use of ZYP-5052 autoinduction media. As a result, strain which contain this DE3 are capable of expressing recombinant genes which have been cloned downstream of the T7 promoter. As already discussed, the pET-21a(+) vector system utilises the T7 promoter, which would allow for the expression of aurodox biosynthesis protein in BL21 via this vector.

In this case, autoinduction media was used for induction of BL21 *E. coli* cultures. Work by Studier (2005) suggested that induction via ZYP-5052 autoinduction media yields expression of target proteins several fold higher than that of induction with IPTG (Studier, 2005). The method is also less labour intensive and utilises a system where cultures are only to be inoculated and grown to saturation, when compared to that of IPTG which required monitoring growth of each culture and adding inducer at the proper stage of growth. During induction, limited concentrations of glucose are metabolised first during growth, preventing lactose uptake until the preferred glucose carbon source is depleted, normally mid-late log phase. As glucose is depleted from the media, lactose is taken up and converted to the inducer allolactose by β -galactosidase. This process causes the release of the lac repressor, inducing expression of the T7 RNA polymerase from the lacUV5 promoter and unblocks the T7 lac promoter allowing expression of target proteins by T7 RNA polymerase (Studier, 2005).

A range of conditions were tested for optimal expression of the three aurodox biosynthesis proteins. In all cases, however, cell lysis was performed with BugBuster™ (Merck) for analysis of proteins allowing for initial optimisation of protein expression. Here, cell lysate was centrifuged at 4 °C before supernatant was boiled for 10 minutes at 95 °C for denaturation prior to SDS-PAGE analysis. Proteins were separated by SDS-PAGE and gels stained with Coomassie Blue dye for visualisation of total protein.

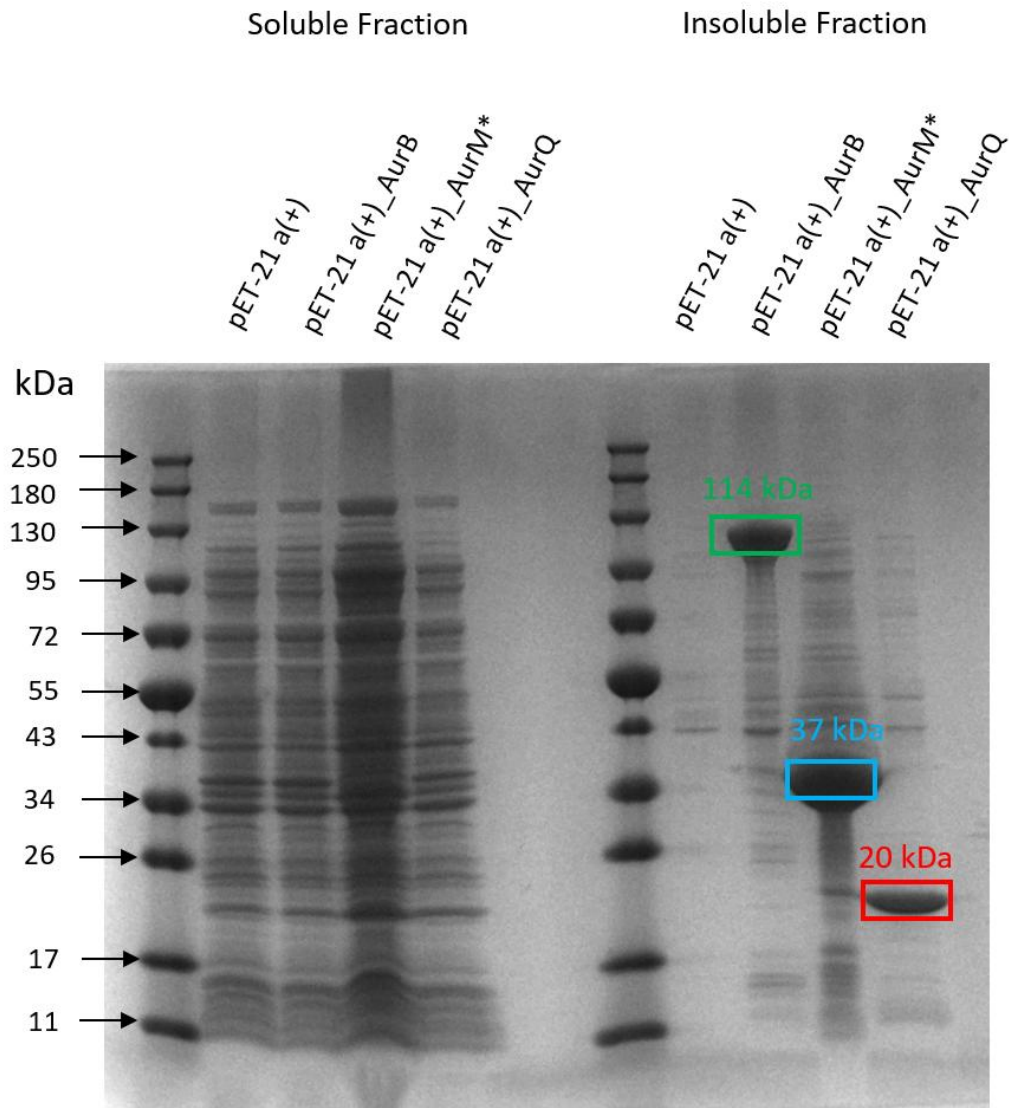
Firstly, cultures of BL21 containing aurodox biosynthesis gene overexpression vectors were grown at 37 °C for 24 hours, 200 rpm, prior to lysis and SDS-PAGE analysis (Fig. 4.25). It can be seen that there is no change in the proteins expressed in the aurodox biosynthesis protein vectors, when compared to that of the empty vector, in the soluble fraction of the cell lysate supernatant. Further processing of the samples with BugBuster™ revealed the proteins of the insoluble fraction, according to manufacturer's protocol. In this case, all three aurodox biosynthesis proteins were found to be expressed a high level when compared to the empty vector control (Fig. 4.25).

To confirm that these proteins were, in fact, the aurodox biosynthesis enzymes of AurB, AurM* and AurQ, the insoluble fraction of the cell lysate supernatants were subjected to analysis by Western Blot (Fig. 4.26). Through the utilisation of the hexahistidine tag on the N terminus of all three proteins, confirmation of these proteins as the aurodox biosynthesis enzymes was made with bands visible at the respective sizes of 114 kDa, 37 kDa and 20 kDa for AurB, AurM* and AurQ. No bands were seen on the empty vector control and confirmation of the Western Blots performance was seen by use of the purified AmtB protein as a positive control (Fig. 4.26). Unfortunately, proteins in insoluble fractions often means that the proteins are forming inclusion bodies, which can lead to incorrect folding of the protein. Therefore, expression in the soluble fraction is preferred (Baneyx and Mujacic, 2004).

To optimise the expression of the proteins and to reduce the amount of insoluble protein, the cultures were subjected to growth at different temperatures and induction times. All *E. coli* BL21 strains were grown at 18 °C for 72 hours, 26°C for 48 hours and again at 37 °C for 24 hours, all with shaking at 200 rpm (Fig. 4.27). It was observed that growth at lower temperatures provide better yields of targeted proteins, particularly in the case of AurM* where it can be observed that as temperature increases the size of the band corresponding to AurM* decreases. The same can be observed for both AurB and AurQ where expression of the proteins is visible compared to the lack of presence in the cell lysate supernatants corresponding to growth at 37 °C for 24 hours.

Lowering the temperature of cultures during recombinant protein expression can encourage correct protein folding and prevent the formation of inclusion bodies (Vera et al., 2007). This is consistent with the observations in this thesis, where lowering the temperature of culture can result in protein expression in the soluble fraction, particularly for BL21 + pET-21a(+)_AurM*. Growth at 18 °C for 72 hours was found to be the best method of expression for all proteins from those tested.

To harvest upscaled volumes of BL21 + pET-21a(+)_AurM* for purification of AurM*, four 50 mL flasks of culture were inoculated and grown at optimum conditions of 18 °C for 72 hours, 200 rpm, and pellets stored for future lysis. For each culture, one mL of sample was processed as previously, and the expressed proteins analysed by SDS-PAGE. For all four cultures, AurM* was found to be expressed at high levels, when compared to the empty vector (Fig. 4.28). AurM* was taken forward for purification and enzymatic characterisation.



E. coli BL21 Autoinduction Media, 37 °C, 24 Hours

Figure 4.25: SDS-PAGE indicates that key aurodox proteins can be overexpressed in *E. coli* BL21 DE3. *E. coli* BL21 DE3 cells containing the overexpression constructs were grown for 24 hours in autoinduction media at 37 °C, 200 rpm. Both the soluble and insoluble fractions are shown, where it can be seen that the proteins are located in the insoluble fraction, with AurB shown in green at 114 kDa , AurM* shown in blue at 37 kDa and AurQ shown in red at 20 kDa.

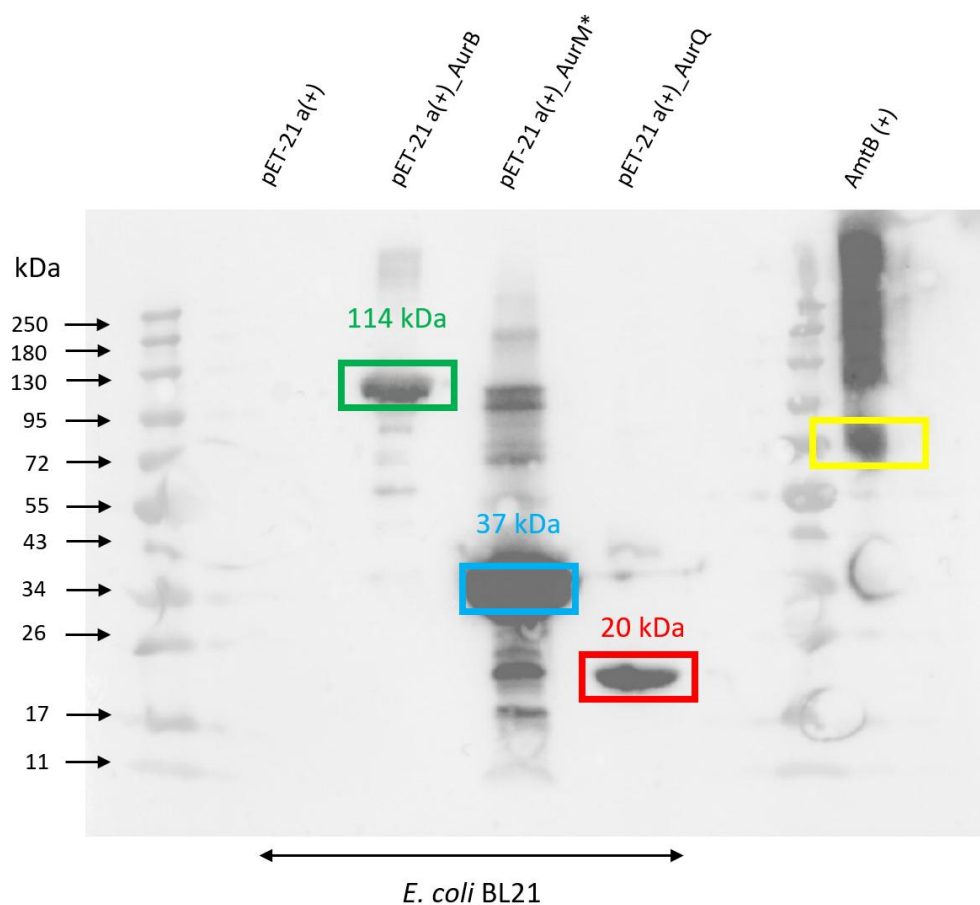


Figure 4.26: Western Blot for the 6x histidine tagged N terminus of aurodox biosynthesis proteins indicate expression by the pET-21 a(+) overexpression constructs in BL21. *E. coli* BL21 DE3 cells containing the overexpression constructs were grown for 24 hours in autoinduction media at 37 °C, 200 rpm. Insoluble fractions are shown, with AurB shown in green at 114 kDa, AurM* shown in blue at 37 kDa and AurQ shown in red at 20 kDa. pET-21 a(+) is used as a negative control, and purified AmtB as a positive control.

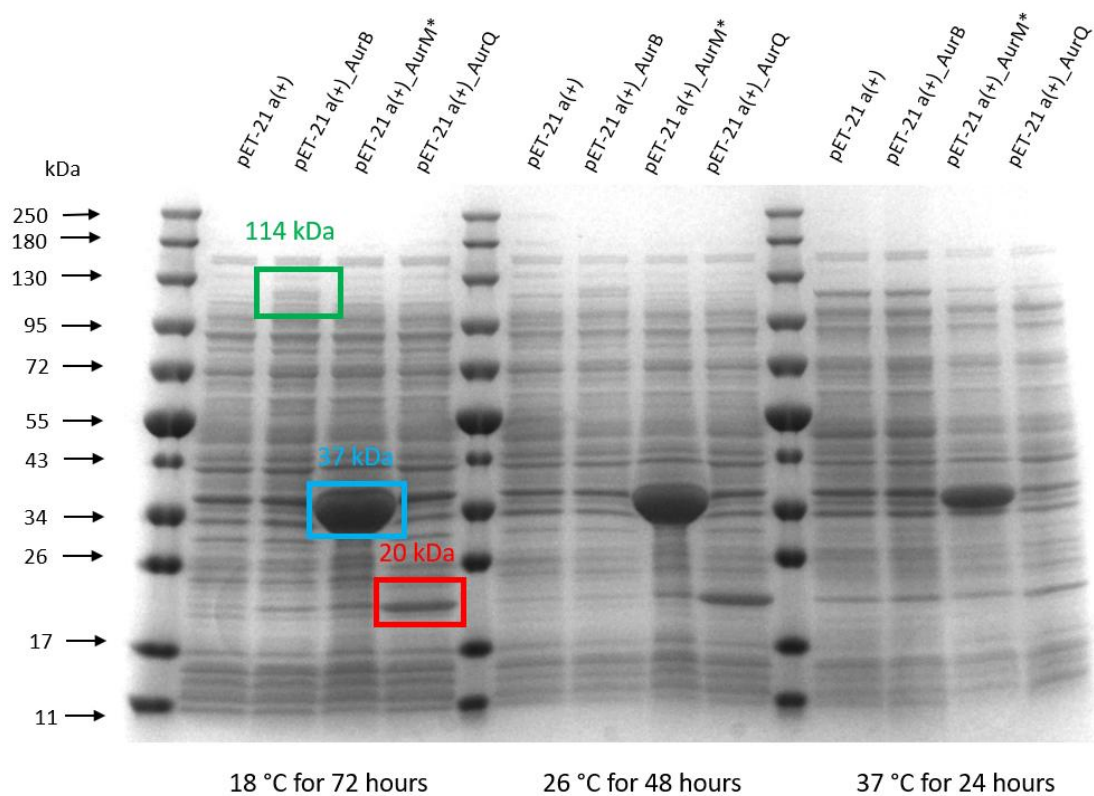


Figure 4.27: Aurodox biosynthesis proteins are optimally expressed in *E. coli* BL21 DE3 when cultured in autoinduction media at 18 °C for 72 hours. AurB shown in green at 114 kDa, AurM* shown in blue at 37 kDa and AurQ shown in red at 20 kDa. pET-21 a(+) is used as a negative control.

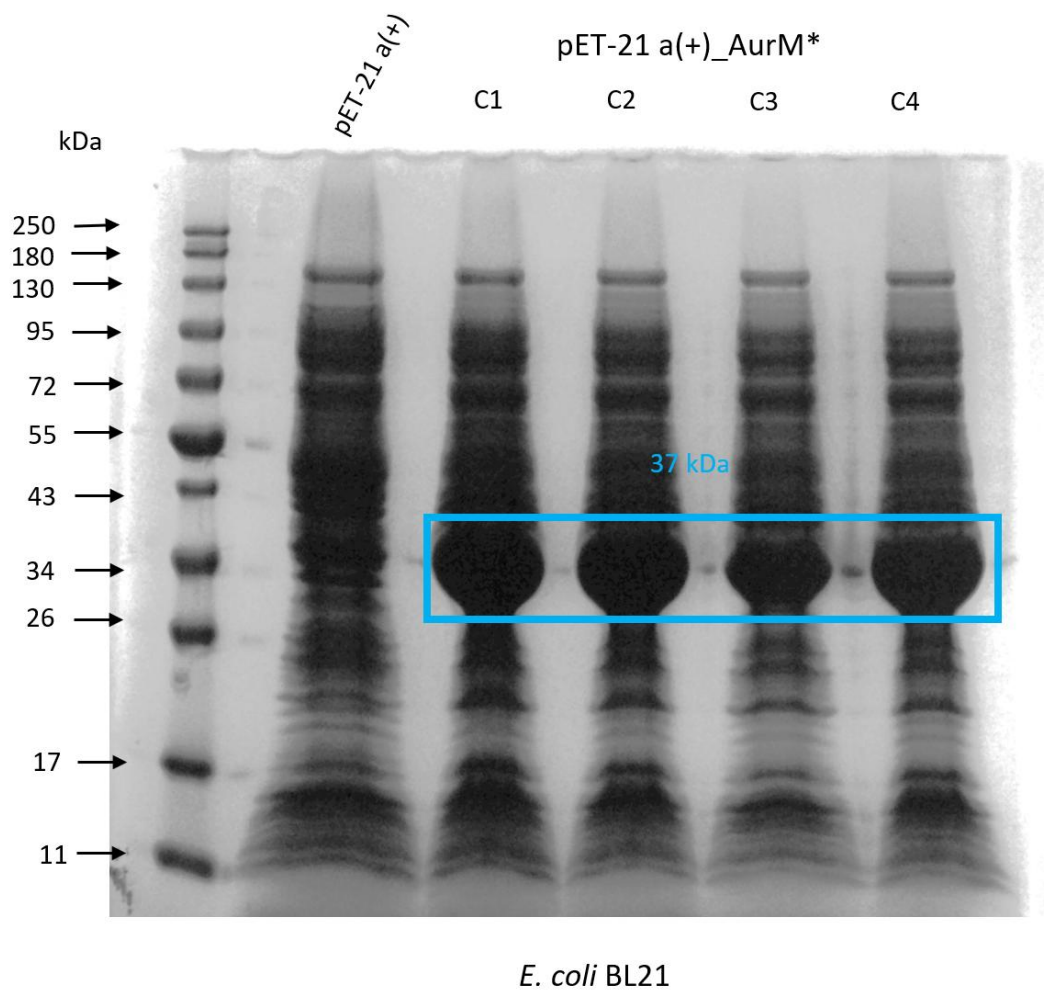


Figure 4.28: Overexpression under optimal conditions for of AurM* from BL21 via the pET-12 a(+)_AurM* overexpression construct. Cultures were grown from 4 individual *E. coli* BL21 + pET-21 a(+)_AurM* cell colonies (C1, C2, C3, C4) and inoculated into 4 flasks for 72 hours in autoinduction media at 18 °C, 200 rpm, before harvesting. AurM* is shown at approximately 37 kDa in blue. pET-21 a(+) is used as a negative control.

4.2.8 Optimising hexahistidine tagged AurM* protein purification by IMAC

Upscaled cultures (4 x 50 ml) of AurM* was overexpressed in BL21 *E. coli* as described (Fig. 4.28) and the cell lysate from overexpression of AurM* in BL21 was solubilised in solubilisation buffer (10mL/g). The solution was then homogenised using a homogeniser and cells lysed using the French pressure cell as described in Chapter 2. After cells were lysed, they were subject to purification via Immobilised Metal Affinity Chromatography (IMAC). As a primary test to assess the success of the IMAC before scaling up, 1 mL of the cell lysate was loaded onto a 1 mL Histrap column packed with cobalt-charged sepharose and the column washed with 5 mL IMAC A buffer supplemented with 40 mM imidazole to remove non-specifically bound protein. AurM* was eluted using a one-step elution of imidazole present in IMAC Buffer B (500 mM) over 10 column volumes. As this was hand purified, the absorbance could not be monitored. The cell lysate was run alongside the loading, wash and elution fractions of the IMAC during SDS PAGE analysis and the fractions analysed for the presence of AurM* (Fig.4.29). AurM* was successfully purified using this method and so the purification was scaled up.

The remaining lysate (40 mL) was again loaded onto a 1 mL Histrap column, this time using the ÄKTA Pure FPLC platform (GE Healthcare) and the column washed with 10 mL IMAC A buffer removing non-specifically bound protein. AurM* was eluted using an imidazole gradient, provided by increasing concentrations of the imidazole rich IMAC Buffer B, increasing from 40-500 mM over 20 column volumes. Throughout the purification process, the protein was continuously monitored by absorbance at 280 nm (Fig. 4.30). The eluent was collected in a 96-well deep well plate in 2 mL fractions. Again, protein size and purity was verified via SDS-PAGE electrophoresis (Fig. 4.31). Present in fractions four onwards in a high concentration, AurM* was eluted and stored for analysis of its enzymatic activity.

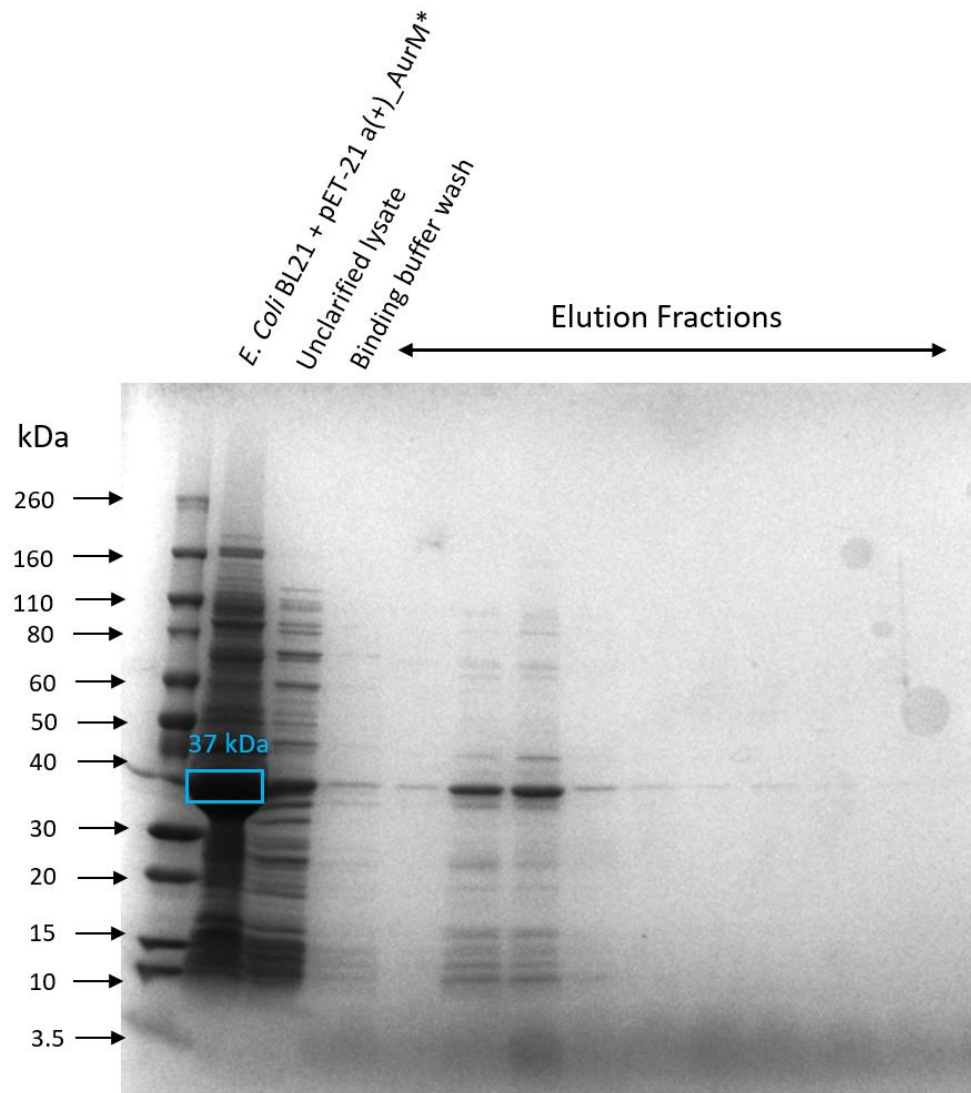


Figure 4.29: Affinity chromatography SDS PAGE gel for *E. coli* BL21 expressing pET-21 a(+)_{AurM}* vector. Crude cell lysate, unclarified lysate, binding buffer wash and elution fractions are shown respectively, with optional elution in fractions 2 and 3, shown in blue at 37 kDa.

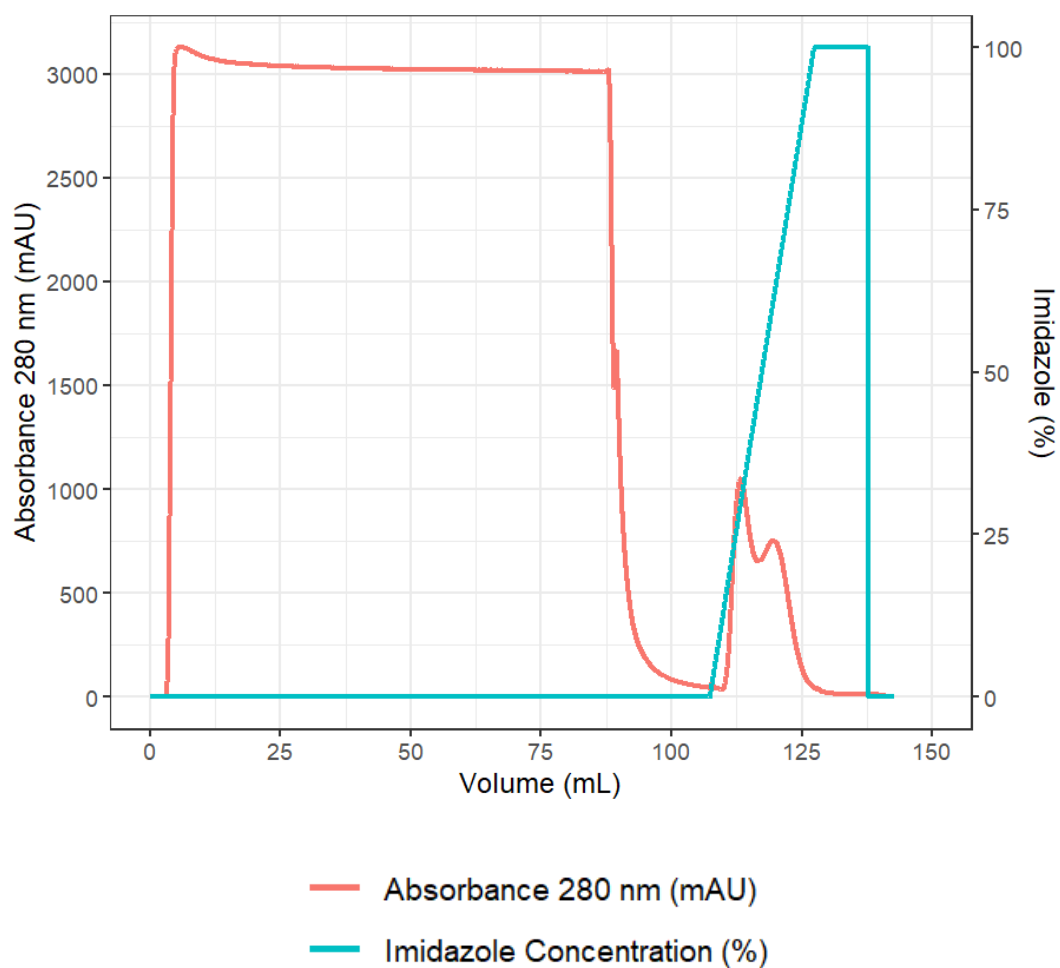


Figure 4.30: Purification of AurM*. IMAC profile of the wash and elution of AurM* from solubilised *E. coli*. The red line represents A280nm and the blue line represents the concentration of imidazole as a percentage (100% = 500 mM).

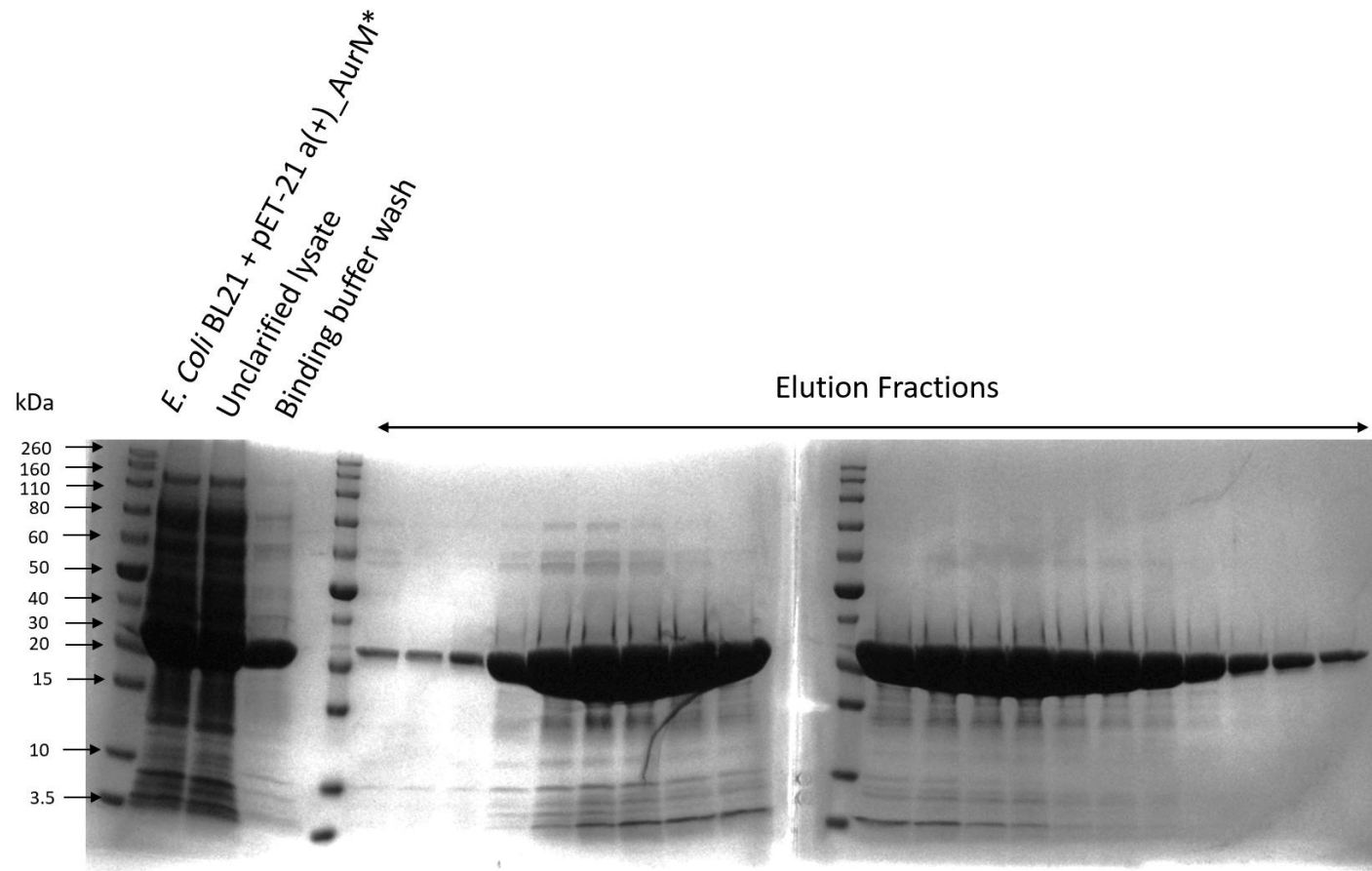


Figure 4.31: SDS PAGE of the Purification of AurM*. SDS-PAGE of the cell lysate loaded, the flow through, the wash, and elution fractions across the peak.

4.2.9 Investigating the enzymatic role of AurM* in aurodox biosynthesis

Based on an adapted version from McKean et al., (2019), methylation enzyme assays were carried out to test the function of AurM* as a SAM-dependant methyltransferase. The protocol, originally used to test C-Alkylation of SAM analogues, was adapted for use here, where the positive control in the original study used was SAM.

S-Adenosyl Methionine (32 mM) was added to an Eppendorf containing phosphate buffer (100 mM) alongside Kirromycin (1 mg/ mL), DTT (100 mM), BSA (1 mg/ mL) all final concentrations. Reactions were incubated using a Thermomixer at 37 °C for 1 h at 500 rpm before addition of AurM* (2.5 µg/ µL). Reactions were incubated for a further 24 h before analysis by LC-MS to analyse the methylation of kirromycin by AurM*. Based on the above reaction, control reactions were set up in parallel, which did not include either Kirromycin, SAM or AurM* to control for the effects of each active component (Table 4A). Volume was adjusted with phosphate buffer, or in the case of Kirromycin, substituted with DMSO.

Mass spectrometry analysis revealed no peaks present that corresponded to that of the aurodox standard (retention time 7.7, M/Z 793.4) in the 'complete reaction'. This indicates that during this reaction, aurodox was not created by the methylation of kirromycin by AurM* in response to the SAM present. As the reaction was unsuccessful, only the data for the 'complete reaction' is shown (Fig. 4.32)

Though it was thought that the reaction was unsuccessful, it was hypothesised that aurodox may have been produced but at too low of a concentration to be detectable amongst the other 'noisy' peaks that exist as part of the reaction (Fig. 4.32). To combat this, a second round of reactions was set up, this time with 10X excess of SAM and AurM* from the previous reaction set (Table 4B).

Similar to the previous reactions, mass spectrometry analysis revealed no peaks present that corresponded to that of the aurodox standard (retention time 7.7, M/Z

793.4; Fig. 4.33) in the 'complete reaction'. This suggests, again, that no kirromycin was converted to aurodox by AurM*.

Further optimisation of the enzymatic methylation assay for AurM* should be done to confirm its activity in the biosynthesis of Aurodox, given the wealth of evidence that exists to suggest the methylation of kirromycin.

Table 4A: AurM* Methyltransferase enzymatic assay reaction components.

Grey boxes indicate no addition of reagent.

Reagent	Aurodox STD	Kirromycin STD	Complete Reaction	No kirromycin	No SAM	No AurM*
Aurodox	x					
Kirromycin		x	x		x	x
SAM			x	x		x
AurM*			x	x	x	
DTT			x	x	x	x
Phos Buff + BSA	x	x	x	x	x	x

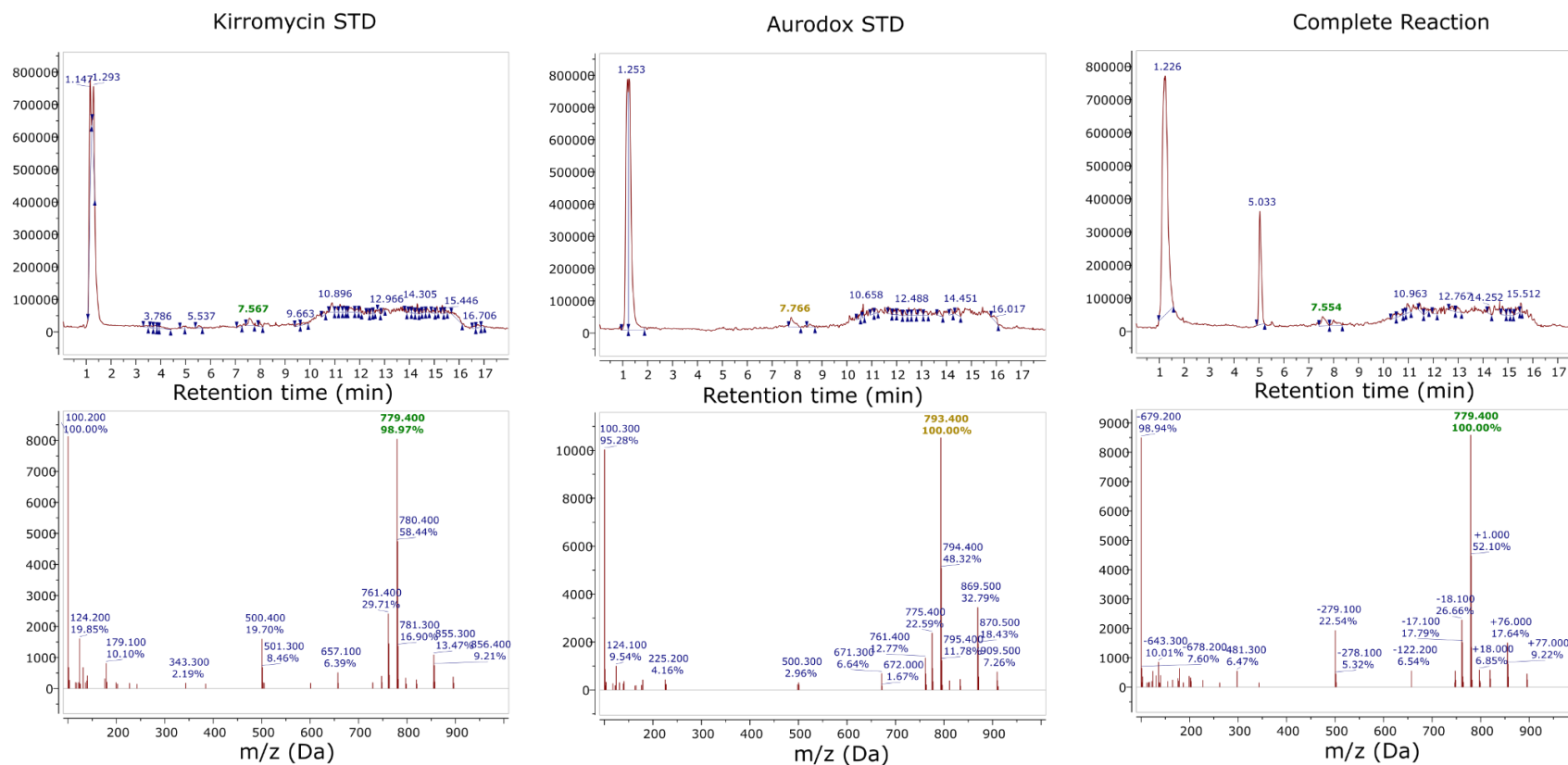


Figure 4.32: Total ion Chromatograms from HPLC indicate that kirromycin has not been converted to Aurodox by the SAM dependant methyltransferase, AurM^{*}. Reactions were prepared as methods (2.10.3). Aurodox and kirromycin standards were purchased from Hello Bio, diluted to 1 mg/ mL and have a retention time of approx. 7.7 and 7.5 minutes, and a corresponding M/Z ratio of 793.4 and 779.4, respectively.

Table 4A: AurM* Methyltransferase enzymatic assay reaction components**with 10x excess of SAM and AurM*.** Grey boxes indicate no addition of reagent.

Reagent	Aurodox STD	Kirromycin STD	Complete Reaction	No kirromycin	No SAM	No AurM*
Aurodox	x					
Kirromycin		x	x		x	X10
SAM			X10	X10		x
AurM*			X10	X10	X10	
DTT			x	x	x	x
Phos Buff + BSA	x	x	x	x	x	x

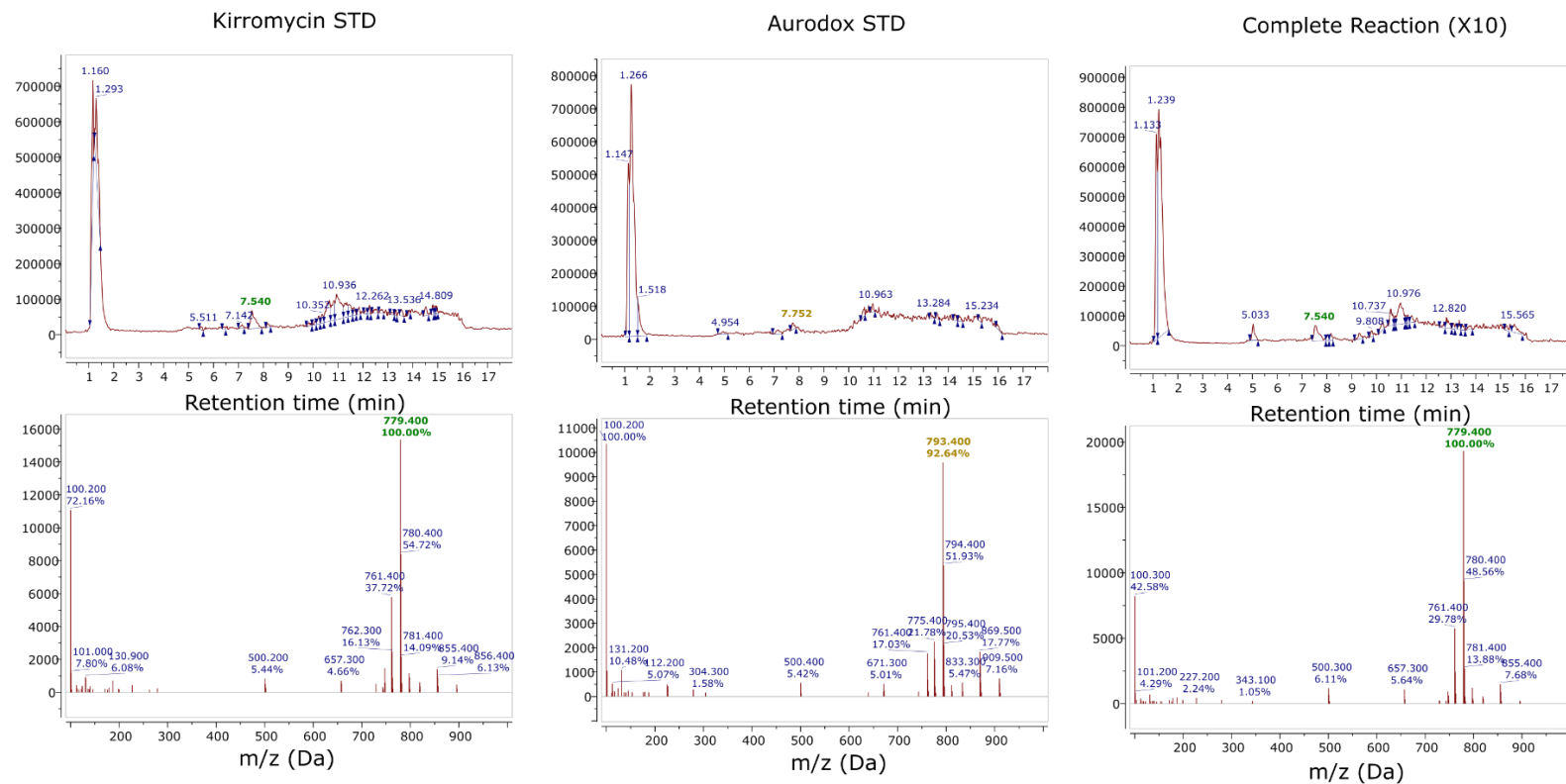


Figure 4.33: Total ion Chromatograms from HPLC indicate that kirromycin has not been converted to Aurodox by the SAM dependant methyltransferase, AurM*, even at a 10 fold excess of SAM and AurM*. Reactions were prepared as methods (2.10.3). Aurodox and kirromycin standards were purchased from Hello Bio, diluted to 1 mg/ mL and have a retention time of approx. 7.7 and 7.5 minutes, and a corresponding M/Z ratio of 793.4 and 779.4, respectively.

4.3 Summary

During this Chapter, the biosynthesis of aurodox was investigated by genetic manipulation of key genes within the aurodox BGC and, in parallel, biosynthetic enzyme assays were performed.

In order to do so, the phage artificial chromosome (PAC) containing the aurodox BGC, generated by Dr McHugh was sequenced using the Oxford Nanopore MinION, where the sequence of the aurodox PAC was then fully annotated based on the annotation of the aurodox BGC from McHugh et al., (2022; Fig. 4.2). The PAC was then validated as a suitable expression system for the biosynthesis of aurodox via a *Streptomyces coelicolor* M1152 heterologous host, where aurodox was shown to be produced in GYM media (Fig. 4.3).

Using the *Streptomyces* re-direct protocol, gene replacements were made on the pESAC-13A_AurI PAC in order to analyse the effect key genes on the aurodox BGC play within the biosynthesis of the aurodox molecule. Deletion of *aurAI*, the first PKS gene of the aurodox BGC, resulted in the loss of aurodox production, though bioactivity against the ESKAPE pathogens was still observed (Fig. 4.14). The same was seen for deletion of *aurHV* and *aurQ*, which encode hypothetical proteins and have no depicted functional homolog in other kirromycin-like elfamycin biosynthesis in the literature, though no bioactivity was observed (Fig. 4.14 & Fig. 4.13). The gene *aurB* was also investigated, encoding a non-ribosomal peptide synthase, KirB, which catalyses the incorporation of β -alanine in to the growing polyketide chain during kirromycin biosynthesis (Laiple et al., 2009; Weber et al., 2008) again, no bioactivity was observed against ESKAPE pathogens.

Finally, the methyltransferase AurM* was investigated by replacement of its gene *aurM**. The observation of bioactivity against the ESKAPE pathogens, coupled with a small amount of kirromycin detected in fermentation extracts of the heterologous

host following the deletion of *aurM**. Suggest that AurM* is responsible for the conversion of kirromycin to aurodox.

Using GFP reporter fusion assays, it was shown that both aurodox and kirromycin can both downregulate the T3SS of EHEC (Fig. 4.18). The same was observed for the derivatives AurAI_ Δ *aurM** and AurAI_ Δ *aurAI*, though to a lesser extent than kirromycin and aurodox, although this is likely a concentration effect as the fermentation extracts are dilute compared to the kirromycin and aurodox standards.

AurB, AurM* and AurQ were cloned into pET-21a(+) vectors for overexpression (Fig. 4.21). Unfortunately, cloning of AurHV was unsuccessful and so optimal expression of proteins was established for three proteins only. After testing a range of conditions, it was found that these proteins were expressed optimally during growth at 18 °C for 72 hours (Fig. 4.28). Therefore, these conditions were used to express and purify AurM* using IMAC for further analysis (Fig. 4.29, 4.30, 4.31). Unfortunately, enzymatic assays were unable to demonstrate AurM* could methylate authentic Kirromycin *in vitro* (Fig. 4.32 & Fig. 4.33), and so further optimisation of this assay should be done to confirm the role of AurM* in the methylation of kirromycin to aurodox.

**Chapter 5: Understanding the self-resistance
mechanisms adopted by kirromycin-like elfamycin
producers.**

5.1 Introduction

To facilitate the biosynthesis of natural products, it is common for the producing bacterial strain to possess resistance mechanisms inferring self-resistance to the producer from the natural product (Almabruk et al., 2018; Cundliffe, 1989). In many antibiotic natural products, these mechanisms of resistance are located within the associated BGC (Alanjary et al., 2017). This is true for the elfamycins, kirromycin, aurodox and factumycin, where a Major facilitator superfamily (MFS) transporter is encoded in the BGC (KirT/AurT/FacT respectively; See Chapter 3). The resistance encoded within the aurodox BGC was identified by McHugh *et al* (2021) but found only to confer partial resistance to aurodox. This was demonstrated through the use of the heterologous hosts, *S. coelicolor* M1152, *S. albus* and *S. venezuelae*. When the aurodox encoding PAC (pESAC-13A_AurI) was introduced into each of the strains, only *S. coelicolor* M1152 was capable of growth and aurodox biosynthesis, with *S. albus* and *S. venezuelae* exhibiting poor growth, which was attributed to incomplete resistance. It has been widely observed that multiple immunity genes are present at distinct genetic loci that also contribute to elfamycin resistance (Vijgenboom et al., 1994).

Elfamycin antibiotics are a group of structurally diverse compounds targeting, and preventing the normal function of Elongation Factor Thermo-unstable (EF-Tu) during the translation phase of protein synthesis (Parmeggiani and Nissen, 2006; Samantha M. Prezioso et al., 2017). Possessing GTPase activity, EF-Tu is a guanine nucleotide-binding protein (GTP binding protein) which is essential during the synthesis of proteins. In the case of kirromycin-like antibiotics such as kirromycin and aurodox, translation is blocked as the compound forms a complex with EF-Tu and GDP, blocking GTP hydrolysis. This binding facilitates an irreversible conformational change in EF-Tu resulting in it binding to the ribosome, unable to detach, preventing

subsequent peptide bond formation and protein synthesis (Parmeggiani and Swart, 1985; Vogeley et al., 2001; Wolf et al., 1974).

The elfamycin target, Ef-Tu, is encoded by the *tuf* gene in bacteria (Sela et al., 1989). As EF-Tu has an essential function in protein synthesis, both the nucleotide sequence identity and the genomic location of the *tuf* gene are conserved between taxa (Lathe et al., 2000). Given EF-Tu performs an essential cellular function, the requirement for self-resistance to elfamycins in producing organisms has likely resulted in the evolution of elfamycin-resistant copies EF-Tu in these strains (Cappellano et al., 1997; Thaker et al., 2012; Yarlagadda et al., 2020). Elfamycin resistant copies of EF-Tu within the genomes of kirromycin-like antibiotic producers often exhibit amino acid changes located at contact sites between the protein and the antibiotic (Mesters et al., 1994; Vogeley et al., 2001). A common amino acid change that is found is the A375T/S, where the basic polar amino acid arginine (A) is converted to a nonpolar threonine (T) at position 375 of the EF-Tu sequence, commonly within the EGLRF(A/T)IREGGR motif. This has been found to confer resistance to kirromycin and is the most common amino acid variant observed within *Streptomyces* species (Cappellano et al., 1997; Mesters et al., 1994; Vijgenboom et al., 1994).

It was hypothesised that kirromycin-like producing elfamycins would harbour a combination of mechanisms to enable self-resistance, given that expression of aurodox in some strains limited growth (McHugh et al., 2020) suggesting BGC derived resistance was insufficient for producing strains. The discovery and exploitation of this could lead to a greater understanding of the resistance mechanism possessed by kirromycin-like elfamycin producers, facilitating further elfamycin production from parental or heterologous strains and a greater understanding of how evolution of kirromycin-like antibiotics may arise.

5.2 Results

5.2.1 Analysis of EF-Tu copy number and phylogeny in kirromycin-like elfamycin producing strains

In many proteobacterial species the *tuf* gene is duplicated, with both *Salmonella typhimurium* and *Escherichia coli*, duplicate *tuf* genes being nearly identical in nucleotide sequence (Kawashima et al., 1996; van der Meide et al., 1983). Evidence also shows that either of the *tuf* genes may be deleted without effect on the viability of the cell (Hughes, 1990; Zuurmond et al., 1999). This duplication has been differentially lost and maintained in a number of bacterial genomes, and in the case of *Streptomyces*, which are common antibiotic producers, multiple copies of *tuf* genes can be found within their genomes encoding EF-Tu (Lathe and Bork, 2001; Vijgenboom et al., 1994). To investigate the resistance mechanisms possessed by kirromycin-like elfamycin producers, the EF-Tu genes possessed by *Streptomyces* strains which are known producers of elfamycins were investigated. Known elfamycin producing strains identified from Chapter 3 of this thesis were included in the analysis if a genome sequence, or their sequences of EF-Tu were available in the literature, where kirromycin-like elfamycins are shown in red. Additionally, the EF-Tu from the four potential kirromycin-like elfamycin producers of also *A. magusensis*, *A. cihanbeyliensis* and *M. rubida*, *Saccharopolyspora* sp. NFXS83 identified during FlaGs analysis in Chapter 3 were also included.

EF-Tu copy number was determined for each strain, where EF-Tu1 (kirromycin sensitive) and EF-Tu3 (kirromycin resistant) from *S. ramocissimus* were used as query sequences to BLAST against genomes. These sequences were used as their resistance/sensitive traits have been well documented (Olsthoorn-Tieleman et al., 2007, 2002). Additionally, their genomes were mined using AntiSMASH (version 6.0)

for identification of any BGCs predicted to encode antibiotics that are known to target translation.

It can be observed that most strains carry a copy of EF-Tu1, the kirromycin sensitive EF-Tu, regardless of whether they encode translation inhibitors or not (Table 5A). This is true for all strains, except for *S. ISL094*, which was not predicted to encode EF-Tu1. This was put down to the sequence quality of the genome being highly fragmented due to its metagenomic assembly (Fig. 3.25), where it is likely that the sequence of EF-Tu1 may be incomplete.

S. goldiniensis, *S. collinus* and *S. ramocissimus* were found to encode both EF-Tu1 (sensitive) and EF-Tu2 (resistant), where *S. ramocissimus* was found to encode two copies of EF-Tu1 (termed EF-Tu2) whose function is unknown (Olsthoorn-Tieleman et al., 2007, 2002). From the strains which were predicted to encode other antibiotics targeting translation (not kirromycin-like elfamycins), all possess a resistant copy of EF-Tu, similar to EF-Tu3, suggesting that having the resistant copy aids in conferring resistance to the strain.

When phylogeny of these distinct sensitive and resistant EF-Tu types was analysed, it was observed that the genome of *Saccharopolyspora* strain of NFXS83, which also possesses a putative kirromycin-like elfamycin BGC, contained one copy of a gene encoding EF-Tu which is distant from the others identified and was therefore used as an outgroup for this analysis (purple, Fig. 5.1).

Initial analysis of the phylogeny reveals two distinct branches of the tree (Fig. 5.1), where one group of EF-Tu sequences is better conserved than the other. The *Micromonospora* and *Amycolatopsis* are found to clade together (orange branch and cyan branch respectively), compared to the other species on the tree.

Streptomyces ramocissimus possesses three copies of genes encoding EF-Tu. The resistance of these encoded proteins to elfamycins is well understood with EF-Tu1 and EF-Tu2 being sensitive and EF-Tu3 being resistant. Analysis revealed the three

copies of EF-Tu to appear distant from each other on the tree (Fig. 5.1, blue). It was observed that EF-Tu1, previously shown to be kirromycin sensitive, appeared in the lower major clade of EF-Tu (Fig. 5.1, bottom half of the tree). *Tuf2* was also found on this lower clade and is also kirromycin sensitive, though, it was found to not for a clade with EF-Tu from any kirromycin-like elfamycin producers. The cryptic nature of the functional role of Tuf2 was noted by Olsthoorn-Tieleman and co-workers (2002), however the short branch length of the lower clade suggests that these proteins are constrained in their evolution suggesting their major role may be in protein synthesis. Moreover, Tuf2 is found on a sub-clade from the Tuf protein which may suggest that the genes encoding these two EF-Tu proteins has expanded either through gene duplication or horizontal gene transfer. In contrast, EF-Tu3 was found to reside on the top half of the phylogenetic tree, alongside the EF-Tu from the elfamycin BGC possessing strains of *S. collinus* (green) *S. ISL-94* strain (red), *S. goldiniensis* (gold) and *S. coelicolor* (pink), which does not produce an elfamycin. Given EF-Tu3 from *S. ramocissimus* is kirromycin resistant, this could indicate that those present in the top clade of the phylogenetic tree may also be resistant (Olsthoorn-Tieleman et al., 2007). The length of the branches in the top clade are also longer, suggesting that there is more divergence in these sequences than in the lower clade, and this may reflect diversification in response to elfamycin selection.

In the case of *Streptomyces collinus*, both EF-Tu proteins are found alongside other kirromycin-resistant EF-Tu such as from *S. ramocissimus*. Interestingly, even though it is a kirromycin producer and the EF-Tu have the resistant genotype, the EF-Tu in this organism do not confer resistance to kirromycin alone. This suggests that additional resistance mechanisms are required such as the Major facilitator superfamily transporter encoded by *kirT* (Robertsen et al., 2018).

Table 5A: EF-Tu copy number of select strains and whether BGCs are predicted to encode the biosynthesis of antibiotics

targeting translation. EF-Tu copy number via NCBI BLAST against the strain's genome with EF-Tu1 and EF-Tu3 from *S. ramocissimus*.

Genomes were ran through AntiSMASH (version 6.0) using strict parameters to identify BGCs. Kirromycin-like elfamycins in red.

	Species name	Tuf1	Tuf3	Encoding a translation inhibitor?
Kirromycin-like elfamycin producers	<i>Streptomyces goldiniensis</i>	1	1	Aurodox
	<i>Streptomyces collinus</i>	1	1	Kirromycin
	<i>Streptomyces ramocissimus</i>	2	1	Kirromycin
	<i>Kitasatospora setae</i> KM-6054	1		Factumycin
	<i>Streptomyces</i> sp. WAC05292	1	1	Factumycin
	<i>Streptantibioticus cattleya</i> NRRL 8057	2		L-681,217
	<i>Planobispora rosea</i>	1	1	GE2770A
	<i>Streptomyces mobaraense</i>	1		Pulvomycin
	<i>Streptomyces netropsis</i>	1		Pulvomycin
	<i>Streptomyces sulphureus</i>	1		Phenelfamycins A and B
	<i>Streptomyces violaceusniger</i>	1		Phenelfamycins A - F
	<i>Streptomyces albospinus</i>	1	1	Phenelfamycins G and H
Potential kirromycin-like elfamycin producers identified in Chapter 3	<i>Streptomyces</i> sp. ISL-094		1	Kirromycin-like BGC
	<i>Amycolatopsis magusensis</i>	1		Kirromycin-like BGC
	<i>Amycolatopsis cihanbeyliensis</i>	1		Kirromycin-like BGC
	<i>Micromonospora rubida</i>	1		Kirromycin-like BGC
	<i>Saccharopolyspora</i> sp. NFXS83	1		Kirromycin-like BGC
Other <i>Streptomyces</i> strains	<i>Streptomyces coelicolor</i> A3(2)	1	1	-
	<i>Streptomyces griseus</i>	1	1	Streptomycin (aminoglycoside)
	<i>Streptomyces fradiae</i>	1	1	Neomycin (aminoglycoside)
	<i>Streptomces rimosus</i>	1	1	Oxytetracycline (tetracycline)
	<i>Streptomyces lividans</i>	1	1	-
	<i>Streptomyces albus</i>	1		-
	<i>Streptomyces venezuelae</i>	1	1	chloramphenicol
	<i>Streptomyces avermitilis</i>	1	1	-
	<i>Streptomyces clavuligerus</i>	1	1	-

Figure 5.1: Phylogenetic analysis of Elongation Factor Thermo-unstable amino acid sequences from kirromycin-like elfamycin producing *Streptomyces* species and their most similar sequences. Evolutionary history was conferred using EF-Tu sequences obtained from the genomes of *Streptomyces* using NCBI BLAST and aligned using MEGA software and used to form a maximum likelihood tree with 500 bootstraps, utilising the JTT matrix-based model. The analysis involved 205 amino acid sequences, where all positions containing gaps and missing data were eliminated.

5.2.2 Predicting the structure of EF-Tu1-3 (*tuf1-3*) from *S. ramocissimus*.

Possessing three different copies of EF-Tu encoding genes, *tuf1-3*, the nature of the function of each of these EF-Tu proteins in *S. ramocissimus* has been explored. During the study by Vijgenboom et al., 1994, only Tuf1 yielded large enough quantities during protein expression to be analysed (Vijgenboom et al., 1994). This standard Tuf1 shared 71% amino acid similarity to EF-TU from *E. coli*, is constitutively expressed and activity is inhibited by kirromycin. During exponential growth, it was shown that EF-Tu3 is produced in minor quantities in *S. ramocissimus*, where this version of EF-Tu shared 65% amino acid similarity to EF-Tu1. EF-Tu3 is resistant to kirromycin, among other classes of EF-Tu-targeted antibiotics, including pulvomycin and GE2270A (Olsthorn-Tieleman et al., 2007). Though this resistance seemed explanatory for kirromycin resistance, coupled with the findings that a homolog of KirT, the Major Facilitator Superfamily transporter was present in the BGC of *S. ramocissimus* kirromycin in this study, it was found that the induction of *tuf3* does not correlate with biosynthesis of kirromycin in this strain, which occurs during stationary phase of growth (Olsthorn-Tieleman et al., 2007; Vijgenboom et al., 1994). While the presence of EF-Tu3 in *S. ramocissimus* would explain how resistance to elfamycins is conferred, the true mechanism is yet to be determined experimentally.

The structure of the three EF-Tu proteins from *S. ramocissimus* were modelled using AlphaFold software (Fig. 5.2). Once aligned, and the structures were overlaid, enabling some insight into protein structure function to be inferred from the 3D predicted models. As EF-Tu is essential to cellular function, the general structure of the proteins is well conserved among the three copies. This was as expected as structural changes of EF-Tu could have deleterious effects on the cell. EF-Tu, EF-Tu2 and EF-Tu3 are similar in structure to one another (Magenta, purple, and green, respectively; Fig. 5.2). When EF-Tu1 and EF-Tu2 are compared, the root mean

square deviation (RMSD) value is 0.56, indicating a minimal level of deviation from aligned pairs of backbone c-alpha atoms between the two structures. When EF-Tu1 and EF-Tu3 are compared, the RMSD value is 0.89 indicating a higher degree of structural variance when compared to EF-Tu1 and EF-Tu2, though still small. Similarly, the TM-score of EF-Tu1 vs EF-Tu2 is higher than EF-Tu1 vs EF-Tu3, at 0.99 and 0.97 respectively, where the TM-score ranges between 0 and 1, with 1 indicating a perfect match and 0 is no match between the two structures. This similarity in structure is likely due to the highly conserved nature of the protein but the slight changes in EF-Tu3 from 1 and 2 support the data from phylogenetic analysis and the RMSD/Tm scores could be result of the difference in amino acid chain length possessed by EF-Tu3 VS EF-Tu1 and 2 (389 vs 397) with EF-Tu3.

The structural variance of EF-Tu3 from *S. ramocissimus* and its kirromycin-resistant phenotype, not possessed by the other two EF-Tu proteins produced by *S. ramocissimus*, suggest it may have an alternative role within *S. ramocissimus*. EF-Tu has been found to possess several moonlighting functions. This means that not only does it have its well documented role as an Elongation Factor, it has also been found involved in many other independent cellular processes such as regulation of cellular shape, adhesion and invasion (Widjaja et al., 2017).

Further work is required to decipher the exact nature of each EF-Tu in *S. ramocissimus*.

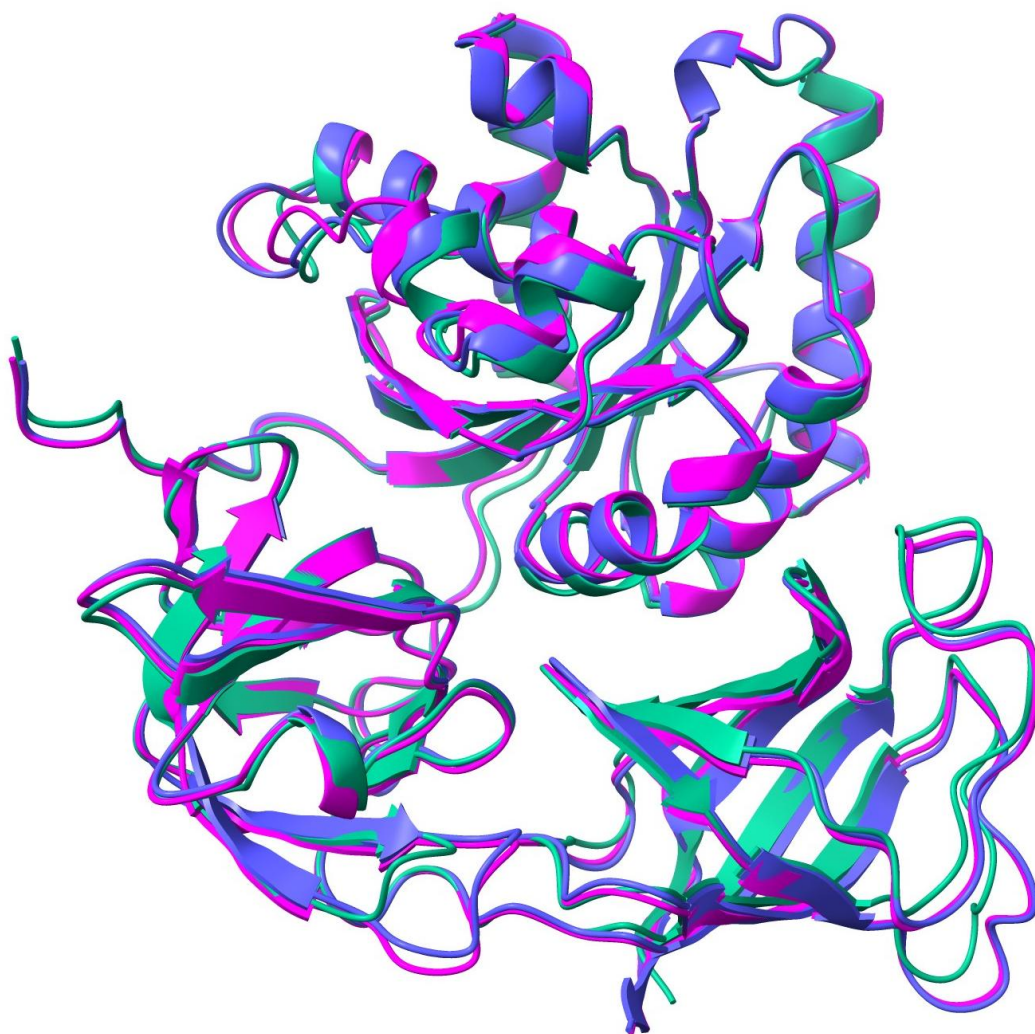


Figure 5.2: The predicted tertiary protein structure of Elongation Factor Thermo unstable 1-3 from *Streptomyces ramocissimus* Are highly conserved . EF-Tu1 in magenta, EF-Tu2 in Purple and EF-Tu3 in green. Structures generated on AlphaFold (accessible at https://colab.research.google.com/github/sokrypton/ColabFold/blob/main/beta/AlphaFold2_advanced.ipynb#scrollTo=Riekgf0KQv_3). Five iterations of protein structure were run for maximum accuracy and structure consensus. Output PDB files were viewed on RCSB PDB-Structure Pairwise Alignment Tool, where they were overlaid and aligned (accessible at <https://www.rcsb.org/alignment>). Images were then edited on ChimeraX software (version 1.6.1).

5.2.3 Predicting the structure of EF-Tu2 (*tuf2*) from *S. goldiniensis*.

Streptomyces goldiniensis, the producer of the kirromycin-like antibiotic aurodox, has two EF-Tu genes, EF-Tu1 and EF-Tu2. Where EF-Tu2 from *S. goldiniensis* was found encoded for by a gene (*tuf2*) located approximately 20 kb upstream of the aurodox supercluster in the genome. It was proposed that this EF-Tu2 aids in the resistance of *S. goldiniensis* during the production of aurodox (McHugh, 2020). From phylogenetic analysis (Fig. 5.1), EF-Tu2 is found alongside a known-resistant EF-Tu3 from *S. ramocissimus*, indicating further the split of the phylogeny between the elfamycin resistant and sensitive EF-Tu, suggesting that EF-Tu2 is kirromycin resistant and may help confer resistance during aurodox production.

Work by McHugh (2020) has shown that *tuf2* plays a role in the internal self-resistance mechanism adopted by *S. goldiniensis* to protect the organism against the effects of the production of aurodox (McHugh, 2020). This was exemplified by the fact heterologous expression of aurodox in heterologous strains such as *Streptomyces venezuelae* and *Streptomyces collinus* was not possible without the expression of *tuf2* from *S. goldiniensis* in the novel hosts.

Several hypotheses exist for the essential role of *tuf2* in aurodox production, the first was that there is specificity within the *tuf2* sequence which is required to confer aurodox resistance, however it is still thought to be possible that changes in amino acids in other regions of EF-Tu may influence sensitivity to aurodox (Berchtold et al., 1993; Cappellano et al., 1997; Glockner and Wolf, 1984; Vijgenboom et al., 1994; Vogeley et al., 2001). The presence of multiple copies of EF-Tu in producing *Streptomyces* strains would support this hypothesis along and that potentially there is a fitness cost to having a single EF-TU copy that is elfamycin resistant. An alternative hypothesis is that the number of copies of EF-Tu could influence aurodox sensitivity, this hypothesis will be tested here.

The tertiary structure of EF-Tu2 from *S. goldiniensis* was also modelled using AlphaFold software, this time modelled against EF-TU from *Thermus thermophilus* HB8 (PDB – 1EXM)(Hogg et al., 2002). Modelling EF-Tu2 from *S. goldiniensis* against the EF-Tu from *Thermus thermophilus* can be justified as the crystal structure is of high resolution due to the thermophilic nature of the strain (Oshima and Imahori, 1974). Having a model EF-Tu is beneficial for this analysis as it can allow an assessment of the accuracy of the AlphaFold predicted structure of EF-Tu2 from *S. goldiniensis*, when compared to the crystal structure of EF-Tu from *Thermus thermophilus*.

As EF-Tu is one of the most conserved proteins in cellular life, it is unsurprising that the structure of EF-Tu from *S. goldiniensis* was predicted to be similar to that of the EF-Tu in *Thermus thermophilus* (Fig. 5.3). For both proteins, domain one is composed of parallel six-stranded β -sheet surrounded by α -helices, where GDP is bound. Domains two and three are comprised of β -barrels of seven and six antiparallel β -strands, respectively, that share an extended interface. The arrangement of these three domains is well-conserved within EF-Tu, where domains two and three are positioned below relative to domain one.

When compared, the RMSD value for comparison of deviation from aligned pairs of backbone c-alpha atoms between the two structures was high of 2.31. However, the Template modelling (TM) score was 0.88, with 1 indicating a perfect match and 0 is no match between the two structures. This indicates that the proteins have the same fold (classified by SCOP/CATH; Xu and Zhang, 2010; Zhang and Skolnick, 2005).

This analysis has allowed preliminary elucidation of the structure of EF-Tu2 from *Streptomyces goldiniensis*, and further analysis will be done on the effect on production and/ or resistance to aurodox in aurodox producing strains.



Figure 5.3: Predicted structure of EF-Tu2 from *Streptomyces goldiniensis* is also well conserved among other EF-Tus. In comparison to the well elucidated crystal structure of Elongation Factor Thermo-unstable from *Thermus thermophilus* HB8. PDB - 1EXM;(Hogg et al., 2002) EF-Tu from *Thermus thermophilus* is shown in blue, EF-Tu2 from *S. goldiniensis* is in gold. Structures were generated on AlphaFold (accessible at https://colab.research.google.com/github/sokrypton/ColabFold/blob/main/beta/AlphaFold2_advanced.ipynb#scrollTo=Riekgf0KQv_3). Five iterations of protein structure were run for maximum accuracy and structure consensus. Output PDB files were viewed on RCSB PDB-Structure Pairwise Alignment Tool, where they were overlayed and aligned (accessible at <https://www.rcsb.org/alignment>). Images were then edited on ChimeraX software (version 1.6.1).

5.2.4 EF-Tu2 increases resistance to aurodox and increases aurodox production in the heterologous host *S. coelicolor* M1152 + pESAC-13A_AurI

To understand the role of *tuf2* from *S. goldiniensis* in aurodox resistance, existing strains were utilised. All strains are shown (red) and all possible combinations of plating (Fig. 5.4). A cloned copy of *tuf2* from *S. goldiniensis* on the integrating vector, pMS82 (*hygR*, ϕ BT integrase), which was introduced alongside the aurodox BGC containing pESAC-13A_AurI in *S. coelicolor* M1152. Empty vector strains containing either pESAC-13A, pMS82 and both respectively, were also generated to as controls. When these strains are cultured on agar adjacent to one another, several interactions can be observed, particularly between those which contain the aurodox producing pESAC-13A_AurI and those which do not (Fig. 5.4). Culturing strains adjacently allows for phenotypic analysis of the different variants against the parental strain. In *S. coelicolor* M1152, it is apparent that the growth of + pMS82_*tuf2* strain, which possesses an extra copy of *tuf2*, is inhibited when grown in proximity to the strain containing the aurodox BGC alone (pESAC-13A_AurI) and the strain containing an additional copy of *tuf2* and the aurodox BGC (+ pESAC-13A_AurI + pMS82_*tuf2*). In the strain containing the empty pESAC-13A vector, sporulation is inhibited compared to strain containing the aurodox BGC alone (pESAC13-A_AurI). This suggests that integration of the aurodox BGC alone provides a competitive advantage over not possessing. The same is observed in the + pESAC-13A_AurI + pMS82_*tuf2* strain where it appears to limit the transition of aerial hyphae to mature spores in *S. coelicolor* + pMS82_*tuf2*, when grown adjacently. This suggests that both the aurodox BGC and *tuf2* are required for full resistance and aurodox production.

With + pESAC13-A_AurI + pMS82_*tuf2* strain showing greater inhibition of sporulation in the associated controls than that of the train with the aurodox cluster

alone, it was hypothesised that possessing EF-Tu2 may increase production of aurodox in the *S. coelicolor* M1152 heterologous host.

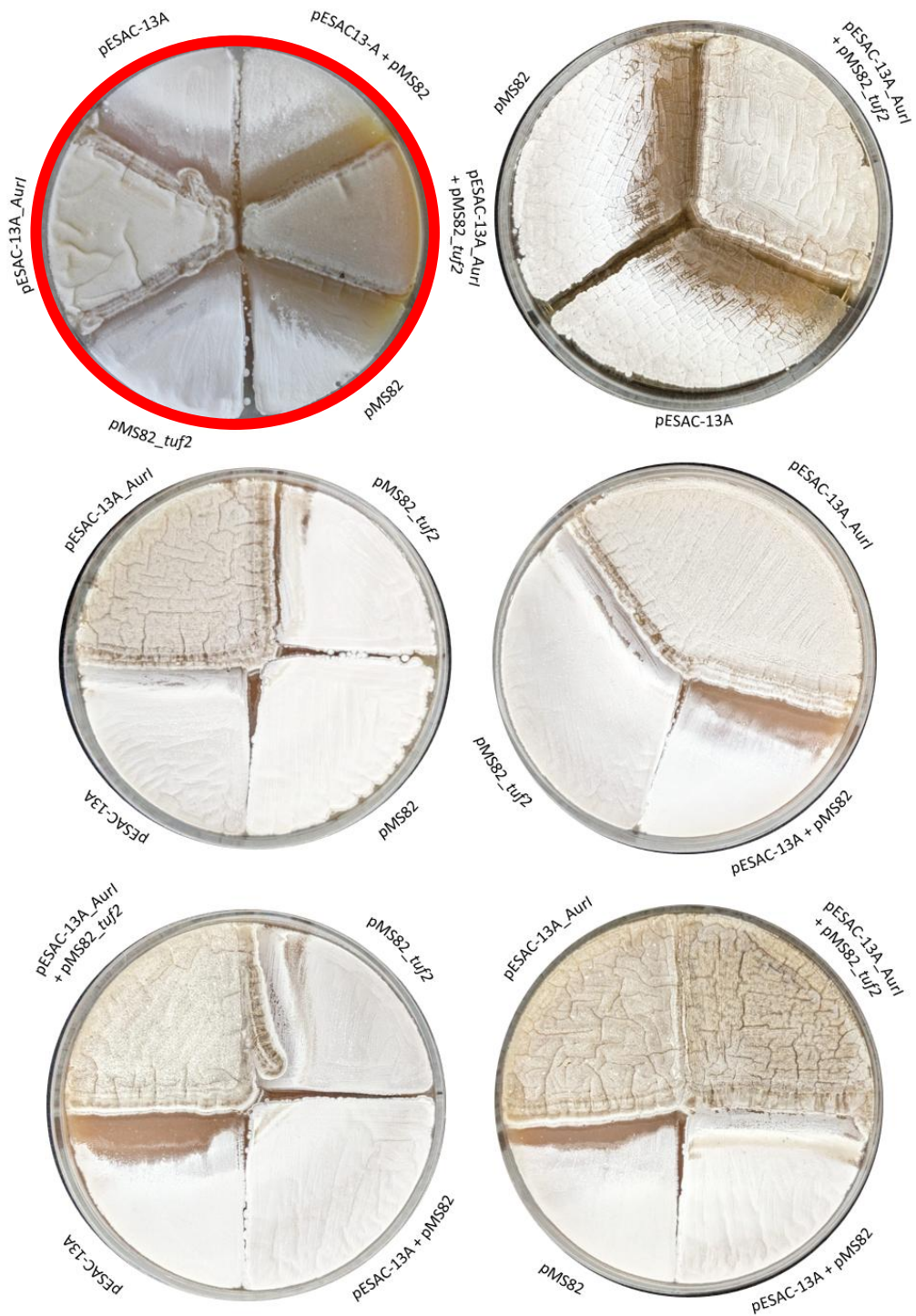


Figure 5.4: *S. coelicolor* M1152 + pESAC-13A_AurI + pMS82_tuf2 appears to produce more aurodox, inhibiting the growth of its singular integration and empty vector controls. Strains were plated in all possible conformations. Strains were cultured for 7 days at 30 °C on MS agar.

The role of *tuf2* in aurodox resistance was explored further by assessing the bioactivity of the heterologous host expressing the aurodox cluster, with and without the addition of *tuf2* expression and the associated empty vector controls, against the ESKAPE pathogens. Agar plug bioassays were undertaken against all ESKAPE pathogens and zones of inhibition were measured in mm with a ruler (Fig. 5.5 & Fig. 5.6). The zone of inhibition produced by *S. coelicolor* M1152 + pESAC-13A_AurI + PMS82_*tuf2* was larger than that produced by *S. coelicolor* M1152 + pESAC-13A-AurI against *S. aureus* ($p=0.003$, Fig. 5.5) and *K. pneumoniae* ($p=0.007$, Fig. 5.6). There was no bioactivity found in the empty vector control for the aurodox cluster, *S. coelicolor* M1152 + pESAC-13A, or the empty vector control, *S. coelicolor* M1152 + pESAC-13A + pMS82. Therefore, the addition of an extra copy of *tuf2* to an aurodox producing strain results in larger zones of inhibition than those without, suggesting an increase in aurodox production. Not only were the zones of inhibition larger for the strains carrying an extra copy of *tuf2*, the zones were also hazier. This could indicate that the indicator strains growth is not as effectively inhibited and a different mechanism, other than bactericidal activity has occurred.

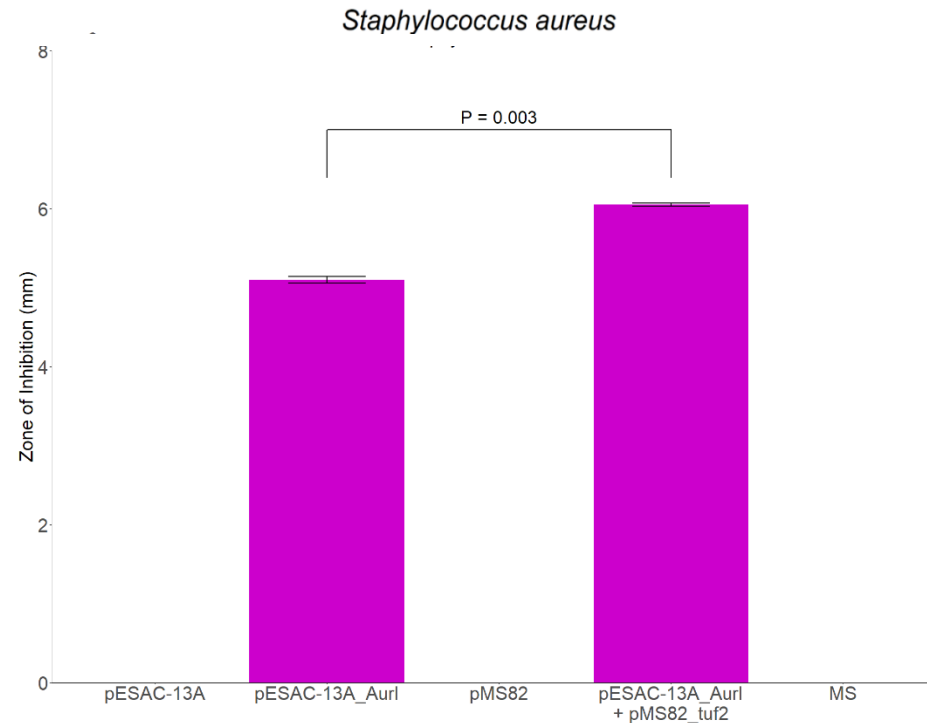


Figure 5.5: An assessment of bioactivity heterologous expression strains supplemented with EF-Tu2 against *Staphylococcus aureus*, where greater bioactivity is observed in strains supplemented with *Tuf2*. Statistical analysis of the data through the use of a two-sample t-test. Error bars show the standard deviation from the mean of zones of inhibition. Agar plugs of strains were harvested after being grown on MS agar after 7 days growth (30 °C) and were plated on indicator strains, *Staphylococcus aureus* ATCC 43300, which was normalised to an OD₆₀₀ of 0.01 in soft nutrient agar. Assay plates were grown for 12 hours at 37°C and zones of inhibition were measured in mm with a ruler

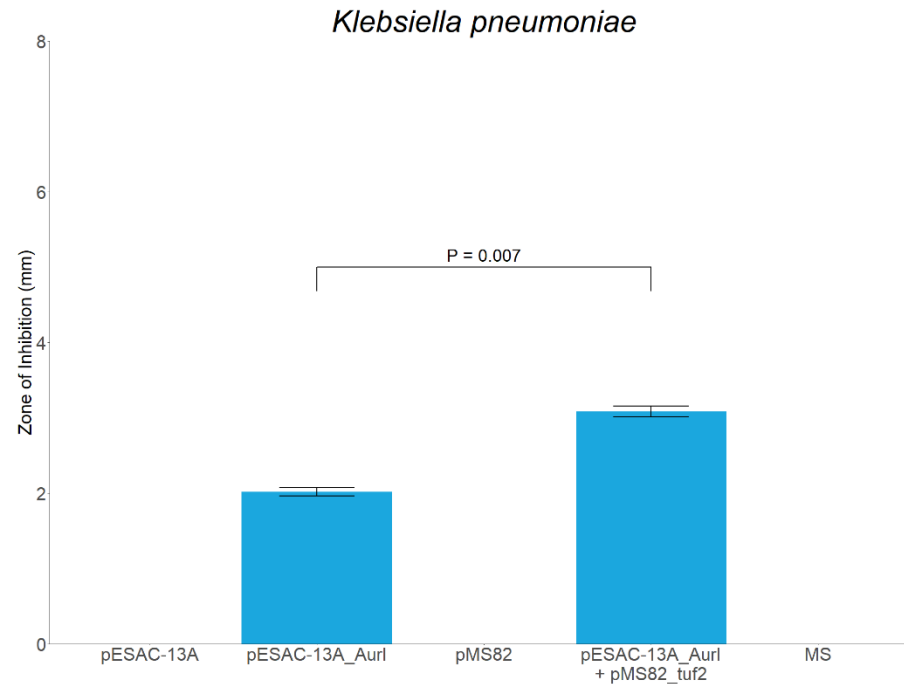


Figure 5.6: An assessment of bioactivity heterologous expression strains supplemented with EF-Tu2 against *Klebsiella pneumoniae*, where greater bioactivity is observed in strains supplemented with *Tuf2*. Statistical analysis of the data through the use of a two-sample t-test. Error bars show standard deviation from the mean of zones of inhibition Agar plugs of strains were harvested after being grown on MS agar after 7 days growth (30 °C) and were plated on indicator strains, *Klebsiella pneumoniae* ATCC 700603, which was normalised to an OD₆₀₀ of 0.01 in soft nutrient agar. Assay plates were grown for 12 hours at 37°C and zones of inhibition were measured in mm with a ruler

5.3 Summary

This Chapter sought to understand the self-resistance mechanisms in kirromycin-like elfamycin producers. One mechanism of resistance is to have additional elfamycin resistant copies of EF-Tu (Prezioso et al., 2017). EF-Tu copy number was established for *Streptomyces* strains who are known producers of elfamycins, and those which are not, in order to assess if there is a relationship between the number of *tuf* genes harboured by *Streptomyces* and whether this is related to encoding the production of antibiotics that affect translation. We established that majority of strains harbour the kirromycin sensitive EF-Tu1, where some strains encoding the production of antibiotics that affect translation possess the kirromycin resistant EF-Tu3. The phylogeny of these EF-Tu were analysed and EF-Tu1 sequences were found to be much closer on the phylogenetic tree with branch lengths suggesting that the protein are more conserved across the genera. In contrast, the elfamycin resistant EF-Tu were found to be much more divergent and phylogenetically distinct from the EF-Tu1 (Fig. 5.1).

As *S. ramocissimus* possesses genes encoding three EF-Tu proteins. We hypothesised that these proteins may be key in understanding the role of each EF-Tu during kirromycin biosynthesis and self-resistance. The protein sequence was modelled using AlphaFold software (Fig. 5.2), with the two copies of kirromycin sensitive EF-Tu being most more similar than the resistant EF-Tu. The same was done for EF-Tu1 and EF-Tu2 from *S. goldiniensis*, where EF-Tu is kirromycin resistant (Fig. 5.4).

Using gifted strains from Dr McHugh, bioactivity screening showed that expression of EF-Tu2 (resistant) within the *S. coelicolor* M1152 + pESAC-13A_Aurl heterologous host results in increased production of aurodox (Fig. 5.5 & Fig. 5.6).

**Chapter 6: Investigating the role of EF-Tu in Type III
Secretion by Enterohemorrhagic *Escherichia coli*.**

6.1 Introduction

EF-Tu has been found to possess several moonlighting functions. This means that not only does it have its well documented role as an Elongation Factor, it has also been found involved in many other independent cellular processes such as stimulating host immune responses and interacting with immune regulators to increase pathogenesis (Widjaja et al., 2017). Given that the T3SS span the periplasm and the inner and outer membrane of Gram-negative bacteria, the discovery of EF-Tu possessing moonlighting function on the cell surface of another Gram-negative organism is intriguing, where in *Mycoplasma pneumoniae* EF-Tu was found to act as a fibronectin-binding protein (Dallo et al., 2002).

Since this discovery, many roles have been discovered for EF-Tu on the surface of cells, where EF-Tu has been identified in the bacterial secretome. In 2019, a review of the diverse role of EF-Tu and its many moonlighting functions was executed, where the literature was evaluated for evidence of EF-Tu presence in non-cytoplasmic locations (Harvey et al., 2019). This work found many examples of EF-Tu present in the surface and secretome of many bacterial species including *E. coli* (Table 6A). These findings were supported by Torres et al, (2020) who identified the presence of EF-Tu in outer membrane protein extracts and culture supernatants of shiga toxin producing *E. coli* O157:H7 (STEC, Fig. 6.1) This discovery was coupled with immunogold electron microscopy showing detection of EF-Tu on the surface of STEC (Torres et al., 2020). Though no specific role was elucidated for EF-Tu in this study, EF-Tu was identified in outer membrane vesicles (OMVs), suggesting it as a possible export mechanism for this protein.

With EF-Tu localising on the outer membrane of EHEC, similar to the positioning of the T3SS, and function and expression of both affected by aurodox and kirromycin,

we hypothesise that there may be a link between the T3SS of EHEC and EF-Tu, which has never previously been demonstrated.

Table 6A: Literature reporting the identification of bacterial EF-Tu in non-cytoplasmic locations. Adapted from Harvey et al., (2019).

Species	Surface Exposed†	Secretome	Immunoproteome
<i>Actinobacillus seminis</i>	Montes-García et al., 2018		
<i>Arsukibacterium ikkense</i>		Lylloff et al., 2016	
<i>Bacillus anthracis</i>		Kim et al., 2014	
<i>Bacillus cereus</i>	Clair et al., 2013; Laouami et al., 2014; Voros et al., 2014; Madeira et al., 2015; Omer et al., 2015		
<i>Bacteroides fragilis</i>	Wilson et al., 2015	Wilson et al., 2015	
<i>Borrelia burgdorferi</i>			Carrasco et al., 2015
<i>Brucella abortus</i>		Jain et al., 2014	
<i>Burkholderia pseudomallei</i>		Burnick et al., 2014; Schwarz et al., 2014	
<i>Caulobacter crescentus</i>	Cao and Bazemore-Walker, 2014		
<i>Cellulomonas fimi</i>		Wakarchuk et al., 2016	
<i>Cellulomonas flavigena</i>		Wakarchuk et al., 2016	
<i>Desulfotomaculum reducens</i>		Dalla Vecchia et al., 2014	
<i>Enterococcus faecalis</i>	Sinnige et al., 2015	Arntzen et al., 2015	
<i>Escherichia coli</i>		Boysen et al., 2015	Kudva et al., 2015
<i>Gallibacterium anatis</i>		López-Ochoa et al., 2017	
<i>Haemophilus influenzae</i>		Thofte et al., 2018	
<i>Helicobacter pylori</i>		Chiu et al., 2016	Snider et al., 2016
<i>Klebsiella pneumonia</i>			Liu et al., 2014
<i>Lactobacillus rhamnosus</i>			Espino et al., 2015
<i>Leptospira biflexa</i>		Wolff et al., 2013; Stewart et al., 2015	
<i>Leptospira borgpetersenii</i>		Wolff et al., 2013	Eshghi et al., 2015
<i>Leptospira interrogans</i>		Wolff et al., 2013	
<i>Leptospira kirschneri</i>		Wolff et al., 2013	
<i>Leptospira noguchii</i>		Wolff et al., 2013	
<i>Leptospira santarosai</i>		Wolff et al., 2013	
<i>Listeria monocytogenes</i>		Tiong et al., 2015	
<i>Mycobacterium avium</i> subsp. <i>paratuberculosis</i>		Rychli et al., 2016; Viale et al., 2014	
<i>Mycobacterium tuberculosis</i>		Viale et al., 2014	
<i>Mycoplasma hyopneumoniae</i>	Tacchi et al., 2016		
<i>Mycoplasma pneumoniae</i>	Yu et al., 2018		
<i>Mycoplasma mycoides</i> subsp. <i>capri</i>	Widjaja et al., 2017		
<i>Neisseria meningitidis</i>		Newcombe et al., 2014	
<i>Propionibacterium freudenreichii</i>	Le Marechal et al., 2015		
<i>Pseudomonas aeruginosa</i>		Kunert et al., 2007	
<i>Pseudomonas syringae</i>		Reales-Calderon et al., 2015	
<i>Roseobacter pomeroyi</i>		Schumacher et al., 2014	
<i>Staphylococcus aureus</i>	Peton et al., 2014; Liew et al., 2015		
<i>Staphylococcus carnosus</i>		Mishra and Horswill, 2017	
<i>Staphylococcus epidermidis</i>		Nega et al., 2015	
<i>Streptococcus gordonii</i>		Siljamaki et al., 2014	
<i>Streptococcus agalactiae</i>	Yang et al., 2018	Maddi et al., 2014	
<i>Streptococcus pneumoniae</i>		Mohan et al., 2014	
<i>Streptococcus thermophilus</i>		Pribyl et al., 2014	
<i>Streptomyces scabiei</i>		Lecomte et al., 2014	

<i>Synechococcus sp.</i>		Komeil et al., 2014	
<i>Tsittia consotensis</i>		Padilla-Reynaud et al., 2015	
<i>Vibrio cholerae</i>		Christie-Oleza et al., 2015b	
<i>Vibrio parahaemolyticus</i>		Rubiano-Labrador et al., 2015	
<i>Xanthomonas citri</i> subsp. <i>citri</i>		Altindis et al., 2015	
<i>Xylella fastidiosa</i>		Nascimento et al., 2016	
<p>Articles searched between 2014–2018 identified EF-Tu present on the surface for in secretions of many bacterial species. Antibodies to this protein were also identified in a number of studies. Key search terms used were, but not limited to: exoproteome, secretome, surfacome, surfaceome, immunoproteome, and secretomic. Table excludes any data that was only bioinformatically determined. [†]Includes surfacome, outer membrane, specific protein analysis under any condition.</p>			

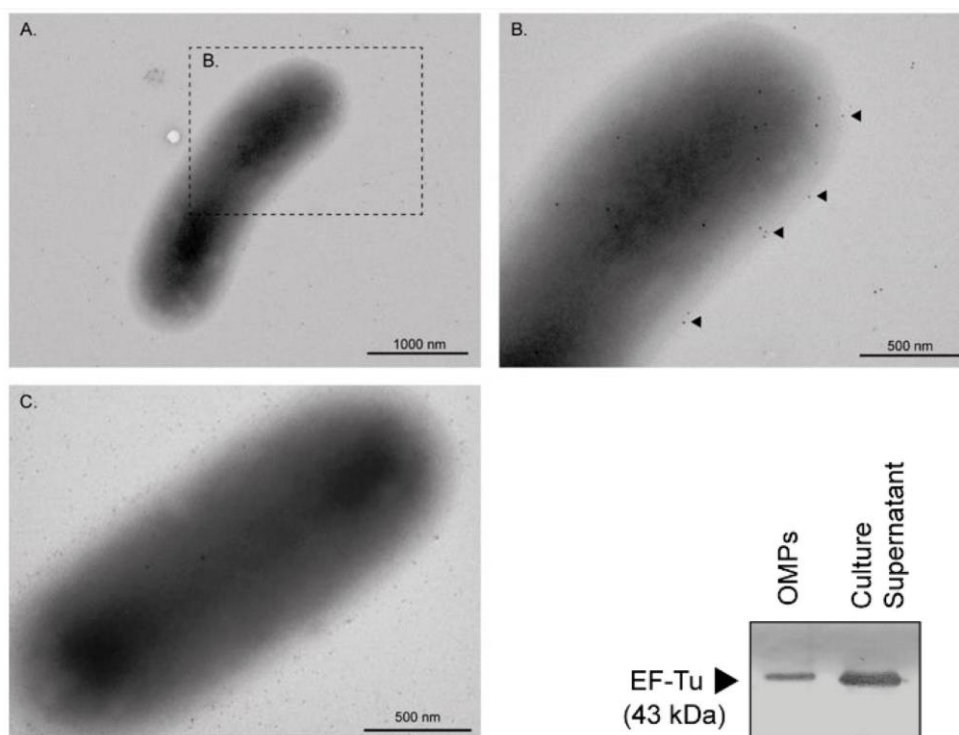


Figure 6.1: Immunogold electron microscopy showing detection of EF-Tu on the surface of STEC O157:H7 str. EDL933 and determination of the presence of EF-Tu, in outer membrane protein (OMP) extracts and culture supernatants. (A&B) The localization of EF-Tu on the cell surface of EDL933 strain was demonstrated by abundant labelling with gold particles (arrows). Bacteria were incubated with monoclonal anti-EF-Tu antibody (mAb 900; 1:200) followed by anti-mouse IgG+IgM (1:100) 10 nm gold particles. (C) As the control, the EDL933 strain was also incubated with anti-mouse IgG+IgM (1:100) gold particles.. Protein extracts were separated by SDS-PAGE (12% acrylamide) and analysed by Western blot assay. Arrows indicate the detection of the corresponding protein. (A) Identification of EF-Tu in OMPs and culture supernatant of the EDL933 strain. Monoclonal anti-EF-Tu antibody (mAb 900) was used in a dilution of 1:2000, followed by anti-mouse IgG, HRP conjugate diluted 1:500. Adapted from Torres et al., (2020)

6.2 Results

6.2.1 EF-Tu is not an effector of the T3SS of EHEC

It was initially hypothesised that EF-Tu may be an effector of the T3SS of EHEC and injected into host cells during infection. Given that EF-Tu has been detected in the secreted proteome of *E. coli* TUV93-0 (McHugh, 2020), and the coupled identification of EF-Tu on the outer membrane (Torres et al., 2020), we sought to determine whether it was a secreted effector of the EHEC T3SS.

Analysis of the EHEC *E. coli* strain TUV93-0 was carried out along with a T3SS knockout of *E. coli* Zap198 Δ escN, where EscN is the ATPase required for T3SS assembly, as a control for secretion via the T3 apparatus. If EF-Tu was present in the secretome of WT *E. coli* TUV93-0 but not in the functional T3SS knockout of *E. coli* Zap198 Δ escN, this suggests that its presence in the secretome is dependent on T3S. Both strains have a similar growth rate of 0.508 h⁻¹ for TUV93-0 and 0.509 hour⁻¹ for Zap198 Δ EscN, making analysis of T3S comparable (Fig. 6.2).

A single colony of each strain was then used to prepare an overnight culture which was subsequently inoculated into T3SS-inducing conditions of growth at 37 °C, 200 rpm, in MEM-Hepes. After approximately 7 hours, the supernatant protein fractions and secreted proteins were then precipitated and analysed using SDS-PAGE as previously explained (Fig. 6.2).

During SDS-PAGE analysis of cell lysate and secreted protein fractions, T3 related proteins were found in the fractions from TUV93-0 but not from Zap198 Δ EscN, confirming its role as a control for T3S. Western Blotting for the EF-Tu in *E. coli* was carried out to elucidate this further, where both the cell lysate and secreted proteins were analysed (Fig. 6.2).

The presence of EF-Tu in the cell lysate of both strains could be detected using this immunoblot method. Interestingly, however, no signal was detected in either secreted protein fraction, demonstrating that in *E. coli* TUV93-0, EF-Tu is not present in secreted proteins under T3S-inducing conditions, and is therefore not an effector of the T3SS.

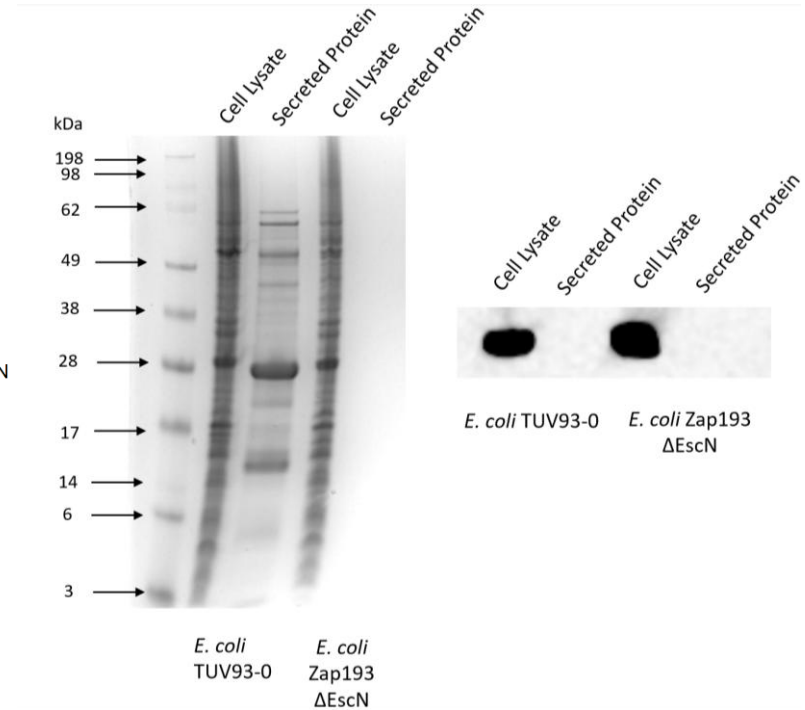
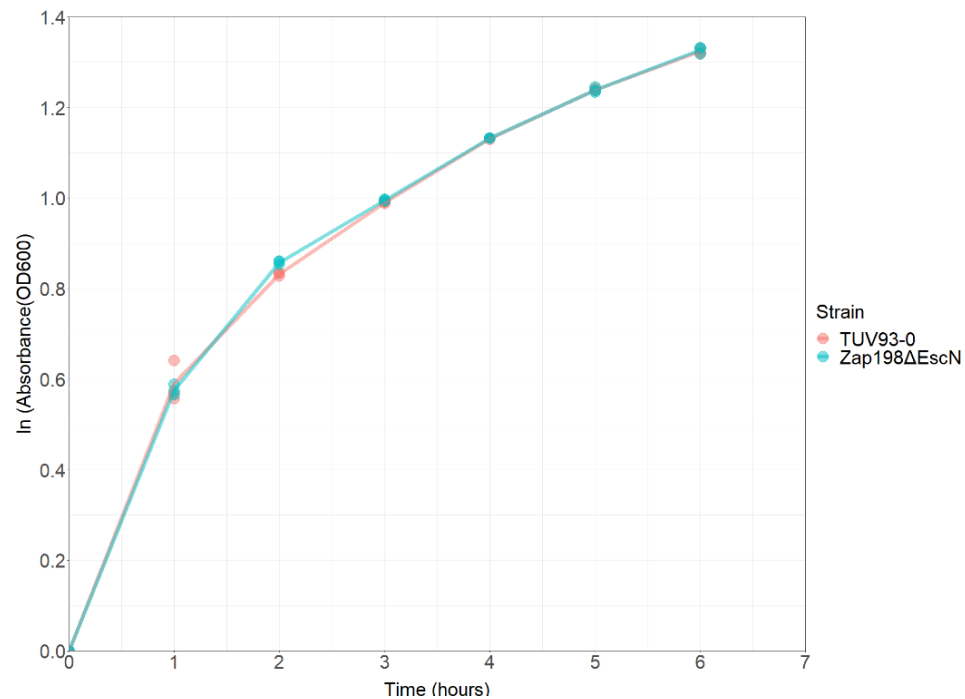


Figure 6.2: EF-Tu is not an effector of the T3SS and is not secreted. Specific growth rate and SDS-PAGE analysis of *E. coli* TUV93-0 and Zap198ΔEscN cell lysate and secreted protein fractions, show EF-Tu was present only in the cell lysate after Western Blotting. Specific growth rates were found as 0.508 h⁻¹ for TUV93-0 and 0.509 hour⁻¹ for Zap198ΔEscN. Strains were cultured in T3S inducing medium (MEM-Hepes, 37 °C, 200 rpm) for 7 hours (left) before harvesting protein. Both cell lysate and secreted proteins are shown (right).

6.2.2 Overexpression of EF-Tu2 in EHEC via the pVS45 expression vector

A bacterial expression vector based on pVS45 (*ampR*) vector (Sperandio et al., 2000) was constructed for expression of EF-Tu2 in EHEC. This vector has been shown previously to be successful in the expression of recombinant proteins in EHEC, including in the EHEC strain *E. coli* TUV93-0 (McHugh et al., 2019; Sperandio et al., 2000). Based upon the pBAD/Myc-His system, this vector is thought to confer tightly controlled bacterial expression with dose-dependent induction via arabinose (Guzman et al., 1995).

This vector was ordered from AddGene (catalogue no. 20059) and cloning of the *tuf2* gene performed by Dr R. McHugh as a collaboration in project (Fig. 6.3). Once received, the plasmid pVS45_*tuf2* was created and the following strains were generated by transformation of the relevant *E. coli* strains with the plasmid: *E. coli* TUV93-0 + pVS45_238, *E. coli* TUV93-0 + *rpsM:gfp*, *E. coli* TUV93-0 + *ler:gfp*, *E. coli* TUV93-0 + *rpsM:gfp* + pVS45_*tuf2*, *E. coli* TUV93-0 + *ler:gfp* + pVS45_*tuf2*, *E. coli* TUV93-0 + pAJR70 and *E. coli* TUV93-0 + pAJR70 + pVS45_*tuf2*. A single transformant was used to prepare an overnight culture in LB broth containing the selective antibiotic ampicillin which was subsequently inoculated into T3SS-inducing conditions of growth at 37 °C, 200 rpm, in MEM-Hepes with selective antibiotics. At an OD₆₀₀ of 0.2, varying concentrations of arabinose were tested for induction of EF-Tu2 expression. The supernatant protein fractions and secreted proteins were then precipitated and analysed using SDS-PAGE as previously explained, after a further four hours incubation (Fig. 6.4).

It can be observed that there is a band present at approximately 44 kDa, consistent with the size predicted for *S. goldiniensis* EF-Tu2. However, given that the native EF-Tu is a similar size and abundant in the cell, and there is no apparent increase in

expression along with increasing arabinose concentration it is difficult to conclude this is the *S. goldiniensis*' EF-Tu2.

Given protein expression within the cell lysate appears to remain unaffected by the varying arabinose concentrations, even though concentration of cells was normalised based on the OD₆₀₀ of the *E. coli* TUV930 cell cultures. The same normalisation based on OD₆₀₀ was carried out for the secreted protein fraction allowing for identification of an increase, or decrease of secreted proteins from the cells, independent of varied OD₆₀₀ of the culture. There is an increase in secreted proteins for *E. coli* TUV93-0 + pVS45_*tuf2* when treated with 0.5, 1.5 and 2.0 % arabinose, when compared to the uninduced control of *E. coli* TUV93-0 + pVS45_*tuf2*. This is interesting as production of T3S related proteins appears to be increased as a result of the expression of EF-Tu2 in *E. coli* TUV93-0.

Due to the vector's documentation as a successful expression vector in EHEC strains, and the link between the secretion of proteins and expression of EF-Tu2, plate reader analysis of the reporter strains was performed to dissect the relationship between the T3SS and EF-Tu2 further. Both induced and uninduced cultures were examined to try to account for this effect on T3S observed by this vector, with and without aurodox. Based on optimum expression conditions for this pVS45_*tuf2* vector, six strains (*E. coli* TUV93-0 with and without the pVS45_*tuf2*, with pAJR7070, *rpsM:gfp* and *ler:gfp*) were grown in the presence of 5 µg/ mL aurodox and DMSO alone as an untreated control (Fig. 6.5). Growth (OD₆₀₀) and expression of GFP driven from the promoters of *rpsM* and *ler* genes (Relative Fluorescence) were analysed on the FLUOstar Optima Microplate Reader System at 5 hours, after 3 hours of initial growth and then a further two hours of growth with induction of arabinose at 2 percent weight by volume. To analyse the effect of aurodox and kirromycin on the T3SS master regulator (*ler*) of EHEC strains, where a housekeeping gene (*rpsM*) acts as a control, pAJR7070 promotorless GFP vectors were used to subtract background fluorescence from the

TUV93-0 strain and GFP reporter fusion autofluorescence.

There was no statistical evidence to suggest a difference in relative fluorescence in the uninduced, treated and both induced, treated ($P=0.237$) and untreated samples ($P=0.150$), therefore, it could be the case that *tuf2* overexpression has no effect on *rpsM* expression, though this will have to be confirmed with further analysis to increase statistical power. This data, however, supports the results of McHugh et al (2019) which demonstrate there is no effect of aurodox on expression of *rpsM* (McHugh et al., 2019).

Expression of *ler* is increased when EF-Tu2 is expressed in the strains treated with aurodox ($P=0.011$) but not for those untreated ($P=0.064$). Most interesting, however, is that expression of *ler* is increased when EF-Tu2 is expressed and the strain is treated with aurodox, compared to the uninduced ($p=0.011$). This suggests that there is a relationship between aurodox, EF-Tu2 and the EHEC T3SS.

To induce Type III Secretion in EHEC, MEM-hepes media must be used for *E. coli* TUV93-0 culture (Roe et al., 2003). However, this media contains 0.2% glucose, which is a known repressor of the arabinose promoter (Siegele and Hu, 1997). Therefore, after three hours, overexpression of EF-Tu2 was repressed. Additionally, recent work by Cottam et al., found that L-arabinose enhances expression of the EHEC T3SS (Cottam et al., 2024).

As a result, design of an inducible expression vector for EF-Tu2 independent of interference with central metabolism essential. Though these data are not without caveats, it is interesting to observe this relationship between aurodox, EF-Tu2 and the increased expression of the EHEC T3SS.

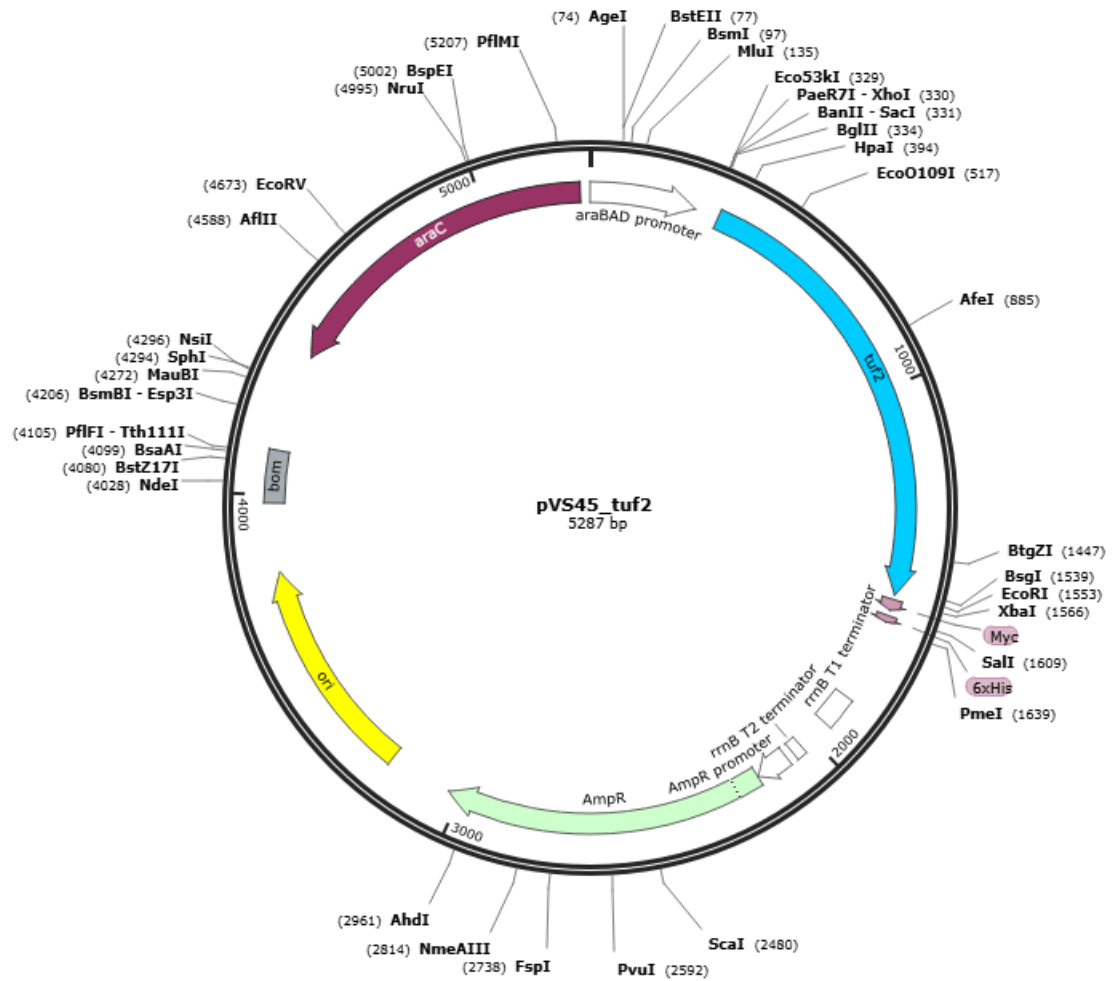


Figure 6.3: Plasmid map of pVS45_tuf2 construct. Vector map generated on **Snapgene**. EF-Tu2 from *S. goldiniensis*, encoded for by *tuf2*, shown in blue with the ampicillin resistance cassette shown in green and araBAD arabinose inducible promoter shown in white.

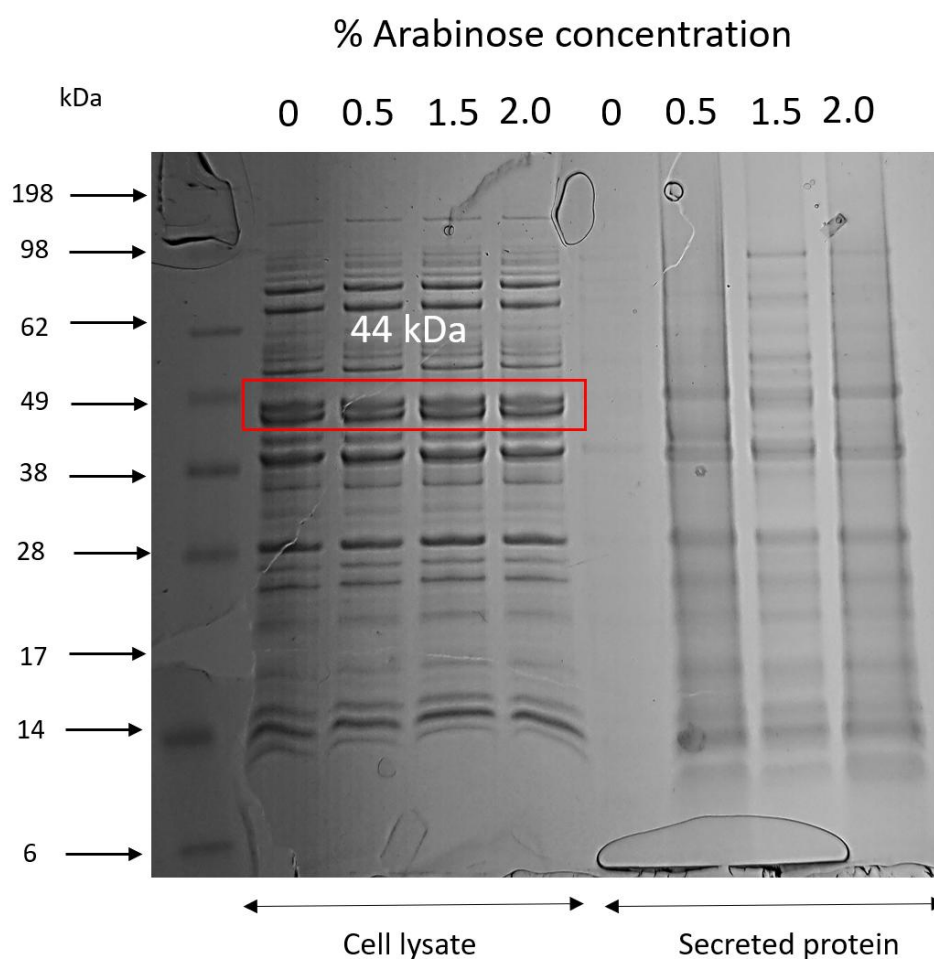


Figure 6.4: SDS-PAGE of TUV93-0 + pVS45_ *tuf2* overexpression of EF-Tu2 from *S. goldiniensis* at varied concentrations of arabinose. Strains were cultured in T3S inducing medium (MEM-Hepes, 37 °C, 200 rpm) till OD 0.2 was reached before induction with arabinose and grown for a further 4 hours before harvesting protein. Both cell lysate and secreted proteins are shown. The location of EF-Tu2 is shown in red at 44 kDa. An increase in secreted proteins in response to EF-Tu2 expression was observed.

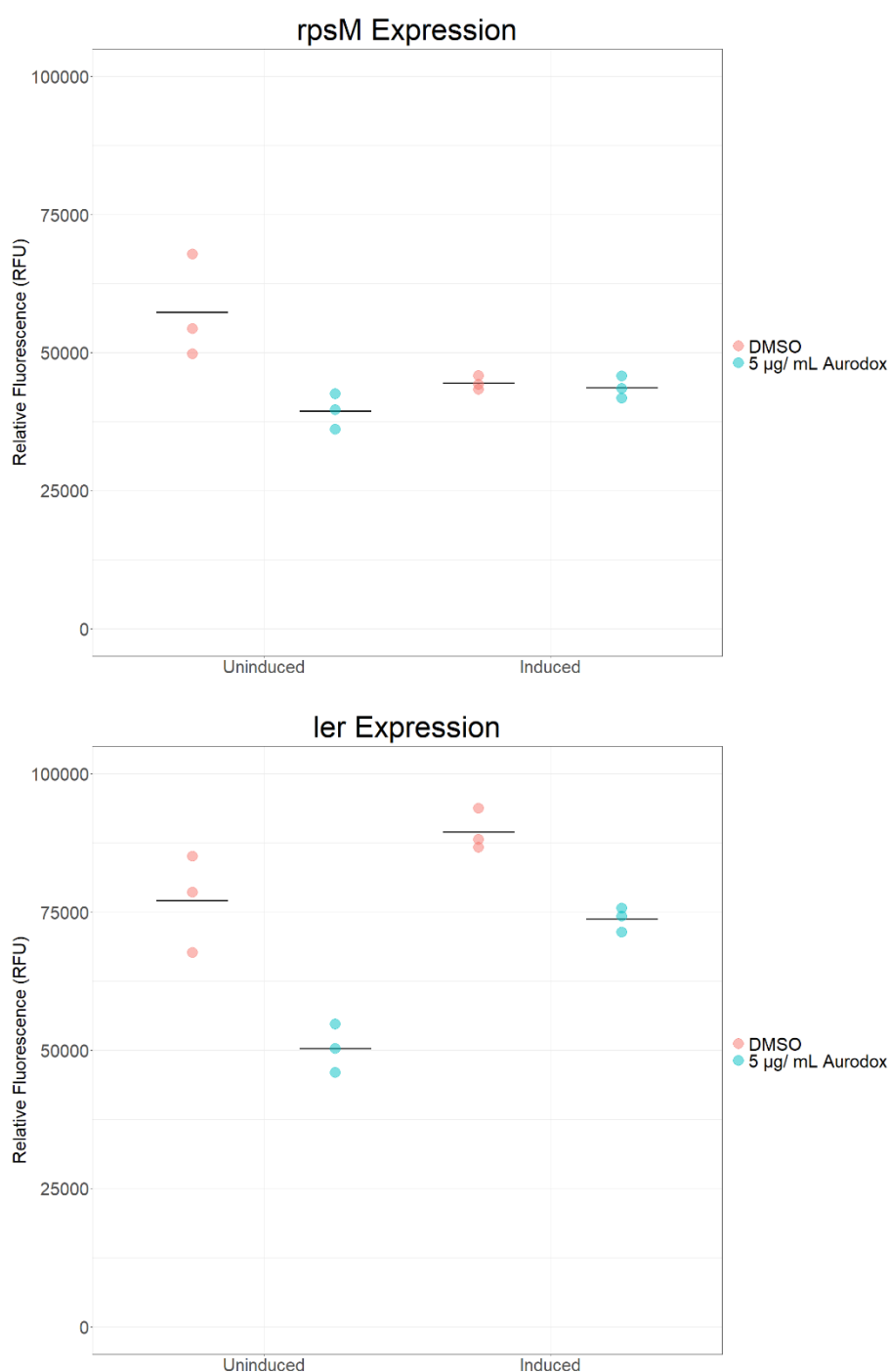


Figure 6.5: Relative fluorescence of *E. coli* TUV93-0 + pVS45_ *tuf2* GFP tagged strains at 7 hrs growth. Strains were grown to OD₆₀₀ 0.2 before induction with 2% arabinose, where the strains were grown for 2 further hours before treatment with 5 µg / mL Aurodox and fluorescence measured after 2 hours. Statistical analysis was performed using a two-sample t-test. Aurodox, shown in blue, DMSO control in red.

6.2.3 Overexpression of EF-Tu2 in EHEC via the pSEVA_238 expression vector reverses the T3SS knockdown effect of aurodox and kirromycin

Due to the repression associated with the arabinose inducible vector pVS45_*tuf2*, one final expression vector, pSEVA238, was chosen for the expression of EF-Tu2 via *tuf2*, where central metabolism was independent of the systems induction (Nikel et al., 2022).

The pSEVA238 expression module was created based on regulatory nodes mined from Gram-negative bacteria, where the XylS/Pm regulatory node was taken from *Pseudomonas putida* (Ramos et al., 1987). The system, which responds to Benzoic acid was found to have excellent performance as an expression tool in *Escherichia coli* (Gawin et al., 2017; Nikel et al., 2022).

This vector, with *tuf2* incorporated, was designed by Dr R McHugh and synthesised (Twist Bio; Fig. 6.6) Once received, the following strains were generated: *E. coli* TUV93-0 _pSEVA_238, *E. coli* TUV93-0 + *rpsM:gfp*, *E. coli* TUV93-0 + *ler:gfp*, *E. coli* TUV93-0 + *rpsM:gfp* + pSEVA238_*tuf2*, *E. coli* TUV93-0 + *ler:gfp* + pSEVA238_*tuf2*, *E. coli* TUV93-0 + pAJR70 and *E. coli* TUV93-0 + pAJR70 + pSEVA238_*tuf2*. As before, a single transformant was used to prepare an overnight culture which was subsequently inoculated into T3SS-inducing conditions of growth at 37 °C, 200 rpm, in MEM-Hepes with selective antibiotics (Kan). At an OD₆₀₀ of 0.2, varying concentrations of benzoic acid were tested for induction of EF-Tu2 protein expression. The cell lysate and secreted proteins were then precipitated and analysed using SDS-PAGE as previously explained, after four further hours.

During analysis of expression, it can be observed that there is a band present at approximately 44 kDa in the cell lysate fraction on an SDS_PAGE gel, consistent with the mass of this EF-Tu2 (Fig. 6.7). As mentioned previously, however, EF-Tu is a similar size and wholly abundant in the cell, so it is difficult to determine the likes of

whether this is *S. goldiniensis*' EF-Tu2. Western Blotting for the HA tag present on by which *tuf2* was tagged was carried out for further confirmation of overexpression (Fig.6.7).

It was observed that no signal from chemiluminescence was found from Western Blotting for the HA tag, present on the pSEVA_*tuf2* vector in the WT strain. The *E. coli* TUV93-0 strain was used as a control for the Western Blot as it was not transformed with the vector. At a concentration of 2.0 mM benzoic acid, signal was observed for Western Blotting of the HA tag, indicating that EF-Tu2, is being induced in *E. coli* TUV93-0 at this concentration. As a result, 2.0 mM was selected as the optimum conditions for inducing the expression of EF-Tu2 via this vector.

Proteins from the cell lysate appear to remain unaffected by the varying benzoic acid concentrations, with cells being normalised based on the OD₆₀₀ of the cell cultures. The same normalisation based on OD₆₀₀ was carried out for the secreted protein fraction allowing for identification of an increase, or decrease of secreted proteins from the cells, independent of varied OD₆₀₀ of the culture. It is apparent that the secreted protein fraction is affected when treated with benzoic acid at all concentrations. There is an increase in secreted proteins for TUV93-0 + pSEVA238_*tuf2* when treated with 0.5, 1.0 and 2.0 mM of benzoic acid, but not for the WT TUV93-0 control or the uninduced control of TUV93-0 + pSEVA238_*tuf2*, where their secretion of proteins was comparable. This indicates that production of T3S related proteins appears to be increased as a result of the expression of EF-Tu2 in TUV93-0.

Based on optimum expression conditions for this pSEVA238_*tuf2* vector, six strains (*E. coli* TUV93-0 with and without the pSEVA_*tuf2*, with pAJR70, *rpsM:gfp* and *ler:gfp*) were grown in the presence of 5 µg/ mL aurodox, 5 µg/ mL kirromycin and DMSO alone as untreated control (Fig. 6.8). Growth (OD₆₀₀) and up/down regulation and expression of *rpsM* and *ler* genes (Relative Fluorescence) was analysed on the

FLUOstar Optima Microplate Reader System (BMG Labtech) over 8 hours after 3 hours of initial growth and then a further two hours of growth with induction of benzoic acid at 2.0 mM. to analyse the effect of aurodox and kirromycin on the T3SS master regulator (*ler*) of EHEC strains, where a housekeeping gene (*rpsM*) acts as a control. pAJR70 promotorless GFP vectors were used to subtract background fluorescence from the TUV93-0 strain and GFP reporter fusion autofluorescence.

When expression of GFP from the *rpsM* promoter was investigated, it can be observed that for all strains, regardless of treatment, expression of EF-Tu2 results in a higher expression of *rpsM:gfp*. Where the expression of *rpsM:gfp* in *E. coli* TUV93-0 +pSEVA238_*tuf2* is increased compared to the WT *rpsM:gfp* strain when treated with DMSO (P=0.022), aurodox (P=0.001) and kirromycin (P=0.0162).

There was no significant difference in *rpsM:gfp* expression when strains containing EF-Tu2 were treated with aurodox (P=0.454) but there was a decrease in *rpsM* expression for those not containing EF-Tu2 when treated with kirromycin (P=0.010) against the untreated control of DMSO, which supports the findings from McHugh et al., (2019), where aurodox had no effect on *rpsM* but kirromycin reduces expression. In strains expressing EF-Tu2, *rpsM* was less affected by aurodox treatment than with treatment with kirromycin (P=0.041), supporting the argument that aurodox does not affect cellular function as much as kirromycin. This is consistent with its use as a T3SS inhibitor not causing disruption to the gut microbiome and less activation of the SOS response (McHugh et al., 2019). Equally, it can also be argued that perhaps these observations are not associated to the mechanism of action of aurodox/kirromycin but instead indicate that EF-Tu2 provides resistance to aurodox but not against kirromycin, resulting in a greater effect of kirromycin on *rpsM* when compared to aurodox under EF-Tu2 expressed conditions.

When *ler* expression was analysed, WT *E. coli* TUV93-0 expressed *ler* at lower levels to that of the untreated control (DMSO) when treated with aurodox (P=0.007) and

kirromycin ($P=0.011$), where there was no significant change in *ler* expression between kirromycin and aurodox treatment ($P=0.951$).

Interestingly, in *E. coli* TUV93-0 expressing the aurodox resistant EF-Tu2 from *S. goldiniensis*, *ler* expression is increased for both the untreated control of DMSO ($P=0.022$) and aurodox ($P=0.004$) compared to that not expressing EF-Tu2. The same, however is not observed with kirromycin ($P=0.835$). These results support the findings of the previous assay (Fig. 6.5) and the secreted proteins of *E. coli* TUV93-0 present on both previous gels (Fig. 6.4 & 6.7) which show that overexpression of EF-Tu2 caused an increase in the expression of the T3SS in *E. coli* TUV93-0.

To summarise the findings of the GFP reporter fusion assay on *rpsM* and *ler* expression in response to EF-Tu2, it can be observed that again, both aurodox and kirromycin downregulate the T3SS of EHEC at concentrations of 5 $\mu\text{g} / \text{mL}$. Additionally, results showed that the overexpression of EF-Tu2 reverses the knockdown phenotype associated with aurodox treatment, increasing expression of *ler*, and therefore the increased expression of the T3SS when compared to the uninduced control.

As we are aware, this is the first experiment that suggests a potential function for EF-Tu2 in T3S, and may help to explain why many enteric pathogens carry two copies of EF-Tu. With the hypothesis being that one is co-expressed alongside T3S.

To determine whether this observation was a result of the EF-Tu2 and other kirromycin-like elfamycin resistant EF-Tu, an aurodox-sensitive EF-Tu was analysed in the same way.

307

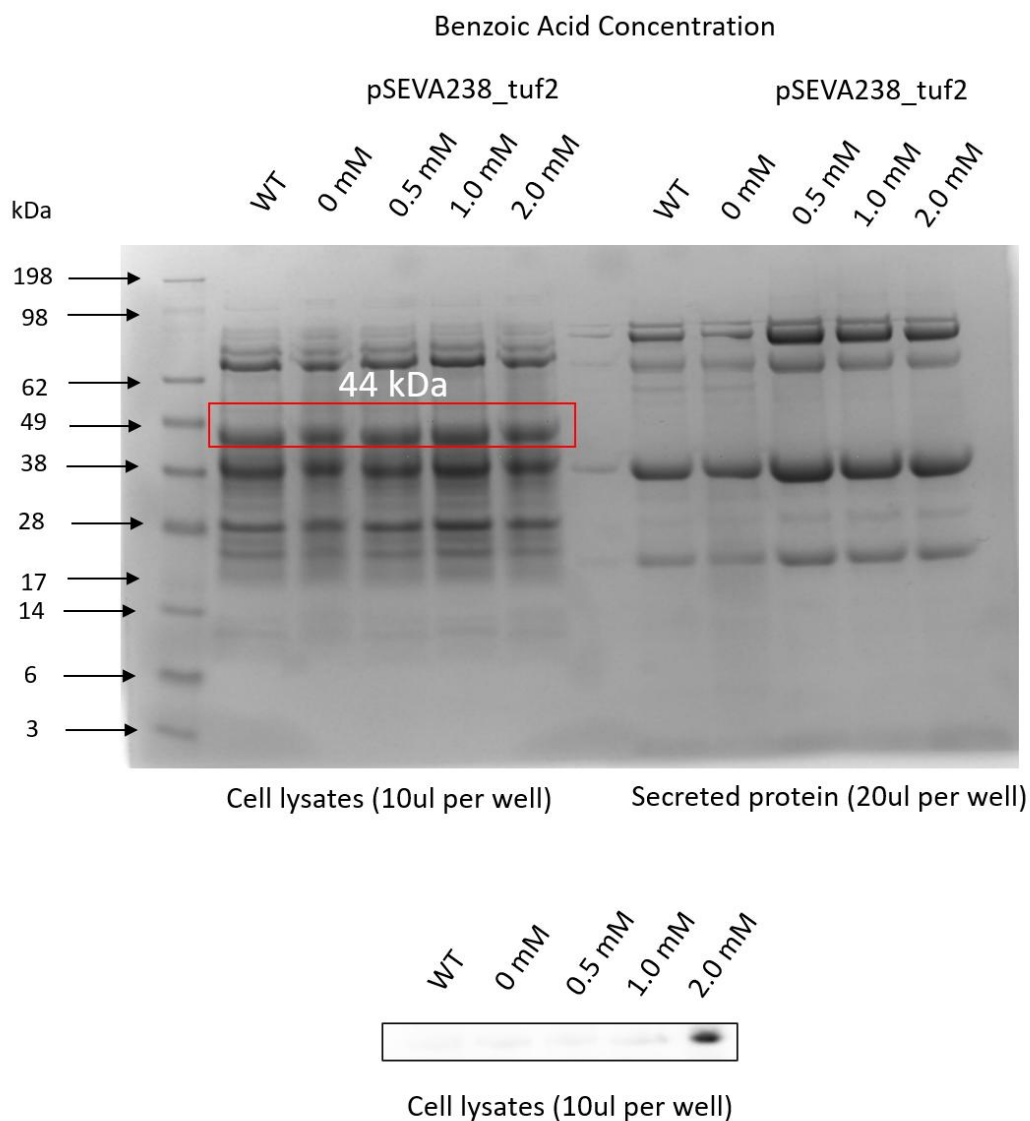


Figure 6.7: *E. coli* TUV93-0 + pVS45_tuf2 optimally expresses EF-Tu2 from *S. goldiniensis* at 2.0 mM and also suggests an increase in secreted protein in response to EF-Tu expression. Strains were cultured in T3S inducing medium (MEM-Hepes, 37 °C, 200 rpm) till OD 0.2 was reached before induction with benzoic acid and grown for a further 4 hours before harvesting protein. Both cell lysate and secreted proteins are shown. The location of EF-Tu2 is shown in red at 44 kDa. An increase in secreted proteins in response to EF-Tu2 expression was observed. Optimum conditions for expression were determined as 2.0 mM via Western Blot.

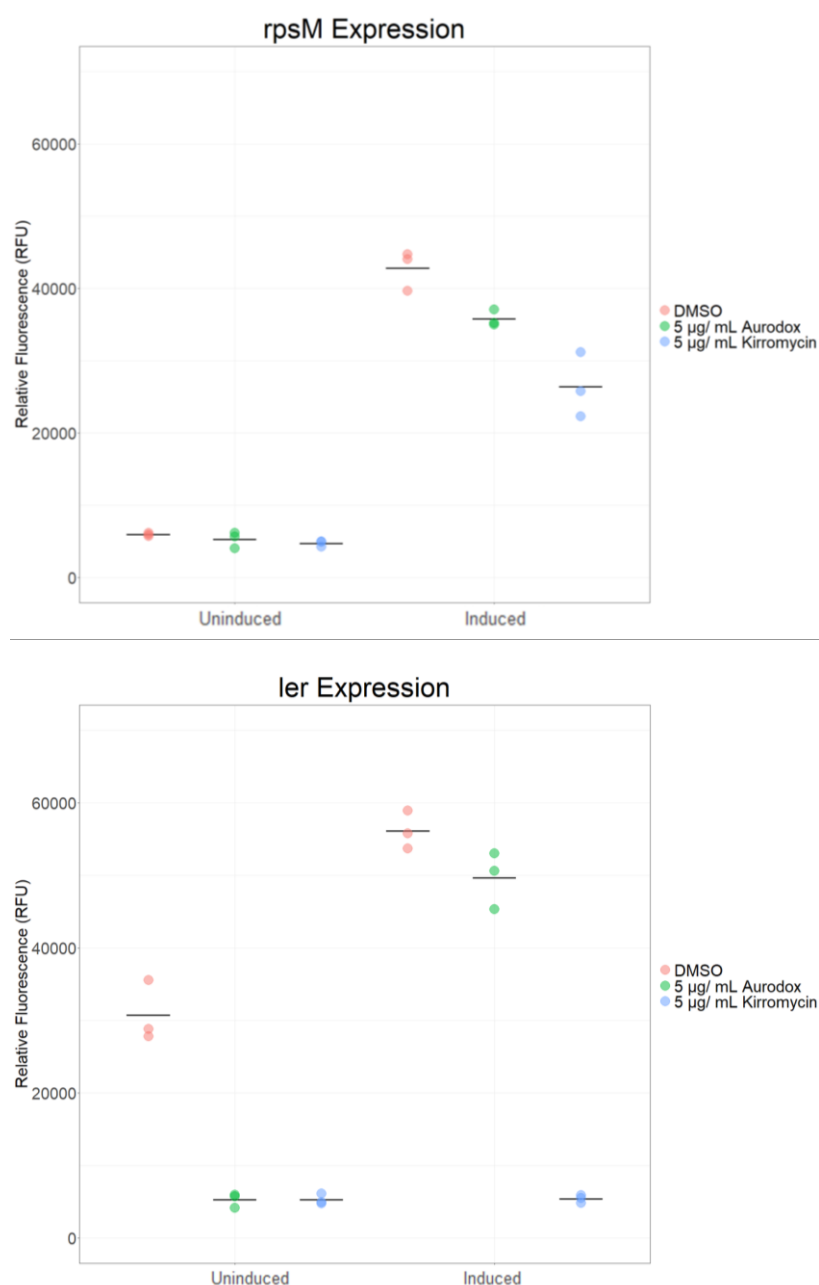


Figure 6.8: Overexpression of EF-Tu2 reverses the knockdown of T3S associated with aurodox treatment, increasing expression of *ler* and therefore, the T3SS. Relative fluorescence of *E. coli* TUV93-0 GFP-tagged strains at 7hrs growth. Strains were grown to OD₆₀₀ 0.2 before induction with 2.0 mM benzoic acid, where the strains were grown for 2 further hours before treatment and measurement during 8 hours of growth. Statistical analysis was performed using a two-sample t-test. Aurodox, shown in green, kirromycin in blue and DMSO control in red.

6.2.4 Expression of the susceptible Ef-TuB from *E. coli* in Enterohemorrhagic *Escherichia coli* via the pSEVA_238 expression vector reverses the T3SS knockdown effect of aurodox and kirromycin

To further dissect the role of EF-Tu and its relationship with T3S of EHEC strains, and whether this is related to kirromycin-like elfamycin resistant EF-Tu only, an EF-Tu, native to *E. coli* which is not resistant to elfamycins was selected. *E. coli* strains contain two genes encoding EF-Tu, *tufA* and *tufB* (van der Meide et al., 1983). The pSEVA238 vector was again ordered from Twist Bio, this time with the *tufB* gene from *E. coli* integrated to test this hypothesis (Fig. 6.9). Once received, the following strains were generated: *E. coli* TUV93-0 _pSEVA_238, *E. coli* TUV93-0 + *rpsM:gfp*, *E. coli* TUV93-0 + *ler:gfp*, *E. coli* TUV93-0 + *rpsM:gfp* + pSEVA238_*tufB*, *E. coli* TUV93-0 + *ler:gfp* + pSEVA238_*tufB*, *E. coli* TUV93-0 + pAJR70 and *E. coli* TUV93-0 + pAJR70 + pSEVA238_*tufB*. As previously, T3S conditions were replicated, and varying concentrations of benzoic acid were tested for induction of EF-TuB expression. The supernatant protein fractions and secreted proteins were then precipitated and analysed using SDS-PAGE as previously explained.

It can be observed that there is a band present at approximately 44 kDa in the cell lysate fraction on an SDS_PAGE gel, consistent with the size of this EF-TuB (Fig. 6.10).

Western Blotting for the HA tag present on the vector in frame with EF-TuB was carried out to elucidate this further. It was observed that no signal from chemiluminescence was found from Western Blotting for the HA tag, in the strain without the vector (WT) present on the pSEVA_*tufB* vector, in the WT strain. However, at all other concentrations an induction signal was detected (Fig. 6.10)

As before, the OD₆₀₀ of cells were normalised before analysis of protein present in cell lysate the secreted fraction. As before, no change was observed within cell lysates,

however, the secreted protein fraction was when treated with benzoic acid at all concentrations (Fig. 6.10). There is a decrease in secreted proteins for *E. coli* TUV93-0 + pSEVA238_ *tufB* when treated with 0.5, 1.0 and 2.0 mM of benzoic acid, but not for the WT TUV93-0 control. Interestingly, the uninduced control also showed less secreted protein, suggesting that presence of the EF-TuB independent of induction has an effect on T3S.

As before, six strains (*E. coli* TUV93-0 with and without the pSEVA238_ *tufB*, with pAJR70, *rpsM::gfp* and *ler::gfp*) were grown in the presence of 5 µg/ mL aurodox, 5 µg/ mL kirromycin and DMSO alone as an untreated control (Fig. 6.11). Growth (OD₆₀₀) and up/down regulation and expression of *rpsM* and *ler* genes (Relative Fluorescence) was analysed on the FLUOstar Optima Microplate Reader System (BMG Labtech) over 8 hours after 3 hours of initial growth and then a further two hours of growth with induction of benzoic acid at 2.0 mM. to analyse, the effect of aurodox and kirromycin on the T3SS master regulator (*ler*) of EHEC strains.

Results from this analysis showed in the WT *E. coli* TUV930 strain, *rpsM* expression is unchanged from the DMSO control, when treated with aurodox (P= 0.048) and kirromycin (P=0.012, Fig. 6.11). Interestingly, when EF-TuB is expressed, *rpsM* levels increase in response to the untreated control of DMSO, compared to the WT (P=0.008). This was not observed for aurodox (P=0.063) or kirromycin (P=0.453) which showed no change in expression of *rpsM*, suggesting an extra copy of EF-TuB provides a metabolic advantage, where treatment with kirromycin-like elfamycin reduces this to levels of *rpsM* similar to that not expressing EF-TuB at all due to its susceptibility to elfamycin antibiotics.

When expression of *ler* was analysed a decrease in *ler*, the master regulator of the T3SS, was observed in response to aurodox (P=0.007) and kirromycin (P=0.007) in the WT strain. This is in line with all three other assays in this study and with findings of McHugh et al., (2019; Fig. 6.11). A decrease in *ler* expression in the untreated

control was also observed when EF-TuB is expressed ($P=0.006$), supporting the phenotypic analysis which showed a decrease in T3SS related proteins in response to the pSEVA238_*tufB* vector (Fig. 6.10). In contrast, expression of *ler* was increased in strains expressing EF-TuB when treated with aurodox ($P=0.014$) and kirromycin ($P=0.001$). Though not seen previously for kirromycin while overexpressing the aurodox resistant EF-Tu2, it is clear here overexpressing EF-Tu reverses the knockdown phenotype of aurodox on the T3SS of *E. coli* TUV93-0. This also suggests that this observation may be linked to all EF-Tu, and not just those resistant to kirromycin-like elfamycins.

These data support the hypothesis of additional functionality (moonlighting) for EF-Tu related to T3S and may explain why many enteric pathogens carry two copies of EF-Tu (Table 5A).

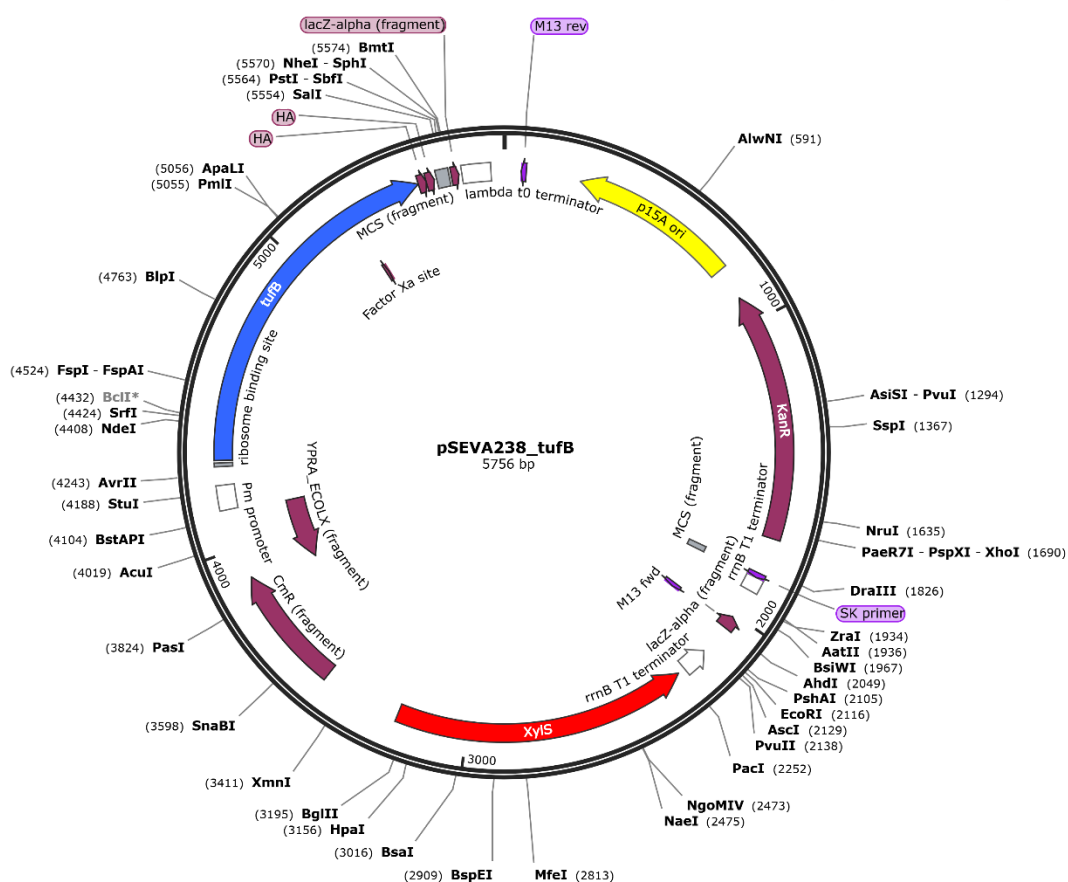


Figure 6.9: Plasmid map of pSEVA238_tufB construct. Vector map generated on Snapgene. EF-TuB from *E. coli* encoded for by tufB, shown in blue with the kanamycin resistance cassette shown in claret and XylS/Pm regulatory node, inducible by benzoic acid, shown in red/white.

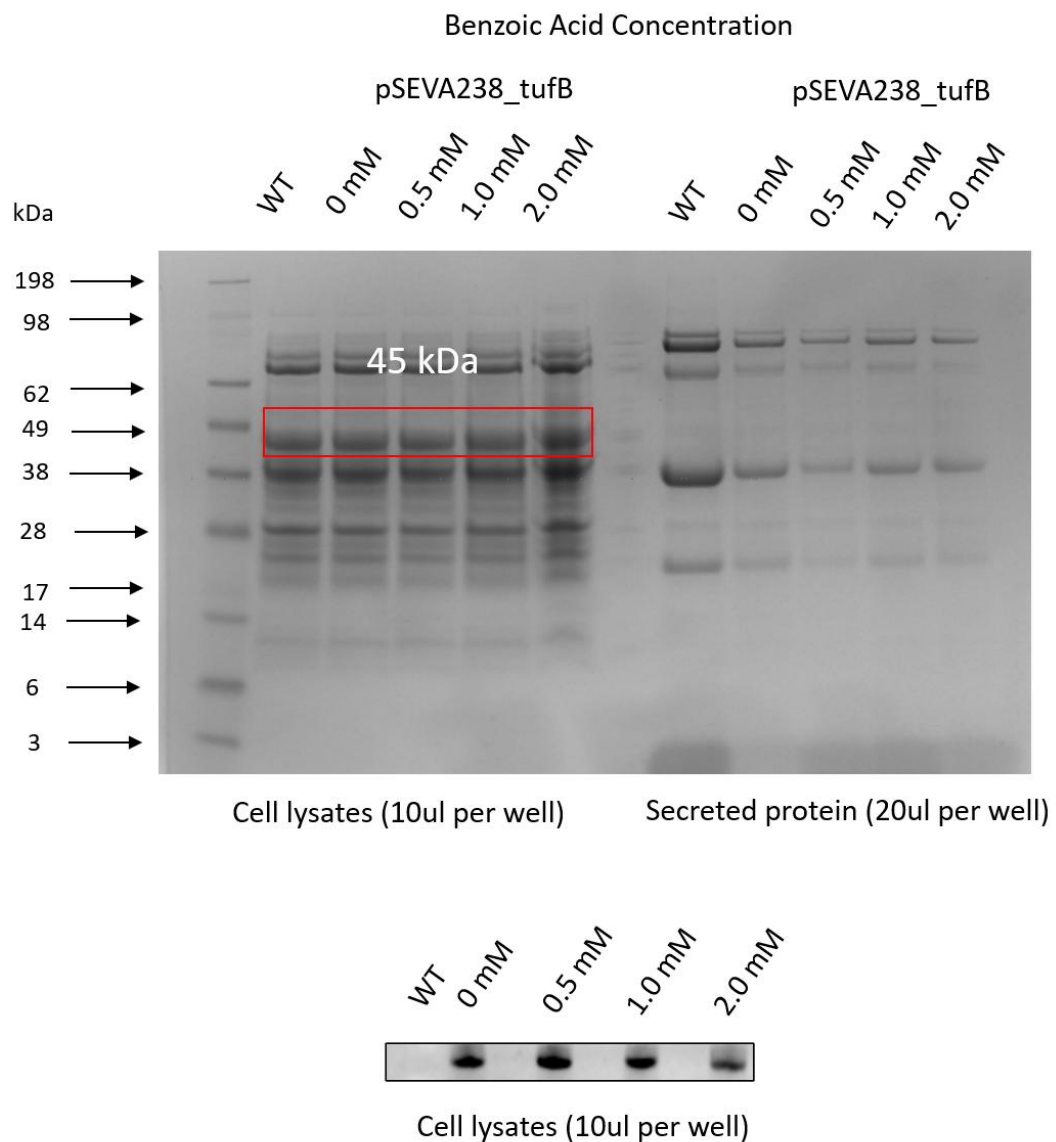


Figure 6.10: SDS-PAGE of TUV93-0 + pVS45_tufB overexpression of EF-TuB from *E. coli* at varied concentrations of benzoic acid. Strains were cultured in T3S inducing medium (MEM-Hepes, 37 °C, 200 rpm) till OD₆₀₀ 0.2 was reached before induction with benzoic acid and grown for a further 4 hours before harvesting protein. Both cell lysate and secreted proteins are shown. The location of EF-TuB is shown in red at 44 kDa. A decrease in secreted proteins in response to EF-TuB expression was observed.

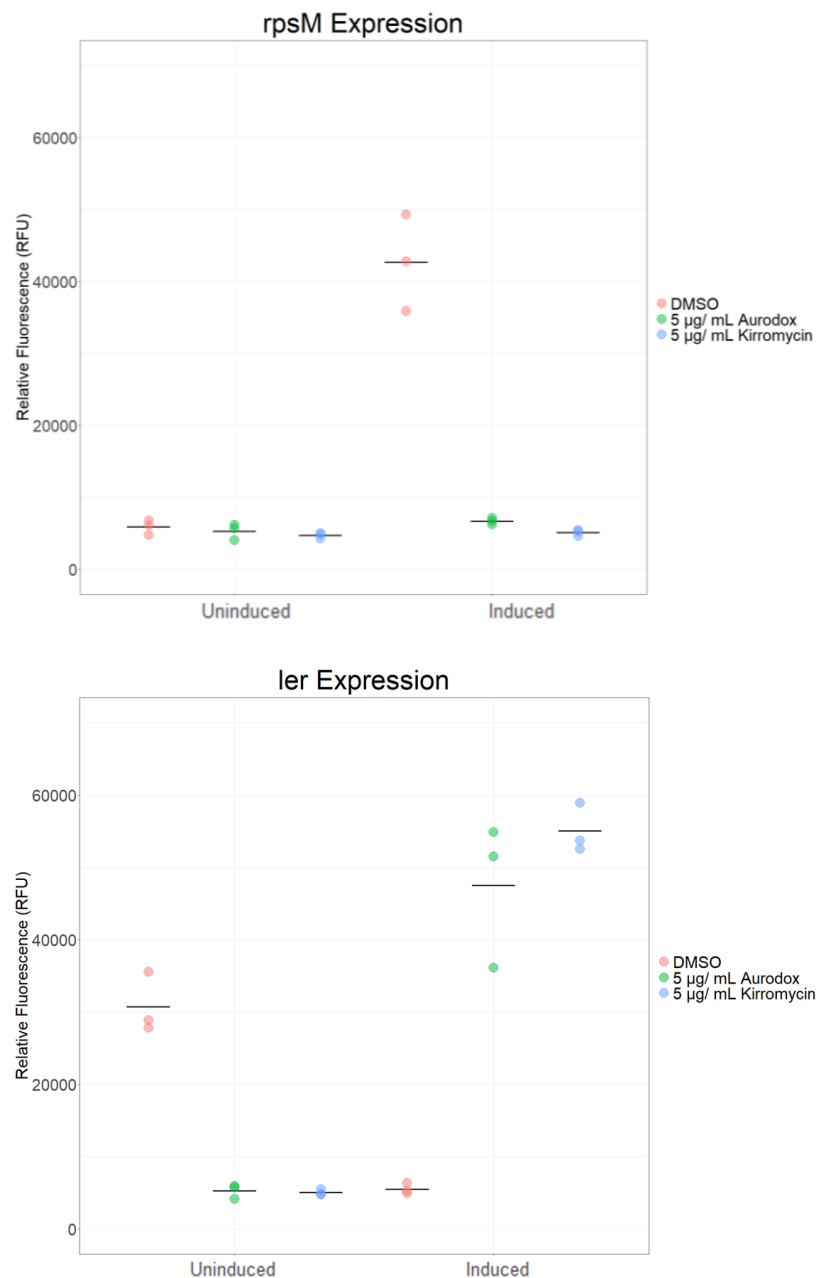


Figure 6.11: Overexpression of EF-TuB reverses the knockdown of T3S associated with aurodox treatment, increasing expression of *ler* and therefore, the T3SS. Relative fluorescence of *E. coli* TUV93-0 GFP-tagged strains at 7hrs growth. Strains were grown to OD₆₀₀ 0.2 before induction with 2.0 mM benzoic acid, where the strains were grown for 2 further hours before treatment and measurement during 8 hours of growth. Statistical analysis was performed using a two-sample t-test. Aurodox, shown in green, kirromycin in blue and DMSO control in red.

6.3 Summary

During this Chapter we investigated the hypothesis that EF-Tu may possess a moonlighting function that is related to T3S. Work by Torres et al., (2020) used immunogold electron microscopy to show the localisation of EF-Tu on the surface of STEC. Given that EF-Tu has been detected in the secreted proteome of *E. coli* TUV93-0 (McHugh, 2020), and the coupled identification of EF-Tu on the outer membrane (Torres et al., 2020), we sought to determine whether it was a secreted effector of the EHEC T3SS.

Western Blotting for the EF-Tu in *E. coli* was carried out to elucidate this further, where both the cell lysate and secreted proteins were analysed (Fig. 6.2). The presence of EF-Tu in the cell lysate of both strains could be detected using this immunoblot method. Interestingly, however, no signal was detected in either secreted protein fraction, demonstrating that in *E. coli* TUV93-0, EF-Tu is not present in secreted proteins under T3S-inducing conditions, and is likely not an effector of the T3SS.

As EF-Tu was shown not to be an effector secreted via the T3SS of EHEC (*E. coli* TUV93-0) it was proposed that perhaps EF-Tu had an alternative role in the T3SS of EHEC. As EF-Tu plays a vital role within the cell, gene knock outs were not possible and so multiple expression vectors were tested for optimum overexpression of the resistant EF-Tu2 within EHEC.

When both EF-Tu2 (resistant) and EF-TuB (sensitive) were expressed in EHEC, this reversed the T3S knockdown phenotype of aurodox on the T3SS of EHEC, suggesting a role within the T3SS. Analysis of the data obtained in this work supports the hypothesis of additional functionality (moonlighting) for EF-Tu related to T3S. The role is not fully elucidated but there is evidence that EF-Tu can act as a protein chaperone under certain conditions (Caldas et al., 1998) These data are the first

experiment that suggests that additional function such as chaperone activity for EF-Tu in T3S may help to explain why many organisms, including enteric pathogens carry two copies of EF-Tu.

Chapter 7: Discussion

7.0 Discussion

Elfamycins represent a relatively poorly understood class of antibiotics that are characterised by their mode of action rather than their chemical class or structure (Prezioso et al., 2017). Moreover, recent work has demonstrated that minor chemical modifications to the structure, as natural variants of elfamycins, can lead to changes in the modes of action (McHugh et al., 2019). The structure of kirromycin and aurodox differ by a methyl group on the pyridone ring of the molecules and this results in aurodox having anti-T3SS activity. This work aimed to understand the diversity of elfamycin biosynthetic gene clusters, their potential evolution, resistance mechanisms, and how biosynthesis could potentially be manipulated to produce elfamycin variants with modified activities.

7.1 Genome sequencing of *S. ramocissimus*

The genome of *S. ramocissimus* was unknown, and therefore the structure of the kirromycin BGC contained within the genome was unknown. Genome sequencing of this kirromycin producer was attempted to further understand the biosynthesis and resistance mechanisms possessed by the strain. It is increasingly evident that the same chemical molecule can be produced through a number of different biosynthetic routes, either variation on a BGC or through a completely different genetic route (Chevrette et al., 2020a; Medema et al., 2015). Using Illumina sequencing, this work resulted in the assembly of a genome which was fragmented (75 contigs; Fig. 3.24). Using a combined approach of Illumina NovaSeq short read sequencing followed by long read sequences would have improved the assembly, such as provided by Oxford Nanopore MinION. Instances where long reads have improved and completed short read assemblies can be noted in the work by Slemc and co-workers, where the highly

complex genome of *Streptomyces rimosus* was elucidated due to a combined sequencing approach (Slemc et al., 2022). The same can be observed when Busarakam et al (2014), where the genome of *Streptomyces leeuwenhoekii* was improved from 658 contigs to just 3 when the Illumina-only assembly was complimented by long reads from PacBio sequencing. Their work also resolved the modularity of a polyketide, where one of the shorter contigs in the initial assembly was found to be a repeat sequence which long reads resolved reducing contig number (Busarakam et al., 2014). Long reads can also resolve the issues around identification of circular or linear replicons, where assembly software can produce linear molecules but do not inform the topology of DNA. Due to the longer reads of PacBio sequencing, some reads will identify terminal inverted repeats of linear replicons allowing indication that this is a circular replicon, removing the duplicated sequence (Gomez-Escribano et al., 2015). In the sequencing of the *S. rimosus* genome, the strains' Giant Linear Plasmid (GLP) was even elucidated using Nanopore data alone, securing the requirement for long read sequencing in the production of high quality reference genomes (Slemc et al., 2022). However, given that the sequencing reads from Illumina allowed us to identify a single contig that contained all of the putative genes for production of kirromycin, it was decided to proceed with comparison of the BGCs.

7.2 Annotation of the *S. ramocissimus* kirromycin BGC

Though the genome was fragmented, the BGC of *S. ramocissimus* was identified and found to be complete based on the genes required for kirromycin biosynthesis from *S. collinus* (Weber et al., 2008). After annotation, and comparison to the kirromycin BGC of *S. collinus*, it was found that the structure of the BGCs were highly similar (Fig. 3.28). Functional annotation of the kirromycin BGC from *S. ramocissimus* (Table 3E), allowed the proposed biosynthesis of kirromycin backbone from *S. ramocissimus*

to be predicted by the enzymes KirAI-KirAVI (Fig. 3.29). This annotation assisted in the resolution of key genes within the kirromycin BGC of *S. collinus*, which have not been previously resolved. In the published, annotated BGC kirromycin from *S. collinus*, (Weber et al., 2008), the Mfs-type exporter KirT protein and the regulator KirR are predicted to have the N and C terminal polypeptide sequences encoded separately (*kirTI/kirTII*, *kirRI/kirRII*). The sequencing technology used to elucidate this sequence was Roche 454, which is known to introduce premature stop codons (Trimble et al., 2012). By comparing the ORF and termini of the protein sequences from the original study by Weber et al., (2008) to the sequences of *KirR* and *KirT* from *S. ramocissimus* here, this confirmed the likelihood of sequencing error as the genes are intact within the BGC of *S. ramocissimus* (Fig. 3.34). These data further our understanding of kirromycin biosynthesis and the structure of the BGC (Weber et al., 2008).

7.3 Identification of a kirromycin-like BGC in a metagenome-assembled genome *S. ISL094*.

A new kirromycin-like elfamycin BGC from *Streptomyces* ISL094 was identified from a metagenomic study (Maza et al., 2019). Each gene present on the BGC was functionally annotated and compared to other kirromycin-like elfamycin BGCs (Fig. 3.28 , 3.30 & Table 3F), not previously described. The methyltransferase, AurM*, of the aurodox BGC of *S. goldiniensis* was found to be responsible for the conversion of kirromycin to aurodox during the last step of biosynthesis (McHugh et al., 2022). This, coupled with the elfamycin BGC of ISL094 showing most genetic similarity to that of the aurodox BGC of *S. goldiniensis* (Fig. 3.28), suggests that the elfamycin BGC of ISL094 could contain the genetic potential for aurodox production.

The additional methyltransferases present on the kirromycin-like BGCs of *S. goldiniensis* and *S. ISL094* were modelled structurally and analysed based on their similarity (Fig. 3.35). The methyltransferase structure was found to be highly conserved between the two, sharing the characteristic Rossman fold, which is highly conserved across all known SAM methyltransferases, despite the ligand/substrate binding domain varying greatly over the family (Martin and McMillan, 2002; Fig. 3.36). The O-methyltransferases thought to be involved in methylation of kirromycin to form aurodox, Kir/AurM* in *S. goldiniensis* and *S. ISL094* were phylogenetically distant to the other O-methyltransferases in the BGCs that are proposed to methylate C-20 on the main kirromycin backbone. These data suggest that it is likely the kirromycin-like BGC of *S. ISL094* encodes the production of aurodox (Fig. 3.37).

Annotation of the kirromycin-like BGCs of *S. ramocissimus* and *S. ISL094* provided further insight into the diversity and evolution of kirromycin-like elfamycin BGCs, where gene duplications, displacements and complete deletions could be observed between the BGCs.

7.4 Analysis of kirromycin-like elfamycin BGC evolution

The four kirromycin-like elfamycin producers identified as being phylogenetically distant (Fig. 3.21) are likely capable of production of such similar elfamycin molecules. Additionally, these molecules are produced from BGCs which have structural and architectural changes, yet similar molecules are capable of being produced (Fig. 3.28). As the clusters possess several structural differences, several recombination events could have occurred to drive the evolution of the order of these clusters, which may explain their presence in such phylogenetically distant *Streptomyces*.

RDP4 has been used to apply algorithms to predict homologous recombination events between BGCs. Where previously it has been shown that several recombination

events could have occurred between the aurodox, kirromycin and bottromycin A2 cluster which lead to the formation of the aurodox BGC (McHugh, 2020). Future work in this study should employ RDP5 (Martin et al., 2021), or other recombination determining software as a means to evaluate the potential recombination and evolution between the BGCs, furthering understanding of BGC evolution within elfamycin producers. While many of these programmes have been designed for the detection of recombination in viruses, they have been employed in detecting recombination in BGCs (Booth et al., 2022)

7.5 Kirromycin, aurodox and its derivatives are capable of downregulation of the T3SS of EHEC

The deletion of genes and the creation of aurodox BGC mutants was carried out on the PAC pESAC13-A_AurI aurodox expression system in *S. coelicolor* M1152 (Fig. 4.1, 4.2, 4.10). It was predicted that the deletion of some of these genes in the BGC may result in the production of aurodox derivatives that may still have bioactivity. These derivatives, alongside kirromycin and aurodox, were tested to analyse the effect of these kirromycin-like elfamycin molecules of the T3SS of EHEC. Using GFP reporter fusion assays, it was shown that both aurodox and kirromycin can both downregulate the T3SS of EHEC (Fig. 4.18), something that was initially thought to be distinct to aurodox (McHugh, 2020; McHugh et al., 2019). The same was observed for the derivatives Aurl_ Δ aurM* and Aurl_ Δ aurAI, though to a lesser extent than kirromycin and aurodox, although this is likely a concentration effect (Fig 4.18). These data suggest that perhaps more kirromycin-like elfamycins may be capable of the downregulation of the T3SS as has been observed for aurodox. This is likely due to the emergence of more moonlighting functions for EF-Tu in terms of the bacterial cell such as adhesion and invasion of host cells, regulation of bacterial cell shape and

stimulation of immune responses by interacting with immune regulators increasing immune system evasion (Harvey et al., 2019; Widjaja et al., 2017).

During this study, another research group based in Kitasato University (Tokyo, Japan), were also investigating aurodox derivatives as potential T3SS inhibitors. Where our work saw biological derivatisation during the production of aurodox, their study synthesized derivatives chemically. In their study, 15 derivatives were synthesized, and structure–activity relationships were elucidated for each by comparing their antibacterial and T3SS inhibitory activities. The benzoyl derivative of aurodox (compound 13 in their study) was found as having the highest selectivity for T3SS inhibitory activity (69-fold selectivity), compared to the rest of their chemical derivatives (Kimishima et al., 2022). These support our findings that more kirromycin-like elfamycins, or derivatives of kirromycin-like elfamycins may be capable of the downregulation of the T3SS of aurodox. Collaboration has initiated with this research group to continue this investigation.

7.6 Cloning and overexpression of key aurodox biosynthesis genes

Key genes with unknown or hypothesised functions in aurodox biosynthesis were cloned into pET-21a(+) vectors for overexpression and eventual protein purification and enzymatic assay to evaluate function (Fig. 4.22, 4.23, 4.24). Unfortunately, this was only achievable for AurM* (Fig 4.28 – 4.31). Future work should complete the cloning of pET-21a(+)_AurHV to assess its function in aurodox biosynthesis, as currently this is unknown, even in its kirromycin homolog KirHV (McHugh et al., 2022; Weber et al., 2008).

Similarly, though, cloning and overexpression were successful, purification of AurQ and AurB was not performed. Though AurQ has no known function, making assay design difficult, the putative non-ribosomal peptide synthetase, AurB is thought to

catalyse the incorporation of β -alanine to the growing polyketide chain during aurodox biosynthesis. Evidence for this includes the role of its kirromycin homolog KirB as discovered during kirromycin biosynthesis (Laiple et al., 2009; Weber et al., 2008). These proteins could be purified, and assays designed to evaluate the function of these proposed biosynthesis enzymes.

7.7 Purification of AurM* and enzymatic characterisation

Purification of AurM* was carried out to assess a potential role as a methyltransferase (Fig 4.28 – 4.31). Genetic data to support this (McHugh et al., 2022) that showed expression of AurM* results in aurodox production in the kirromycin producer, *S. collinus*. This resulted in the prediction that AurM* catalyses the final reaction of aurodox biosynthesis. Unfortunately, enzymatic assays were unable to demonstrate AurM* could methylate authentic Kirromycin *in vitro* (Fig. 4.32 & 4.33). It is possible that methylation by AurM* is not the final step in Aurodox biosynthesis, and AurM* was able to act in concert with the kirromycin biosynthetic machinery, methylating the pyridone ring at an earlier stage of biosynthesis rather than at the last stage acting on kirromycin (McHugh et al., 2022). To confirm this, further optimisation of the methyltransferase assay would be required. The promiscuous nature of O-methyltransferases could then be exploited to produce novel kirromycin-like elfamycins such as ethylated and tetrazole variants using SAM analogues as was demonstrated by McKean et al., (2019).

7.8 EF-Tu copy number and elfamycin resistance profile varies among *Streptomyces*

Elfamycins target elongation factor EF-Tu and one mechanism of resistance is to have additional elfamycin resistant copies of EF-Tu (Prezioso et al., 2017). Investigation of EF-Tu copy number in *Streptomyces*, established that majority of strains harbour the kirromycin sensitive EF-Tu1, where some strains encoding the production of antibiotics that affect translation possess the kirromycin resistant EF-Tu3 in addition. The EF-Tu1 sequences were found to be much closer on the phylogenetic tree with branch lengths suggesting that these proteins are more highly conserved across the genera. This would indicate that purifying selection was acting upon these sequences constraining variation. In contrast, the elfamycin resistant EF-Tu were found to be much more divergent and phylogenetically distinct from the EF-Tu1 (Fig. 5.1). *S. ramocissimus* possesses genes encoding three EF-Tu proteins. Further work is required to decipher the exact nature and role of each EF-Tu in *S. ramocissimus*, but during fermentation of *S. ramocissimus* in kirromycin-producing conditions (Chapter 3), samples were taken every 12 hours. During their study, Vijgenboom et al., (1994) were unable to determine the exact point at which stage of kirromycin production each *tuf* gene was expressed. EF-Tu1 was always present under kirromycin production conditions in submerged and surface-grown cultures of *S. ramocissimus* and in germinating spores. The expression of *tuf2* and *tuf3* was, however, below the detection level. It was hypothesised that during fermentation, and kirromycin production, that different EF-Tu genes would be active. Unfortunately, due to time constraints this could not be explored further in this study, but if the work should continue reverse transcriptase-PCR experiments should be done to determine the onset of each of the EF-Tu1-3 expression.

Given multiple proteins encode a similar function within the cell, there is the potential that this functional redundancy may be an effect of duplicated targets for antibiotics. This functional redundancy is not new for essential genes within *Streptomyces* species, it was discovered that *Streptomyces* have two redundant copies of most glycolytic enzymes, and several other metabolic features in early diverging Actinobacteria (Chevrette et al., 2020). Here it was shown that expression of EF-Tu2 (resistant) within *Streptomyces* results in increased production of aurodox in the heterologous host *S. coelicolor* M1152, and that this aurodox product is still active against the T3SS of EHEC (Fig. 5.4, 5.5, 5.6).

7.9 EF-Tu reversed the T3S knockdown phenotype of Aurodox and Kirromycin and potentially plays a role in T3SSs in EHEC

When both EF-Tu2 (resistant) and EF-TuB (sensitive) were expressed in EHEC, this reversed the T3S knockdown phenotype of aurodox on the T3SS of EHEC, suggesting a role within the T3SS (Fig. 6.8 & 6.11). Analysis of the data obtained in this work supports the hypothesis of additional functionality (moonlighting) for EF-Tu related to T3S. The role is not fully elucidated but there is evidence that EF-Tu can act as a protein chaperone under certain conditions (Caldas et al., 1998). These data are the first experiment that suggests that additional function for EF-TU within T3S, such as chaperone activity, and may help to explain why many organisms, including enteric pathogens carry two copies of EF-Tu.

Further work is required to elucidate the full role of EF-Tu in T3S, further studies should be done such as harnessing the technology employed by Torres et al., (2020), immunogold electron microscopy, and in addition to tagging EF-Tu during the

analysis, T3S related proteins such as EspA could be tagged with an alternative size to find the localisation of these in respect to EF-Tu.

Chapter 8: Conclusions and Future Work

8.0 Conclusions and Future Work

This thesis sought to contribute to the understanding of kirromycin-like elfamycin biosynthesis and resistance mechanisms adopted by their producing strains. The study itself had three key aims.

The first aim was to determine the sequence of the kirromycin BGC from *S. ramocissimus*, with a view to expand the knowledge of kirromycin-like Elfamycin biosynthesis and evolution of related BGCs. Sequencing of the *S. ramocissimus* genome and analysis of the gene cluster responsible for kirromycin production allowed for the improved annotation of the kirromycin BGC from *S. collinus*. Additionally, the dissection of the cluster and comparison with other kirromycin-like BGCs allowed to infer function to genes involved in kirromycin and aurodox biosynthesis which had not previously been described. Several examples of gene duplication, gene displacement, and acquisition were identified and suggest evolution between these kirromycin-like elfamycin BGCs. Future work should see the assembly of *S. ramocissimus* genome improved by the addition of long read sequencing to reduce the number of contigs and facilitate a better understanding of the *S. ramocissimus* genome. Secondly, recombination between the kirromycin-like BGCs, and in turn, all elfamycin BGCs should be investigated to understand the enzyme evolution within elfamycin BGCs. This would further our understanding of enzyme evolution, not only within the elfamycins but within other BGCs too.

The second aim of the study was to dissect the biosynthesis of aurodox by finding roles for undefined key genes within the BGC through gene deletion and enzymatic characterisation. Though we did not manage to assign new function of aurodox biosynthesis genes based on enzymatic assay, our findings showed that aurodox derivatives were also capable of downregulation of the T3SS of EHEC, something which was planned to be investigated via targeted derivatisation should the

biosynthesis dissection reveal interesting roles for genes. Future work should continue on the purification of AurB, AurHV and AurQ, with enzymatic assays designed to allow for the confirmation or to assign function to these proteins in order to understand their role in aurodox biosynthesis. Further derivatisation of the aurodox/kirromycin molecule, either through collaboration with Kitasato University (Tokyo, Japan), or through similar method from our research group such as ethylated and tetrazole variants, should be done to improve aurodox T3SS downregulation furthering the strength of aurodox as an antivirulence candidate.

Finally, we sought to determine the immunity mechanisms used by kirromycin-like elfamycin producing strains and their effect on the antibiotic and anti-virulent activity. The true functions of EF-Tu1-3 in *S. ramocissimus*, and EF-Tu1 and EF-Tu2 in *S. goldiniensis*, should be investigated by reverse transcriptase-PCR experiments or RNA Seq during kirromycin-like elfamycin production to assign a function other than aiding in elfamycin resistance which was observed by increased aurodox production in the Aurl heterologous host.

Finally, the addition of both resistant (*tuf2*) and susceptible (*tufB*) to kirromycin Ef-Tu reversed the knockdown phenotype of kirromycin/Aurodox on the T3SS of EHEC, suggesting a never, before seen function of EF-Tu in T3S. Future work should continue to elucidate this role that EF-Tu has on the T3SS of EHEC, where immunogold electron microscopy of EF-Tu and T3S related proteins such as EspA in parallel could reveal the localisation of these proteins, potentially together.

Chapter 9: References

- Abel, K., Yoder, M.D., Hilgenfeld, R., Jurnak, F., 1996. An α to β conformational switch in EF-Tu. *Structure* 4, 1153–1159. [https://doi.org/10.1016/S0969-2126\(96\)00123-2](https://doi.org/10.1016/S0969-2126(96)00123-2)
- Abellan-Schneyder, I., Matchado, M.S., Reitmeier, S., Sommer, A., Sewald, Z., Baumbach, J., List, M., Neuhaus, K., 2021. Primer, Pipelines, Parameters: Issues in 16S rRNA Gene Sequencing. *mSphere* 6. <https://doi.org/10.1128/mSphere.01202-20>
- Abraham, E.P., Chain, E., 1988. An enzyme from bacteria able to destroy penicillin. 1940. *Rev. Infect. Dis.* 10, 677–678.
- Abutaleb, N.S., Seleem, M.N., 2020. Antivirulence activity of auranofin against vancomycin-resistant enterococci: in vitro and in vivo studies. *Int. J. Antimicrob. Agents* 55, 105828. <https://doi.org/10.1016/j.ijantimicag.2019.10.009>
- Akbarzadeh, A., Norouzian, D., Farhang, A., Mehrabi, M.R., Shafiei, M., Zare, D., Saffari, Z., Mortazavi, M., Mardaneh, M., Nemati, Z., 2007. Mutation of *Streptomyces griseoflavus* in order to obtain high yield desferrioxamine producing fused cells. *Pak. J. Biol. Sci. PJS* 10, 4527–4530. <https://doi.org/10.3923/pjbs.2007.4527.4530>
- Al-Abri, S.S., Beeching, N.J., Nye, F.J., 2005. Traveller's diarrhoea. *Lancet Infect. Dis.* 5, 349–360. [https://doi.org/10.1016/S1473-3099\(05\)70139-0](https://doi.org/10.1016/S1473-3099(05)70139-0)
- Alanjary, M., Kronmiller, B., Adamek, M., Blin, K., Weber, T., Huson, D., Philmus, B., Ziemert, N., 2017. The Antibiotic Resistant Target Seeker (ARTS), an exploration engine for antibiotic cluster prioritization and novel drug target discovery. *Nucleic Acids Res.* 45, W42–W48. <https://doi.org/10.1093/nar/gkx360>
- Alanjary, M., Steinke, K., Ziemert, N., 2019. AutoMLST: An automated web server for generating multi-locus species trees highlighting natural product potential. *Nucleic Acids Res.* 47, W276–W282. <https://doi.org/10.1093/nar/gkz282>
- Alberti, F., Corre, C., 2019. Editing streptomycete genomes in the CRISPR/Cas9 age. *Nat. Prod. Rep.* 36, 1237–1248. <https://doi.org/10.1039/c8np00081f>
- Aldred, K.J., Kerns, R.J., Osherooff, N., 2014. Mechanism of Quinolone Action and Resistance. *Biochemistry* 53, 1565–1574. <https://doi.org/10.1021/bi5000564>
- Allen, R.C., Popat, R., Diggle, S.P., Brown, S.P., 2014. Targeting virulence: Can we make evolution-proof drugs? *Nat. Rev. Microbiol.* 12, 300–308. <https://doi.org/10.1038/nrmicro3232>
- Allocati, N., Masulli, M., Alexeyev, M.F., Di Ilio, C., 2013. *Escherichia coli* in Europe: An overview. *Int. J. Environ. Res. Public Health* 10, 6235–6254. <https://doi.org/10.3390/ijerph10126235>
- Almabruk, K.H., Dinh, L.K., Philmus, B., 2018. Self-Resistance of Natural Product Producers: Past, Present, and Future Focusing on Self-Resistant Protein Variants. *ACS Chem. Biol.* 13, 1426–1437. <https://doi.org/10.1021/acscchembio.8b00173>
- Almagro Armenteros, J.J., Tsirigos, K.D., Sønderby, C.K., Petersen, T.N., Winther, O., Brunak, S., von Heijne, G., Nielsen, H., 2019. SignalP 5.0 improves signal peptide predictions using

deep neural networks. *Nat. Biotechnol.* 37, 420–423. <https://doi.org/10.1038/s41587-019-0036-z>

Altschul, S.F., Gish, W., Miller, W., Myers, E.W., Lipman, D.J., 1990. Basic local alignment search tool. *J. Mol. Biol.* [https://doi.org/10.1016/S0022-2836\(05\)80360-2](https://doi.org/10.1016/S0022-2836(05)80360-2)

Aminov, R., 2017. History of antimicrobial drug discovery: Major classes and health impact. *Biochem. Pharmacol.* 133, 4–19. <https://doi.org/10.1016/j.bcp.2016.10.001>

Aoki, Y., Matsumoto, D., Kawaide, H., Natsume, M., 2011. Physiological role of germicidins in spore germination and hyphal elongation in *Streptomyces coelicolor* A3(2). *J. Antibiot. (Tokyo)* 64, 607–611. <https://doi.org/10.1038/ja.2011.59>

Assmann, D., Wolf, H., 1979. Pulvomycin, an inhibitor of prokaryotic protein biosynthesis. *Arch. Microbiol.* 120, 297–299. <https://doi.org/10.1007/BF00423079>

Baba, T., Ara, T., Hasegawa, M., Takai, Y., Okumura, Y., Baba, M., Datsenko, K.A., Tomita, M., Wanner, B.L., Mori, H., 2006. Construction of *Escherichia coli* K-12 in-frame, single-gene knockout mutants: The Keio collection. *Mol. Syst. Biol.* 2. <https://doi.org/10.1038/msb4100050>

Baltz, R.H., 2017. Gifted microbes for genome mining and natural product discovery. *J. Ind. Microbiol. Biotechnol.* 44, 573–588. <https://doi.org/10.1007/s10295-016-1815-x>

Baltz, R.H., 2014. Model for Synthetic Biology To Accelerate the Evolution of Secondary Metabolite Biosynthetic Pathways. *ACS Synth. Biol.* 3, 748–758.

Baltz, R.H., 2010. *Streptomyces* and *Saccharopolyspora* hosts for heterologous expression of secondary metabolite gene clusters. *J. Ind. Microbiol. Biotechnol.* 37, 759–772. <https://doi.org/10.1007/s10295-010-0730-9>

Baneyx, F., Mujacic, M., 2004. Recombinant protein folding and misfolding in *Escherichia coli*. *Nat. Biotechnol.* 22, 1399–1408. <https://doi.org/10.1038/nbt1029>

Barajas, J.F., McAndrew, R.P., Thompson, M.G., Backman, T.W.H., Pang, B., de Rond, T., Pereira, J.H., Benites, V.T., Martín, H.G., Baidoo, E.E.K., Hillson, N.J., Adams, P.D., Keasling, J.D., 2019. Structural insights into dehydratase substrate selection for the borrelidin and fluvirucin polyketide synthases. *J. Ind. Microbiol. Biotechnol.* 46, 1225–1235. <https://doi.org/10.1007/s10295-019-02189-z>

Baran, A., Kwiatkowska, A., Potocki, L., 2023. Antibiotics and Bacterial Resistance-A Short Story of an Endless Arms Race. *Int. J. Mol. Sci.* 24, 5777. <https://doi.org/10.3390/ijms24065777>

Barke, J., Seipke, R.F., Grünschow, S., Heavens, D., Drou, N., Bibb, M.J., Goss, R.J., Yu, D.W., Hutchings, M.I., 2010. A mixed community of actinomycetes produce multiple antibiotics for the fungus farming ant *Acromyrmex octospinosus*. *BMC Biol.* 8, 109. <https://doi.org/10.1186/1741-7007-8-109>

Barona-Gómez, F., Chevrette, M.G., Hoskisson, P.A., 2023. On the evolution of natural product biosynthesis, in: *Advances in Microbial Physiology*. Academic Press. <https://doi.org/10.1016/bs.ampbs.2023.05.001>

- Barreales, E.G., Rumbero, Á., Payero, T.D., de Pedro, A., Jambrina, E., Aparicio, J.F., 2020. Structural and bioactivity characterization of filipin derivatives from engineered streptomyces filipinensis strains reveals clues for reduced haemolytic action. *Antibiotics* 9, 1–11. <https://doi.org/10.3390/antibiotics9070413>
- Batey, S.F.D., Greco, C., Hutchings, M.I., Wilkinson, B., 2020. Chemical warfare between fungus-growing ants and their pathogens. *Curr. Opin. Chem. Biol.* 59, 172–181. <https://doi.org/10.1016/j.cbpa.2020.08.001>
- Baunach, M., Chowdhury, S., Stallforth, P., Dittmann, E., 2021. The Landscape of Recombination Events That Create Nonribosomal Peptide Diversity. *Mol. Biol. Evol.* 1–15. <https://doi.org/10.1093/molbev/msab015>
- Beckham, K.S.H., Roe, A.J., 2014. From screen to target: Insights and approaches for the development of anti-virulence compounds. *Front. Cell. Infect. Microbiol.* 4, 1–8. <https://doi.org/10.3389/fcimb.2014.00139>
- Belknap, K.C., Park, C.J., Barth, B.M., Andam, C.P., 2020. Genome mining of biosynthetic and chemotherapeutic gene clusters in *Streptomyces* bacteria. *Sci. Rep.* 10, 1–9. <https://doi.org/10.1038/s41598-020-58904-9>
- Bender, K.S., Buckley, D.H., Madigan, M.T., Martinko, J.M., Stahl, D.A., 2015. Brock Biology of Microorganisms, in: Brock Biology of Microorganisms. Pearson, United Kingdom, pp. 252–258.
- Bentley, R., Meganathan, R., 1982. Biosynthesis of vitamin K (menaquinone) in bacteria. *Microbiol. Rev.* 46, 241–280. <https://doi.org/10.1128/mr.46.3.241-280.1982>
- Berchtold, H., Reshetnikova, L., Reiser, C.O.A., Schirmer, N.K., Sprinzl, M., Hilgenfeld, R., 1993. Erratum: Crystal structure of active elongation factor Tu reveals major domain rearrangements (*Nature* (1993) 365 (126-132)). *Nature* 365, 368. <https://doi.org/10.1038/365368a0>
- Bérdy, J., 2005. Bioactive Microbial Metabolites. *J. Antibiot. (Tokyo)* 58, 1–26.
- Berger, J., Lehr, H.H., Teitel, S., Maehr, H., Grunberg, E., 1973. A new antibiotic X-5108 of streptomyces origin: I. Production, isolation and properties. *J. Antibiot. (Tokyo)* 26, 15–22. <https://doi.org/10.7164/antibiotics.26.15>
- Berks, B.C., 1996. A common export pathway for proteins binding complex redox cofactors? *Mol. Microbiol.* 22, 393–404. <https://doi.org/10.1046/j.1365-2958.1996.00114.x>
- Biliński, P., Kapka-Skrzypczak, L., Posobkiewicz, M., Bondaryk, M., Hołownia, P., Wojtyła, A., 2012. Public health hazards in Poland posed by foodstuffs contaminated with *E. coli* O104:H4 bacterium from the recent European outbreak. *Ann. Agric. Environ. Med.* 19, 3–10.
- Bingle, L.E.H., Constantinidou, C., Shaw, R.K., Islam, M.S., Patel, M., Snyder, L.A.S., Lee, D.J., Penn, C.W., Busby, S.J.W., Pallen, M.J., 2014. Microarray analysis of the Ler regulon in enteropathogenic and enterohaemorrhagic *Escherichia coli* strains. *PLoS ONE* 9, 1–12. <https://doi.org/10.1371/journal.pone.0080160>

- Bittrich, S., Segura, J., Duarte, J.M., Burley, S.K., Rose, Y., 2024. RCSB protein Data Bank: exploring protein 3D similarities via comprehensive structural alignments. *Bioinformatics* 40, btae370. <https://doi.org/10.1093/bioinformatics/btae370>
- Bizuye, A., Moges, F., Andualem, B., 2013. Isolation and screening of antibiotic producing actinomycetes from soils in Gondar town, North West Ethiopia. *Asian Pac. J. Trop. Dis.* 3, 375–381. [https://doi.org/10.1016/S2222-1808\(13\)60087-0](https://doi.org/10.1016/S2222-1808(13)60087-0)
- Blair, J.M.A., Richmond, G.E., Piddock, L.J.V., 2014. Multidrug efflux pumps in Gram-negative bacteria and their role in antibiotic resistance. *Future Microbiol.* 9, 1165–1177. <https://doi.org/10.2217/fmb.14.66>
- Blair, J.M.A., Webber, M.A., Baylay, A.J., Ogbolu, D.O., Piddock, L.J.V., 2015. Molecular mechanisms of antibiotic resistance. *Nat. Rev. Microbiol.* 13, 42–51. <https://doi.org/10.1038/nrmicro3380>
- Blanco, P., Hernando-Amado, S., Reales-Calderon, J., Corona, F., Lira, F., Alcalde-Rico, M., Bernardini, A., Sanchez, M., Martinez, J., 2016. Bacterial Multidrug Efflux Pumps: Much More Than Antibiotic Resistance Determinants. *Microorganisms* 4, 14. <https://doi.org/10.3390/microorganisms4010014>
- Blattner, F.R., Plunkett, G., Bloch, C.A., Perna, N.T., Burland, V., Riley, M., Collado-Vides, J., Glasner, J.D., Rode, C.K., Mayhew, G.F., Gregor, J., Davis, N.W., Kirkpatrick, H.A., Goeden, M.A., Rose, D.J., Mau, B., Shao, Y., 1997. The Complete Genome Sequence of *Escherichia coli* K-12.
- Blin, K., Shaw, S., Kloosterman, A.M., Charlop-Powers, Z., van Wezel, G.P., Medema, M.H., Weber, T., 2021. antiSMASH 6.0: improving cluster detection and comparison capabilities. *Nucleic Acids Res.* 49, W29–W35. <https://doi.org/10.1093/nar/gkab335>
- Blin, K., Shaw, S., Steinke, K., Villebro, R., Ziemert, N., Lee, S.Y., Medema, M.H., Weber, T., 2019. AntiSMASH 5.0: Updates to the secondary metabolite genome mining pipeline. *Nucleic Acids Res.* 47, W81–W87. <https://doi.org/10.1093/nar/gkz310>
- Böhnlein, C., Kabisch, J., Meske, D., Franz, C.M.A.P., Pichner, R., 2016. Fitness of Enterohemorrhagic *Escherichia coli* (EHEC)/Enteroaggregative *E. coli* O104:H4 in Comparison to That of EHEC O157: Survival Studies in Food and In Vitro. *Appl. Environ. Microbiol.* 82, 6326–6334. <https://doi.org/10.1128/AEM.01796-16>
- Bolotin, E., Melamed, D., Livnat, A., 2023. Genes that are Used Together are More Likely to be Fused Together in Evolution by Mutational Mechanisms: A Bioinformatic Test of the Used-Fused Hypothesis. *Evol. Biol.* 50, 30–55. <https://doi.org/10.1007/s11692-022-09579-9>
- Bonacorsi, S., Bingen, E., 2005. Molecular epidemiology of *Escherichia coli* causing neonatal meningitis. *Int. J. Med. Microbiol.* 295, 373–381. <https://doi.org/10.1016/j.ijmm.2005.07.011>
- Booth, T.J., Bozhüyük, K.A.J., Liston, J.D., Batey, S.F.D., Lacey, E., Wilkinson, B., 2022. Bifurcation drives the evolution of assembly-line biosynthesis. *Nat. Commun.* 13, 3498. <https://doi.org/10.1038/s41467-022-30950-z>

- Bosi, E., Donati, B., Galardini, M., Brunetti, S., Sagot, M.F., Lió, P., Crescenzi, P., Fani, R., Fondi, M., 2015. MeDuSa: A multi-draft based scaffolder. *Bioinformatics* 31, 2443–2451. <https://doi.org/10.1093/bioinformatics/btv171>
- Brady, S.F., Li, L., MacIntyre, L.W., Ali, T., Russo, R., Koirala, B., Hernandez, Y., 2021. Biosynthetic interrogation of soil metagenomes reveals metamarin, an uncommon cyclomarin congener with activity against mycobacterium tuberculosis. *J. Nat. Prod.* <https://doi.org/10.1021/acs.jnatprod.0c01104>
- Brötz, E., Kulik, A., Vikineswary, S., Lim, C.-T., Tan, G.Y.A., Zinecker, H., Imhoff, J.F., Paululat, T., Fiedler, H.-P., 2011. Phenelfamycins G and H, new elfamycin-type antibiotics produced by *Streptomyces albospinus* Acta 3619. *J. Antibiot. (Tokyo)* 64, 257–266. <https://doi.org/10.1038/ja.2010.170>
- Bull, A.T., Asenjo, J.A., Goodfellow, M., Gómez-Silva, B., 2016. The Atacama Desert: Technical Resources and the Growing Importance of Novel Microbial Diversity. *Annu. Rev. Microbiol.* 70, 215–234. <https://doi.org/10.1146/annurev-micro-102215-095236>
- Busarakam, K., Bull, A.T., Girard, G., Labeda, D.P., Van Wezel, G.P., Goodfellow, M., 2014. *Streptomyces leeuwenhoekii* sp. nov., the producer of chaxalactins and chaxamycins, forms a distinct branch in *Streptomyces* gene trees. *Antonie Van Leeuwenhoek Int. J. Gen. Mol. Microbiol.* 105, 849–861. <https://doi.org/10.1007/s10482-014-0139-y>
- Bush, M.J., Tschowri, N., Schlimpert, S., Flärdh, K., Buttner, M.J., 2015. C-di-GMP signalling and the regulation of developmental transitions in streptomycetes. *Nat. Rev. Microbiol.* 13, 749–760. <https://doi.org/10.1038/nrmicro3546>
- Cafaro, M.J., Poulsen, M., Little, A.E.F., Price, S.L., Gerardo, N.M., Wong, B., Stuart, A.E., Larget, B., Abbot, P., Currie, C.R., 2010. Specificity in the symbiotic association between fungus-growing ants and protective *Pseudonocardia* bacteria. *Proc. R. Soc. B Biol. Sci.* 278, 1814–1822. <https://doi.org/10.1098/rspb.2010.2118>
- Caldas, T.D., Yaagoubi, A.E., Richarme, G., 1998. Chaperone Properties of Bacterial Elongation Factor EF-Tu *. *J. Biol. Chem.* 273, 11478–11482. <https://doi.org/10.1074/jbc.273.19.11478>
- Calvert, M.B., Jumde, V.R., Titz, A., 2018. Pathoblockers or antivirulence drugs as a new option for the treatment of bacterial infections. *Beilstein J. Org. Chem.* 14, 2607–2617. <https://doi.org/10.3762/bjoc.14.239>
- Campbell, E.A., Korzheva, N., Mustaev, A., Murakami, K., Nair, S., Goldfarb, A., Darst, S.A., 2001. Structural mechanism for rifampicin inhibition of bacterial rna polymerase. *Cell* 104, 901–912. [https://doi.org/10.1016/s0092-8674\(01\)00286-0](https://doi.org/10.1016/s0092-8674(01)00286-0)
- Cappellano, C., Monti, F., Sosio, M., Donadio, S., Sarubbi, E., 1997. Natural kirromycin resistance of elongation factor Tu from the kirrothricin producer *Streptomyces cinnamoneus*. *Microbiology* 143, 617.
- Cegelski, L., Marshall, G.R., Eldridge, G.R., Hultgren, S.J., 2008. The biology and future prospects of antivirulence therapies. *Nat. Rev. Microbiol.* 6, 17–27.

- Champness, W.C., 1988. New loci required for *Streptomyces coelicolor* morphological and physiological differentiation. *J. Bacteriol.* 170, 1168–1174.
<https://doi.org/10.1128/jb.170.3.1168-1174.1988>
- Chase-Topping, M.E., McKendrick, I.J., Pearce, M.C., MacDonald, P., Matthews, L., Halliday, J., Allison, L., Fenlon, D., Low, J.C., Gunn, G., Woolhouse, M.E.J., 2007. Risk factors for the presence of high-level shedders of *Escherichia coli* O157 on Scottish farms. *J. Clin. Microbiol.* 45, 1594–1603. <https://doi.org/10.1128/JCM.01690-06>
- Chater, K.F., 1972. A Morphological and Genetic Mapping Study of White Colony Mutants of *Streptomyces coelicolor*, *Journal of General Microbiology*.
- Chater, K.F., Chandra, G., 2006. The evolution of development in *Streptomyces* analysed by genome comparisons. *FEMS Microbiol. Rev.* 30, 651–672. <https://doi.org/10.1111/j.1574-6976.2006.00033.x>
- Chen, I., Christie, P.J., Dubnau, D., 2005. The Ins and Outs of DNA Transfer in Bacteria. *Science* 310, 1456–1460. <https://doi.org/10.1126/science.1114021>
- Chevrette, M.G., Gutiérrez-García, K., Selem-Mojica, N., Aguilar-Martínez, C., Yañez-Olvera, A., Ramos-Aboites, H.E., Hoskisson, P.A., Barona-Gómez, F., 2020a. Evolutionary dynamics of natural product biosynthesis in bacteria. *Nat. Prod. Rep.* 37, 566–599.
<https://doi.org/10.1039/c9np00048h>
- Chevrette, M.G., Hoskisson, P.A., Barona-Gómez, F., 2020b. Enzyme Evolution in Secondary Metabolism, *Comprehensive Natural Products III*. Elsevier Inc.
<https://doi.org/10.1016/b978-0-12-409547-2.14712-2>
- Cieza, R.J., Hu, J., Ross, B.N., Sbrana, E., Torres, A.G., 2015. The IbeA Invasin of Adherent-Invasive *Escherichia coli* Mediates Interaction with Intestinal Epithelia and Macrophages. *Infect. Immun.* 83, 1904–1918. <https://doi.org/10.1128/IAI.03003-14>
- Cimermancic, P., Medema, M.H., Claesen, J., Kurita, K., Wieland Brown, L.C., Mavrommatis, K., Pati, A., Godfrey, P.A., Koehrsen, M., Clardy, J., Birren, B.W., Takano, E., Sali, A., Lington, R.G., Fischbach, M.A., 2014. Insights into secondary metabolism from a global analysis of prokaryotic biosynthetic gene clusters. *Cell* 158, 412–421.
<https://doi.org/10.1016/j.cell.2014.06.034>
- Claessen, D., Rink, R., De Jong, W., Siebring, J., De Vreugd, P., Boersma, F.G.H., Dijkhuizen, L., Wösten, H.A.B., 2003. A novel class of secreted hydrophobic proteins is involved in aerial hyphae formation in *Streptomyces coelicolor* by forming amyloid-like fibrils. *Genes Dev.* 17, 1714–1726. <https://doi.org/10.1101/gad.264303>
- Clatworthy, A.E., Pierson, E., Hung, D.T., 2007. Targeting virulence: a new paradigm for antimicrobial therapy. *Nat. Chem. Biol.* 3, 541–548.
<https://doi.org/10.1038/nchembio.2007.24>
- Clokier, M.R., Millard, A.D., Letarov, A.V., Heaphy, S., 2011. Phages in nature. *Bacteriophage* 1, 31–45. <https://doi.org/10.4161/bact.1.1.14942>

- Coburn, B., Sekirov, I., Finlay, B.B., 2007. Type III Secretion Systems and Disease. *Clin. Microbiol. Rev.* 20, 535–549. <https://doi.org/10.1128/CMR.00013-07>
- Connell, S.R., Tracz, D.M., Nierhaus, K.H., Taylor, D.E., 2003. Ribosomal Protection Proteins and Their Mechanism of Tetracycline Resistance. *Antimicrob. Agents Chemother.* 47, 3675–3681. <https://doi.org/10.1128/AAC.47.12.3675-3681.2003>
- Corporation, P., 2009. Wizard(R) SV Gel and PCR Clean-Up System Quick Protocol 9281–9282.
- Costa, T.R.D., Felisberto-Rodrigues, C., Meir, A., Prevost, M.S., Redzej, A., Trokter, M., Waksman, G., 2015. Secretion systems in Gram-negative bacteria: structural and mechanistic insights. *Nat. Rev. Microbiol.* 13, 343. <https://doi.org/10.1038/nrmicro3456>
- Cottam, C., White, R.T., Beck, L.C., Stewart, C.J., Beatson, S.A., Lowe, E.C., Grinter, R., Connolly, J.P.R., 2024. Metabolism of l-arabinose converges with virulence regulation to promote enteric pathogen fitness. *Nat. Commun.* 15, 4462. <https://doi.org/10.1038/s41467-024-48933-7>
- Crits-Christoph, A., Diamond, S., Butterfield, C.N., Thomas, B.C., Banfield, J.F., 2018. Novel soil bacteria possess diverse genes for secondary metabolite biosynthesis. *Nature* 558, 440–444. <https://doi.org/10.1038/s41586-018-0207-y>
- Croes, K., Foulon, V., Casteels, M., Van Veldhoven, P.P., Mannaerts, G.P., 2000. Phytanoyl-CoA hydroxylase: recognition of 3-methyl-branched acyl-CoAs and requirement for GTP or ATP and Mg²⁺ in addition to its known hydroxylation cofactors. *J. Lipid Res.* 41, 629–636. [https://doi.org/10.1016/S0022-2275\(20\)32411-1](https://doi.org/10.1016/S0022-2275(20)32411-1)
- Crone, W.J.K., Leeper, F.J., Truman, A.W., 2012. Identification and characterisation of the gene cluster for the anti-MRSA antibiotic bottromycin: expanding the biosynthetic diversity of ribosomal peptides. *Chem. Sci.* 3, 3516–3521. <https://doi.org/10.1039/C2SC21190D>
- Cundliffe, E., 1989. How Antibiotic-Producing Organisms Avoid Suicide. *Annu. Rev. Microbiol.* 43, 207–233. <https://doi.org/10.1146/annurev.mi.43.100189.001231>
- Daer, R., Barrett, C.M., Melendez, E.L., Wu, J., Tekel, S.J., Xu, J., Dennison, B., Muller, R., Haynes, K.A., 2018. Characterization of diverse homoserine lactone synthases in *Escherichia coli*. *PLOS ONE* 13, e0202294. <https://doi.org/10.1371/journal.pone.0202294>
- Dallo, S.F., Kannan, T.R., Blaylock, M.W., Baseman, J.B., 2002. Elongation factor Tu and E1 β subunit of pyruvate dehydrogenase complex act as fibronectin binding proteins in *Mycoplasma pneumoniae*. *Mol. Microbiol.* 46, 1041–1051. <https://doi.org/10.1046/j.1365-2958.2002.03207.x>
- Datsenko, K.A., Wanner, B.L., 2000. One-step inactivation of chromosomal genes in *Escherichia coli* K-12 using PCR products. *Proc. Natl. Acad. Sci. U. S. A.* 97, 6640–6645. <https://doi.org/10.1073/pnas.120163297>
- Davies, J., 2013. Specialized microbial metabolites: functions and origins. *J. Antibiot. (Tokyo)* 66, 361–364. <https://doi.org/10.1038/ja.2013.61>

- Davies, J., Davies, D., 2010. Origins and Evolution of Antibiotic Resistance. *Microbiol. Mol. Biol. Rev.* MMBR 74, 417–433. <https://doi.org/10.1128/MMBR.00016-10>
- Davies, J., Ryan, K.S., 2012. Introducing the parvome: Bioactive compounds in the microbial world. *ACS Chem. Biol.* 7, 252–259. <https://doi.org/10.1021/cb200337h>
- D’Costa, V.M., King, C.E., Kalan, L., Morar, M., Sung, W.W.L., Schwarz, C., Froese, D., Zazula, G., Calmels, F., Debruyne, R., Golding, G.B., Poinar, H.N., Wright, G.D., 2011. Antibiotic resistance is ancient. *Nature* 477, 457–461. <https://doi.org/10.1038/nature10388>
- de Lima Procópio, R.E., da Silva, I.R., Martins, M.K., de Azevedo, J.L., de Araújo, J.M., 2012. Antibiotics produced by *Streptomyces*. *Braz. J. Infect. Dis.* 16, 466–471. <https://doi.org/10.1016/j.bjid.2012.08.014>
- Deng, W., Puente, J.L., Gruenheid, S., Li, Y., Vallance, B.A., Vázquez, A., Barba, J., Ibarra, J.A., O’Donnell, P., Metalnikov, P., Ashman, K., Lee, S., Goode, D., Pawson, T., Finlay, B.B., 2004. Dissecting virulence: Systematic and functional analyses of a pathogenicity island. *Proc. Natl. Acad. Sci. U. S. A.* 101, 3597–3602. <https://doi.org/10.1073/pnas.0400326101>
- Dewey, R.S., Arison, B.H., Hannah, J., Shih, D.H., Albers-Schönberg, G., 1985. The structure of efrotomycin. *J. Antibiot. (Tokyo)* 38, 1691–1698. <https://doi.org/10.7164/antibiotics.38.1691>
- Dhar, S., Kumari, H., Balasubramanian, D., Mathee, K., 2018. Cell-wall recycling and synthesis in *Escherichia coli* and *Pseudomonas aeruginosa* - their role in the development of resistance. *J. Med. Microbiol.* 67, 1–21. <https://doi.org/10.1099/jmm.0.000636>
- Dror, B., Wang, Z., Brady, S.F., Jurkevitch, E., Cytryn, E., 2020. Elucidating the Diversity and Potential Function of Nonribosomal Peptide and Polyketide Biosynthetic Gene Clusters in the Root Microbiome. *mSystems* 5, 1–15. <https://doi.org/10.1128/msystems.00866-20>
- Du, Y.-L., Shen, X.-L., Yu, P., Bai, L.-Q., Li, Y.-Q., 2011. Gamma-Butyrolactone Regulatory System of *Streptomyces chattanoogensis* Links Nutrient Utilization, Metabolism, and Development. *Appl. Environ. Microbiol.* 77, 8415–8426. <https://doi.org/10.1128/AEM.05898-11>
- Dubnau, D., 1999. DNA Uptake in Bacteria. *Annu. Rev. Microbiol.* 53, 217–244. <https://doi.org/10.1146/annurev.micro.53.1.217>
- Dubnau, D., Blokesch, M., 2019. Mechanisms of DNA Uptake by Naturally Competent Bacteria. *Annu. Rev. Genet.* 53, 217–237. <https://doi.org/10.1146/annurev-genet-112618-043641>
- Duncan, K.R., Haltli, B., Gill, K.A., Correa, H., Berru  , F., Kerr, R.G., 2015. Exploring the diversity and metabolic potential of actinomycetes from temperate marine sediments from Newfoundland, Canada. *J. Ind. Microbiol. Biotechnol.* 42, 57–72. <https://doi.org/10.1007/s10295-014-1529-x>
- Dunne, K.A., Chaudhuri, R.R., Rossiter, A.E., Beriotto, I., Browning, D.F., Squire, D., Cunningham, A.F., Cole, J.A., Loman, N., Henderson, I.R., 2017. Sequencing a piece of

- history: Complete genome sequence of the original *Escherichia coli* strain. *Microb. Genomics* 3. <https://doi.org/10.1099/mgen.0.000106>
- Eddy, S.R., 2004. What is a hidden Markov model? *Nat. Biotechnol.* 22, 1315–1316. <https://doi.org/10.1038/nbt1004-1315>
- Edison, L.K., Dan, V.M., R, R.S., S, P.N., 2020. A Strategic Production Improvement of *Streptomyces* Beta Glucanase Enzymes with Aid of Codon Optimization and Heterologous Expression. *Biosci. Biotechnol. Res. Asia* 17, 587–599. <https://doi.org/10.13005/bbra/2862>
- Elliot, M., Damji, F., Passantino, R., Chater, K., Leskiw, B., 1998. The *bldD* gene of *Streptomyces coelicolor* A3(2): A regulatory gene involved in morphogenesis and antibiotic production. *J. Bacteriol.* 180, 1549–1555. <https://doi.org/10.1128/jb.180.6.1549-1555.1998>
- Elliot, M.A., Bibb, M.J., Buttner, M.J., Leskiw, B.K., 2001. *BldD* is a direct regulator of key developmental genes in *Streptomyces coelicolor* A3(2). *Mol. Microbiol.* 40, 257–269. <https://doi.org/10.1046/j.1365-2958.2001.02387.x>
- Elliot, M.A., Karoonuthaisiri, N., Huang, J., Bibb, M.J., Cohen, S.N., Kao, C.M., Buttner, M.J., 2003. The chaplins: A family of hydrophobic cell-surface proteins involved in aerial mycelium formation in *Streptomyces coelicolor*. *Genes Dev.* 17, 1727–1740. <https://doi.org/10.1101/gad.264403>
- Fani, R., Brilli, M., Fondi, M., Lió, P., 2007. The role of gene fusions in the evolution of metabolic pathways: the histidine biosynthesis case. *BMC Evol. Biol.* 7 Suppl 2, S4. <https://doi.org/10.1186/1471-2148-7-S2-S4>
- Feeney, M.A., Newitt, J.T., Addington, E., Algora-Gallardo, L., Allan, C., Balis, L., Birke, A.S., Castaño-Espriu, L., Charkoudian, L.K., Devine, R., Gayard, D., Hamilton, J., Hennrich, O., Hoskisson, P.A., Keith-Baker, M., Klein, J.G., Kruasuwana, W., Mark, D.R., Mast, Y., McHugh, R.E., McLean, T.C., Mohit, E., Munnoch, J.T., Murray, J., Noble, K., Otani, H., Parra, J., Pereira, C.F., Perry, L., Pintor-Escobar, L., Pritchard, L., Prudence, S.M.M., Russell, A.H., Schniete, J.K., Seipke, R.F., Sélem-Mojica, N., Undabarrena, A., Vind, K., van Wezel, G.P., Wilkinson, B., Worsley, S.F., Duncan, K.R., Fernández-Martínez, L.T., Hutchings, M.I., 2022. ActinoBase: tools and protocols for researchers working on *Streptomyces* and other filamentous actinobacteria. *Microb. Genomics* 8. <https://doi.org/10.1099/mgen.0.000824>
- Ferens, W.A., Hovde, C.J., 2011. *Escherichia coli* O157:H7: Animal reservoir and sources of human infection. *Foodborne Pathog. Dis.* 8, 465–487. <https://doi.org/10.1089/fpd.2010.0673>
- Fondi, M., Emiliani, G., Fani, R., 2009. Origin and evolution of operons and metabolic pathways. *Res. Microbiol., Special issue on the origin of life and microbiology* 160, 502–512. <https://doi.org/10.1016/j.resmic.2009.05.001>
- Forterre, P., 1999. Displacement of cellular proteins by functional analogues from plasmids or viruses could explain puzzling phylogenies of many DNA informational proteins. *Mol. Microbiol.* 33, 457–465. <https://doi.org/10.1046/j.1365-2958.1999.01497.x>
- Friedmann, H.C., 2006. *Escherich* and *Escherichia*. *EcoSal Plus* 6. <https://doi.org/10.1128/ecosalplus.esp-0025-2013>

Fuchs, S., Mühldorfer, I., Donohue-Rolfe, A., Kerényi, M., Emödy, L., Alexiev, R., Nenkov, P., Hacker, J., 1999. Influence of RecA on in vivo virulence and Shiga toxin 2 production in *Escherichia coli* pathogens. *Microb. Pathog.* 27, 13–23.
<https://doi.org/10.1006/mpat.1999.0279>

Fuhrman, J.A., Cram, J.A., Needham, D.M., 2015. Marine microbial community dynamics and their ecological interpretation. *Nat. Rev. Microbiol.* 13, 133–146.
<https://doi.org/10.1038/nrmicro3417>

Gambushe, S.M., Zishiri, O.T., El Zowalaty, M.E., 2022. Review of *Escherichia coli* O157:H7 Prevalence, Pathogenicity, Heavy Metal and Antimicrobial Resistance, African Perspective. *Infect. Drug Resist.* 15, 4645–4673. <https://doi.org/10.2147/IDR.S365269>

Gaschignard, J., Levy, C., Romain, O., Cohen, R., Bingen, E., Aujard, Y., Boileau, P., 2011. Neonatal Bacterial Meningitis: 444 Cases in 7 Years. *Pediatr. Infect. Dis. J.* 30, 212–217.
<https://doi.org/10.1097/inf.0b013e3181fab1e7>

Gawin, A., Valla, S., Brautaset, T., 2017. The XylS/Pm regulator/promoter system and its use in fundamental studies of bacterial gene expression, recombinant protein production and metabolic engineering. *Microb. Biotechnol.* 10, 702–718. <https://doi.org/10.1111/1751-7915.12701>

Gebreyohannes, G., Moges, F., Sahile, S., Raja, N., 2013. Isolation and characterization of potential antibiotic producing actinomycetes from water and sediments of Lake Tana, Ethiopia. *Asian Pac. J. Trop. Biomed.* 3, 426–435. [https://doi.org/10.1016/S2221-1691\(13\)60092-1](https://doi.org/10.1016/S2221-1691(13)60092-1)

Genilloud, O., 2017. Actinomycetes: Still a source of novel antibiotics. *Nat. Prod. Rep.* 34, 1203–1232. <https://doi.org/10.1039/c7np00026j>

Gerlach, R.G., Hensel, M., 2007. Protein secretion systems and adhesins: The molecular armory of Gram-negative pathogens. *Int. J. Med. Microbiol.* 297, 401–415.
<https://doi.org/10.1016/j.ijmm.2007.03.017>

Gilchrist, C.L.M., Chooi, Y.-H., 2021. clinker & clustermap.js: automatic generation of gene cluster comparison figures. *Bioinformatics* 37, 2473–2475.
<https://doi.org/10.1093/bioinformatics/btab007>

Gill, S., Catchpole, R., Forterre, P., 2019. Extracellular membrane vesicles in the three domains of life and beyond. *FEMS Microbiol. Rev.* 43, 273–303.
<https://doi.org/10.1093/femsre/fuy042>

Girard, F., Dziva, F., van Diemen, P., Phillips, A.D., Stevens, M.P., Frankel, G., 2007. Adherence of Enterohemorrhagic *Escherichia coli* O157, O26, and O111 Strains to Bovine Intestinal Explants Ex Vivo. *Appl. Environ. Microbiol.* 73, 3084–3090.
<https://doi.org/10.1128/AEM.02893-06>

Girard, G., Traag, B.A., Sangal, V., Mascini, N., Hoskisson, P.A., Goodfellow, M., Wezel, G.P.V., 2013. A novel taxonomic marker that discriminates between morphologically complex actinomycetes. *Open Biol.* 3, 130073.

- Glockner, C., Wolf, H., 1984. Mechanism of natural resistance to kirromycin-type antibiotics in actinomycetes. *FEMS Microbiol Lett* 25, 121.
- Goldwater, P.N., Bettelheim, K.A., 2012. Treatment of enterohemorrhagic *Escherichia coli* (EHEC) infection and hemolytic uremic syndrome (HUS). *BMC Med.* 10, 12. <https://doi.org/10.1186/1741-7015-10-12>
- Gomez-Escribano, J.P., Alt, S., Bibb, M.J., 2016. Next generation sequencing of actinobacteria for the discovery of novel natural products. *Mar. Drugs* 14, 6–8. <https://doi.org/10.3390/md14040078>
- Gomez-Escribano, J.P., Bibb, M.J., 2012. *Streptomyces coelicolor* as an expression host for heterologous gene clusters, *Methods in Enzymology*. Elsevier Inc. <https://doi.org/10.1016/B978-0-12-404634-4.00014-0>
- Gomez-Escribano, J.P., Bibb, M.J., 2011. Engineering *Streptomyces coelicolor* for heterologous expression of secondary metabolite gene clusters. *Microb. Biotechnol.* 4, 207–215. <https://doi.org/10.1111/j.1751-7915.2010.00219.x>
- Gomez-Escribano, J.P., Castro, J.F., Razmilic, V., Chandra, G., Andrews, B., Asenjo, J.A., Bibb, M.J., 2015. The *Streptomyces leeuwenhoekii* genome: De novo sequencing and assembly in single contigs of the chromosome, circular plasmid pSLE1 and linear plasmid pSLE2. *BMC Genomics* 16, 1–11. <https://doi.org/10.1186/s12864-015-1652-8>
- Goodfellow, M., 2015. Actinobacteria, in: *Bergey's Manual of Systematics of Archaea and Bacteria*. John Wiley & Sons, Ltd, pp. 1–2. <https://doi.org/10.1002/9781118960608.cbm00004>
- Goukulan, K., Khare, S., Cerniglia, C., 2014. METABOLIC PATHWAYS | Production of Secondary Metabolites of Bacteria.
- Graf, F.E., Palm, M., Warringer, J., Farewell, A., 2019. Inhibiting conjugation as a tool in the fight against antibiotic resistance. *Drug Dev. Res.* 80, 19–23. <https://doi.org/10.1002/ddr.21457>
- Grant, S.G.N., Jessee, J., Bloom, F.R., Hanahan, D., 1990. Differential plasmid rescue from transgenic mouse DNAs into *Escherichia coli* methylation-restriction mutants. *Proc. Natl. Acad. Sci. U. S. A.* 87, 4645–4649. <https://doi.org/10.1073/pnas.87.12.4645>
- Gregory, M.A., Till, R., Smith, M.C.M., 2003. Integration site for *Streptomyces* phage ϕ BT1 and development of site-specific integrating vectors. *J. Bacteriol.* 185, 5320–5323. <https://doi.org/10.1128/JB.185.17.5320-5323.2003>
- Gui, C., Li, Q., Mo, X., Qin, X., Ma, J., Ju, J., 2015. Discovery of a New Family of Dieckmann Cyclases Essential to Tetramic Acid and Pyridone-Based Natural Products Biosynthesis. *Org. Lett.* 17, 628–631. <https://doi.org/10.1021/ol5036497>
- Gullo, V.P., Zimmerman, S.B., Dewey, R.S., Hensens, O., Cassidy, P.J., Oiwa, R., Omura, S., 1982. Factumycin, a new antibiotic (A40A): fermentation, isolation and antibacterial spectrum. *J. Antibiot. (Tokyo)* 35, 1705–1707. <https://doi.org/10.7164/antibiotics.35.1705>

- Gullón, S., Olano, C., Abdelfattah, M.S., Braña, A.F., Rohr, J., Méndez, C., Salas, J.A., 2006. Isolation, Characterization, and Heterologous Expression of the Biosynthesis Gene Cluster for the Antitumor Anthracycline Steffimycin. *Appl. Environ. Microbiol.* 72, 4172–4183. <https://doi.org/10.1128/AEM.00734-06>
- Gurevich, A., Saveliev, V., Vyahhi, N., Tesler, G., 2013. QUAST: quality assessment tool for genome assemblies. *Bioinformatics* 29, 1072–1075. <https://doi.org/10.1093/bioinformatics/btt086>
- Gust, B., Challis, G.L., Fowler, K., Kieser, T., Chater, K.F., 2003. PCR-targeted *Streptomyces* gene replacement identifies a protein domain needed for biosynthesis of the sesquiterpene soil odor geosmin. *Proc. Natl. Acad. Sci.* 100, 1541–1546. <https://doi.org/10.1073/pnas.0337542100>
- Guzman, L.M., Belin, D., Carson, M.J., Beckwith, J., 1995. Tight regulation, modulation, and high-level expression by vectors containing the arabinose PBAD promoter. *J. Bacteriol.* 177, 4121–4130. <https://doi.org/10.1128/jb.177.14.4121-4130.1995>
- Guzmán-Chávez, F., Zwahlen, R.D., Bovenberg, R.A.L., Driessen, A.J.M., 2018. Engineering of the filamentous fungus *penicillium chrysogenum* as cell factory for natural products. *Front. Microbiol.* 9. <https://doi.org/10.3389/fmicb.2018.02768>
- Hall, C.C., Watkins, J.D., Georgopapadakou, N.H., 1989. Effects of elfamycins on elongation factor Tu from *Escherichia coli* and *Staphylococcus aureus*. *Antimicrob. Agents Chemother.* 33, 322–325. <https://doi.org/10.1128/AAC.33.3.322>
- Harvey, K.L., Jarocki, V.M., Charles, I.G., Djordjevic, S.P., 2019. The Diverse Functional Roles of Elongation Factor Tu (EF-Tu) in Microbial Pathogenesis. *Front. Microbiol.* 10.
- Hedge, D.D., Strain, J.D., Heins, J.R., Farver, D.K., 2008. New advances in the treatment of *Clostridium difficile* infection (CDI). *Ther. Clin. Risk Manag.* 4, 949–964.
- Hempel, A.M., Cantlay, S., Molle, V., Wang, S.B., Naldrett, M.J., Parker, J.L., Richards, D.M., Jung, Y.G., Buttner, M.J., Flärdh, K., 2012. The Ser/Thr protein kinase AfsK regulates polar growth and hyphal branching in the filamentous bacteria *Streptomyces*. *Proc. Natl. Acad. Sci. U. S. A.* 109. <https://doi.org/10.1073/pnas.1207409109>
- Heng, E., Tan, L.L., Tay, D.W.P., Lim, Y.H., Yang, L.-K., Seow, D.C.S., Leong, C.Y., Ng, V., Ng, S.B., Kanagasundaram, Y., Wong, F.T., Koduru, L., 2023. Cost-effective hybrid long-short read assembly delineates alternative GC-rich *Streptomyces* hosts for natural product discovery. *Synth. Syst. Biotechnol.* 8, 253–261. <https://doi.org/10.1016/j.synbio.2023.03.001>
- Herbert, L.J., Vali, L., Hoyle, D.V., Innocent, G., McKendrick, I.J., Pearce, M.C., Mellor, D., Porphyre, T., Locking, M., Allison, L., Hanson, M., Matthews, L., Gunn, G.J., Woolhouse, M.E.J., Chase-Topping, M.E., 2014. *E. coli* O157 on Scottish cattle farms: Evidence of local spread and persistence using repeat cross-sectional data. *BMC Vet. Res.* 10, 1–10. <https://doi.org/10.1186/1746-6148-10-95>

- Hernandes, R.T., Elias, W.P., Vieira, M.A.M., Gomes, T.A.T., 2009. An overview of atypical enteropathogenic *Escherichia coli*. *FEMS Microbiol. Lett.* 297, 137–149.
<https://doi.org/10.1111/j.1574-6968.2009.01664.x>
- Hews, C.L., Tran, S.-L., Wegmann, U., Brett, B., Walsham, A.D.S., Kavanaugh, D., Ward, N.J., Juge, N., Schüller, S., 2017. The StcE metalloprotease of enterohaemorrhagic *Escherichia coli* reduces the inner mucus layer and promotes adherence to human colonic epithelium ex vivo. *Cell. Microbiol.* 19, e12717. <https://doi.org/10.1111/cmi.12717>
- Hobbs, G., Frazer, C.M., Gardner, D.C.J., Cullum, J.A., Oliver, S.G., 1989. Dispersed growth of *Streptomyces* in liquid culture. *Appl. Microbiol. Biotechnol.* 31, 272–277.
<https://doi.org/10.1007/BF00258408>
- Hochlowski, J.E., Buytendorp, M.H., Whittern, D.N., Buko, A.M., Chen, R.H., McAlpine, J.B., 1988. Phenelfamycins, a novel complex of elfamycin-type antibiotics. II. Isolation and structure determination. *J Antibiot* 41, 1300.
- Hodgson, D.A., 2000. Primary Metabolism and it's Control in *Streptomyces*: A Most Unusual Group of Bacteria. *Adv. Microb. Physiol.*
- Hogg, T., Mesters, J.R., Hilgenfeld, R., 2002. Inhibitory mechanisms of antibiotics targeting elongation factor Tu. *Curr. Protein Pept. Sci.* 3, 121–131.
<https://doi.org/10.2174/1389203023380855>
- Hokisson, P.A., Seipke, R.F., 2020. Cryptic or Silent? The Known Unknowns, Unknown Knowns, and Unknown Unknowns of Secondary Metabolism. *mBio* 11, 1–6.
<https://doi.org/10.1128/mBio.02642-20>
- Homma, T., Nuxoll, A., Gandt, A.B., Ebner, P., Engels, I., Schneider, T., Götz, F., Lewis, K., Conlon, B.P., 2016. Dual targeting of cell wall precursors by teixobactin leads to cell lysis. *Antimicrob. Agents Chemother.* 60, 6510–6517. <https://doi.org/10.1128/AAC.01050-16>
- Hooper, D.C., 2002. Fluoroquinolone resistance among Gram-positive cocci. *Lancet Infect. Dis.* 2, 530–538. [https://doi.org/10.1016/s1473-3099\(02\)00369-9](https://doi.org/10.1016/s1473-3099(02)00369-9)
- Hoskisson, P.A., Fernández-Martínez, L.T., 2018. Regulation of specialised metabolites in *Actinobacteria* – expanding the paradigms. *Environ. Microbiol. Rep.* 10, 231–238.
<https://doi.org/10.1111/1758-2229.12629>
- Hoskisson, P.A., Hobbs, G., Sharples, G.P., 2001. Antibiotic production, accumulation of intracellular carbon reserves, and sporulation in *Micromonospora echinospora* (ATCC 15837). *Can. J. Microbiol.* 47, 148–152.
- Hotinger, J.A., Morris, S.T., May, A.E., 2021. The Case against Antibiotics and for Anti-Virulence Therapeutics. *Microorganisms* 9, 2049.
<https://doi.org/10.3390/microorganisms9102049>
- Huerta-Urbe, A., Marjenberg, Z.R., Yamaguchi, N., Fitzgerald, S., Connolly, J.P.R., Carpena, N., Uvell, H., Douce, G., Elofsson, M., Byron, O., Marquez, R., Gally, D.L., Roe, A.J., 2016. Identification and characterization of novel compounds blocking Shiga toxin expression in

- Escherichia coli O157:H7. *Front. Microbiol.* 7, 1–9.
<https://doi.org/10.3389/fmicb.2016.01930>
- Hughes, D., 1990. Both genes for EF-Tu in *Salmonella typhimurium* are individually dispensable for growth. *J. Mol. Biol.* 215, 41–51. [https://doi.org/10.1016/S0022-2836\(05\)80093-2](https://doi.org/10.1016/S0022-2836(05)80093-2)
- Hutchings, M., Truman, A., Wilkinson, B., 2019. Antibiotics: past, present and future. *Curr. Opin. Microbiol.* 51, 72–80. <https://doi.org/10.1016/j.mib.2019.10.008>
- Hwang, S., Lee, Y., Kim, J.H., Kim, G., Kim, H., Kim, W., Cho, S., Palsson, B.O., Cho, B.-K., 2021. *Streptomyces* as Microbial Chassis for Heterologous Protein Expression. *Front. Bioeng. Biotechnol.* 9, 804295. <https://doi.org/10.3389/fbioe.2021.804295>
- Ichikawa, N., Oguchi, A., Ikeda, H., Ishikawa, J., Kitani, S., Watanabe, Y., Nakamura, S., Katano, Y., Kishi, E., Sasagawa, M., Ankai, A., Fukui, S., Hashimoto, Y., Kamata, S., Otaguro, M., Tanikawa, S., Nihira, T., Horinouchi, S., Ohnishi, Y., Hayakawa, M., Kuzuyama, T., Arisawa, A., Nomoto, F., Miura, H., Takahashi, Y., Fujita, N., 2010. Genome Sequence of *Kitasatospora setae* NBRC 14216T: An Evolutionary Snapshot of the Family *Streptomycetaceae*. *DNA Res.* 17, 393–406. <https://doi.org/10.1093/dnares/dsq026>
- Iftime, D., Kulik, A., Härtner, T., Rohrer, S., Niedermeyer, T.H.J., Stegmann, E., Weber, T., Wohlleben, W., 2016. Identification and activation of novel biosynthetic gene clusters by genome mining in the kirromycin producer *Streptomyces collinus* Tü 365. *J. Ind. Microbiol. Biotechnol.* 43, 277–291. <https://doi.org/10.1007/s10295-015-1685-7>
- Iguchi, A., Thomson, N.R., Ogura, Y., Saunders, D., Ooka, T., Henderson, I.R., Harris, D., Asadulghani, M., Kurokawa, K., Dean, P., Kenny, B., Quail, M.A., Thurston, S., Dougan, G., Hayashi, T., Parkhill, J., Frankel, G., 2009. Complete genome sequence and comparative genome analysis of enteropathogenic *Escherichia coli* O127:H6 strain E2348/69. *J. Bacteriol.* 191, 347–354. <https://doi.org/10.1128/JB.01238-08>
- Ikeda, H., Shin-Ya, K., Omura, S., 2014. Genome mining of the *Streptomyces avermitilis* genome and development of genome-minimized hosts for heterologous expression of biosynthetic gene clusters. *J. Ind. Microbiol. Biotechnol.* 41, 233–250.
<https://doi.org/10.1007/s10295-013-1327-x>
- Imamovic, L., Muniesa, M., 2012. Characterizing RecA-independent induction of Shiga toxin2-encoding phages by EDTA treatment. *PLoS ONE* 7.
<https://doi.org/10.1371/journal.pone.0032393>
- Iqbal, H.A., Low-Beinart, L., Obiajulu, J.U., Brady, S.F., 2016. Natural Product Discovery through Improved Functional Metagenomics in *Streptomyces*. *J Am Chem Soc* 138, 9341–9344.
- Iyoda, S., Koizumi, N., Satou, H., Lu, Y., Saitoh, T., Ohnishi, M., Watanabe, H., 2006. The GrIR-GrIA regulatory system coordinately controls the expression of flagellar and LEE-encoded type III protein secretion systems in enterohemorrhagic *Escherichia coli*. *J. Bacteriol.* 188, 5682–5692. <https://doi.org/10.1128/JB.00352-06>

- Janardhan, A., Kumar, A.P., Viswanath, B., Saigopal, D.V.R., Narasimha, G., 2014. Production of Bioactive Compounds by Actinomycetes and Their Antioxidant Properties. *Biotechnol. Res. Int.* 2014, 217030. <https://doi.org/10.1155/2014/217030>
- Jarvis, K.G., Girón, J.A., Jerse, A.E., Mcdaniel, T.K., Donnenberg, M.S., Kaper, J.B., 1995. Enteropathogenic *Escherichia coli* contains a putative type III secretion system necessary for the export of proteins involved in attaching and effacing lesion formation. *Proc. Natl. Acad. Sci. U. S. A.* 92, 7996–8000. <https://doi.org/10.1073/pnas.92.17.7996>
- Ji, C.-H., Kim, H., Kang, H.-S., 2019. Synthetic Inducible Regulatory Systems Optimized for the Modulation of Secondary Metabolite Production in *Streptomyces*. *ACS Synth. Biol.* 8, 577–586. <https://doi.org/10.1021/acssynbio.9b00001>
- Ji, C.-H., Kim, J.-P., Kang, H.-S., 2018. Library of Synthetic *Streptomyces* Regulatory Sequences for Use in Promoter Engineering of Natural Product Biosynthetic Gene Clusters. *ACS Synth. Biol.* 7, 1946–1955. <https://doi.org/10.1021/acssynbio.8b00175>
- Johnson, C.M., Grossman, A.D., 2015. Integrative and Conjugative Elements (ICEs): What They Do and How They Work. *Annu. Rev. Genet.* 49, 577–601. <https://doi.org/10.1146/annurev-genet-112414-055018>
- Johnson, J.R., Stell, A.L., 2000. Extended Virulence Genotypes of *Escherichia coli* Strains from Patients with Urosepsis in Relation to Phylogeny and Host Compromise. *J. Infect. Dis.* 181, 261–272. <https://doi.org/10.1086/315217>
- Johnson, T.J., Kariyawasam, S., Wannemuehler, Y., Mangiamale, P., Johnson, S.J., Doetkott, C., Skyberg, J.A., Lynne, A.M., Johnson, J.R., Nolan, L.K., 2007. The Genome Sequence of Avian Pathogenic *Escherichia coli* Strain O1:K1:H7 Shares Strong Similarities with Human Extraintestinal Pathogenic *E. coli* Genomes. *J. Bacteriol.* 189, 3228–3236. <https://doi.org/10.1128/JB.01726-06>
- Jones, A.C., Gust, B., Kulik, A., Heide, L., Buttner, M.J., Bibb, M.J., 2013. Phage p1-derived artificial chromosomes facilitate heterologous expression of the FK506 gene cluster. *PloS One* 8, e69319. <https://doi.org/10.1371/journal.pone.0069319>
- Juárez-Rodríguez, M.M., Cortes-López, H., García-Contreras, R., González-Pedrajo, B., Díaz-Guerrero, M., Martínez-Vázquez, M., Rivera-Chávez, J.A., Soto-Hernández, R.M., Castillo-Juárez, I., 2020. Tetradecanoic Acids With Anti-Virulence Properties Increase the Pathogenicity of *Pseudomonas aeruginosa* in a Murine Cutaneous Infection Model. *Front. Cell. Infect. Microbiol.* 10, 597517. <https://doi.org/10.3389/fcimb.2020.597517>
- Kaltenpoth, M., 2009. Actinobacteria as mutualists: general healthcare for insects? *Trends Microbiol.* 17, 529–535. <https://doi.org/10.1016/j.tim.2009.09.006>
- Kang, H.-S., Kim, E.-S., 2021. Recent advances in heterologous expression of natural product biosynthetic gene clusters in *Streptomyces* hosts. *Curr. Opin. Biotechnol., Chemical Biotechnology • Pharmaceutical Biotechnology* 69, 118–127. <https://doi.org/10.1016/j.copbio.2020.12.016>
- Kaper, J.B., Nataro, J.P., Mobley, H.L.T., 2004. Pathogenic *Escherichia coli*. *Nat. Rev. Microbiol.* 2, 123–140. <https://doi.org/10.1038/nrmicro818>

- Karmali, M.A., 1989. Infection by verocytotoxin-producing *Escherichia coli*. *Clin. Microbiol. Rev.* 2, 15–38. <https://doi.org/10.1128/CMR.2.1.15>
- Kataoka, M., Ueda, K., Kudo, T., Seki, T., Yoshida, T., 1997. Application of the variable region in 16S rDNA to create an index for rapid species identification in the genus *Streptomyces*. *FEMS Microbiol. Lett.* 151, 249–255. <https://doi.org/10.1111/j.1574-6968.1997.tb12578.x>
- Kato, J., Funa, N., Watanabe, H., Ohnishi, Y., Horinouchi, S., 2007. Biosynthesis of gamma-butyrolactone autoregulators that switch on secondary metabolism and morphological development in *Streptomyces*. *Proc. Natl. Acad. Sci. U. S. A.* 104, 2378–2383. <https://doi.org/10.1073/pnas.0607472104>
- Katz, L., Baltz, R.H., 2016. Natural product discovery: past, present, and future. *J. Ind. Microbiol. Biotechnol.* 43, 155–176. <https://doi.org/10.1007/s10295-015-1723-5>
- Kautsar, S.A., van der Hooft, J.J.J., de Ridder, D., Medema, M.H., 2021. BiG-SLiCE: A highly scalable tool maps the diversity of 1.2 million biosynthetic gene clusters. *GigaScience* 10, giaa154. <https://doi.org/10.1093/gigascience/giaa154>
- Kawashima, T., Berthet-Colominas, C., Wulff, M., Cusack, S., Leberman, R., 1996. The structure of the *Escherichia coli* EF-Tu·EF-Ts complex at 2.5 Å resolution. *Nature* 379, 511–518. <https://doi.org/10.1038/379511a0>
- Keijser, B.J.F., Noens, E.E.E., Kraal, B., Koerten, H.K., van Wezel, G.P., 2003. The *Streptomyces coelicolor* *ssgB* gene is required for early stages of sporulation. *FEMS Microbiol. Lett.* 225, 59–67. [https://doi.org/10.1016/S0378-1097\(03\)00481-6](https://doi.org/10.1016/S0378-1097(03)00481-6)
- Kempf, A.J., Wilson, K.E., Hensens, O.D., Monaghan, R.L., Zimmerman, S.B., Dulaney, E.L., 1986. L-681,217, a new and novel member of the efrotomycin family of antibiotics. *J. Antibiot. (Tokyo)* 39, 1361–1367. <https://doi.org/10.7164/antibiotics.39.1361>
- Kettenring, J., Colombo, L., Ferrari, P., Tavecchia, P., Nebuloni, M., Vékey, K., Gallo, G.G., Selva, E., 1991. Antibiotic GE2270 a: a novel inhibitor of bacterial protein synthesis. II. Structure elucidation. *J. Antibiot. (Tokyo)* 44, 702–715. <https://doi.org/10.7164/antibiotics.44.702>
- Kiepas, A.B., Hoskisson, P.A., Pritchard, L., 2023. 16S rRNA phylogeny and clustering is not a reliable proxy for genome-based taxonomy in *Streptomyces*. <https://doi.org/10.1101/2023.08.15.553377>
- Kieser, T., Bibb, M., Chater, K., Butter, M., Hopwood, D., Bittner, M., Buttner, M., 2000. *Practical Streptomyces Genetics: A Laboratory Manual*.
- Kim, N.H., Cho, T.J., Rhee, M.S., 2017. Current Interventions for Controlling Pathogenic *Escherichia coli*. *Adv. Appl. Microbiol.* 100, 1–47. <https://doi.org/10.1016/bs.aambs.2017.02.001>
- Kimishima, A., Hagimoto, D., Honsho, M., Watanabe, Y., Iwatsuki, M., Tsutsumi, H., Inahashi, Y., Naher, K., Sakai, K., Kuwae, A., Abe, A., Asami, Y., 2022. Insights into the structure–activity relationship of a type III secretion system inhibitor, aurodox. *Bioorg. Med. Chem. Lett.* 69, 128779. <https://doi.org/10.1016/j.bmcl.2022.128779>

- Kimura, K., Iwatsuki, M., Nagai, T., Matsumoto, A., Takahashi, Y., Shiomi, K., Omura, S., Abe, A., 2011. A small-molecule inhibitor of the bacterial type III secretion system protects against in vivo infection with *Citrobacter rodentium*. *J. Antibiot. (Tokyo)* 64, 197–203. <https://doi.org/10.1038/ja.2010.155>
- Kitov, P.I., Sadowska, J.M., Mulvey, G., Armstrong, G.D., Ling, H., Pannu, N.S., Read, R.J., Bundle, D.R., 2000. Shiga-like toxins are neutralized by tailored multivalent carbohydrate ligands. *Nature* 403, 669–672. <https://doi.org/10.1038/35001095>
- Kleinteich, J., Hildebrand, F., Bahram, M., Voigt, A.Y., Wood, S.A., Jungblut, A.D., Küpper, F.C., Quesada, A., Camacho, A., Pearce, D.A., Convey, P., Vincent, W.F., Zarfl, C., Bork, P., Dietrich, D.R., 2017. Pole-to-Pole Connections: Similarities between Arctic and Antarctic Microbiomes and Their Vulnerability to Environmental Change. *Front. Ecol. Evol.* 5. <https://doi.org/10.3389/fevo.2017.00137>
- Kodani, S., Hudson, M.E., Durrant, M.C., Buttner, M.J., Nodwell, J.R., Willey, J.M., 2004. The SapB morphogen is a lantibiotic-like peptide derived from the product of the developmental gene *ramS* in *Streptomyces coelicolor*. *Proc. Natl. Acad. Sci. U. S. A.* 101, 11448–11453. <https://doi.org/10.1073/pnas.0404220101>
- Kodani, S., Lodato, M.A., Durrant, M.C., Picart, F., Willey, J.M., 2005. SapT, a lanthionine-containing peptide involved in aerial hyphae formation in the streptomycetes. *Mol. Microbiol.* 58, 1368–1380. <https://doi.org/10.1111/j.1365-2958.2005.04921.x>
- Kramer, J., Özkaya, Ö., Kümmerli, R., 2020. Bacterial siderophores in community and host interactions. *Nat. Rev. Microbiol.* 18, 152–163. <https://doi.org/10.1038/s41579-019-0284-4>
- Krause, J., Handayani, I., Blin, K., Kulik, A., Mast, Y., 2020. Disclosing the Potential of the SARP-Type Regulator PapR2 for the Activation of Antibiotic Gene Clusters in Streptomycetes. *Front. Microbiol.* 11, 1–17. <https://doi.org/10.3389/fmicb.2020.00225>
- Kruasuwan, W., Lohmaneeratana, K., Munnoch, J.T., Vongsangnak, W., Jantrasuriyarat, C., Hoskisson, P.A., Thamchaipenet, A., 2023. Transcriptome Landscapes of Salt-Susceptible Rice Cultivar IR29 Associated with a Plant Growth Promoting Endophytic Streptomyces. *Rice* 16, 6. <https://doi.org/10.1186/s12284-023-00622-7>
- Kudo, Y., Awakawa, T., Du, Y.-L., Jordan, P.A., Creamer, K.E., Jensen, P.R., Lington, R.G., Ryan, K.S., Moore, B.S., 2020. Expansion of Gamma-Butyrolactone Signaling Molecule Biosynthesis to Phosphotriester Natural Products. *ACS Chem. Biol.* 15, 3253–3261. <https://doi.org/10.1021/acschembio.0c00824>
- Kumar, S., Stecher, G., Li, M., Knyaz, C., Tamura, K., 2018. MEGA X: Molecular evolutionary genetics analysis across computing platforms. *Mol. Biol. Evol.* 35, 1547–1549. <https://doi.org/10.1093/molbev/msy096>
- Labeda, D.P., Goodfellow, M., Brown, R., Ward, A.C., Lanoot, B., Vannanneyt, M., Swings, J., Kim, S.B., Liu, Z., Chun, J., Tamura, T., Oguchi, A., Kikuchi, T., Kikuchi, H., Nishii, T., Tsuji, K., Yamaguchi, Y., Tase, A., Takahashi, M., Sakane, T., Suzuki, K.I., Hatano, K., 2012. Phylogenetic study of the species within the family Streptomycetaceae. *Antonie Van*

- Leeuwenhoek Int. J. Gen. Mol. Microbiol. 101, 73–104. <https://doi.org/10.1007/s10482-011-9656-0>
- Laiple, K.J., Härtner, T., Fiedler, H.P., Wohlleben, W., Weber, T., 2009. The kirromycin gene cluster of *Streptomyces collinus* Tü 365 codes for an aspartate- α -decarboxylase, KirD, which is involved in the biosynthesis of the precursor B-alanine. *J. Antibiot. (Tokyo)* 62, 465–468. <https://doi.org/10.1038/ja.2009.67>
- Lambalot, R.H., Gehring, A.M., Flugel, R.S., Zuber, P., LaCelle, M., Marahiel, M.A., Reid, R., Khosla, C., Walsh, C.T., 1996. A new enzyme superfamily - the phosphopantetheinyl transferases. *Chem. Biol.* 3, 923–936. [https://doi.org/10.1016/s1074-5521\(96\)90181-7](https://doi.org/10.1016/s1074-5521(96)90181-7)
- Lamoureux, C., Guilloux, C.-A., Beauruelle, C., Gouriou, S., Ramel, S., Dirou, A., Le Bihan, J., Revert, K., Ropars, T., Lagrèfeuille, R., Vallet, S., Le Berre, R., Nowak, E., Héry-Arnaud, G., 2021. An observational study of anaerobic bacteria in cystic fibrosis lung using culture dependant and independent approaches. *Sci. Rep.* 11, 6845. <https://doi.org/10.1038/s41598-021-85592-w>
- Larcombe, D.E., Braes, R.E., Croxford, J.T., Wilson, J.W., Figurski, D.H., Hoskisson, P.A., 2024. Sequence and origin of the *Streptomyces* intergenetic-conjugation helper plasmid pUZ8002. *Access Microbiol.* 6. <https://doi.org/10.1099/acmi.0.000808.v3>
- Lathe, W.C., Bork, P., 2001. Evolution of *tuf* genes: ancient duplication, differential loss and gene conversion. *FEBS Lett.* 502, 113–116. [https://doi.org/10.1016/S0014-5793\(01\)02639-4](https://doi.org/10.1016/S0014-5793(01)02639-4)
- Lathe, W.C., Snel, B., Bork, P., 2000. Gene context conservation of a higher order than operons. *Trends Biochem. Sci.* 25, 474–479. [https://doi.org/10.1016/s0968-0004\(00\)01663-7](https://doi.org/10.1016/s0968-0004(00)01663-7)
- Latoscha, A., Drexler, D.J., Al-Bassam, M.M., Bandera, A.M., Kaefer, V., Findlay, K.C., Witte, G., Tschowri, N., 2020. C-di-AMP hydrolysis by the phosphodiesterase AtaC promotes differentiation of multicellular bacteria. *Proc. Natl. Acad. Sci. U. S. A.* 117, 7392–7400. <https://doi.org/10.1073/pnas.1917080117>
- Latoscha, A., Wörmann, M.E., Tschowri, N., 2019. Nucleotide second messengers in streptomyces. *Microbiol. U. K.* 165, 1153–1165. <https://doi.org/10.1099/mic.0.000846>
- Lauber, F., Deme, J.C., Lea, S.M., Berks, B.C., 2018. Type 9 secretion system structures reveal a new protein transport mechanism. *Nature* 564, 77–82. <https://doi.org/10.1038/s41586-018-0693-y>
- Leal, M.C., Anaya-Rojas, J.M., Munro, M.H.G., Blunt, J.W., Melian, C.J., Calado, R., Lürig, M.D., 2020. Fifty years of capacity building in the search for new marine natural products. *Proc. Natl. Acad. Sci.* 117, 24165–24172. <https://doi.org/10.1073/pnas.2007610117>
- Leclerc, Q.J., Wildfire, J., Gupta, A., Lindsay, J.A., Knight, G.M., 2022. Growth-Dependent Predation and Generalized Transduction of Antimicrobial Resistance by Bacteriophage. *mSystems* 7, e00135-22. <https://doi.org/10.1128/msystems.00135-22>

- Leclercq, R., 2002. Mechanisms of resistance to macrolides and lincosamides: nature of the resistance elements and their clinical implications. *Clin. Infect. Dis. Off. Publ. Infect. Dis. Soc. Am.* 34, 482–492. <https://doi.org/10.1086/324626>
- Lee, J.H., Kim, Y.G., Cho, H.S., Ryu, S.Y., Cho, M.H., Lee, J., 2014. Coumarins reduce biofilm formation and the virulence of *Escherichia coli* O157:H7. *Phytomedicine* 21, 1037–1042. <https://doi.org/10.1016/j.phymed.2014.04.008>
- Lee, N., Hwang, S., Kim, W., Lee, Y., Kim, J.H., Cho, S., Kim, H.U., Yoon, Y.J., Oh, M.-K., Palsson, B.O., Cho, B.-K., 2021. Systems and synthetic biology to elucidate secondary metabolite biosynthetic gene clusters encoded in *Streptomyces* genomes. *Nat. Prod. Rep.* 38, 1330–1361. <https://doi.org/10.1039/d0np00071j>
- Li, C., Swofford, C.A., Sinskey, A.J., 2020. Modular engineering for microbial production of carotenoids. *Metab. Eng. Commun.* 10, e00118. <https://doi.org/10.1016/j.mec.2019.e00118>
- Li, Z., Jaroszewski, L., Iyer, M., Sedova, M., Godzik, A., 2020. FATCAT 2.0: towards a better understanding of the structural diversity of proteins. *Nucleic Acids Res.* 48, W60–W64. <https://doi.org/10.1093/nar/gkaa443>
- Ling, L.L., Schneider, T., Peoples, A.J., Spoering, A.L., Engels, I., Conlon, B.P., Mueller, A., Schäberle, T.F., Hughes, D.E., Epstein, S., Jones, M., Lazarides, L., Steadman, V.A., Cohen, D.R., Felix, C.R., Fetterman, K.A., Millett, W.P., Nitti, A.G., Zullo, A.M., Chen, C., Lewis, K., 2015. A new antibiotic kills pathogens without detectable resistance. *Nature* 517, 455–459.
- Liu, L, Johnson, H L, Perin, J, Li MSPH, M., Black, R E, Black, Robert E, Liu, Li, Johnson, Hope L, Cousens, S., Perin, Jamie, Scott, S., Lawn, J.E., Rudan, I., Campbell, H., Cibulskis, R., Li, M., Mathers, C., 2012. Global, regional, and national causes of child mortality: an updated systematic analysis for 2010 with time trends since 2000. *www.thelancet.com* 379, 2151–61. [https://doi.org/10.1016/S0140-6736\(12\)60560-1](https://doi.org/10.1016/S0140-6736(12)60560-1)
- Liu, Z., Zhao, Y., Huang, C., Luo, Y., 2021. Recent Advances in Silent Gene Cluster Activation in *Streptomyces*. *Front. Bioeng. Biotechnol.* 9.
- Lombó, F., Velasco, A., Castro, A., De La Calle, F., Braña, A.F., Sánchez-Puelles, J.M., Méndez, C., Salas, J.A., 2006. Deciphering the Biosynthesis Pathway of the Antitumor Thiocoraline from a Marine Actinomycete and Its Expression in Two *Streptomyces* Species. *ChemBioChem* 7, 366–376. <https://doi.org/10.1002/cbic.200500325>
- Lopatniuk, M., Ostash, B., Luzhetskyy, A., Walker, S., Fedorenko, V., 2014. Generation and study of the strains of streptomycetes - heterologous hosts for production of moenomycin. *Russ. J. Genet.* 50, 360–365. <https://doi.org/10.1134/S1022795414040085>
- Lorusso, A.B., Carrara, J.A., Barroso, C.D.N., Tuon, F.F., Faoro, H., 2022. Role of Efflux Pumps on Antimicrobial Resistance in *Pseudomonas aeruginosa*. *Int. J. Mol. Sci.* 23, 15779. <https://doi.org/10.3390/ijms232415779>
- Madhaiyan, M., Saravanan, V.S., See-Too, W.-S., Volpiano, C.G., Sant’Anna, F.H., Faria da Mota, F., Sutcliffe, I., Sangal, V., Passaglia, L.M.P., Rosado, A.S., 2022. Genomic and

- phylogenomic insights into the family Streptomycetaceae lead to the proposal of six novel genera. *Int. J. Syst. Evol. Microbiol.* 72, 005570. <https://doi.org/10.1099/ijsem.0.005570>
- Maehr, H., Leach, M., Yarmchuk, L., Mitrovic, M., 1979. Antibiotic x-5108. ix chemical conversion of mocimycin to aurodox and derivatives of aurodox, goldinamine and mocimycin. *J. Antibiot. (Tokyo)* 32, 361–367. <https://doi.org/10.7164/antibiotics.32.361>
- Maehr, Hubert., Leach, Michael., Yarmchuk, Linda., Stempel, Arthur., 1973. Antibiotic X-5108. V. Structures of antibiotic X-5108 and mocimycin. *J. Am. Chem. Soc.* 95, 8449–8450. <https://doi.org/10.1021/ja00806a043>
- Mahenthiralingam, E., Song, L., Sass, A., White, J., Wilmot, C., Marchbank, A., Boaisha, O., Paine, J., Knight, D., Challis, G.L., 2011. Enacyloxins are products of an unusual hybrid modular polyketide synthase encoded by a cryptic *Burkholderia ambifaria* Genomic Island. *Chem Biol* 18, 665.
- Marinelli, F., 2009. Antibiotics and Streptomyces: The future of antibiotic discovery. *Microbiol. Today* 36, 20–23.
- Martin, D.P., Varsani, A., Roumagnac, P., Botha, G., Maslamoney, S., Schwab, T., Kelz, Z., Kumar, V., Murrell, B., 2021. RDP5: a computer program for analyzing recombination in, and removing signals of recombination from, nucleotide sequence datasets. *Virus Evol.* 7, veaa087. <https://doi.org/10.1093/ve/veaa087>
- Martin, J.L., McMillan, F.M., 2002. SAM (dependent) I AM: the S-adenosylmethionine-dependent methyltransferase fold. *Curr. Opin. Struct. Biol.* 12, 783–793. [https://doi.org/10.1016/S0959-440X\(02\)00391-3](https://doi.org/10.1016/S0959-440X(02)00391-3)
- Maza, F., Maldonado, J., Vásquez-Dean, J., Mandakovic, D., Gaete, A., Cambiazo, V., González, M., 2019. Soil Bacterial Communities From the Chilean Andean Highlands: Taxonomic Composition and Culturability. *Front. Bioeng. Biotechnol.* 7.
- Mcewen, S.A., Collignon, P.J., 2017. Antimicrobial Resistance: A One Health Colloquium. *Microbiol. Spectr.* 6, 1–26. <https://doi.org/10.1128/microbiolspec.ARBA-0009-2017>.Correspondence
- Mchugh, R.E., 2020. Characterising the biosynthesis and mechanism of action of aurodox from *Streptomyces goldiniensis*.
- Mchugh, R.E., Munnoch, J.T., Braes, R.E., Mckean, I.J.W., Giard, J., Taladriz-Sender, A., Peschke, F., Burley, G.A., Roe, A.J., Hoskisson, P.A., 2022. Biosynthesis of Aurodox, a Type III Secretion System Inhibitor from *Streptomyces goldiniensis*. *Appl. Environ. Microbiol.* 88. <https://doi.org/10.1128/aem.00692-22>
- Mchugh, R.E., Munnoch, J.T., Roe, A.J., Hoskisson, P.A., 2021. Genome sequence of the aurodox-producing bacterium *Streptomyces goldiniensis* ATCC 21386 44, 1–13.
- McHugh, R.E., O’Boyle, N., Connolly, J.P.R., Hoskisson, P.A., Roe, A.J., 2019. Characterization of the mode of action of aurodox, a type III secretion system inhibitor from *streptomyces goldiniensis*. *Infect. Immun.* 87, 1–12. <https://doi.org/10.1128/IAI.00595-18>

- McHugh, Rebecca, Munnoch, John, Roe, Andrew J, Hoskisson, Paul A, 2022. Genome sequence of the aurodox-producing bacterium *Streptomyces goldiniensis* ATCC 21386 - ACMI-D-22-00033R1. <https://doi.org/10.6084/M9.FIGSHARE.19487693.V2>
- McInnes, R.S., McCallum, G.E., Lamberte, L.E., van Schaik, W., 2020. Horizontal transfer of antibiotic resistance genes in the human gut microbiome. *Curr. Opin. Microbiol., Host-Microbe Interactions: Bacteria* 53, 35–43. <https://doi.org/10.1016/j.mib.2020.02.002>
- McKean, I.J.W., Sadler, J.C., Cuetos, A., Frese, A., Humphreys, L.D., Grogan, G., Hoskisson, P.A., Burley, G.A., 2019. S-Adenosyl Methionine Cofactor Modifications Enhance the Biocatalytic Repertoire of Small Molecule C-Alkylation. *Angew. Chem. Int. Ed Engl.* 58, 17583–17588. <https://doi.org/10.1002/anie.201908681>
- McKenzie, N.L., Thaker, M., Koteva, K., Hughes, D.W., Wright, G.D., Nodwell, J.R., 2010. Induction of antimicrobial activities in heterologous streptomyces using alleles of the *Streptomyces coelicolor* gene *absA1*. *J. Antibiot. (Tokyo)* 63, 177–182. <https://doi.org/10.1038/ja.2010.13>
- McLean, T.C., Lo, R., Tschowri, N., Hoskisson, P.A., Al Bassam, M.M., Hutchings, M.I., Som, N.F., 2019a. Sensing and responding to diverse extracellular signals: An updated analysis of the sensor kinases and response regulators of streptomyces species. *Microbiol. U. K.* 165, 929–952. <https://doi.org/10.1099/mic.0.000817>
- McLean, T.C., Wilkinson, B., Hutchings, M.I., Devine, R., 2019b. Dissolution of the disparate: Co-ordinate regulation in antibiotic biosynthesis. *Antibiotics* 8. <https://doi.org/10.3390/antibiotics8020083>
- McMurry, L., Petrucci, R.E., Levy, S.B., 1980. Active efflux of tetracycline encoded by four genetically different tetracycline resistance determinants in *Escherichia coli*. *Proc. Natl. Acad. Sci. U. S. A.* 77, 3974–3977. <https://doi.org/10.1073/pnas.77.7.3974>
- Medema, M.H., Blin, K., Cimermanic, P., De Jager, V., Zakrzewski, P., Fischbach, M.A., Weber, T., Takano, E., Breitling, R., 2011. AntiSMASH: Rapid identification, annotation and analysis of secondary metabolite biosynthesis gene clusters in bacterial and fungal genome sequences. *Nucleic Acids Res.* 39, 339–346. <https://doi.org/10.1093/nar/gkr466>
- Medema, M.H., Cimermanic, P., Sali, A., Takano, E., Fischbach, M.A., 2014. A Systematic Computational Analysis of Biosynthetic Gene Cluster Evolution: Lessons for Engineering Biosynthesis. *PLOS Comput. Biol.* 10, e1004016. <https://doi.org/10.1371/journal.pcbi.1004016>
- Medema, M.H., Kottmann, R., Yilmaz, P., Cummings, M., Biggins, J.B., Blin, K., De Bruijn, I., Chooi, Y.H., Claesen, J., Coates, R.C., Cruz-Morales, P., Duddela, S., Düsterhus, S., Edwards, D.J., Fewer, D.P., Garg, N., Geiger, C., Gomez-Escribano, J.P., Greule, A., Hadjithomas, M., Haines, A.S., Helfrich, E.J.N., Hillwig, M.L., Ishida, K., Jones, A.C., Jones, C.S., Jungmann, K., Kegler, C., Kim, H.U., Kötter, P., Krug, D., Masschelein, J., Melnik, A.V., Mantovani, S.M., Monroe, E.A., Moore, M., Moss, N., Nützmann, H.W., Pan, G., Pati, A., Petras, D., Reen, F.J., Rosconi, F., Rui, Z., Tian, Z., Tobias, N.J., Tsunematsu, Y., Wiemann, P., Wyckoff, E., Yan, X., Yim, G., Yu, F., Xie, Y., Aigle, B., Apel, A.K., Balibar, C.J., Balskus, E.P., Barona-Gómez, F., Bechthold, A., Bode, H.B., Borriss, R., Brady, S.F., Brakhage, A.A., Caffrey, P., Cheng, Y.Q.,

Clardy, J., Cox, R.J., De Mot, R., Donadio, S., Donia, M.S., Van Der Donk, W.A., Dorrestein, P.C., Doyle, S., Driessen, A.J.M., Ehling-Schulz, M., Entian, K.D., Fischbach, M.A., Gerwick, L., Gerwick, W.H., Gross, H., Gust, B., Hertweck, C., Höfte, M., Jensen, S.E., Ju, J., Katz, L., Kaysser, L., Klassen, J.L., Keller, N.P., Kormanec, J., Kuipers, O.P., Kuzuyama, T., Kyrpides, N.C., Kwon, H.J., Lautru, S., Lavigne, R., Lee, C.Y., Linquan, B., Liu, X., Liu, W., Luzhetskyy, A., Mahmud, T., Mast, Y., Méndez, C., Metsä-Ketelä, M., Micklefield, J., Mitchell, D.A., Moore, B.S., Moreira, L.M., Müller, R., Neilan, B.A., Nett, M., Nielsen, J., O’Gara, F., Oikawa, H., Osbourn, A., Osburne, M.S., Ostash, B., Payne, S.M., Pernodet, J.L., Petricek, M., Piel, J., Ploux, O., Raaijmakers, J.M., Salas, J.A., Schmitt, E.K., Scott, B., Seipke, R.F., Shen, B., Sherman, D.H., Sivonen, K., Smanski, M.J., Sosio, M., Stegmann, E., Süßmuth, R.D., Tahlan, K., Thomas, C.M., Tang, Y., Truman, A.W., Viaud, M., Walton, J.D., Walsh, C.T., Weber, T., Van Wezel, G.P., Wilkinson, B., Willey, J.M., Wohlleben, W., Wright, G.D., Ziemert, N., Zhang, C., Zotchev, S.B., Breitling, R., Takano, E., Glöckner, F.O., 2015. Minimum Information about a Biosynthetic Gene cluster. *Nat. Chem. Biol.* 11, 625–631. <https://doi.org/10.1038/nchembio.1890>

Mellmann, A., Harmsen, D., Cummings, C.A., Zentz, E.B., Leopold, S.R., Rico, A., Prior, K., Szczepanowski, R., Ji, Y., Zhang, W., McLaughlin, S.F., Henkhaus, J.K., Leopold, B., Bielaszewska, M., Prager, R., Brzoska, P.M., Moore, R.L., Guenther, S., Rothberg, J.M., Karch, H., 2011. Prospective genomic characterization of the german enterohemorrhagic *Escherichia coli* O104:H4 outbreak by rapid next generation sequencing technology. *PLoS ONE* 6. <https://doi.org/10.1371/journal.pone.0022751>

Mennicken, S., de Paula, C.C.P., Vogt-Schilb, H., Jersáková, J., 2024. Diversity of Mycorrhizal Fungi in Temperate Orchid Species: Comparison of Culture-Dependent and Culture-Independent Methods. *J. Fungi* 10, 92. <https://doi.org/10.3390/jof10020092>

Mesters, J.R., Zeef, L.A., Hilgenfeld, R., de Graaf, J.M., Kraal, B., Bosch, L., 1994. The structural and functional basis for the kirromycin resistance of mutant EF-Tu species in *Escherichia coli*. *EMBO J* 13, 4877.

Mills, E., Baruch, K., Charpentier, X., Kobi, S., Rosenshine, I., 2008. Real-Time Analysis of Effector Translocation by the Type III Secretion System of Enteropathogenic *Escherichia coli*. *Cell Host Microbe* 3, 104–113. <https://doi.org/10.1016/j.chom.2007.11.007>

Mirhoseini, A., Amani, J., Nazarian, S., 2018. Review on pathogenicity mechanism of enterotoxigenic *Escherichia coli* and vaccines against it. *Microb. Pathog.* 117, 162–169. <https://doi.org/10.1016/j.micpath.2018.02.032>

Modi, S.R., Collins, J.J., Relman, D.A., 2014. Antibiotics and the gut microbiota. *J. Clin. Invest.* 124, 4212–4218. <https://doi.org/10.1172/JCI72333>

Moore, S.J., Lai, H.-E., Chee, S.-M., Toh, M., Coode, S., Chengan, K., Capel, P., Corre, C., de los Santos, E.L., Freemont, P.S., 2021. A *Streptomyces venezuelae* Cell-Free Toolkit for Synthetic Biology. *ACS Synth. Biol.* 10, 402–411. <https://doi.org/10.1021/acssynbio.0c00581>

Mori, H., Kataoka, M., Yang, X., 2022. Past, Present, and Future of Genome Modification in *Escherichia coli*. *Microorganisms* 10, 1835. <https://doi.org/10.3390/microorganisms10091835>

- Morse, J.C., Girodat, D., Burnett, B.J., Holm, M., Altman, R.B., Sanbonmatsu, K.Y., Wieden, H.-J., Blanchard, S.C., 2020. Elongation factor-Tu can repetitively engage aminoacyl-tRNA within the ribosome during the proofreading stage of tRNA selection. *Proc. Natl. Acad. Sci. U. S. A.* 117, 3610–3620. <https://doi.org/10.1073/pnas.1904469117>
- Mühlen, S., Dersch, P., 2015. Anti-virulence Strategies to Target Bacterial Infections. https://doi.org/10.1007/82_2015_490
- Muir, P., Li, S., Lou, S., Wang, D., Spakowicz, D.J., Salichos, L., Zhang, J., Weinstock, G.M., Isaacs, F., Rozowsky, J., Gerstein, M., 2016. The real cost of sequencing: scaling computation to keep pace with data generation. *Genome Biol.* 17, 53. <https://doi.org/10.1186/s13059-016-0917-0>
- Mulani, M.S., Kamble, E.E., Kumkar, S.N., Tawre, M.S., Pardesi, K.R., 2019. Emerging Strategies to Combat ESKAPE Pathogens in the Era of Antimicrobial Resistance: A Review. *Front. Microbiol.* 10, 539. <https://doi.org/10.3389/fmicb.2019.00539>
- Munita, J.M., Arias, C.A., Unit, A.R., Santiago, A.D., 2016. Mechanisms of Antibiotic Resistance. *HHS Public Access* 4, 1–37. <https://doi.org/10.1128/microbiolspec.VMBF-0016-2015.Mechanisms>
- Murata, M., Sugiyama, S., Matsuoka, S., Matsumori, N., 2015. Bioactive Structure of Membrane Lipids and Natural Products Elucidated by a Chemistry-Based Approach. *Chem. Rec.* 15, 675–690. <https://doi.org/10.1002/tcr.201402097>
- Nair, A.V., Robson, A., Ackrill, T.D., Till, M., Byrne, M.J., Back, C.R., Tiwari, K., Davies, J.A., Willis, C.L., Race, P.R., 2020. Structure and mechanism of a dehydratase/decarboxylase enzyme couple involved in polyketide β -methyl branch incorporation. *Sci. Rep.* 10, 15323. <https://doi.org/10.1038/s41598-020-71850-w>
- Näsvall, J., Sun, L., Roth, J.R., Andersson, D.I., 2012. Real-Time Evolution of New Genes by Innovation, Amplification, and Divergence. *Science* 338, 384–387. <https://doi.org/10.1126/science.1226521>
- Nataro, J.P., Steiner, T., Guerrant, R.L., 1998. Enterohemorrhagic *Escherichia coli*. *Emerg. Infect. Dis.* 4, 251–261.
- Navarro-Muñoz, J.C., Selem-Mojica, N., Mullaney, M.W., Kautsar, S.A., Tryon, J.H., Parkinson, E.I., De Los Santos, E.L.C., Yeong, M., Cruz-Morales, P., Abubucker, S., Roeters, A., Lokhorst, W., Fernandez-Guerra, A., Cappelini, L.T.D., Goering, A.W., Thomson, R.J., Metcalf, W.W., Kelleher, N.L., Barona-Gomez, F., Medema, M.H., 2020. A computational framework to explore large-scale biosynthetic diversity. *Nat. Chem. Biol.* 16, 60–68. <https://doi.org/10.1038/s41589-019-0400-9>
- Nepal, K.K., Wang, G., 2019. Streptomyces: Surrogate Hosts for the Genetic Manipulation of Biosynthetic Gene Clusters and Production of Natural Products. *Biotechnol. Adv.* 37, 1–20. <https://doi.org/10.1016/j.biotechadv.2018.10.003>
- Nguyen, Y., Sperandio, V., 2012. Enterohemorrhagic *E. coli* (EHEC) pathogenesis. *Front. Cell. Infect. Microbiol.* 2, 90. <https://doi.org/10.3389/fcimb.2012.00090>

- Nichols, D., Cahoon, N., Trakhtenberg, E.M., Pham, L., Mehta, A., Belanger, A., Kanigan, T., Lewis, K., Epstein, S.S., 2010. Use of ichip for high-throughput in situ cultivation of "uncultivable microbial species". *Appl. Environ. Microbiol.* 76, 2445–2450. <https://doi.org/10.1128/AEM.01754-09>
- Nieminen, L., Webb, S., Smith, M.C.M., Hoskisson, P.A., 2013. A Flexible Mathematical Model Platform for Studying Branching Networks: Experimentally Validated Using the Model Actinomycete, *Streptomyces coelicolor*. *PLoS ONE* 8. <https://doi.org/10.1371/journal.pone.0054316>
- Nikel, P.I., Benedetti, I., Wirth, N.T., de Lorenzo, V., Calles, B., 2022. Standardization of regulatory nodes for engineering heterologous gene expression: a feasibility study. *Microb. Biotechnol.* 15, 2250–2265. <https://doi.org/10.1111/1751-7915.14063>
- Noda-García, L., Barona-Gómez, F., 2013. Enzyme evolution beyond gene duplication. *Mob. Genet. Elem.* 3, e26439. <https://doi.org/10.4161/mge.26439>
- Nouioui, I., Carro, L., García-López, M., Meier-Kolthoff, J.P., Woyke, T., Kyrpides, N.C., Pukall, R., Klenk, H.-P., Goodfellow, M., Göker, M., 2018. Genome-Based Taxonomic Classification of the Phylum Actinobacteria. *Front. Microbiol.* 9, 2007. <https://doi.org/10.3389/fmicb.2018.02007>
- Ochoa, T.J., Contreras, C.A., 2011. Enteropathogenic *Escherichia coli* infection in children. *Curr. Opin. Infect. Dis.* 24, 478–483. <https://doi.org/10.1097/QCO.0b013e32834a8b8b>
- Ogawara, H., 2016. Self-resistance in streptomycetes, with special reference to β -lactam antibiotics. *Molecules* 21, 1–30. <https://doi.org/10.3390/molecules21050605>
- Ohnishi, Y., Seo, J.W., Horinouchi, S., 2002. Deprogrammed sporulation in *Streptomyces*. *FEMS Microbiol. Lett.* 216, 1–7. [https://doi.org/10.1016/S0378-1097\(02\)00996-5](https://doi.org/10.1016/S0378-1097(02)00996-5)
- Olsthoorn-Tieleman, L.N., Fischer, S.E.J., Kraal, B., 2002. The unique *tuf2* gene from the kirromycin producer *Streptomyces ramocissimus* encodes a minor and kirromycin-sensitive elongation factor Tu. *J. Bacteriol.* 184, 4211–4218. <https://doi.org/10.1128/JB.184.15.4211-4218.2002>
- Olsthoorn-Tieleman, L.N., Palstra, R.-J.T.S., van Wezel, G.P., Bibb, M.J., Pleij, C.W.A., 2007. Elongation factor Tu3 (EF-Tu3) from the kirromycin producer *Streptomyces ramocissimus* is resistant to three classes of EF-Tu-specific inhibitors. *J. Bacteriol.* 189, 3581–3590. <https://doi.org/10.1128/JB.01810-06>
- O'Neill, J., 2016. Review on Antimicrobial Resistance.
- Oren, A., Garrity, G.M., 2021. Valid publication of the names of forty-two phyla of prokaryotes. *Int. J. Syst. Evol. Microbiol.* 71, 005056. <https://doi.org/10.1099/ijsem.0.005056>
- Oshima, T., Imahori, K., 1974. Description of *Thermus thermophilus* (Yoshida and Oshima) comb. nov., a Nonsporulating Thermophilic Bacterium from a Japanese Thermal Spa. *Int. J. Syst. Evol. Microbiol.* 24, 102–112. <https://doi.org/10.1099/00207713-24-1-102>

- Overmann, J., Scholz, A.H., 2017. Microbiological Research Under the Nagoya Protocol: Facts and Fiction. *Trends Microbiol.* 25, 85–88. <https://doi.org/10.1016/j.tim.2016.11.001>
- Owen, J.G., Copp, J.N., Ackerley, D.F., 2011. Rapid and flexible biochemical assays for evaluating 4'-phosphopantetheinyl transferase activity. *Biochem. J.* 436, 709–717. <https://doi.org/10.1042/BJ20110321>
- Pagès, J.-M., James, C.E., Winterhalter, M., 2008. The porin and the permeating antibiotic: a selective diffusion barrier in Gram-negative bacteria. *Nat. Rev. Microbiol.* 6, 893–903. <https://doi.org/10.1038/nrmicro1994>
- Paget, M.S., Chamberlin, L., Atrih, A., Foster, S.J., Buttner, M.J., 1999. Evidence that the extracytoplasmic function sigma factor sigmaE is required for normal cell wall structure in *Streptomyces coelicolor* A3(2). *J. Bacteriol.* 181, 204–211. <https://doi.org/10.1128/JB.181.1.204-211.1999>
- Pakbin, B., Brück, W.M., Rossen, J.W.A., 2021. Virulence Factors of Enteric Pathogenic *Escherichia coli*: A Review. *Int. J. Mol. Sci.* 22, 9922. <https://doi.org/10.3390/ijms22189922>
- Palmer, T., Finney, A.J., Saha, C.K., Atkinson, G.C., Sargent, F., 2021. A holin/peptidoglycan hydrolase-dependent protein secretion system. *Mol. Microbiol.* 115, 345–355. <https://doi.org/10.1111/mmi.14599>
- Parmeggiani, A., Krab, I.M., Okamura, S., Nielsen, R.C., Nyborg, J., Nissen, P., 2006. Structural basis of the action of pulvomycin and GE2270 A on elongation factor Tu. *Biochemistry* 45, 6846.
- Parmeggiani, A., Nissen, P., 2006. Elongation factor Tu-targeted antibiotics: four different structures, two mechanisms of action. *FEBS Lett* 580, 4576.
- Parmeggiani, A., Swart, G.W.M., 1985. Mechanism of Action of Kirromycin-Like Antibiotics. *Annu. Rev. Microbiol.* 39, 557–577. <https://doi.org/10.1146/annurev.mi.39.100185.003013>
- Pavlidou, M., Pross, E.K., Musiol, E.M., Kulik, A., Wohlleben, W., Weber, T., 2011. The phosphopantetheinyl transferase KirP activates the ACP and PCP domains of the kirromycin NRPS/PKS of *Streptomyces collinus* Tü 365. *FEMS Microbiol. Lett.* 319, 26–33. <https://doi.org/10.1111/j.1574-6968.2011.02263.x>
- Paysan-Lafosse, T., Blum, M., Chuguransky, S., Grego, T., Pinto, B.L., Salazar, G.A., Bileschi, M.L., Bork, P., Bridge, A., Colwell, L., Gough, J., Haft, D.H., Letunić, I., Marchler-Bauer, A., Mi, H., Natale, D.A., Orengo, C.A., Pandurangan, A.P., Rivoire, C., Sigrist, C.J.A., Sillitoe, I., Thanki, N., Thomas, P.D., Tosatto, S.C.E., Wu, C.H., Bateman, A., 2022. InterPro in 2022. *Nucleic Acids Res.* 51, D418–D427. <https://doi.org/10.1093/nar/gkac993>
- Pendergrass, H.A., May, A.E., 2019. Natural product type III secretion system inhibitors. *Antibiotics* 8. <https://doi.org/10.3390/antibiotics8040162>
- Pogliano, J., Poglian, N., Silverman, J.A., 2012. Daptomycin-mediated reorganization of membrane architecture causes mislocalization of essential cell division proteins. *J. Bacteriol.* 194, 4494–4504. <https://doi.org/10.1128/JB.00011-12>

- Polapally, R., Mansani, M., Rajkumar, K., Burgula, S., Hameeda, B., Alhazmi, A., Bantun, F., Almalki, A.H., Haque, S., El Enshasy, H.A., Sayyed, R.Z., 2022. Melanin pigment of *Streptomyces puniceus* RHP9 exhibits antibacterial, antioxidant and anticancer activities. *PloS One* 17, e0266676. <https://doi.org/10.1371/journal.pone.0266676>
- Pouillot, F., Chomton, M., Blois, H., Courroux, C., Noelig, J., Bidet, P., Bingen, E., Bonacorsi, S., 2012. Efficacy of Bacteriophage Therapy in Experimental Sepsis and Meningitis Caused by a Clone O25b:H4-ST131 *Escherichia coli* Strain Producing CTX-M-15. *Antimicrob. Agents Chemother.* 56, 3568–3575. <https://doi.org/10.1128/AAC.06330-11>
- Prezioso, Samantha M., Brown, N.E., Goldberg, J.B., 2017. Elfamycins: Inhibitors of Elongation Factor-Tu. *Mol. Microbiol.* 106, 22–34. <https://doi.org/10.1111/mmi.13750>
- Prezioso, S. M., Brown, N.E., Goldberg, J.B., 2017. Elfamycins: inhibitors of elongation factor-Tu. *Mol Microbiol* 106, 22.
- Proft, T., Baker, E.N., 2009. Pili in Gram-negative and Gram-positive bacteria - structure, assembly and their role in disease. *Cell. Mol. Life Sci. CMLS* 66, 613–635. <https://doi.org/10.1007/s00018-008-8477-4>
- Prosser, B.L.T., Palleroni, N.J., 1976. *Streptomyces longwoodensis* sp. nov. *Int. J. Syst. Evol. Microbiol.* 26, 319–322. <https://doi.org/10.1099/00207713-26-3-319>
- Qadri, F., Svennerholm, A.-M., Faruque, A.S.G., Sack, R.B., 2005. Enterotoxigenic *Escherichia coli* in developing countries: epidemiology, microbiology, clinical features, treatment, and prevention. *Clin. Microbiol. Rev.* 18, 465–483. <https://doi.org/10.1128/CMR.18.3.465-483.2005>
- Qin, Z., Munnoch, J.T., Devine, R., Holmes, N.A., Seipke, R.F., Wilkinson, K.A., Wilkinson, B., Hutchings, M.I., 2017. Formicamycins, antibacterial polyketides produced by *Streptomyces formicae* isolated from African *Tetraponera* plant-ants. *Chem. Sci.* 8, 3218–3227. <https://doi.org/10.1039/C6SC04265A>
- Ramos, J.L., Mermod, N., Timmis, K.N., 1987. Regulatory circuits controlling transcription of TOL plasmid operon encoding meta-cleavage pathway for degradation of alkylbenzoates by *Pseudomonas*. *Mol. Microbiol.* 1, 293–300. <https://doi.org/10.1111/j.1365-2958.1987.tb01935.x>
- Rasko, D.A., Sperandio, V., 2010. Anti-virulence strategies to combat bacteria-mediated disease. *Nat. Rev. Drug Discov.* 9, 117–128. <https://doi.org/10.1038/nrd3013>
- Rausch, C., Weber, T., Kohlbacher, O., Wohlleben, W., Huson, D.H., 2005. Specificity prediction of adenylation domains in nonribosomal peptide synthetases (NRPS) using transductive support vector machines (TSVMs). *Nucleic Acids Res.* 33, 5799–5808. <https://doi.org/10.1093/nar/gki885>
- Robertsen, H.L., Musiol-Kroll, E.M., Ding, L., Laiple, K.J., Hofeditz, T., Wohlleben, W., Lee, S.Y., Grond, S., Weber, T., 2018. Filling the Gaps in the Kirromycin Biosynthesis: Deciphering the Role of Genes Involved in Ethylmalonyl-CoA Supply and Tailoring Reactions. *Sci. Rep.* 8. <https://doi.org/10.1038/s41598-018-21507-6>

- Rodrigues, I.C., Rodrigues, S.C., Duarte, F.V., Costa, Paula M. da, Costa, Paulo M. da, 2022. The Role of Outer Membrane Proteins in UPEC Antimicrobial Resistance: A Systematic Review. *Membranes* 12, 981. <https://doi.org/10.3390/membranes12100981>
- Rodriguez-Siek, K.E., Giddings, C.W., Doetkott, C., Johnson, T.J., Fakh, M.K., Nolan, L.K., 2005. Comparison of *Escherichia coli* isolates implicated in human urinary tract infection and avian colibacillosis. *Microbiology* 151, 2097–2110. <https://doi.org/10.1099/mic.0.27499-0>
- Roe, A.J., Yull, H., Naylor, S.W., Woodward, M.J., Smith, D.G.E., Gally, D.L., 2003. Heterogeneous surface expression of EspA translocon filaments by *Escherichia coli* O157:H7 is controlled at the posttranscriptional level. *Infect. Immun.* 71, 5900–5909. <https://doi.org/10.1128/IAI.71.10.5900-5909.2003>
- Ross-Gillespie, A., Weigert, M., Brown, S.P., Kümmerli, R., 2014. Gallium-mediated siderophore quenching as an evolutionarily robust antibacterial treatment. *Evol. Med. Public Health* 2014, 18–29. <https://doi.org/10.1093/emph/eou003>
- Rückert, C., Szczepanowski, R., Albersmeier, A., Goesmann, A., Iftime, D., Musiol, E.M., Blin, K., Wohlleben, W., Pühler, A., Kalinowski, J., Weber, T., 2013. Complete genome sequence of the kirromycin producer *Streptomyces collinus* Tü 365 consisting of a linear chromosome and two linear plasmids. *J. Biotechnol.* 168, 739–740. <https://doi.org/10.1016/j.jbiotec.2013.10.004>
- Rudolf, J.D., Chang, C.-Y., Ma, M., Shen, B., 2017. Cytochromes P450 for natural product biosynthesis in *Streptomyces*: sequence, structure, and function. *Nat. Prod. Rep.* 34, 1141–1172. <https://doi.org/10.1039/c7np00034k>
- Saha, C.K., Sanches Pires, R., Brolin, H., Delannoy, M., Atkinson, G.C., 2021. FlaGs and webFlaGs: discovering novel biology through the analysis of gene neighbourhood conservation. *Bioinforma. Oxf. Engl.* 37, 1312–1314. <https://doi.org/10.1093/bioinformatics/btaa788>
- Saitou, N., Nei, M., 1987. The neighbor-joining method: a new method for reconstructing phylogenetic trees. *Mol. Biol. Evol.* 4, 406–425. <https://doi.org/10.1093/oxfordjournals.molbev.a040454>
- Salerno, P., Persson, J., Bucca, G., Laing, E., Ausmees, N., Smith, C.P., Flärdh, K., 2013. Identification of new developmentally regulated genes involved in *Streptomyces coelicolor* sporulation. *BMC Microbiol.* 13. <https://doi.org/10.1186/1471-2180-13-281>
- Sambrook, J., Fritsch, E.F., Maniatis, T., 1989. *Molecular cloning: a laboratory manual*. Cold Spring Harbor Laboratory Press, Cold Spring Harbor, NY.
- Savoia, D., 2016. New Antimicrobial Approaches: Reuse of Old Drugs. *Curr. Drug Targets* 6, 731–738.
- Schatz, A., Bugie, E., Waksman, S.A., 1944. Streptomycin, a substance exhibiting antibiotic activity against gram-positive and gram-negative bacteria. 1944. *Proc. Soc. Exp. Biol. Med.* 55, 66–69. <https://doi.org/10.1097/01.blo.0000175887.98112.fe>

- Schiavo, G., van der Goot, F.G., 2001. The bacterial toxin toolkit. *Nat. Rev. Mol. Cell Biol.* 2, 530–537. <https://doi.org/10.1038/35080089>
- Schmidt, M.A., 2010. LEEways: Tales of EPEC, ATEC and EHEC. *Cell. Microbiol.* 12, 1544–1552. <https://doi.org/10.1111/j.1462-5822.2010.01518.x>
- Schmidt, S., Sunyaev, S., Bork, P., Dandekar, T., 2003. Metabolites: a helping hand for pathway evolution? *Trends Biochem. Sci.* 28, 336–341. [https://doi.org/10.1016/S0968-0004\(03\)00114-2](https://doi.org/10.1016/S0968-0004(03)00114-2)
- Schniete, J.K., Cruz-Morales, P., Selem-Mojica, N., Fernández-Martínez, L.T., Hunter, I.S., Barona-Gómez, F., Hoskisson, P.A., 2018. Expanding primary metabolism helps generate the metabolic robustness to facilitate antibiotic biosynthesis in *Streptomyces*. *mBio* 9. <https://doi.org/10.1128/mBio.02283-17>
- Schwartz, J.L., Tishler, M., Arison, B.H., Shafer, H.M., Omura, S., 1976. Identification of mycolutein and pulvomycin as aureothin and labilomycin respectively. *J. Antibiot. (Tokyo)* 29, 236–241. <https://doi.org/10.7164/antibiotics.29.236>
- Seipke, R.F., Barke, J., Brearley, C., Hill, L., Yu, D.W., Goss, R.J.M., Hutchings, M.I., 2011. A Single *Streptomyces* Symbiont Makes Multiple Antifungals to Support the Fungus Farming Ant *Acromyrmex octospinosus*. *PLOS ONE* 6, e22028. <https://doi.org/10.1371/journal.pone.0022028>
- Seipke, R.F., Barke, J., Heavens, D., Yu, D.W., Hutchings, M.I., 2013. Analysis of the bacterial communities associated with two ant–plant symbioses. *MicrobiologyOpen* 2, 276–283. <https://doi.org/10.1002/mbo3.73>
- Seipke, R.F., Kaltenpoth, M., Hutchings, M.I., 2012. *Streptomyces* as symbionts: an emerging and widespread theme? *FEMS Microbiol. Rev.* 36, 862–876. <https://doi.org/10.1111/j.1574-6976.2011.00313.x>
- Selva, E., Beretta, G., Montanini, N., Saddler, G.S., Gastaldo, L., Ferrari, P., Lorenzetti, R., Landini, P., Ripamonti, F., Goldstein, B.P., 1991a. Antibiotic GE2270 a: a novel inhibitor of bacterial protein synthesis. I. Isolation and characterization. *J. Antibiot. (Tokyo)* 44, 693–701. <https://doi.org/10.7164/antibiotics.44.693>
- Selva, E., Beretta, G., Montanini, N., Saddler, G.S., Gastaldo, L., Ferrari, P., Lorenzetti, R., Landini, P., Ripamonti, F., Goldstein, B.P., 1991b. Antibiotic GE2270 a: a novel inhibitor of bacterial protein synthesis. I. Isolation and characterization. *J. Antibiot. (Tokyo)* 44, 693–701. <https://doi.org/10.7164/antibiotics.44.693>
- Selva, E., Ferrari, P., Kurz, M., Tavecchia, P., Colombo, L., Stella, S., Restelli, E., Goldstein, B.P., Ripamonti, F., Denaro, M., 1995. Components of the GE2270 complex produced by *Planobispora rosea* ATCC 53773. *J. Antibiot. (Tokyo)* 48, 1039–1042. <https://doi.org/10.7164/antibiotics.48.1039>
- Selvin, J., Shanmugha Priya, S., Seghal Kiran, G., Thangavelu, T., Sapna Bai, N., 2009. Sponge-associated marine bacteria as indicators of heavy metal pollution. *Microbiol. Res.* 164, 352–363. <https://doi.org/10.1016/j.micres.2007.05.005>

- Servin, A.L., 2005. Pathogenesis of Afa/Dr Diffusely Adhering *Escherichia coli*. Clin. Microbiol. Rev. 18, 264–292. <https://doi.org/10.1128/CMR.18.2.264-292.2005>
- Shaw, R.K., Berger, C.N., Feys, B., Knutton, S., Pallen, M.J., Frankel, G., 2008. Enterohemorrhagic *Escherichia coli* Exploits EspA Filaments for Attachment to Salad Leaves. Appl. Environ. Microbiol. 74, 2908–2914. <https://doi.org/10.1128/AEM.02704-07>
- Shen, Y., Loessner, M.J., 2021. Beyond antibacterials - exploring bacteriophages as antivirulence agents. Curr. Opin. Biotechnol. 68, 166–173. <https://doi.org/10.1016/j.copbio.2020.11.004>
- Shentu, X.-P., Cao, Z.-Y., Xiao, Y., Tang, G., Ochi, K., Yu, X.-P., 2018. Substantial improvement of toyocamycin production in *Streptomyces diastatochromogenes* by cumulative drug-resistance mutations. PLOS ONE 13, e0203006. <https://doi.org/10.1371/journal.pone.0203006>
- Shin, M., 2017. The mechanism underlying Ler-mediated alleviation of gene repression by H-NS. Biochem. Biophys. Res. Commun. 483, 392–396. <https://doi.org/10.1016/j.bbrc.2016.12.132>
- Sidda, J.D., Corre, C., 2012. Gamma-Butyrolactone and Furan Signaling Systems in *Streptomyces*, in: Hopwood, D.A. (Ed.), Methods in Enzymology, Natural Product Biosynthesis by Microorganisms and Plants, Part C. Academic Press, pp. 71–87. <https://doi.org/10.1016/B978-0-12-404634-4.00004-8>
- Sidda, J.D., Poon, V., Song, L., Wang, W., Yang, K., Corre, C., 2016. Overproduction and identification of butyrolactones SCB1-8 in the antibiotic production superhost *Streptomyces* M1152. Org. Biomol. Chem. 14, 6390–6393. <https://doi.org/10.1039/c6ob00840b>
- Siegele, D.A., Hu, J.C., 1997. Gene expression from plasmids containing the araBAD promoter at subsaturating inducer concentrations represents mixed populations. Proc. Natl. Acad. Sci. U. S. A. 94, 8168–8172.
- Sievers, F., Wilm, A., Dineen, D., Gibson, T.J., Karplus, K., Li, W., Lopez, R., McWilliam, H., Remmert, M., Söding, J., Thompson, J.D., Higgins, D.G., 2011. Fast, scalable generation of high-quality protein multiple sequence alignments using Clustal Omega. Mol. Syst. Biol. 7, 539. <https://doi.org/10.1038/msb.2011.75>
- Sigle, S., Ladwig, N., Wohlleben, W., Muth, G., 2015. Synthesis of the spore envelope in the developmental life cycle of *Streptomyces coelicolor*. Int. J. Med. Microbiol. 305, 183–189. <https://doi.org/10.1016/j.ijmm.2014.12.014>
- Simpson, K.L., Wilson, A.W., Burton, E., Nakayama, T.O.M., Chichester, C.O., 1963. MODIFIED FRENCH PRESS FOR THE DISRUPTION OF MICROORGANISMS. J. Bacteriol. 86, 1126–1127. <https://doi.org/10.1128/jb.86.5.1126-1127.1963>
- Singh, S.B., Zink, D.L., Dorso, K., Motyl, M., Salazar, O., Basilio, A., Vicente, F., Byrne, K.M., Ha, S., Genilloud, O., 2009. Isolation, structure, and antibacterial activities of lucensimycins D-G, discovered from *streptomyces lucensis* MA7349 using an antisense strategy. J. Nat. Prod. 72, 345–352. <https://doi.org/10.1021/np8005106>

- Sit, C.S., Ruzzini, A.C., Van Arnem, E.B., Ramadhar, T.R., Currie, C.R., Clardy, J., 2015. Variable genetic architectures produce virtually identical molecules in bacterial symbionts of fungus-growing ants. *Proc. Natl. Acad. Sci.* 112, 13150–13154. <https://doi.org/10.1073/pnas.1515348112>
- Skinninger, M.A., Johnston, C.W., Gunabalasingam, M., Merwin, N.J., Kieliszek, A.M., MacLellan, R.J., Li, H., Ranieri, M.R.M., Webster, A.L.H., Cao, M.P.T., Pfeifle, A., Spencer, N., To, Q.H., Wallace, D.P., Dejong, C.A., Magarvey, N.A., 2020. Comprehensive prediction of secondary metabolite structure and biological activity from microbial genome sequences. *Nat. Commun.* 11, 6058. <https://doi.org/10.1038/s41467-020-19986-1>
- Slemc, L., Jakše, J., Filisetti, A., Baranasic, D., Rodríguez-García, A., Del Carratore, F., Marino, S.M., Zucko, J., Starcevic, A., Šala, M., Pérez-Bonilla, M., Sánchez-Hidalgo, M., González, I., Reyes, F., Genilloud, O., Springthorpe, V., Goranovič, D., Kosec, G., Thomas, G.H., Lucrezia, D.D., Petković, H., Tome, M., n.d. Reference-Grade Genome and Large Linear Plasmid of *Streptomyces rimosus*: Pushing the Limits of Nanopore Sequencing. *Microbiol. Spectr.* 10, e02434-21. <https://doi.org/10.1128/spectrum.02434-21>
- Slot, J.C., 2017. Fungal Gene Cluster Diversity and Evolution. *Adv. Genet.* 100, 141–178. <https://doi.org/10.1016/bs.adgen.2017.09.005>
- Sørensen, S.J., Bailey, M., Hansen, L.H., Kroer, N., Wuertz, S., 2005. Studying plasmid horizontal transfer in situ: a critical review. *Nat. Rev. Microbiol.* 3, 700–710. <https://doi.org/10.1038/nrmicro1232>
- Sosio, M., Bossi, E., Donadio, S., 2001. Assembly of large genomic segments in artificial chromosomes by homologous recombination in *Escherichia coli*. *Nucleic Acids Res.* 29, 1–8. <https://doi.org/10.1093/nar/29.7.e37>
- Sousa, J.A. de J., Olivares, F.L., 2016. Plant growth promotion by streptomycetes: ecophysiology, mechanisms and applications. *Chem. Biol. Technol. Agric.* 3, 24. <https://doi.org/10.1186/s40538-016-0073-5>
- Sperandio, V., Mellies, J.L., Delahay, R.M., Frankel, G., Adam Crawford, J., Nguyen, W., Kaper, J.B., 2000. Activation of enteropathogenic *Escherichia coli* (EPEC) LEE2 and LEE3 operons by Ler. *Mol. Microbiol.* 38, 781–793. <https://doi.org/10.1046/j.1365-2958.2000.02168.x>
- Sprinzl, M., 1994. Elongation factor Tu: a regulatory GTPase with an integrated effector. *Trends Biochem. Sci.* 19, 245–250. [https://doi.org/10.1016/0968-0004\(94\)90149-x](https://doi.org/10.1016/0968-0004(94)90149-x)
- Stackebrandt, E., Witt, D., Kemmerling, C., Kroppenstedt, R., Liesack, W., 1991. Designation of *Streptomyces* 16S and 23S rRNA-based target regions for oligonucleotide probes. *Appl. Environ. Microbiol.* 57, 1468–1477.
- Stentz, R., Horn, N., Cross, K., Salt, L., Brearley, C., Livermore, D.M., Carding, S.R., 2015. Cephalosporinases associated with outer membrane vesicles released by *Bacteroides* spp. protect gut pathogens and commensals against β -lactam antibiotics. *J. Antimicrob. Chemother.* 70, 701–709. <https://doi.org/10.1093/jac/dku466>

- Stokes, H.W., Gillings, M.R., 2011. Gene flow, mobile genetic elements and the recruitment of antibiotic resistance genes into Gram-negative pathogens. *FEMS Microbiol. Rev.* 35, 790–819. <https://doi.org/10.1111/j.1574-6976.2011.00273.x>
- Strieker, M., Tanović, A., Marahiel, M.A., 2010. Nonribosomal peptide synthetases: Structures and dynamics. *Curr. Opin. Struct. Biol.* 20, 234–240. <https://doi.org/10.1016/j.sbi.2010.01.009>
- Studier, F.W., 2005. Protein production by auto-induction in high-density shaking cultures. *Protein Expr. Purif.* 41, 207–234. <https://doi.org/10.1016/j.pep.2005.01.016>
- Studier, F.W., Moffatt, B.A., 1986. Use of bacteriophage T7 RNA polymerase to direct selective high-level expression of cloned genes. *J. Mol. Biol.* 189, 113–130. [https://doi.org/10.1016/0022-2836\(86\)90385-2](https://doi.org/10.1016/0022-2836(86)90385-2)
- Sugai, S., Komaki, H., Hemmi, H., Kodani, S., 2016. Isolation and structural determination of a new antibacterial compound demethyl-L-681,217 from *Streptomyces cattleya*. *J. Antibiot. (Tokyo)* 69, 839–842. <https://doi.org/10.1038/ja.2016.53>
- Surette, M.D., Spanogiannopoulos, P., Wright, G.D., 2021. The Enzymes of the Rifamycin Antibiotic Resistome. *Acc. Chem. Res.* 54, 2065–2075. <https://doi.org/10.1021/acs.accounts.1c00048>
- Takano, E., 2006. γ -Butyrolactones: *Streptomyces* signalling molecules regulating antibiotic production and differentiation. *Curr. Opin. Microbiol., Ecology and industrial microbiology / Techniques* 9, 287–294. <https://doi.org/10.1016/j.mib.2006.04.003>
- Tan, S., Cho, K., Nodwell, J.R., 2022. A defect in cell wall recycling confers antibiotic resistance and sensitivity in *Staphylococcus aureus*. *J. Biol. Chem.* 298, 102473. <https://doi.org/10.1016/j.jbc.2022.102473>
- Tanaka, Y., Kasahara, K., Hirose, Y., Murakami, K., Kugimiya, R., Ochi, K., 2013. Activation and products of the cryptic secondary metabolite biosynthetic gene clusters by rifampin resistance (*rpoB*) mutations in actinomycetes. *J. Bacteriol.* 195, 2959–2970. <https://doi.org/10.1128/JB.00147-13>
- Tarr, P.I., Gordon, C.A., Chandler, W.L., 2005. Shiga-toxin-producing *Escherichia coli* and haemolytic uraemic syndrome. *Lancet* 365, 1073–1086. [https://doi.org/10.1016/S0140-6736\(05\)71144-2](https://doi.org/10.1016/S0140-6736(05)71144-2)
- Taylor, M.W., Hill, R.T., Piel, J., Thacker, R.W., Hentschel, U., 2007. Soaking it up: the complex lives of marine sponges and their microbial associates. *ISME J.* 1, 187–190. <https://doi.org/10.1038/ismej.2007.32>
- Terlizzi, M.E., Gribaudo, G., Maffei, M.E., 2017. UroPathogenic *Escherichia coli* (UPEC) Infections: Virulence Factors, Bladder Responses, Antibiotic, and Non-antibiotic Antimicrobial Strategies. *Front. Microbiol.* 8, 1566. <https://doi.org/10.3389/fmicb.2017.01566>
- Thaker, M., Spanogiannopoulos, P., Wright, G.D., 2010. The tetracycline resistome. *Cell. Mol. Life Sci.* 67, 419–431. <https://doi.org/10.1007/s00018-009-0172-6>

- Thaker, M.N., García, M., Koteva, K., Waglechner, N., Sorensen, D., Medina, R., Wright, G.D., 2012. Biosynthetic gene cluster and antimicrobial activity of the elfamycin antibiotic factumycin. *MedChemComm* 3, 1020–1026. <https://doi.org/10.1039/c2md20038d>
- Theuretzbacher, U., Gottwalt, S., Beyer, P., Butler, M., Czaplewski, L., Lienhardt, C., Moja, L., Paul, M., Paulin, S., Rex, J.H., Silver, L.L., Spigelman, M., Thwaites, G.E., Paccaud, J.P., Harbarth, S., 2019. Analysis of the clinical antibacterial and antituberculosis pipeline. *Lancet Infect. Dis.* 19, e40–e50. [https://doi.org/10.1016/S1473-3099\(18\)30513-9](https://doi.org/10.1016/S1473-3099(18)30513-9)
- Tieleman, L.N., van Wezel, G.P., Bibb, M.J., Kraal, B., 1997. Growth phase-dependent transcription of the *Streptomyces ramocissimus* *tuf1* gene occurs from two promoters. *J. Bacteriol.* 179, 3619–3624.
- Torres, A.N., Chamorro-Veloso, N., Costa, P., Cádiz, L., Del Canto, F., Venegas, S.A., López Nitsche, M., Coloma-Rivero, R.F., Montero, D.A., Vidal, R.M., 2020. Deciphering Additional Roles for the EF-Tu, l-Asparaginase II and OmpT Proteins of Shiga Toxin-Producing *Escherichia coli*. *Microorganisms* 8, 1184. <https://doi.org/10.3390/microorganisms8081184>
- Torsvik, V., Goksoyr, J., Daae, F.L., 1990. High Diversity in Soil Bacteria. *Appl. Environ. Microbiol.* 56, 782–787.
- Totsika, M., 2016. Benefits and Challenges of Antivirulence Antimicrobials at the Dawn of the Post-Antibiotic Era. *Drug Deliv. Lett.* 6, 30–37. <https://doi.org/10.2174/22103031066661605061200>
- Tringe, S.G., Hugenholtz, P., Brinkman, F., Parkhill, J., 2008. A renaissance for the pioneering 16S rRNA gene This review comes from a themed issue on Genomics Edited by. *Curr. Opin. Microbiol.* 11, 442–446. <https://doi.org/10.1016/j.mib.2008.09.011>
- Understanding Moore's law : four decades of innovation, 2006. . Philadelphia, Pa. : Chemical Heritage Foundation.
- van Bergeijk, D.A., Terlouw, B.R., Medema, M.H., van Wezel, G.P., 2020. Ecology and genomics of Actinobacteria: new concepts for natural product discovery. *Nat. Rev. Microbiol.* 18, 546–558. <https://doi.org/10.1038/s41579-020-0379-y>
- van der Meide, P.H., Vijgenboom, E., Talens, A., Bosch, L., 1983. The role of EF-Tu in the expression of *tufA* and *tufB* genes. *Eur. J. Biochem.* 130, 397–407. <https://doi.org/10.1111/j.1432-1033.1983.tb07166.x>
- Van Wezel, G.P., McDowall, K.J., 2011. The regulation of the secondary metabolism of *Streptomyces*: New links and experimental advances. *Nat. Prod. Rep.* 28, 1311–1333. <https://doi.org/10.1039/c1np00003a>
- vanWezel, G.P., van derMeulen, J., Kawamoto, S., Luiten, R.G.M., Koerten, H.K., Kraal, B., 2000. *ssgA* Is Essential for Sporulation of *Streptomyces coelicolor* A3(2) and Affects Hyphal Development by Stimulating Septum Formation. *J. Bacteriol.* 182, 5653–5662.
- Veenendaal, A.K.J., Sundin, C., Blocker, A.J., 2009. Small-molecule type III secretion system inhibitors block assembly of the shigella type III secreton. *J. Bacteriol.* 191, 563–570. <https://doi.org/10.1128/JB.01004-08>

- Vera, A., González-Montalbán, N., Arís, A., Villaverde, A., 2007. The conformational quality of insoluble recombinant proteins is enhanced at low growth temperatures. *Biotechnol. Bioeng.* 96, 1101–1106. <https://doi.org/10.1002/bit.21218>
- Vidgren, J., Svensson, L.A., Liljas, A., 1994. Crystal structure of catechol O-methyltransferase. *Nature* 368, 354–358. <https://doi.org/10.1038/368354a0>
- Vijgenboom, E., Woudt, L.P., Heinstra, P.W.H., Rietveld, K., Van Haarlem, J., Van Wezel, G.P., Shochat, S., Bosch, L., 1994. Three tuf-like genes in the kirromycin producer *Streptomyces ramocissimus*. *Microbiology* 140, 983–998. <https://doi.org/10.1099/00221287-140-4-983>
- Vogele, L., Palm, G.J., Mesters, J.R., Hilgenfeld, R., 2001. Conformational change of elongation factor Tu (EF-Tu) induced by antibiotic binding. Crystal structure of the complex between EF-Tu-GDP and aurodox. *J. Biol. Chem.* 276, 17149–17155. <https://doi.org/10.1074/jbc.M100017200>
- von Wintersdorff, C.J.H., Penders, J., van Niekerk, J.M., Mills, N.D., Majumder, S., van Alphen, L.B., Savelkoul, P.H.M., Wolffs, P.F.G., 2016. Dissemination of Antimicrobial Resistance in Microbial Ecosystems through Horizontal Gene Transfer. *Front. Microbiol.* 7, 173. <https://doi.org/10.3389/fmicb.2016.00173>
- Waksman, S.A., 1919. Cultural studies of species of *Actinomyces*.
- Waksman, S.A., Curtis, R.E., 1916. The actinomycetes of the soil.
- Waksman, S.A., Henrici, A.T., 1943. The nomenclature and classification of the Actinomycetes. *J. Bacteriol.* 7, 190–200. <https://doi.org/10.1179/sre.1944.7.51.190>
- Walsh, C.T., 2008. The chemical versatility of natural-product assembly lines. *Acc. Chem. Res.* 41, 4–10. <https://doi.org/10.1021/ar7000414>
- Wang, W., Yang, T., Li, Y., Li, S., Yin, S., Styles, K., Corre, C., Yang, K., 2016. Development of a Synthetic Oxytetracycline-Inducible Expression System for *Streptomyces* Using de Novo Characterized Genetic Parts. *ACS Synth. Biol.* 5, 765–773. <https://doi.org/10.1021/acssynbio.6b00087>
- Waschulin, V., Borsetto, C., Corre, C., Wellington, E.M., 2023. Design and validation of a PCR screen for γ -butyrolactone-like regulatory systems in *Streptomyces*. *Access Microbiol.* 5, 000661.v3. <https://doi.org/10.1099/acmi.0.000661.v3>
- Waschulin, V., Borsetto, C., James, R., Newsham, K.K., Donadio, S., Corre, C., Wellington, E., 2022. Biosynthetic potential of uncultured Antarctic soil bacteria revealed through long-read metagenomic sequencing. *ISME J.* 16, 101–111. <https://doi.org/10.1038/s41396-021-01052-3>
- Wasteson, Y., 2001. Zoonotic *Escherichia coli*. *Acta Vet. Scand. Suppl.* 95, 79–84.
- Watanabe, T., Izaki, K., Takahashi, H., 1982. New polyenic antibiotics active against gram-positive and -negative bacteria. I. Isolation and purification of antibiotics produced by *Gluconobacter* sp. W-315. *J. Antibiot. (Tokyo)* 35, 1141–1147. <https://doi.org/10.7164/antibiotics.35.1141>

Watanabe, T., Okubo, N., Suzuki, T., Izaki, K., 1992. NEW POLYENIC ANTIBIOTICS ACTIVE AGAINST GRAM-POSITIVE AND GRAM-NEGATIVE BACTERIA VI. NON-LACTONIC POLYENE ANTIBIOTIC, ENACYLOXIN IIa, INHIBITS BINDING OF AMINOACYL-tRNA TO A SITE OF RIBOSOMES. *J. Antibiot. (Tokyo)* 45, 572–574. <https://doi.org/10.7164/antibiotics.45.572>

Watanabe, Y., Haneda, T., Kimishima, A., Kuwae, A., Suga, T., Suzuki, T., Iwabuchi, Y., Honsho, M., Honma, S., Iwatsuki, M., Matsui, H., Hanaki, H., Kanoh, N., Abe, A., Asami, Y., Ōmura, S., n.d. PurA is the main target of aurodox, a type III secretion system inhibitor. *Proc. Natl. Acad. Sci. U. S. A.* 121, e2322363121. <https://doi.org/10.1073/pnas.2322363121>

Weber, Tilmann, Laible, K.J., Pross, E.K., Textor, A., Grond, S., Welzel, K., Pelzer, S., Vente, A., Wohlleben, W., 2008a. Molecular Analysis of the Kirromycin Biosynthetic Gene Cluster Revealed β -Alanine as Precursor of the Pyridone Moiety. *Chem. Biol.* 15, 175–188. <https://doi.org/10.1016/j.chembiol.2007.12.009>

Weber, Tilmann, Laible, K.J., Pross, E.K., Textor, A., Grond, S., Welzel, K., Pelzer, S., Vente, A., Wohlleben, W., 2008b. Molecular Analysis of the Kirromycin Biosynthetic Gene Cluster Revealed β -Alanine as Precursor of the Pyridone Moiety. *Chem. Biol.* 15, 175–188. <https://doi.org/10.1016/j.chembiol.2007.12.009>

Weber, T., Laible, K.J., Pross, E.K., Textor, A., Grond, S., Welzel, K., Pelzer, S., Vente, A., Wohlleben, W., 2008. Molecular analysis of the kirromycin biosynthetic gene cluster revealed beta-alanine as precursor of the pyridone moiety. *Chem Biol* 15, 175.

Weisblum, B., 1995. Erythromycin resistance by ribosome modification. *Antimicrob. Agents Chemother.* 39, 577–585. <https://doi.org/10.1128/AAC.39.3.577>

Weng, Y., Bina, T.F., Bina, X.R., Bina, J.E., 2021. ToxR Mediates the Antivirulence Activity of Phenyl-Arginine- β -Naphthylamide To Attenuate *Vibrio cholerae* Virulence. *Infect. Immun.* 89, e0014721. <https://doi.org/10.1128/IAI.00147-21>

Whelan, S., Lucey, B., Finn, K., 2023. Uropathogenic *Escherichia coli* (UPEC)-Associated Urinary Tract Infections: The Molecular Basis for Challenges to Effective Treatment. *Microorganisms* 11, 2169. <https://doi.org/10.3390/microorganisms11092169>

Wick, R.R., Judd, L.M., Gorrie, C.L., Holt, K.E., 2016. Unicycler: resolving bacterial genome assemblies from short and long sequencing reads. <https://doi.org/10.1101/096412>

Wick, R.R., Schultz, M.B., Zobel, J., Holt, K.E., 2015. Bandage: interactive visualization of de novo genome assemblies. *Bioinformatics* 31, 3350–3352. <https://doi.org/10.1093/bioinformatics/btv383>

Widjaja, M., Harvey, K.L., Hagemann, L., Berry, I.J., Jarocki, V.M., Raymond, B.B.A., Tacchi, J.L., Gründel, A., Steele, J.R., Padula, M.P., Charles, I.G., Dumke, R., Djordjevic, S.P., 2017. Elongation factor Tu is a multifunctional and processed moonlighting protein. *Sci. Rep.* 7, 11227. <https://doi.org/10.1038/s41598-017-10644-z>

Wiles, T.J., Kulesus, R.R., Mulvey, M.A., 2008. Origins and virulence mechanisms of uropathogenic *Escherichia coli*. *Exp. Mol. Pathol.* 85, 11–19. <https://doi.org/10.1016/j.yexmp.2008.03.007>

- Willey, J.M., Gaskell, A.A., 2011. Morphogenetic signaling molecules of the streptomycetes. *Chem. Rev.* 111, 174–187. <https://doi.org/10.1021/cr1000404>
- Williams, S.T., Goodfellow, M., Alderson, G., Wellington, E.M.H., Sneath, P.H.A., Sackin, M.J., 1983. Numerical Classification of *Streptomyces* and Related Genera, *Journal of General Microbiology*.
- Wilson, D.N., 2014. Ribosome-targeting antibiotics and mechanisms of bacterial resistance. *Nat. Rev. Microbiol.* 12, 35–48. <https://doi.org/10.1038/nrmicro3155>
- Wl, T., Kp, K., M, D., A, W., J, W., J, G., F, M., 2012. Short-read reading-frame predictors are not created equal: sequence error causes loss of signal. *BMC Bioinformatics* 13. <https://doi.org/10.1186/1471-2105-13-183>
- Wolf, H., Chinali, G., Parmeggiani, A., 1974. Kirromycin, an Inhibitor of Protein Biosynthesis that Acts on Elongation Factor Tu. *Proc. Natl. Acad. Sci. U. S. A.* 71, 4910–4914.
- Wolf, H., Zähler, H., 1972. [Metabolic products of microorganisms. 99. Kirromycin]. *Arch. Mikrobiol.* 83, 147–154.
- Wolf, H., Zähler, H., Nierhaus, K., 1972. Kirromycin, an inhibitor of the 30 S ribosomal subunits function. *FEBS Lett.* 21, 347–350. [https://doi.org/10.1016/0014-5793\(72\)80199-6](https://doi.org/10.1016/0014-5793(72)80199-6)
- Worsley, S.F., Newitt, J., Rassbach, J., Batey, S.F.D., Holmes, N.A., Murrell, J.C., Wilkinson, B., Hutchings, M.I., 2020. *Streptomyces* Endophytes Promote Host Health and Enhance Growth across Plant Species. *Appl. Environ. Microbiol.* 86, e01053-20. <https://doi.org/10.1128/AEM.01053-20>
- Wu, L., Zhang, Q., Deng, Z., Yu, Y., 2022. From solo to duet, intersections of natural product assembly with self-resistance. *Nat. Prod. Rep.* 39, 919–925. <https://doi.org/10.1039/D1NP00064K>
- Xu, G., Yang, S., 2019. Regulatory and evolutionary roles of pseudo γ -butyrolactone receptors in antibiotic biosynthesis and resistance. *Appl. Microbiol. Biotechnol.* 103, 9373–9378. <https://doi.org/10.1007/s00253-019-10219-0>
- Xu, J., Zhang, Y., 2010. How significant is a protein structure similarity with TM-score = 0.5? *Bioinformatics* 26, 889. <https://doi.org/10.1093/bioinformatics/btq066>
- Yagüe, P., Willemse, J., Koning, R.I., Rioseras, B., López-García, M.T., Gonzalez-Quirón, N., Lopez-Iglesias, C., Shliaha, P.V., Rogowska-Wrzesinska, A., Koster, A.J., Jensen, O.N., Van Wezel, G.P., Manteca, Á., 2016. Subcompartmentalization by cross-membranes during early growth of *Streptomyces* hyphae. *Nat. Commun.* 7, 1–11. <https://doi.org/10.1038/ncomms12467>
- Yarlagadda, V., Medina, R., Johnson, T.A., Koteva, K.P., Cox, G., Thaker, M.N., Wright, G.D., 2020. Resistance-Guided Discovery of Elfamycin Antibiotic Producers with Antagonococcal Activity. *ACS Infect. Dis.* 6, 3163–3173. <https://doi.org/10.1021/acsinfecdis.0c00467>
- Yashiro, E., Spear, R.N., McManus, P.S., 2011. Culture-dependent and culture-independent assessment of bacteria in the apple phyllosphere. *J. Appl. Microbiol.* 110, 1284–1296. <https://doi.org/10.1111/j.1365-2672.2011.04975.x>

- Yin, Z., Dickschat, J.S., 2021. Cis double bond formation in polyketide biosynthesis. *Nat. Prod. Rep.* 38, 1445–1468. <https://doi.org/10.1039/D0NP00091D>
- Zambelloni, R., Marquez, R., Roe, A.J., 2015. Development of antivirulence compounds: A biochemical review. *Chem. Biol. Drug Des.* 85, 43–55. <https://doi.org/10.1111/cbdd.12430>
- Zaroubi, L., Ozugergin, I., Mastronardi, K., Imfeld, A., Law, C., Gélinas, Y., Piekny, A., Findlay, B.L., 2022. The Ubiquitous Soil Terpene Geosmin Acts as a Warning Chemical. *Appl. Environ. Microbiol.* 88, e0009322. <https://doi.org/10.1128/aem.00093-22>
- Zettler, J., Xia, H., Burkard, N., Kulik, A., Grond, S., Heide, L., Apel, A.K., 2014. New aminocoumarins from the rare actinomycete *Catenulispora acidiphila* DSM 44928: identification, structure elucidation, and heterologous production. *Chembiochem Eur. J. Chem. Biol.* 15, 612–621. <https://doi.org/10.1002/cbic.201300712>
- Zhang, J.-W., Wang, R., Liang, X., Han, P., Zheng, Y.-L., Li, X.-F., Gao, D.-Z., Liu, M., Hou, L.-J., Dong, H.-P., 2023. Novel Gene Clusters for Natural Product Synthesis Are Abundant in the Mangrove Swamp Microbiome. *Appl. Environ. Microbiol.* 89, e0010223. <https://doi.org/10.1128/aem.00102-23>
- Zhang, Y., Skolnick, J., 2005. TM-align: a protein structure alignment algorithm based on the TM-score. *Nucleic Acids Res.* 33, 2302–2309. <https://doi.org/10.1093/nar/gki524>
- Zhou, H., Wang, Y., Yu, Y., Bai, T., Chen, L., Liu, P., Guo, H., Zhu, C., Tao, M., Deng, Z., 2012. A non-restricting and non-methylating *Escherichia coli* strain for DNA cloning and high-throughput conjugation to *Streptomyces coelicolor*. *Curr. Microbiol.* 64, 185–190. <https://doi.org/10.1007/s00284-011-0048-5>
- Zhou, S., Bhukya, H., Malet, N., Harrison, P.J., Rea, D., Belousoff, M.J., Venugopal, H., Sydor, P.K., Styles, K.M., Song, L., Cryle, M.J., Alkhalaf, L.M., Fülöp, V., Challis, G.L., Corre, C., 2021. Molecular basis for control of antibiotic production by a bacterial hormone. *Nature* 590, 463–467. <https://doi.org/10.1038/s41586-021-03195-x>
- Zhou, Z., Sun, N., Wu, S., Li, Y.Q., Wang, Y., 2016. Genomic data mining reveals a rich repertoire of transport proteins in *Streptomyces*. *BMC Genomics* 17. <https://doi.org/10.1186/s12864-016-2899-4>
- Zuurmond, A.M., Rundlöf, A.K., Kraal, B., 1999. Either of the chromosomal *tuf* genes of *E. coli* K-12 can be deleted without loss of cell viability. *Mol. Gen. Genet. MGG* 260, 603–607. <https://doi.org/10.1007/s004380050934>